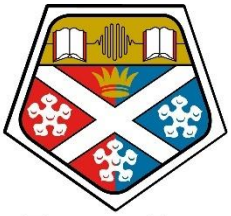

University of Strathclyde Glasgow

Mechanistic Characterisation of the Rh50 Ammonium Transporter Protein from *Nitrosomonas europaea*

Adriana Bizior

Supervisor 1: Dr Arnaud Javelle Supervisor 2: Prof. Paul Hoskisson

Strathclyde Institute of Pharmaceutical and Biomedical Sciences

A thesis submitted in fulfilment of the requirements for the degree of Doctor of Philosophy at the University of Strathclyde.

December 2022

Declaration

‘This thesis is the result of the author’s original research. It has been composed by the author and has not been previously submitted for examination which has led to the award of a degree.’

Signed: 

Date: December 2022

Acknowledgments

First and foremost, I would like to thank my primary supervisor Dr Arnaud Javelle for his constant support, encouragement, and for always believing in me. Arnaud has provided me with much guidance whilst giving me scope to drive my own project and explore my own ideas. I truly cannot imagine having a better mentor, thank you, Arnaud. Many thanks to Prof. Paul Hoskisson, my secondary supervisor, for all the insightful discussions and comments throughout my PhD.

I would like to thank the academics on level 6 namely, Paul Herron, Kate Duncan, Iain Hunter, Morgan Feeney, Leighton Pritchard and Craig Roberts. All of the above have influenced my work and their feedback has been of great value. I also want to express my gratitude to all our collaborators. This includes Dr Ana Sofia Brito, Dr Mélanie Boeckstaens and Dr Anna-Maria Marini for all their efforts and expertise in yeast complementation work, and for all the constructive and insightful discussions during our collaborations. I would also like to thank both Prof. Luke Chamberlain and Dr Laura Lehtovirta-Morley for agreeing to be my viva examiners.

Now turning to the Javelle group, aka the protein experts. I remember Gaëtan from my honours project when he was in the final stages of his PhD. I remember his advice very well “Don’t do a PhD”, and yet I did it anyway because Gordon said it is fun. Gordon, a PhD student in the Javelle lab taught me everything I needed to know to complete my journey on level 6 Hamnet Wing. I am forever grateful for his help and friendship which I am certain will last forever. In my final year, I had a chance to pass this gift of knowledge to Thomas Harris, the newest addition to our group. I can sleep peacefully knowing that ÄKTA and SURFE^{2}R are in good hands. Thank you for all your hard work, Tom.

This section would not have been complete if I have not mentioned all the wonderful people I have met during this journey. I would like to thank every member of the Microgroup, past and present for their continued help, advice, and support. So, to Ainsley, Ally, Anna, Anil, Bea, Becca, Charlie, Charlotte, Connie, Dan, Darya, David, Darren, Diana, Eilidh, Emily, Elmira, Gaëtan,

Gareth, Gordon, Holly, Jack, James, John M, John B, Jonny, Jordan, Liam, Lily, Lis, Logan, Marla, Molly, Moira, Parra, Stuart, Tiago, Tom Ha and Tom He and Walid.

Now I want to specifically thank some individuals who have become so special to me over the years. To Eilidh, for being my lab cheerleader and a massive source of encouragement. You infected me with your positivity - thanks to you I learnt to cherish every little thing in my life. To Elmira (aka Chimken), for appreciating my dark humour and level of honesty only acceptable in mainland Europe. Thank you for keeping me physically and mentally fit with our regular pad sessions at the gym. To Molly, for the laugh which cannot be stopped even by the thickest of walls, for all the cheese chat and heavenly good cakes. I hope to see you on Bake Off one day. Last but not least, to my little Robyn(ean). Your chaotic energy and smiley face brighten up many long days in the lab and office <smiles mischievously from behind desk divider>. Thank you for always being there for me, gals. I am forever grateful I could share this journey with you. I look forward to our annual trips to Hawick and dinners that turn into therapeutic dance sessions.

While I have met so many incredible people during my PhD, which I am fortunate to call my friends now, this section is dedicated to people who were around since before, those who turned Scotland into a new home. Special thanks to Paula, you helped me turn this awkward, scared girl who moved to Edinburgh over 9 years ago into a confident woman that I am now. To Pauline and Hannah for all the time spent in the library studying for exams and to my little Polish “family” Kasia, Aleks, Gosia and Filip for giving me so many memories and for keeping my work-life balance in check.

A massive THANK YOU to my family. To my parents, Alicja and Aleksander, for supporting my every decision and for always showing interest in what I do (I really appreciated “Are your bacteria behaving?” or “Are your little bugs growing?” questions). *Dziękuję za wszystko*. To my brothers, Marcin and Rafał - I know that to this day you have no idea what I do but it doesn’t matter, I appreciate all the memes you send me daily, science and non-science related. To my sister-in-law Marta for keeping Marcin in check and Asia for being the

sister I never had. Special thanks to my godmother Dorota, for being my inspiration to pursue a PhD and for always praising my achievements. Finally, and most importantly, I want to thank my best friend and partner, Wojtek. Thank you for providing me with an unmeasurable amount of laughter and distraction from every experiment that has failed over the past three years. You have seen me at my worst and still believed in me, encouraged, and supported me - I couldn’t have done it without you. I promise I will get a real job now and will make it up to you for putting up with a PhD me.

Abstract

The exchange of ammonium across cellular membranes is a fundamental process in all domains of life which is facilitated by the ubiquitous Amt/Mep/Rh transporter superfamily. The functional diversity of Amt/Mep and Rh has been known for decades: bacteria, fungi, and plants use Amt/Mep proteins to scavenge ammonium for biosynthetic assimilation. Mammals on the other hand use the Rh proteins for ammonium detoxification in erythrocytes, kidney, and liver tissues. Crucially Rh malfunction is associated with various pathologies, including hereditary anaemias, overhydrated stomatocytosis, and early-onset depressive disorders. However, their mechanism and the substrate translocated (NH_4^+/NH_3) remain elusive. Recently, our group proposed a new model for the mechanism of electrogenic ammonium transport in AmtB protein from *E. coli*, where NH_4^+ undergoes deprotonation, allowing NH_3 and H^+ to follow two separate pathways, and join in the cytoplasm. Despite their fundamentally divergent physiological functions, the Amt/Mep/Rh proteins are structurally very similar, raising the possibility of a conserved transport mechanism across the family. In this context, we investigated the mechanism of ammonium translocation through rhesus protein (Rh50) from *Nitrosomonas europaea,* as a first step towards expanding the Rh protein research and understanding of their mechanism.

An *in vitro* assay based on Solid Supported Membrane Electrophysiology (SSME) was developed and the electrogenic activity in Rh50 was confirmed (Chapter 3). We provided a detailed characterisation of the activity, selectivity, and kinetics of WT Rh50 (Chapter 4). Further characterisation of WT Rh50 and Rh50 variants led to the proposal of the coexistence of two mechanisms in the protein: mechanism I wherein NH_4^+ is deprotonated and H^+ and NH_3 are carried separately across the membrane, and mechanism II, where NH_4^+ is directly translocated through by-passing deprotonation (Chapter 4). Through mutagenesis studies, we also revealed valuable information on bidirectionality of the protein which we propose to be directly linked with a hydration pattern of the protein (Chapter 5). The body of this work provides a basis for future Rh protein research which will enable us to better understand how Rh mutations lead to pathologies in humans.

Publications

Two papers have been published throughout the course of this PhD. Some of the contents of the first paper have been presented in Chapter 4. Both papers can be found in the Appendix of this thesis, and the references are listed below:

Gordon Williamson, Giulia Tamburrino, **Adriana Bizior,** Mélanie Boeckstaens, Gaëtan Dias Mirandela, Marcus G Bage, Andrei Pisliakov, Callum M Ives, Eilidh Terras, Paul A Hoskisson, Anna Maria Marini, Ulrich Zachariae, and Arnaud Javelle. (2020) 'A two-lane mechanism for selective biological ammonium transport', *eLife*., 9, p. e57183.

Gordon Williamson, Ana Sofia Brito, **Adriana Bizior**, Giulia Tamburrino, Gaëtan Dias Mirandela, Thomas Harris, Paul A. Hoskisson, Ulrich Zachariae, Anna Maria Marini, Mélanie Boeckstaens, Arnaud Javellea 'Coexistence of Ammonium Transporter and Channel Mechanisms in Amt/Mep/Rh twin-His Variants Impairs the Filamentation Signaling Capacity of Fungal Mep2 Transceptors'. *mBio*, e0291321.

Parts of the Introduction to this thesis will be published in the following review articles:

Adriana Bizior, Gordon Williamson, Gaetan Dias Mirandela, Paul A. Hoskisson, and Arnaud Javelle 'Prokaryotic ammonium transporters: After three decades of research, is the mystery solved?' *Microbiology Society* manuscript in review

Adriana Bizior, Gordon Williamson, Thomas Harris, Paul A. Hoskisson, and Arnaud Javelle 'New insights into Rh protein research – a review' *Biochemical Society* manuscript in review

The data presented in Chapter 4 and 5 will form the core of another paper which is currently in preparation:

Adriana Bizior, Gordon Williamson, Ana Sofia Brito, Thomas Harris, Mélanie Boeckstaens, Paul A Hoskisson, Anna Maria Marini, and Arnaud Javelle 'Rh50 protein from *Nitrosomonas europaea* is an electrogenic ammonium transporter' manuscript in preparation

List of Abbreviations

°C	Degrees Celsius
A	solution Activating solution
Å	A
*Af*Amt1	*Archaeoglobus fulgidus* ammonium transporter 1
Amt	Ammonium transporter
*Ca*Mep2	*Candida albicans* Methylpermease 2
CV	Column Volume
DDM	dodecyl-β-maltopyranoside
DNA	Deoxyribonucleic acid
EcAmtB	*Escherichia coli* ammonium transporter
IMAC	Immobilised Metal Affinity Chromatography
KDa	KiloDalton
Ki	Inhibition constant
Km	Michaelis constant
*Ks*Amt5	*Kuenenia stuttgartiensis* ammonium transporter 5
LB	Luria Britani
LDAO	lauryldecylamine oxide
LPR	Lipid Protein Ratio
MeA	Methylammonium
Mep	Methylammonium permease
MDS	Molecular Dynamic Simulation
nA	NanoAmpere
NA solution	Non-activating solution
*Ne*Rh50	*Nitrosomonas europaea* rhesus protein 50
nF	NanoFaraday
nS	Nanoseconds
OG	n-octyl-β-D-glucopyranoside
PAGE	Polyacrylamide gel electrophoresis
PDB	Protein Database

pH	Power of hydrogen
PMSF	Phenylmethylsulfonyl fluoride
POPC	1-palmitoyl-2-oleoyl phosphatidylcholine
Rsat	Saturation Constant
Rsol	Solubilisation Constant
Rh	Rhesus
RMSD	Root Mean Square Deviation
*Sc*Mep	*Saccharomyces cerevisiae* Methylpermease
SDS	Sodium Dodecyl Sulfate
SEC	Size Exclusion Chromatography
SSME	Solid Supported Membrane Electrophysiology
TEMED	Tetramethylethylenediamine
Tris	Tris(hydroxymethyl)aminomethane
WB	Western Blott
g	x gravity

Table of Contents

Chapter 1

Chapter 1: Introduction

1.1 Biological Importance of Ammonium

The transport of ammonium (NH_4^+) across cell membranes is a fundamental process in all domains of life. Apart from N_2, ammonium is the most prevalent nitrogenous compound on earth, and for most higher plants (Britto *et al.*, 2001), prokaryotes, and fungi (Reitzer, 2003) it is a preferred nitrogen (N) source (Kleiner, 1981). Ammonium is also an important intermediate released by symbiotic fungi (Behie and Bidochka, 2014) and during many metabolic reactions, such as symbiotic fixation of atmospheric dinitrogen (F.J, 1965). It also provides energy and reducing power for ammonia-oxidising organisms (Bock and Wagner, 2006).

Whilst ammonium is an important biosynthetic compound in plants and microorganisms, it is also the end product of nitrogen metabolism (Kleiner, 1981), and a key metabolite in the control of systemic acid-base balance in higher organisms (Pitts, 1971; Knepper *et al.*, 1991). In humans, elevated concentrations of ammonium can lead to a wide variety of clinical problems, such as neurological conditions, and growth retardation in neonates and children (Auron and Brophy, 2012). Thus, efficient ammonium excretion is essential in detoxifying erythrocytes, kidney, and liver cells (Wright *et al.*, 2011).

Ammonium is not merely a toxic waste product. It appears to activate an autophagy, an intracellular degradative pathway which maintains cell homeostasis, by controlling turnover of proteins and organelles, and in the survival of cells during stressful conditions, such as starvation (Eng and Abraham, 2010). Moreover, ammonia accumulation in the tumour microenvironment was proposed to contribute to proliferation of cancerous cells by serving as a nitrogen source for amino acid synthesis (Spinelli *et al.*, 2017).

1.1.1 Ammonium Provides Energy for Ammonia-Oxidising Bacteria

Ammonia-oxidizing bacteria (AOB), such as *Nitrosomonas europaea,* are obligate chemolithoautotrophs which use NH_3 as a sole energy source and reducing power (Bock and Wagner, 2006). AOB participate in the biogeochemical N cycle in the process of nitrification, by catalysing oxidation of inorganic nitrogen in the form of ammonia (NH_3) or ammonium (NH_4^+) to oxidized nitrogen in the form of nitrite (NO_2^-). AOB such as *N. europaea* achieve aerobic nitrification via the successive action of ammonia monooxygenase (AMO) and hydroxylamine oxidoreductase (HAO) (Hooper *et al.,* 1997). The soluble forms are readily released increasing the nitrogen availability to plants. AOB are also important to the treatment of wastewater and have potential for the bioremediation of sites contaminated with chlorinated aliphatic hydrocarbons (Juliette, Hyman and Arp, 1993; Keener and Arp, 1994). In addition, ammonia appears to play a critical role serving as a signal leading to regulation of gene transcription (Sayavedra-Soto *et al.*, 1996; Wei, Sayavedra-Soto and Arp, 2004), and as a metabolic substrate in *N. europaea*.

Despite extensive studies focusing on the ability of *N. europaea* to utilise ammonia, (Arp, Sayavedra-Soto and Hommes, 2002), little is known about how ammonium enters the cell. It was suggested by Chain *et al.* that in *N. europaea* ammonium uptake is mediated passively at low pH (Chain *et al.*, 2003). However, high ammonium uptake rates observed in *N. europaea,* and its ability to accumulate ammonium during ammonia oxidation (Schmidt *et al.*, 2004) highly suggests active ammonium transport system.

1.1.2 Ammonium Metabolism is Critical for Acid-Base Homeostasis

In mammals, the liver plays a central role in nitrogen metabolism, and conversion of toxic ammonia to urea via the ornithine cycle (also called urea cycle), forming urea that is excreted in urine by kidneys (**Figure 1.1**) (Bode and Souba, 1994). Ammonium escaping from the urea cycle is transformed into glutamine by glutamine synthetase (GS) in the perivenous hepatocytes. Glutamine is then transported in the blood to the proximal tubules in the renal

cortex, where, along with other amino acids, it is converted into ammonia (Tannen, 1978). Free ammonium ions are either excreted in the urine as a result of specialised transport process in several nephron segments or reabsorbed and returned to blood stream via renal vein (**Figure 1.2**). Renal ammonium metabolism is the primary component of net acid excretion and thereby is critical for acid-base homeostasis (Pitts, 1971; Knepper *et al.*, 1991).

1.1.3 Ammonium Exchange Across Biological Membranes

For many years, the transport of ammonium produced in the kidney was through to occur by the rapid NH_3 diffusion across renal tubule epithelia. Here, NH_3 would be at a concentration equilibrium throughout the kidney, while in compartments with the lowest pH it would be trapped as ionic NH_4^+ (Pitts, 1948). Such equilibrium between NH_4^+/NH_3 is of a high importance as upon it depends on the systemic pH balance. This view, however, was later challenged by studies demonstrating that NH_3 permeability is a significant barrier to ammonia transport (Kikeri *et al.*, 1989), and that NH_3 concentrations differ along the renal cortex (Simon, Martin and Buerkert, 1985; Good and DuBose, 1987). In addition, the neutral molecule NH_3 is a weak base, thus at physiological pH, 99% of the ammonium is protonated to yield NH_4^+ (Bates and Pinching, 1950).

This observation led to a new model of NH_3 and NH_4^+ transport across plasma membranes mediated by specific proteins. Studies using brush-border membrane vesicles suggested that the apical Na^+/H^+ exchanger (NHE-3) (**Figure 1.2**) and an apical Ba^{2+}-sensitive K^+ channel play important roles in NH_4^+ secretion in proximal tubule (Nagami, 1989; Hamm and Simon, 1990). In the thick ascending limb of Henle loop, which is an important site for reabsorbing luminal ammonia, the apical Na^+-K^+-$2Cl^-$ cotransporter (NKCC2) was proposed to be a major contributor, where NH_4^+ is transported at the K^+-binding site (**Figure 1.2**) (Amlal, Paillard and Bichara, 1994). The exit of ammonia across the basolateral plasma membrane was proposed to be mediated by the basolateral Na^+/NH_4^+ exchanger or via Na^+-K^+-ATPase (NHE-4) (Wall and Koger, 1994; Bourgeois *et al.*, 2010). Finally, parallel H^+ and NH_3 secretion occurs in the collecting duct (**Figure 1.2**).

While mentioned above proteins might aid in ammonium transport, later studies demonstrated that the transporter-mediated NH_3 movement in apical and basolateral collecting duct cells was not altered by Na^+-K^+-ATPase, Na^+-K^+-$2Cl^-$ cotransporter inhibitors, nor by excess potassium or by varying membrane potential (Handlogten *et al.*, 2004; Handlogten *et al.*, 2005). These findings suggested the presence of unidentified ammonium-specific proteins enabling efficient ammonium transport mechanism.

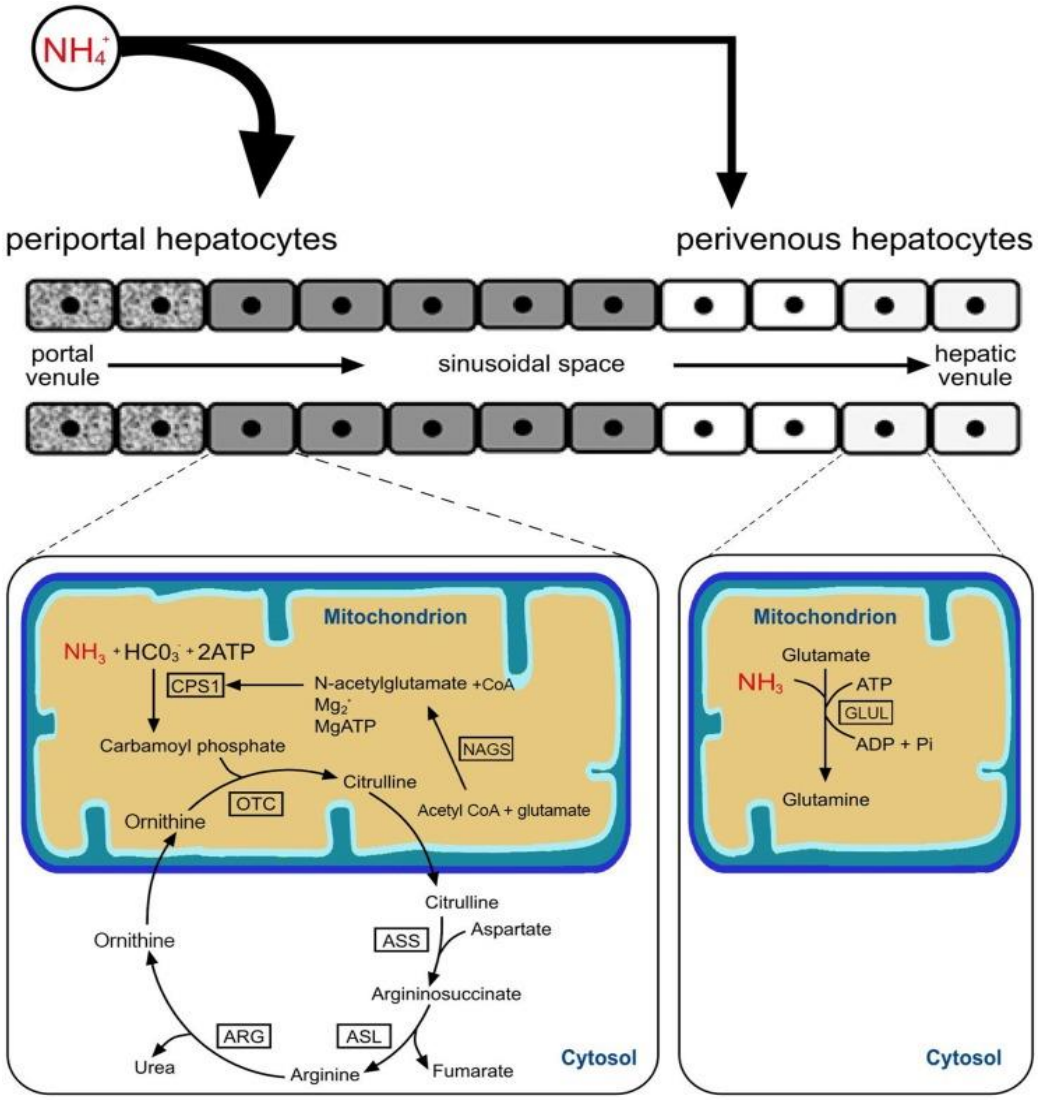

Figure 1.1 The two major pathways metabolizing ammonia in the liver: the urea cycle (periportal), and glutamine synthesis (pericentral). In the urea cycle ammonia is converted to into urea is a sequence of biochemical reactions. Ammonia 'escaping' the urea cycle is metabolized to glutamine. *Carbamoyl phosphate synthetase1 (CPS1), N-acetylglutamate synthase (NAGS), ornithine carbamoyltransferase (OTC), argininosuccinate synthetase (ASS1), argininosuccinate lyase (ASL), Arginase (ARG1), glutamate–ammonia ligase (GLUL).* Figure adapted from van Straten *et at.,* 2004.

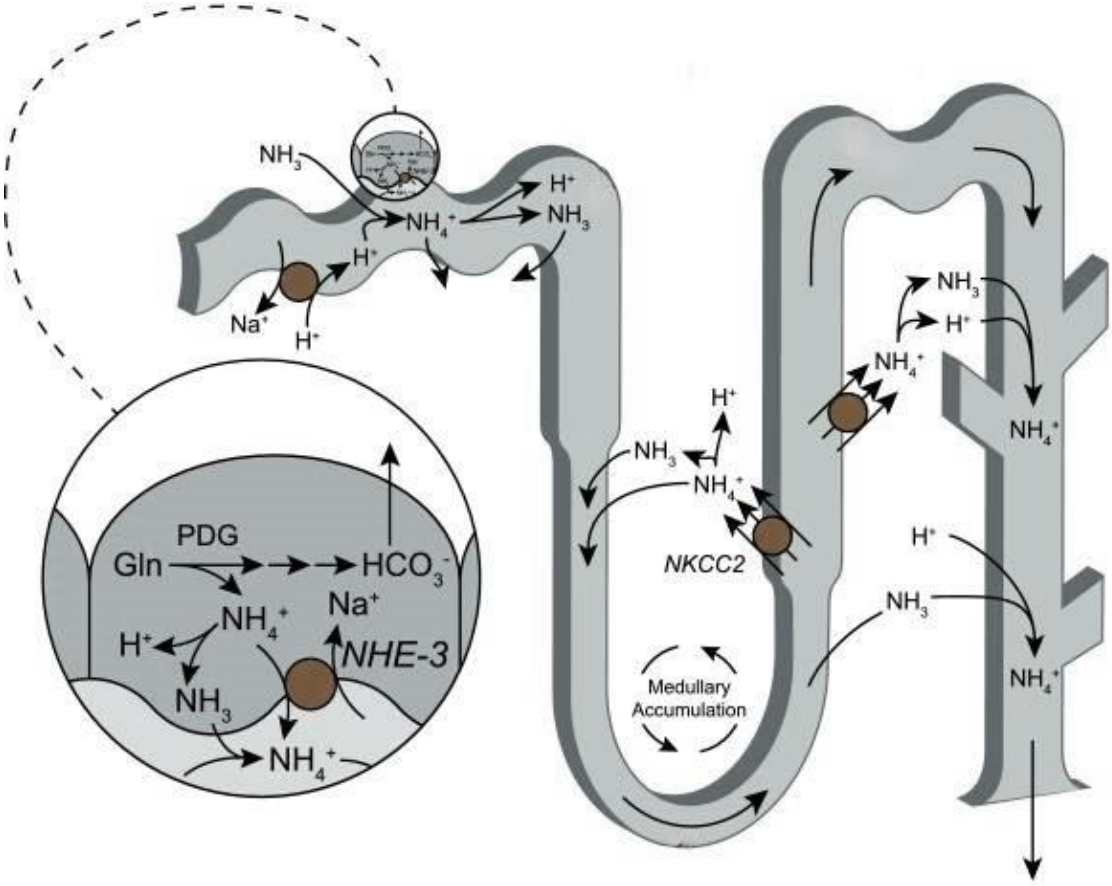

Figure 1.2 Renal amino acid and ammonia metabolism. The proximal tubule produces ammonia, as NH_4^+, through glutamine (Gln) metabolism by phosphate-dependent glutaminase (PDG). NH_4^+ is then secreted preferentially into the luminal fluid, primarily by Na^+/H^+ exchanger (NHE-3), and, in addition, there is a component of NH_3 secretion. Ammonia is reabsorbed by the thick ascending limb through a process primarily involving Na^+-K^+-$2Cl^-$ cotransporter (NKCC2)-mediated NH_4^+ reabsorption, resulting in ammonia delivery to the distal nephron. The remaining urinary ammonia is secreted in the collecting duct through parallel NH_3 and H^+ transport. Figure adapted and modified from Weiner and Verlander, 2013.

1.2 History of Ammonium Transporter Family

1.2.1 The First Evidence for Ammonium Transport Systems

The existence of active ammonia/ammonium (NH_3/NH_4^+) transport systems were first reported in 70's, while investigating the role of amino acid transport in the nitrogen starvation response in the fungus *Penicillium chrysogenum* (Benko, Wood and Segel, 1969, Hackette *et al.*, 1970). The study demonstrated that presence of ammonium inhibited a key, non-specific amino acid permease suggesting the existence of a specific system for ammonium transport (Benko, Wood and Segel, 1969). A later study led by Hackett *et al.,* measured the uptake of an analogue of ammonium: ^{14}C labelled methylammonium (MeA) in *P. chrysogenum,* and confirmed the presence of a highly specific membrane transport system for NH_4^+. Though, it was not until 1994 when the cloning of two genes, one from *Saccharomyces cerevisiae* and one from *Arabidopsis thaliana*, led to the recognition of the first two members of the ammonium transporter family of proteins. Subsequently, the plant protein was named AMT, for AMmonium Transporter, and the fungal protein was named MEP, for MEthylammonium Permease. Soon, the first prokaryotic Amt gene was sequenced and characterised in *Corynebacterium glutamicum* (Siewe *et al.*, 1996) and the Amt/Mep family members were identified in other organisms including *Escherichia coli* (van Heeswijk *et al.*, 1996), *Archaeglobus fulgidus* (Klenk *et al.*, 1997), and *Candidia albicans* (Biswas and Morschhäuser, 2005)

1.2.2 Identification of Mammalian Ammonium Transporter Genes

In 1997, Marini *et al.* reported that the human red blood cell (RBC) Rh-associated glycoprotein (RhAG) was a distant relative of the Amt/Mep family (Marini *et al.*, 1997b). Based on a sequence similarity of 20-25%, between RhAG and existing Amt/Mep family members, Rhesus (Rh) protein was identified as potential mammalian ammonium transporter. (Marini *et al.*, 1997b; Matassi *et al.*, 1999). However, RhAG are only expressed in RBCs, thus could not participate in ammonium transport in organs accountable for ammonium metabolism and excretion, such as the liver and kidney.

A few years later, Liu *et al.,* characterized a pair of Rh homologues (RhBG and RhCG) present in human and mouse nonerythroid tissues. Both RhBG and RhCG were localised in organs involved in ammonia metabolism including the liver and kidneys as well as the central nervous system, testes, and intestines (Liu *et al.*, 2000; Liu *et al.*, 2001). More specifically, RhBG and RhCG are expressed on epithelium of the kidney cells involved in ammonium secretion including connecting tubules and collecting ducts. Interestingly, both proteins are co-expressed in the same cell types but with opposite polarity: RhBG is localized at the basolateral domain, while RhCG at the apical domain of the plasma membrane (Eladari *et al.*, 2002; Quentin *et al.*, 2003). These findings further supported the notion that Rh proteins might be the long-sought mammalian ammonium transporter proteins.

Hard evidence of this hypothesis was presented by Marini *et al.*, when she demonstrated that human RhAG and RhCG (previously known as RhGK for kidney) proteins were able to sufficiently complement transport activity of a mutant *Saccharomyces cerevisiae* strain deprived of three endogenous *Mep* ammonium transporters (triple-Δ*mep*) (Marini *et al.*, 2000a).

1.2.2.1 Identification of Rh Proteins in Lower Organisms

Despite being prevalent in vertebrates, Rh homologues were later identified in many lower organisms including green alga *Chlamydomonas reinhardtii*, the worm *Caenorhabditis elegans* (Kitano and Saitou, 2000; Huang and Peng, 2005). Interestingly, Rh and Amt genes were found together in organisms as diverse as unicellular eukaryotic microbes (e.g., green alga, slime mould, and

water moulds) and invertebrate animals (e.g., nematodes, arthropods, echinoderms, and ascidians) (Huang and Peng, 2005). Rh proteins were also found to replace AMT proteins altogether like in the nitrifying bacterium *N. europaea* (Huang and Peng, 2005). Identifying *rh1* gene in the genome of *N. europaea* genome was the first evidence to argue against passive ammonium uptake in *N. europaea,* as suggested before (Chain *et al.*, 2003).

1.3 Phylogeny of Rh and Amt/Mep Protein Family

1.3.1 Rh and Amt/Mep Distribution

While the family of Rh and Amt/Mep proteins spans the entire tree of life, little is known about their evolutionary history. The first attempt to reconstruct the phylogeny of the Rh family, and study its relationship with Amt, was carried out in 2005. In this study, Huang and Peng analysed 111 Rh genes and 260 non-redundant Amt genes from Genbank files (C. H. Huang and Peng, 2005). Phylogenetical and bioinformatical analysis revealed evolutionary divergence between Rh and Amt proteins, segregating them into two distinct families (**Figure 1.3 A**) (Huang and Peng, 2005)**.** Another study demonstrated that although Mep proteins are phylogenetically closer to Amt, they still show distinct clustering (**Figure 1.3 B**) (Pitts *et al.*, 2014).

Huang and Peng also observed that all vertebrates possessed Rh but not Amt proteins, and whilst present in 41 organisms, ranging from humans to prokaryote *Nitrosomonas europaea,* Rh were absent in vascular plants and archaea. As mentioned already, some organisms including unicellular eukaryotic microorganisms and invertebrates, were found to possess both Rh and Amt proteins. This suggests that Amt and Rh have co-existed over a long evolutionary period (Huang and Liu, 2001; Huang and Peng, 2005).

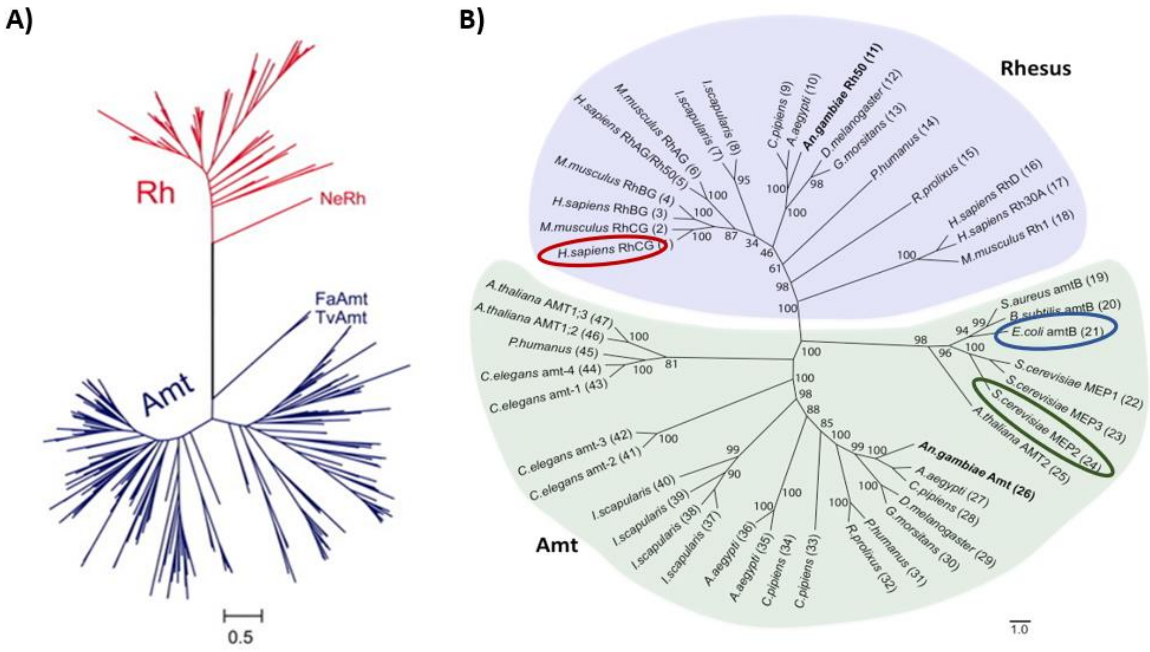

Figure 1.3 Rh and Amt are distantly related families. A) maximum likelihood tree of Amt (blue), Rh proteins (red), NeRh50 (bacterial Rhesus), FaAntB/TvAmtB (archaeal AMT) (Figure from Huang and Peng, 2005). B) Neighbour-joining tree comparing ammonium transporter proteins from prokaryotes and eukaryotes. Rhesus (purple region) and Amt (green region) proteins segregate into distinct families, with Mep grouping with Amt proteins. An example for each of Rh (red), Amt (blue), and Mep (green) have been highlighted. Figure adapted and modified form Pitts *et al*., 2014.

1.3.2 Rh Gene Clusters

More detailed examination of the Rh evolutionary pathway identified four distinct clusters; Rh30 (RhD and RhCE) and Rh50 (RhAG, RhBG and RHCG) in vertebrates, and two primitive clusters; Rhp1 in microorganisms and invertebrates, and Rph2 in a non-mammalian vertebrates (**Figure 1.4**) (Huang and Peng, 2005).

The Rh50 proteins can be further divided into erythroid (RhAG) and non-erythroid proteins (RhBG and RhCG), basing on their tissue specificity. Erythroid RhAG, and Rh30 appeared to share a common ancestor, different to the one shared by RhBG and RhCG (**Figure 1.4**). In addition, all Rh50 are transport competent, while Rh30 are not. It appears that the Rh30 cluster underwent faster evolution, suggesting it may have diverged for a red cell-specific functional modification at the same time losing their transporting abilities (Huang and Peng, 2005). In addition, Rh50 genes have a much longer evolutionary history than Rh30, which is likely derived by duplication from a Rh50-like ancestor.

The Rhp2 cluster appeared ancient, due to its genetic stability and for being expressed the gut, which is the oldest organ. Out of all Rh genes, Rhp2 is most closely linked to the bacterial Rhesus protein from *Nitrosomonas europaea* (*Ne*Rh50), the lowest in species order, and to Rhp1 genes (**Figure 1.4**). In contrast, Rhp1 is the most diverse cluster found in organisms expressing both the Rh and Amt proteins. Species of this group have up to 3 Rh genes, thought to have risen from gene duplication events (**Figure 1.4**) (Huang and Peng, 2005).

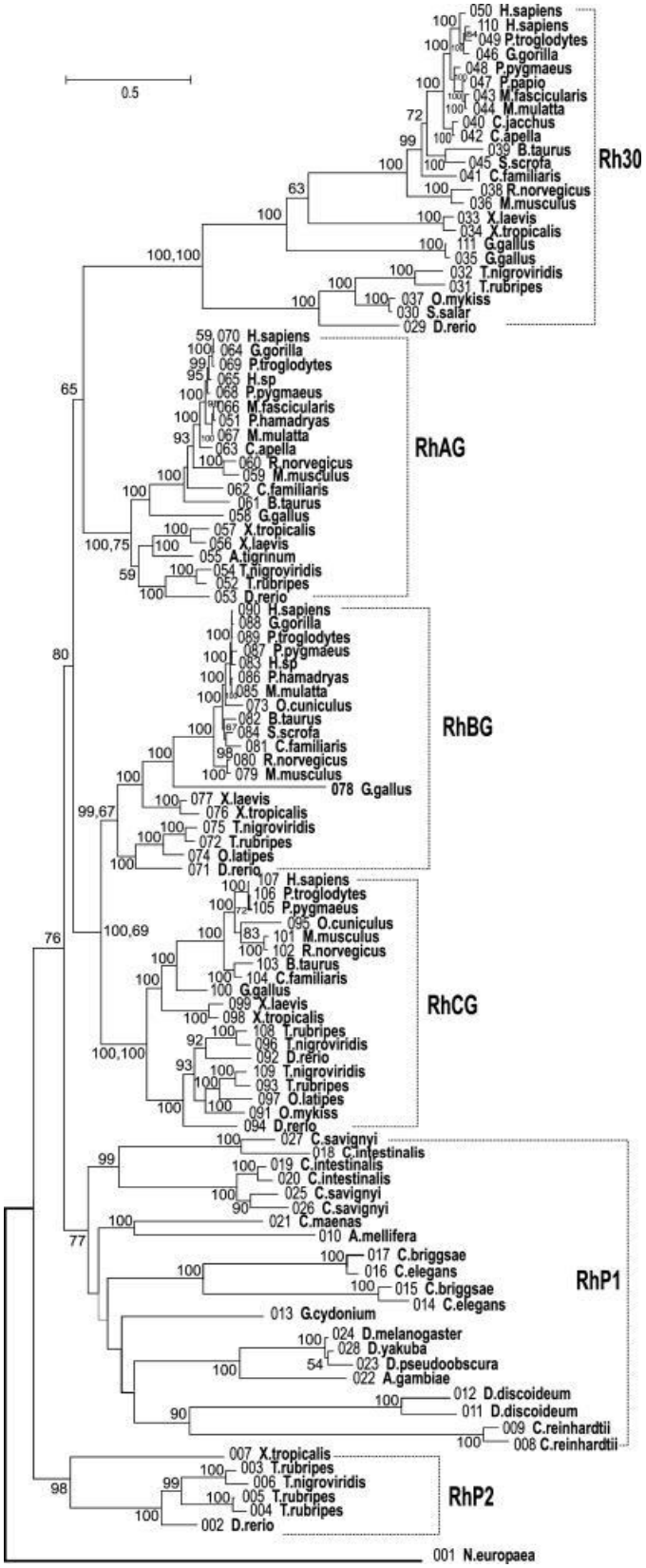

Figure 1.4 Rh family gene tree. The binary tree of 111 Rh genes. Four increasingly heated. *N. europaea* forms an outgroup, because is at the base of the family and is the lowest in species order. Scale bar: 0.5 substitutions per nucleotide. (Figure adapted from Huang and Peng 2005.)

1.3.3 Rh Gene Evolution

While still not clear, the evolutionary history of Rh and Amt/Mep family appears to be filled with expansion, contraction, gene loss and horizontal gene transfer (HGT). It was proposed that *Amt* genes were vertically transferred from parent to offspring, while *Mep* were horizontally transferred from a different species (McDonald, Dietrich and Lutzoni, 2012; McDonald and Ward, 2016). For this reason, McDonald *et al.* argued existence of only two clades namely Amt and Rh, excluding Mep as a true clade.

The Rh family, on the other hand, was believed to have a common ancestor of prokaryotic origins due to the presence of Rh homologs in bacteria (Huang and Peng, 2005). Two independent studies suggested that *N. europaea* acquired the Rh50 gene by HGT and was regarded as a case of non-orthologous gene displacement, due to the lack of AMT genes in the *N. europaea* genome (Cherif-Zahar *et al.*, 2007; Matassi, 2017). Nevertheless, although duplications of genes occurred in many species ranging from unicellular eukaryotes to sea squirts, no distinct clusters were formed in these taxonomic groups (**Figure 1.4**) (Huang and Peng, 2005). In addition, Huang and Peng concluded that the paralogous clusters appeared only after vertebrate speciation (**Figure 1.4**) (Huang and Peng, 2005), raising the possibility that mammalian Rh have acquired a distinct functional role not only from Amt/Mep but also from prokaryotic Rh.

The long history of Rh and Amt/Mep evolution poses a challenging question regarding their biological function: why would two proteins, Rh and Amt, coexist in so many organisms to fulfil the same function; and what is the selective advantage of possessing one over the other? Whilst these proteins are undoubtedly ubiquitous, the universality of their function and mechanism must be elucidated to answer these questions.

1.4 Biological Role and Medical Implications of Rh and Amt/Mep Family

1.4.1 Amt Protein

Amt proteins are not limited to scavenging ammonium from the external environment. They engage in diverse physiological roles, and their activities are modulated not only at the transcriptional level, but also at the protein level. One of many examples is the ammonium transporter AmtB, which plays a central role in tightly regulated nitrogen metabolism in *Escherichia coli* (Coutts *et al.*, 2002). Another example is one of seven Amt/Mep/Rh orthologues, *Ks*Amt5, from planctomycete *Candida Kuenenia stuttgartiensis,* which was demonstrated to act as an ammonium sensor/transducer, due to an elongated cytoplasmic domain with significant homology to histidine kinases (**section 1.6.1.4**) (Pflüger *et al.*, 2018). In addition, Amt proteins not only scavenge ammonium from surroundings, but also mediate its transfer into host plant cytoplasm from symbiotic fungi (López-Pedrosa *et al.*, 2006; Behie and Bidochka, 2014).

1.4.2 Mep Protein

The three Mep isoforms from *Saccharomyces cerevisiae* underpin the precise control of ammonium uptake in the yeast. Interestingly, not all three Mep proteins are essential for yeast growth, presenting functional possibilities for their additional roles. Closer investigation of Mep1-3 revealed their different kinetic properties: the Mep2 protein displays the highest affinity for NH_4^+ (Km 1-2 µM), followed by Mep1 (Km 5-10 µM), and finally Mep3, which displays the lowest affinity (Km ~ 1.4-2.1 mM) (Marini *et al.*, 1997a). Just like Amt/Rh, Mep genes are subject to nitrogen control, however their expression levels are governed by different general nitrogen regulatory factors (Marini *et al.*, 1997a). In addition, Mep1 and Mep2 are not essential for just scavenging. They also retain ammonium, highlighting another physiological role of these transporters (Marini *et al.*, 1997a).

Aside from scavenging ammonium, Mep2 protein was found to act as sensor in filamentous development in some fungal species (Lorenz and Heitman,

1998). In search of environmental nutrients the *S. cerevisiae* undergo dimorphic transition from unipolar yeast to hyphal growth (Gimeno *et al.*, 1992). This dimorphic change is an essential process in the virulence of human pathogens such as *Candida albicans* and *Aspergillus fumigatus* (Lo *et al.*, 1997; Lee, Morrow and Fraser, 2013). In result, Mep2 was recognised as a transceptor, which senses and responds to nitrogen limitation by initiating downstream signalling pathways resulting in filamentation (Lorenz and Heitman, 1998; Boeckstaens, André and Marini, 2008; van den Berg *et al.*, 2016).

1.4.3 Rhesus Protein

While Amt/Mep proteins were demonstrated to facilitate only the import of the ammonium, the mammalian rhesus proteins were noted to facilitate both, uptake and excretion when expressed in yeast (Marini *et al.*, 2000a). This unique ability was revealed when expression of human RhAG and RhCG in triple-*mepΔ* yeast prevented toxicity induced by high methylammonium concentrations, revealing the role of Rh proteins in methylammonium excretion (Marini *et al.*, 2000a). Collectively, the biological role of Rh proteins was proposed to be distinct from the Amt/Mep proteins. They were pronounced to be responsible for detoxification in erythrocytes, maintaining pH balance, and reabsorption of ammonium through the renal tubule epithelial cells (Knepper *et al.*, 1991; Wright *et al.*, 2011). But what role do they play in lower organisms?

Over the last two decades, significant progress has been made in our understanding of the role of Rh protein in vertebrates. In fish, the role of Rh in NH_4^+ transport was first demonstrated by Nakada *et al* in 2007. The Rh protein from the gills of *Takifugu rubripes* was able to facilitate uptake of MeA when expressed in *Xenopus oocytes*, challenging the classic view of passive ammonia diffusion in the fish gill (Nakada *et al.*, 2007). Indeed, various species of amphibious fish were demonstrated to excrete ammonium via cutaneous Rh proteins, in the absence of water-flow over the gills, in order to avoid ammonia toxicity (Livingston *et al.*, 2018).

The role of Rh50 in development of eukaryotic organisms has also been reported. Knock-out (KO)/knock-down (KD) mutants were demonstrated to affect embryonic development of *Dictyostelium discoideum* amoeba (Singleton, Kirsten and Dinsmore, 2006) and the nematode *Caenorhabditis elegans* (Ji *et al.*, 2006). A study on *Aedes aegypti*, which mostly occupies sewage contaminated water, demonstrated that the larvae owe its resistance to lethal ammonia concentrations to Rh proteins. The larvae can efficiently excrete ammonium against a steep concentration gradient by upregulating expression of their rhesus protein within a "physiological triad" of organs (Durant and Donini, 2019). Rh protein was also found to be essential for development and function in the tunicate *Ciona intestinalis* larvae (Marino *et al.*, 2007).

A crucial role of Rh50 proteins was also noted in prokaryotes. When expressed in *S. cerevisiae*, Rh50 from *N. europaea* mediated bidirectional methylammonium (MeA) transport, as seen previously with the human Rhesus proteins (Marini *et al.*, 2000a; Weidinger *et al.*, 2007; Cherif-Zahar *et al.*, 2007). Weidinger *et al* also demonstrated that MeA uptake rate relies on transcription level of *rh50* in *N. europaea* (Weidinger *et al.*, 2007). Another study compared MeA influx of wild-type and KO *N. europaea* strains, showing decreased uptake rate in mutant cells (Cherif-Zahar *et al.*, 2007). These experiments provided evidence for the Rh50 involvement in ammonium transport in *N. europaea.*

1.4.3.1 Human Rh Protein: Malfunction and Associated Diseases

Interest in the human Rh protein family arose from the seminal discovery of Rh factors and their involvement in immunogenic characteristics, and haemolytic disease in the foetus and new born (Landsteiner and Wiener, 1941). Today they are recognised as ammonium transporters (Marini *et al.*, 2000a), essential in detoxification of erythrocytes, maintaining pH balance, and reabsorption of ammonium through the renal tubule epithelial cells (Knepper *et al.*, 1991; Wright *et al.*, 2011). Consequently, mutations in Rh are associated with numerous pathologies.

Genetic mutations of RhAG were found to cause Rh deficiency syndrome ($Rh_{null\ or}$ Rh_{nod}) characterised by the lack of Rh antigens on RBCs (Schmidt and Vos, 1967; Huang *et al.*, 1998), or dominant Overhydrated Stomatocytosis (OHSt), a rare hereditary haemolytic anaemia, characterised by uncontrolled entry of monovalent cations (K^+ and Na^+) into erythrocytes (Bruce *et al.*, 2009;Stewart *et al.*, 2011). In addition, a human RhAG was also linked to a subtype of migraine (Norberg *et al.*, 2006).

The physiological importance of non-erythroid RhBG and RhCG proteins, also became more evident in NH_3/NH_4^+ handling. Studies on *Rhbg* knockout (KO) mice demonstrated lowered urinary ammonium excretion, while HCl-induced acidosis increased Rhbg protein expression in healthy mice (Bishop *et al.*, 2010). Studies on *Rhcg* KO mice demonstrated impaired urinary NH_4^+ excretion when exposed to increased acid loads. It was noted that both apical permeability to NH_3 and transepithelial NH_3/NH_4^+ transport, were reduced (Biver *et al.*, 2008). Mutations in Rhcg were found to disrupt acid-base homeostasis, which has been linked to male infertility and distal Renal Tubular Acidosis (dRTA) (Biver *et al.*, 2008), which in human can lead to development of kidney stones, and, in extreme cases, renal failure (Laing *et al.*, 2005). In addition, human RhCG has been identified as a candidate gene for early-onset major depressive disorder (Verma *et al.*, 2008). Finally, the *rhbc* and *rhcg* genes were proposed to act as potential tumour suppressors by inducing sharp down-regulation in human oesophageal squamous epithelial cancers (Chen *et al.*, 2002) and mouse brain tumours (Johansson *et al.*, 2004).

Despite their clear fundamental and biomedical importance knowledge of the actual mechanism of Rh in mediating ammonium transport and more detailed function is lacking. It was expected that crystal structures would aid in establishing the role the Rh proteins and open new avenues of research aiming to tackle multiple diseases linked with Rh malfunction.

1.5 Structural Characterisation of Ammonium Transporters

1.5.1 Topology and Secondary Structure

The topology of Amt/Mep/Rh proteins was determined *in-vivo* using the ammonium transporter AmtB from *E. coli* as a model system. Two reporter proteins, PhoA and LacZ, were fused to the C-terminus of each of the 12, previously predicted, transmembrane (TM) helices (van Heeswijk *et al.*, 1996; Thomas, Mullins and Merrick, 2000). The PhoA- and LacZ- insertions are active in the periplasm and the cytoplasm, respectively enabling determination of the orientation of the helix. The results revealed 11 TM helices, suggesting that the 1st theoretical helix was a signal peptide that would be cleaved off following folding or insertion into the membrane (**Figure 1.5 A**) (Thomas, Mullins and Merrick, 2000). Further studies demonstrated that the 11 TM helix model and general topology observed in AmtB is conserved across Amt/Mep proteins (**Figure 1.6**).

In contrast, both Rh50 and Rh30 proteins, have been shown to possess 12 TM helices with both the N-terminus and C-terminus located in the cytoplasm (**Figure 1.5 B**). For consistency the additional N-terminal helix relative to Amt/Mep, was termed M0 (**Figure 1.6**) (Eyers *et al.*, 1994; Lupo *et al.*, 2007; Gruswitz *et al.*, 2010).

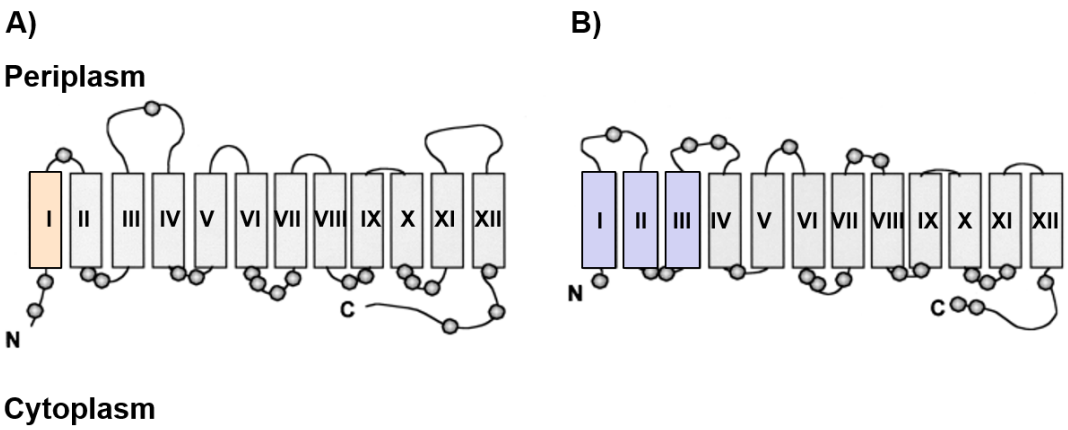

Figure 1.5 Membrane topology of the Amt/Mep and Rh family of ammonium transporters. A) Schematic model of *E. coli* AmtB protein with cleavable signal sequence in peach. B) Schematic model of the human Rh50 protein. Grey boxes represent helices whose topology is conserved across the Mep/Amt and Rh families, while lilac boxes represent helices that are not homologous. The balls represent positive charge in these protein sequences. Figure adapted and modified from Thomas, Mullins and Merrick, 2000.

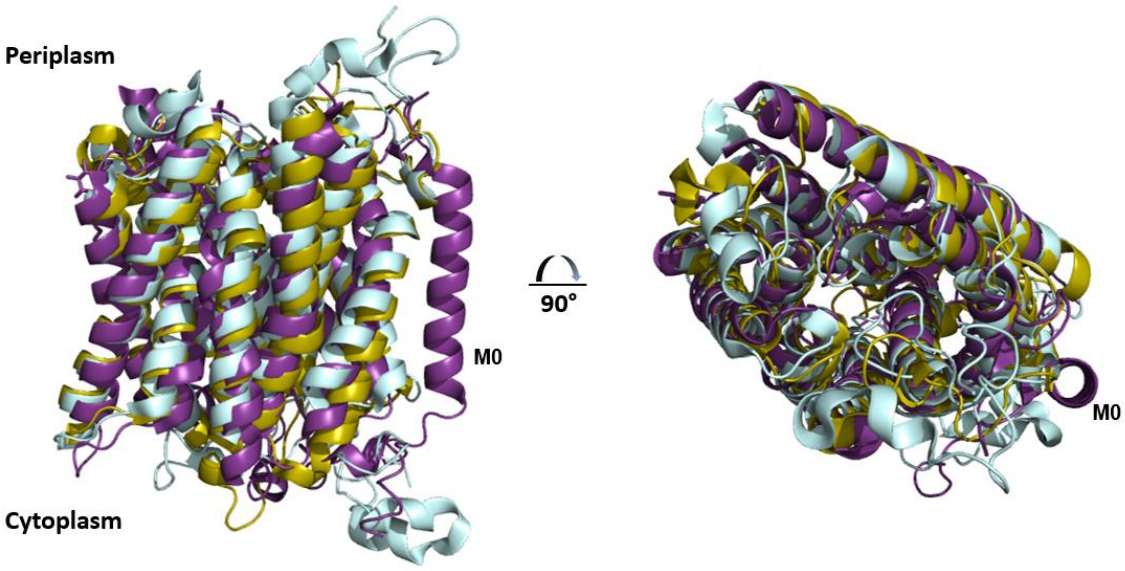

Figure 1.6 Structural Conservation of Amt/Mep/Rh protein. A monomer from *E. coli* AmtB (olive), *S. cerevisiae* Mep2 (cyan), and *H. sapiens* RhCG (purple), shown from sideview of proteins as inserted in the membrane (left), and with N-terminus at the top and C-terminus at the bottom (right). The additional helix is present in RhCG is denoted as M0. Crystal structures for AmtB, Mep2, and RhCG were obtained from PDB (1u7g, 5af1, and 3hd6 respectively) and aligned in pymol.

1.5.2 Tertiary and Quaternary Structure

The first evidence suggesting the oligomeric state of Amt/Mep/Rh proteins came from a study where expression of an inactive Mep1 inhibited the activity of Mep2 and Mep3 in *S. cerevisiae* (Marini *et al.*, 2000b). However, the first Amt/Mep protein to be purified was AmtB from *E. coli*. Analytical ultracentrifugation (AUC) and size exclusion chromatography (SEC) techniques revealed trimeric organisation of AmtB with a molecular mass of ~90 kDa (Blakey *et al.*, 2002). Soon afterwards, the first ordered 2D crystals of AmtB were obtained (Conroy *et al.,* 2004*)*. The authors suggested a pseudo-two-fold symmetry and a presence of potential translocation pathway in each monomer of the trimer (Conroy *et al.*, 2004). This was soon confirmed by the high-resolution crystal structures of AmtB enabling investigation of the mechanism of ammonium transport at the molecular level for the first time (Khademi *et al.*, 2004; Zheng *et al.*, 2004).

To date, high resolution crystal structures representing each member of the Amt/Mep/Rh family have been solved, including Amt from *Archaeoglobus fulgidus* and *K. stuttgartiensis* (Andrade et al., 2005; Pflüger et al., 2018)*,* Mep2 from *S. cerevisiae* and *Candida albicans* (van den Berg *et al.*, 2016), as well as rhesus proteins from *N. europaea* and human (Li *et al.*, 2007; Lupo *et al.*, 2007; Gruswitz *et al.*, 2010)

As the model for the ammonium transport presented in **Chapter 4** (**Section 4.1.1**) is based on *Ec*AmtB, particular emphasis will be placed on its structure, followed by a detailed analysis of Amt/Mep mechanism. Finally, structure of prokaryotic and mammalian Rh proteins as well as their mechanism will be discussed.

1.6 Amt/Mep Proteins

1.6.1 Crystal Structure of Amt/Mep Proteins

The crystal structure of *E. coli* ammonium transporter AmtB was published in 2004 and has since became the most intensely studied member of the Amt/Mep family, with more than 20 high-resolution structures, including numerous variants, deposited in the Protein Data Bank (PDB) (Khademi *et al.*, 2004; Zheng *et al.*, 2004; Javelle *et al.*, 2006; Javelle *et al.*, 2008). AmtB exists as a homotrimer, with each monomer composed of 11 transmembrane (TM) helices (**Figure 1.7 A and B**)**.** The fold of AmtB divides into two contiguous, right-handed, five-helix bundles (TM1–5 and TM6–10) forming a two-fold axis. A long C-terminal helix TM11, lies perpendicular to the membrane interface surrounding the lipid accessible portion of the monomer (Khademi *et al.*, 2004; Zheng *et al.*, 2004). The subunit interface was notably hydrophobic, owing it to hydrophobic side-chains from each TM1 forming a tight contact ~20Å into the membrane. The contact between neighbouring monomers occurs via interaction of TM1-3 of one monomer with the TM1, TM6-8 of another (Zheng *et al.*, 2004). Of the most significant for the mechanism was identification of a potential substrate translocation pathway located in the centre of each monomer. The pathway outlines four key features of mechanistic interest amely: the S1 binding site, the “Phe-gate”, the hydrophobic pore and cytoplasmic vestibule (**Figure 1.7 C**).

Topologies of bacterial *Af*Amt1 from *A. fulgidus* and *Ks*Amt5 from *K. stuttgartiensis* are similar to *Ec*AmtB. Both proteins follow pseudo-two-fold symmetry across the 11TM helices in the monomers with only the signal sequence missing (Khademi *et al.*, 2004; Andrade *et al.*, 2005; Pflüger *et al.*, 2018). Highly alike, with mean root square deviation of 0.7 Å, Mep 2 proteins from *S. cerevisiae* and from *C. albicans* also share the above features with prokaryotic Amt proteins (van den Berg *et al.*, 2016).

Most importantly, all crystals structures of Amt/Mep proteins reported the presence of the signature translocation pathway within each monomer. Each four structural features, composing the translocation pathway, will be discussed in context of Amt/Mep proteins in the following paragraphs.

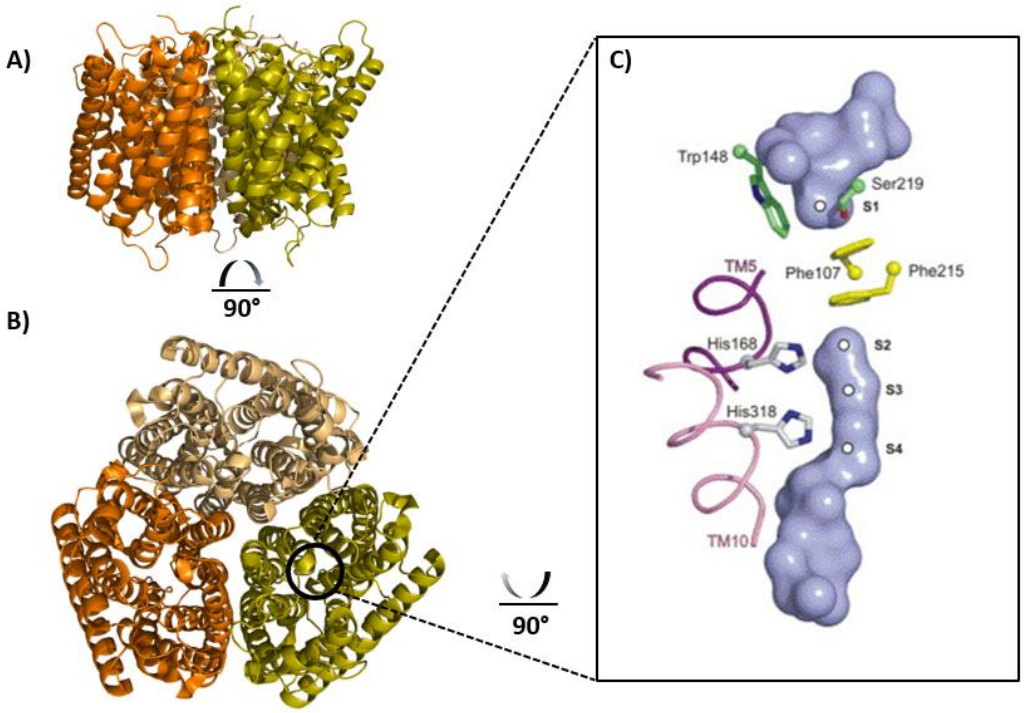

Figure 1.7 Structure of AmtB: A) View of the AmtB trimer from the side, and B) from the top, with each monomer coloured in olive, orange, or yellow. C) Expanded view of the pore region of a single monomer with the water-accessible volume represented in purple. Highly conserved residues are shown in ball-and- stick representation for the ammonium binding site (green), phenylalanine gate (yellow) and central pore (grey), where parts of the two transmembrane helices TM5 (His168) and TM10 (His318) are also shown. Figure C adapted from Javelle *et al.,* 2007.

1.6.1.1 S1 Binding Site

In AmtB a potential NH_4^+ binding site named S1 lies within a vestibule in the periplasmic face of the protein. The S1 site is formed by S219, W148 and F107 residues, where NH_4^+ could be potentially stabilised via the hydrogen bond with S219 and π-cation interactions with the phenyl rings of W148 and F107 (Khademi *et al.*, 2004; Zheng *et al.*, 2004). Based on free energy calculations the binding affinity of this site is in the µM range, favouring NH_4^+ and NH_3 over Na^+ or K^+ (Zheng *et al.*, 2004; Javelle *et al.*, 2007). Another potential acceptor is a highly conserved aspartic acid residue (D160 in AmtB) which resides close to S1 site (Thomas, Mullins and Merrick, 2000; Javelle *et al.*, 2004). Previous studies implied a mechanistically important role for D160, due to complete loss of transporting abilities of $AmtB^{D160A}$ (Javelle *et al.*, 2004). However, no density around D160 was observed in the presence of ammonium. In addition, the carboxyl functional group of the D160 is buried into the structure and not in contact with the lumen at the S1 site. Consequently, it was suggested to have a structural role only (Khademi *et al.*, 2004).

No major differences were noted in the S1 binding site of bacterial AMTs (Andrade *et al.*, 2005; Pflüger *et al.*, 2018). In contrast to bacterial ammonium transporters, the binding site is slightly wider in Mep2 proteins. This is the result of an additional 20-25 residues at N-terminus in Mep2 proteins, which enables contract with the Extra Cellular Loop 5 (ECL5) of the neighbouring monomer (van den Berg *et al.*, 2016).

The presence of a binding site in Amt/Mep proteins is consistent with the fact that the transporter is only expressed under ammonium-limited conditions, most probably in the µM range (Javelle *et al.*, 2006), thus ensuring high affinity for the substrate and efficient scavenging for ammonium (Wirén and Merrick, 2004).

1.6.1.2 The Phenylalanine Gate

The second key structural feature of the translocation pathway is the phenylalanine gate, also called “Phe-gate”. In AmtB, two stacked phenyl rings

of F107 and F215 block the access to the pore from the S1 site (Khademi *et al.*, 2004). Such arrangement was identical in all the AmtB crystal structures, but Khademi *et al* suggested that the rings would have to be dynamic to facilitate any conduction event (Khademi *et al.*, 2004) and Molecular Dynamic (MD) simulations studies supported this view (Lin, Cao and Mo, 2006; Nygaard *et al.*, 2006).

The Phe-gate is highly conserved in all of the Amt/Mep proteins (Andrade *et al.*, 2005; van den Berg *et al.*, 2016; Pflüger *et al.*, 2018). In agreement with Khademi and Zheng suggestion, higher flexibility in the sidechain of F204 of *Af*Amt1 was observed, suggesting movement during the translocation event (Andrade *et al.*, 2005).

1.6.1.3 Hydrophobic Pore

Below the Phe-gate lies a strongly hydrophobic pore that leads to the cytoplasm. In AmtB it is lined by two histidine residues, H168 and H318 forming the characteristic “twin-His” motif (Khademi *et al.*, 2004; Javelle *et al.*, 2006). In a series of experiments Khademi *et al* observed three electron densities (Am 2, 3, and 4) within the hydrophobic pore, but only in the presence of 25 mM $(NH_4)_2SO_4$, concluding they corresponded to ammonium molecules (Khademi *et al.*, 2004). This was questioned by Zheng *et al* as the authors observed those densities regardless of the presence or absence of ammonium. Since it is difficult to distinguish H_2O from NH_3 at a resolution of 1.35Å the authors suggested that the densities could also be water molecules (Zheng *et al.*, 2004). The experiment was repeated with methylammonium which is more easily distinguishable from water in the electron density. The electron density was only observed on the periplasmic side in the recognition pocket (Khademi *et al.*, 2004).

In contrast, no such electron densities were observed within the hydrophobic pore of *Af*Amt1 in either presence or absence of ammonium (Andrade *et al.*, 2005). While the hydrophobic pore is conserved in both bacterial and fungal proteins (Andrade *et al.*, 2005; van den Berg *et al.*, 2016; Pflüger *et al.*, 2018), the crystal structure of *Ks*Amt5 revealed three additional residues (F27, Y30,

F34) in the translocation pore. Their sidechains and a slight shift of the twin-His motif occludes the translocation pathway (Pflüger *et al.*, 2018). In addition, an *in vitro* electrophysiology method demonstrated that in *Ks*Amt5 ammonium binds but is not translocated across the membrane, suggesting a different or additional role of the protein (Pflüger *et al.*, 2018). Lastly, in a number of fungal ammonium transporter proteins the first histidine is replaced by a glutamic acid residue (Javelle *et al.*, 2006). It was argued that in its neutral form glutamic acid could occupy a space equivalent to histidine and make the same hydrogen bonding interactions, hence not affecting transporting abilities (Winkler, 2006; Javelle *et al.*, 2006). It is not known whether this substitution has provided a specific biochemical or physiological function.

Such a high conservation of the twin-His motif across the family indicates a functionally important role of this sturcture for the functionality of these transporter proteins (Zheng *et al.*, 2004; Javelle *et al.*, 2006).

1.6.1.4 A Cytoplasmic Vestibule

The translocation pathway terminates at a water accessible vestibule in the cytoplasmic face of the protein, lacking an apparent binding site. Remarkably, AmtB was crystallised in two different spatial groups, and the cytoplasmic vestibule was in different states in each crystal (Zheng *et al.*, 2004). This conformational change within the vestibule suggested a functionally significant role, which is still unknown.

Unlike *Ec*AmtB and *Af*Amt1, the C-terminal tail in *Ks*Amt5 is extended resembling the histidine kinase (HK) domain observed in two-component systems (Khademi *et al.*, 2004; Andrade *et al.*, 2005; Pflüger *et al.*, 2018). This modification was proposed to allow this specific ammonium transporter to be repurposed and to act as an ammonium sensor/transducer (Pflüger *et al.*, 2018). The cytoplasmic exit of the *Sc*Mep2 translocation channel also differs from other ammonium transporters. In Mep2, the cytoplasmic vestibule is at closed state; a feature not observed in prokaryotic AMTs. It is due to a hydrogen bond interaction between Y49 (located at the C-terminus of TM1) and H324, the second histidine of the twin-His motif. Lastly, the C-terminal

region does not interact with the main core of the protein, resulting in elongated Mep2 proteins (van den Berg *et al.*, 2016).

The high-resolution X-ray structures of ammonium transporters from different species were a breakthrough in the Amt/Mep/Rh research field. Slight structural differences can be observed in the extracellular loops and C-terminal tail of Amt/Mep proteins. Nevertheless, the central subunit of the pore is highly conserved as visualised in **Figure 1.8 C**. Evolutionary conservation scores, estimated using the ConSurf server (Ashkenazy *et al.*, 2016) indicate that the residues that line internal hydrophobic pathway show a large degree of conservation among homologous proteins. This suggests a possibility of a conserved mechanism across this enormous family.

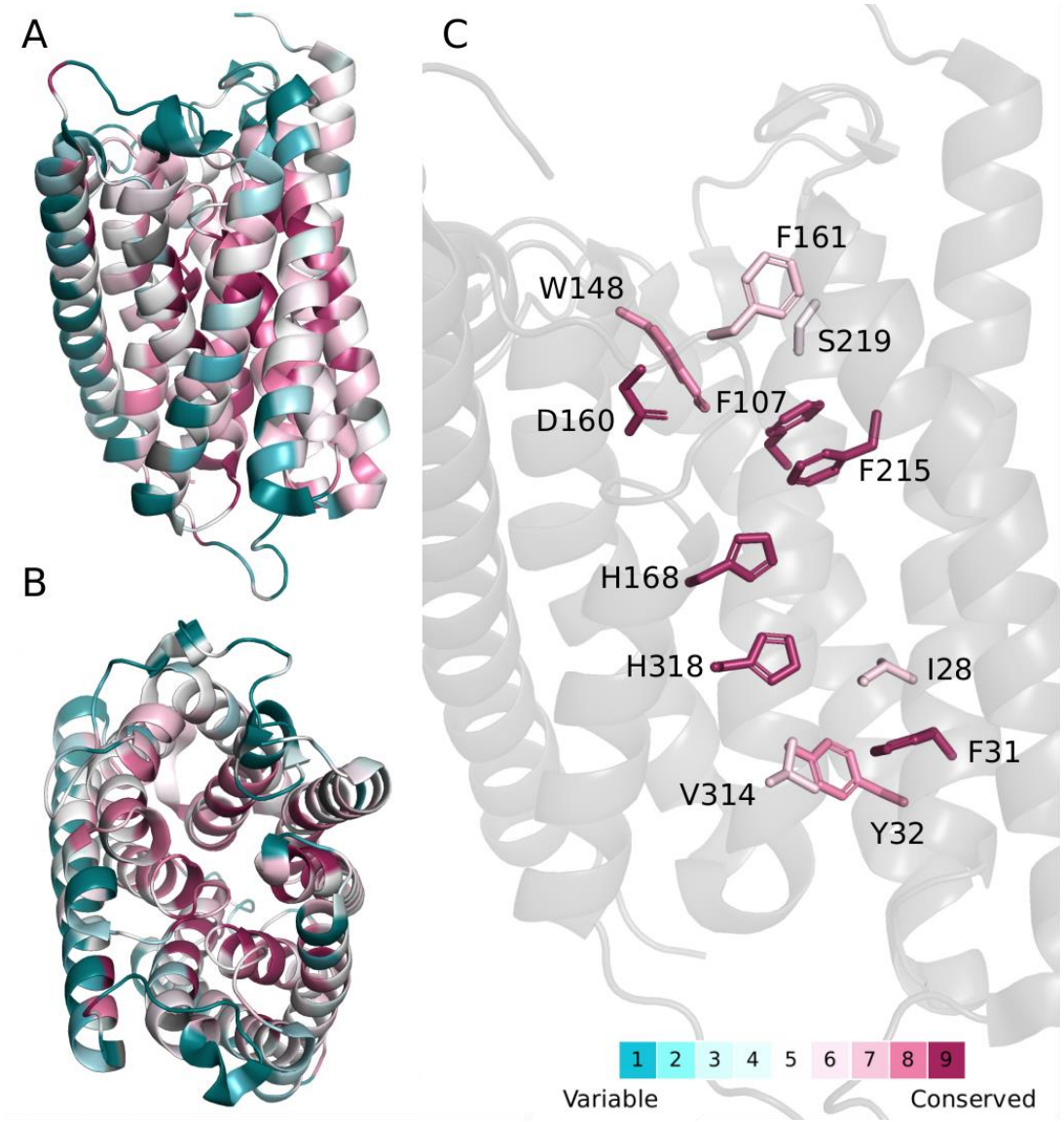

Figure 1.8 Evolutionary conservation of residues forming a translocation pathway in Amt/Mep proteins. Evolutionary conservation scores indicate that the residues that line internal hydrophobic pathway show a large degree of conservation among homologous proteins. Evolutionary conservation scores were estimated using the ConSurf server (Ashkenazy *et al.*, 2016). Briefly, a multiple sequence alignment (MSA) was built of homologues collected from the SWISS-PROT database. Homologues were identified by five iterations of HMMER, producing an MSA of 64 sequences. The evolutionary conservation scores are projected onto an AmtB monomer (PDB code: 1U7G), with some helices removed for clarity. (A) Side view. (B) Top view from periplasmic side. (C) Close-up view of key residues of the translocation pathway.

1.6.2 Functional Characterisation of Amt/Mep

The first functional studies, aiming to characterise the mechanism of Amt/Mep transporters, measured the uptake of an ammonium analogue [^{14}C]-methylammonium (MeA). These studies demonstrated that Amt/Mep proteins facilitate MeA uptake in *S. cerevisiae*, while ammonium competition assays demonstrated that they are strongly selective towards ammonium (Marini *et al.*, 1994). This approach also discriminated proteins by their substrate capacity and transport rate such as the Mep1-3 proteins in *S. cerevisiae* (Marini *et al.*, 1997). However, these studies did not dissect the precise mechanisms of Amt/Mep proteins. The lack of a robust *in vitro* assay that would allow for direct measurement of the true substrate NH_4^+ and the lack of structural information were the bottle neck for the mechanism elucidation.

As a result, all functional assays relying on different techniques did not lead to a clear consensus concerning the mechanism of the Amt/Mep/Rh transporter family. Instead, they proposed different mechanisms where some Amt/Mep function as NH_3 gas channels, and some as active transporters either as NH_4^+ uniporters, or NH_3/H^+ symporters (**Figure 1.9**). In this section, each of the proposed mechanisms for Amt/Mep ammonium transport will be reviewed. The transport mechanism for each Amt/Mep protein discussed was summarised and presented in **Table 1.1**.

1.6.2.1 NH_3 Gas Channel

For years, it has been generally accepted that ammonium uptake by organisms occur via passive diffusion (**Figure 1.9 A**). But ions such as NH_4^+ are not able to freely diffuse through the hydrophobic bilayer, thus early studies suggested that Amt and Mep proteins serve as electroneutral NH_3 channels (**Figure 1.9 B**). Radiolabelled [^{14}C]-methylammonium uptake assays provided the evidence that fungal Mep proteins (Soupene, Ramirez and Kustu, 2001) as well as the *S. typhimurium* AmtB mediate diffusion of the uncharged species NH_3 (Soupene *et al.*, 1998; Soupene, Lee and Kustu, 2002). This was concluded basing on their finding that accumulation was due to diffusion and

metabolic trapping of MeA by the glutamine synthetase in fungi and bacteria, respectively (Soupene, Lee and Kustu, 2002).

This transport mechanisms was also proposed for some AMTs found in plant species, such as AMT2 from *Arabidopsis thaliana*.(Neuhäuser, Dynowski and Ludewig, 2009). Functional analysis of *At*AMT2 in yeast and *Xenopus laevis* oocytes suggested that NH_4^+ is recruited by the binding site but uncharged NH_3 was mediated through (Neuhäuser, Dynowski and Ludewig, 2009). In addition, *in vivo* studies on *E. coli* AmtB showed that Amt/Mep might act as electroneutral channels (Javelle *et al.*, 2005).

These observations were supported by bacterial as well as fungal crystal structures, and presence of the hydrophobic pore (Khademi *et al.*, 2004; Andrade *et al.*, 2005; van den Berg *et al.*, 2016), leading to a conclusion that Amt/Mep proteins serve as channels mediating transport of uncharged NH_3 species.

1.6.2.2 Active Transport of NH_4^+

Facilitated passive transport is consistent with the hydrophobicity of the pore, but it is limited by the predominance of NH_4^+ at physiological pH. The pKa of the NH_4^+/NH_3 equilibrium is 9.25, thus at physiological pH 99% of ammonium is protonated (Bates and Pinching, 1950). In addition, while passive diffusion might be true for some ammonium transporters, it does not explain how most organisms, such as *E. coli*, are able to grow in an ammonium limited environment within a pH well below the pKa for the equilibrium NH_4^+/NH_3 (pKa 9.25). Moreover, Amt/Mep ammonium transporters are expressed under nitrogen limiting conditions, again arguing against the passive conductance. A hope for clarification arose when electrogenic transport has been noted for some of Amt/Mep proteins. However, the actual mechanism has not been settled to date. Some studies insisted on uniport of charged species NH_4^+, while others suggested symport of NH_3 and H^+.

1.6.2.2.1 NH_4^+ Uniport

In solution ammonium occurs in two forms: ionic NH_4^+ and molecular NH_3, implying the possibility of diverse transport mechanisms in Amt/Mep. A patch-clump electrophysiology assay showed that AMT1;1 form *L. esculentum* mediates an electrogenic ammonium influx (Ludewig, von Wirén and Frommer, 2002). Since the influx was pH independent the authors concluded that *Le*AMT1;1 function as an NH_4^+ uniporter (**Figure 1.9 C**). This theory was further supported by the finding that each [C^{14}]-methylammonium ion transported by *Le*AMT1;1 carries a positive elementary charge (Mayer, Dynowski and Ludewig, 2006). A similar NH_4^+ uniport mechanism has been suggested for *At*AMT1;1 (Loqué *et al.*, 2009) and *Os*AMT1;1 (Yang *et al.*, 2015).

While the experimental measurements suggest an NH_4^+ uniport mechanism, crystal structures strongly oppose this view. The presence of the hydrophobic pore creates a high energetic barrier and movement of ions would be extremely unfavourable (Khademi *et al.*, 2004). Moreover, mutagenesis studies on AmtB showed that variants lacking Phe-gate lost MeA transporting abilities, and did not become permeable to H^+ nor K^+ (Javelle *et al.*, 2008). Since, opening the accessibly to the pore does not change the selectivity of AmtB another mechanism should be considered.

1.6.2.2.2 NH_3/H^+ Symport

Similar to results from Mayer *el al*, were obtained when studying an ammonium transporter AMT1;1 from *Triticum aestivum* found in wheat. Inward currents were activated by NH_4^+ or methylammonium ions (MeA^+) measured by two-electrode voltage clamp and radio-labelled uptakes (Mayer, Dynowski and Ludewig, 2006; Søgaard *et al.*, 2009). The clear sensitivity to pH lead authors to conclude that NH_4^+ is perceived at the binding site but transported as NH_3 and H^+ via two separate pathways, and subsequently recombined in the cytoplasm (**Figure 1.9 D**) (Søgaard *et al.*, 2009).

Arabidopsis thaliana poses 6 AMTs protein organise in two AMT sub-families AMT1 and AMT2. While AMT2 family was proved to act as an electroneutral NH_3 transporters, the AMT1, has been demonstrated to facilitate electrogenic transport using yeast complementation and electrophysiology assay (Neuhäuser, Dynowski and Ludewig, 2009; Neuhäuser, Dynowski and Ludewig, 2014). In the net NH_4^+ transporter *At*AMT1;2 mutations led to a change in coupling of NH_3 and H^+ transport, supporting that *At*AMT1;2 functions as an NH_3/H^+ symporter (Neuhäuser and Ludewig, 2014). *E. coli* AmtB was also found electrogenic and similarly, the co-transport of NH_3/H^+ was proposed (Mirandela *et al.*, 2018). Indeed, evidence suggesting the importance of NH_4^+ deprotonation in ammonium transport has been suggested by Ariz *et al* (Ariz *et al.*, 2018). The authors used N^{15} isotope fractionations associated with pH dependent NH_4^+ deprotonation and determined the kinetic isotope effect linked to the protein transport, to elucidate the nature of transported species (NH_4^+ or NH_3/H^+).

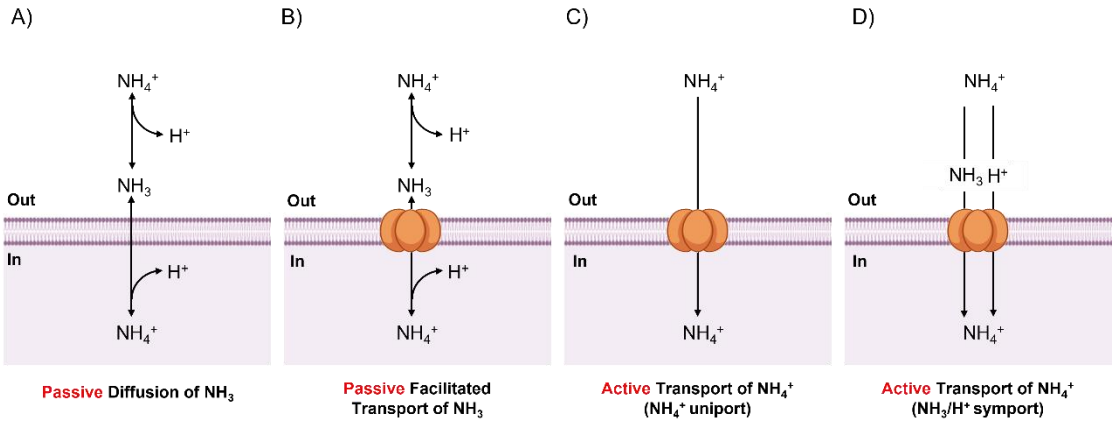

Figure 1.9 Four modes of ammonium transport. The homotrimer in the membrane represents the ammonium carrier. Four mechanisms of transport are shown. A) Transport via passive diffusion of NH_3, B) Passive facilitated transport of NH_3, C) Active transport of NH_4^+ (uniport), D) Active transport of NH_4^+ where NH_3 and H^+ follow two separate routes. (Figure adapted and modified from van Heeswijk, Westerhoff and Boogerd, 2013.

Table 1.1 Transport mechanism in Amt/Mep proteins

Protein	Mechanism	Supporting evidence	References
*Sc*Mep	NH_3 transport	(i) Diffusion trapping dependent on H^+ ATPase (ii) Growth defects of Mep mutant on low ammonium concentrations at acid pH	(Soupene, Ramirez and Kustu, 2001)
*St*AmtB	NH_3 transport	(i) Metabolic trapping dependent on glutamine synthetase (ii) Growth defects of Amt mutant on low ammonium concentrations at acid pH	(Soupene, Lee and Kustu, 2002)
*At*AMT2	NH_3 transport	(i) Electroneutral transport (ii) pH independent	(Neuhäuser, Dynowski and Ludewig, 2009)
*Le*AMT1;1	NH_4^+ uniport	(i) Electrogenic transport (ii) Highly negative membrane potential, and small the Km value, suggests cationic transport (iii) pH independent (iv) MeA ion associated by a positive elementary charge	(Ludewig, von Wirén and Frommer, 2002)
*At*AMT1;1	NH_4^+ uniport	(i) Electrogenic transport of ammonium (ii) pH independent	(Loqué *et al.*, 2009)
*At*AMT1;2	NH_3/H^+ symport	(i) Electrogenic transport of ammonium (ii) Mutation of Q67H and W145S results in uncoupling transport of NH_3 and H^+	(Neuhäuser and Ludewig, 2014)
*Ec*AmtB	NH_3/H^+ symport	(i) Electrogenic transport of ammonium (ii) pH independent (iii) Deprotonation mechanism	(Mirandela *et al.*, 2018;Ariz *et al.*, 2018)

1.6.3 Deprotonation Site and H^+ Acceptor

To prove NH_3/H^+ symport theory, many functional studies tried to find a potential deprotonation site and acceptor of H^+. Consequently, four (4) hypotheses regarding deprotonation were considered:

1. Deprotonation at the Binding Site S1 via Water Molecule

A deprotonation mechanism was first proposed by Khademi *et al*. The authors predicted that NH_4^+ would be deprotonated at the binding site (S1) of AmtB by a water molecule, followed by the proton release into periplasm (**Figure 1.10 A**) (Khademi *et al.*, 2004). Consistent with this view, Michaelis-Menten kinetics model suggested that recruitment and deprotonation of NH_4^+ at the S1 site was required for conduction (Winkler, 2006). This however, would result in electroneutral transport which did not agree with the results obtained by Mirandela *el al* who have demonstrated that AmtB mediates electrogenic ammonium transport (Mirandela *et al.*, 2018).

2. Deprotonation at the Binding site S1 via Serine Residue

Computational modelling on AmtB suggested that S219 residue might act as a proton acceptor to facilitate deprotonation (**Figure 1.10 B)** (Ishikita and Knapp, 2007). However, Javelle *et al* showed that $AmtB^{S219A}$ displayed enhanced MeA uptake in comparison to the WT, questioning the involvement of this residue in deprotonation (Javelle *et al.*, 2008). $AmtB^{S219A}$ variant was also tested in our lab using electrophysiology measurements, and while the conduction was lower in comparison to the WT, it was still able to translocate ammonium (Unpublished data, Dr. Williamson PhD thesis).

3. Deprotonation via Aspartic Acid Residue

Aspartic acid residue (D160 in *Ec*AmtB) near S1, is highly conserved across the entire family, and thus has become yet another candidate for a H^+ acceptor (**Figure 1.10 C**) (Javelle *et al.*, 2004). The molecular dynamic simulations

(MDS) predicted that D160 in AmtB would be available for interaction (Luzhkov *et al.*, 2006). Another MDS study concluded that it would be very likely for D160 to accept protons from ammonium ions (Lin, Cao and Mo, 2006). Indeed, the methylammonium uptake assays revealed that AmtB^{D160A} was inactive, while AmtB^{D160E} variant retained only ~70% of WT transporting activity (Javelle *et al.*, 2004). A study on *Sc*Mep2, further strengthen the functional importance of this residue (D182 in *Sc*Mep2) suggesting it is it was implicated in methylammonium binding affinity (Marini *et al.*, 2006).

4. Deprotonation via First Histidine Residue

The conservation of imidazole rings pair arrangement of twin-His motif has given rise to speculations that it may have a role in the deprotonation of ammonium ions before they cross the central part of the pore (Zheng *et al.*, 2004). Indeed, MDS showed a water wire composed of three water molecules, present in the pore of *Ec*AmtB (Lamoureux, Klein and Bernèche, 2007). Argued by mean force calculations authors suggested that first histidine (H168 in AmtB) could serve in deprotonation (**Figure 1.10 D**) (Lamoureux, Klein and Bernèche, 2007). However, in a number of fungal ammonium transporter proteins the first histidine is replaced by glutamic acid residue, what speaks against this hypothesis (Javelle *et al.*, 2006). Moreover, analysis of numerous variants of the twin-His motif of *Ec*AmtB and *Sc*Mep2 using growth experiments or MeA uptake, further challenged this view (Javelle *et al.*, 2006; Wang *et al.*, 2013). A single H to A variants of AmtB were capable of complementing growth, while failing to transport MeA. MDS clearly showed that a single histidine variants (H168A or H318A) of AmtB allows hydrophobic MeA to bind with higher affinity than ammonia around the mutated sites, preventing its conduction (Wang *et al.*, 2013). Therefore, this work not only proved that first histidine is not involved in deprotonation in AmtB, but also emphasised that MeA is not a suitable analogue of ammonium (Wang *et al.*, 2013).

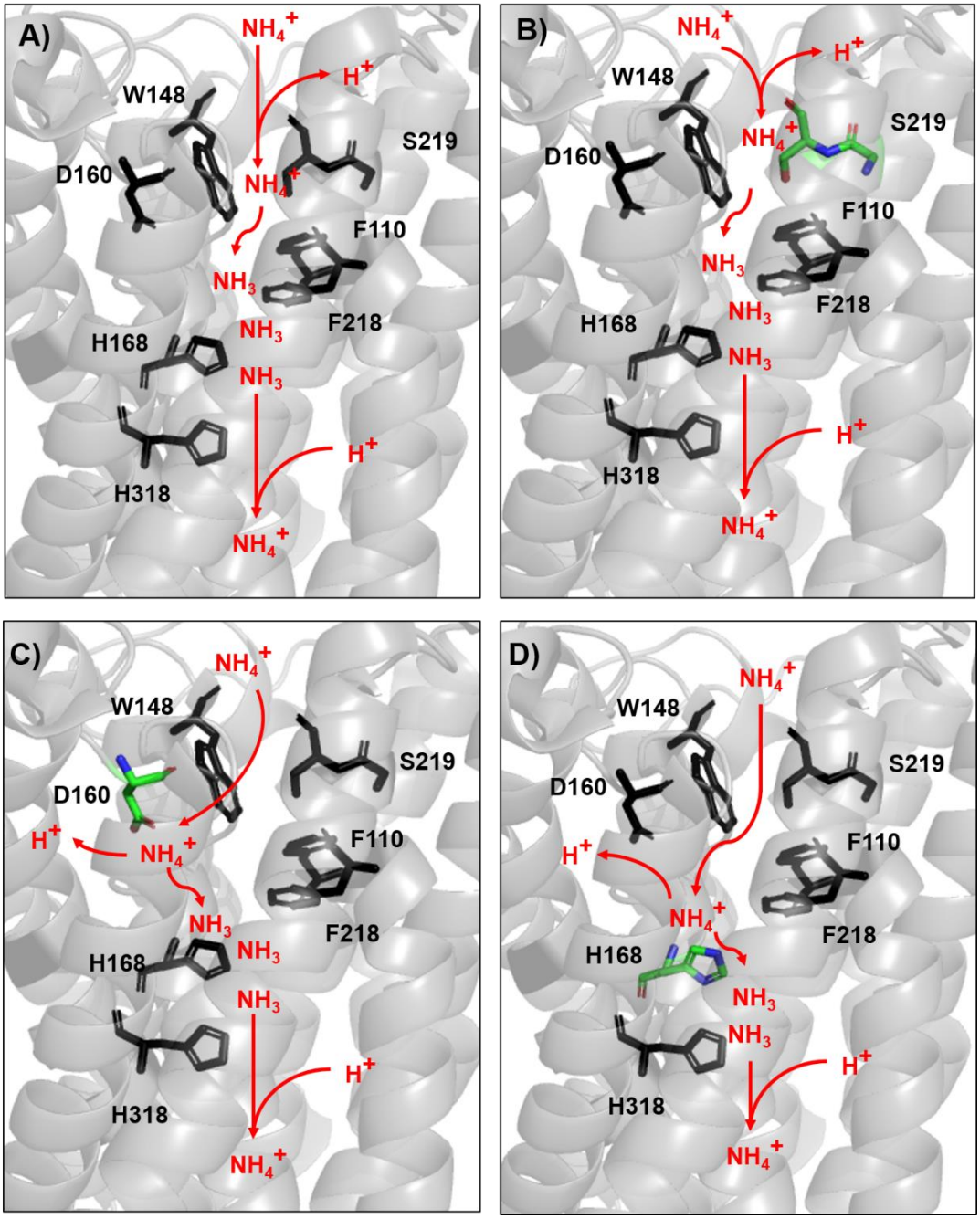

Figure 1.10 Proposed deprotonation mechanisms of NH_4^+ in *Ec*AmtB. Deprotonation *via:* A) water molecule, B) Serine residue, C) Aspartic acid residue, D) Histidine residue.

The deprotonation itself does not explain the phenomenon of electrogenic transport though. For electrogenic transport the proton must somehow be translocated through the hydrophobic pore (Khademi *et al.*, 2004). Consequently, if NH_4^+ undergo deprotonation, there must be a separate pathway for H^+ conduction into the cytoplasm. Remarkable observations were made via MDS, which revealed a chain of water molecules forming at the twin-His motif, parallel to the central pore in *Ec*AmtB (Baday *et al.*, 2013). Such a chain could function as a water wire, creating a potential route for H^+ transport. In addition, *Ec*AmtB discriminates against ions of similar ionic radii and charge to NH_4^+, such as K^+ and Na^+, possibly because these ions cannot be deprotonated (Javelle *et al.*, 2008). While this theory seems very plausible, the presence of water wires predicted by MDS must be verified experimentally.

1.7 Rhesus protein

1.7.1 Crystal Structure of Rh Proteins

In 2007, the crystal structure of the first rhesus protein (Rh50) was resolved from *N. europaea* by two independent groups (Lupo *et al.*, 2007; Li *et al.*, 2007). This was a breakthrough moment for rhesus protein research, enabling the comparison of Rh to the pre-established structures of bacterial AMTs, such as *Ec*AmtB or *Af*Amt1 as well as more precise modelling of human Rh proteins (Khademi *et al.*, 2004; Andrade *et al.*, 2005). Soon afterwards the crystal structure of mammalian RhCG was resolved by Gruswitz *et al* (Gruswitz *et al.*, 2010).

It was demonstrated that Rh is not a tetramer, as previously suggested (Eyers *et al.*, 1994). Instead, both bacterial Rh50 and RhCG retain trimeric organisation and the pseudo-two-fold symmetry between TMH1-5 and TMH6-10 observed in AMTs. Consistent with previous prediction, human Rh features 12th N-terminal TMH, called TM0, localised at the subunit interface of the trimer (**Figure 1.6**) (Eyers *et al.*, 1994; Gruswitz *et al.*, 2010). TM0 and TMH11 are linked by loops to the 10-helix core, breaking the two-fold symmetry. These loops varies in length and sequence in different Rh isoforms (Gruswitz *et al.*, 2010). In contrast, the crystal structure of Rh50 revealed only 11 TMH. The authors hypothesised that the Rh50 N-terminal end TMH0 was recognised as a signal peptide and removed when heterogeneously expressed in *E. coli* (Lupo *et al.*, 2007). But whether it is so processed in the native host *N. europaea* remains unclear (Cherif-Zahar *et al.*, 2007; Weidinger *et al.*, 2007).

These structures demonstrated that both, bacterial and human Rh proteins adhered to a trimeric organisation and confirmed ubiquity of this conformation across the Amt/Mep/Rh superfamily. More importantly, both structures revealed the presence of the previously mentioned translocation pathway within each of the monomers (**Figure 1.11**). My primary interest is to discuss the structural differences that discriminate Amt from Rh proteins in functionally critical regions of the translocation pathway.

1.7.2 An Extracellular Vestibule

The first striking difference between Rh50 and AMTs is the lack of the ammonium binding site S1. Out of the F107, W148, S219 residues, forming the binding site of *Ec*AmtB, only the F residue is conserved in *Ne*Rh50 (Khademi *et al.*, 2004; Lupo *et al.*, 2007). In addition, much shorter loops between transmembrane helices M2 and M3 and helices M10 and M11 were observed in *Ne*Rh50. This makes the periplasmic surface of *Ne*Rh50 smaller in contrast to those seen in other AMT proteins (Li *et al.*, 2007). Likewise, no S1 binding site was observed in the structure of human RhCG (Li *et al.*, 2007; Lupo *et al.*, 2007; Gruswitz *et al.*, 2010). However, at the bottom of the periplasmic vestibule, A144 of AmtB is replaced by a conserved residue E146 in Rh50 and E166 in RhCG (**Figure 1.11 A)**. This residues was proposed to present a prime candidate for a charged substrate recruitment site (Hoyhtya, 2020). In addition to acidic E166 residue at the periplasmic site of RhCG, the residues D218, D278 and E329 at the cytoplasmic site (**Figure 1.11 B** labelled with *), were proposed to create a recruitment site for NH_4^+ in human protein (Gruswitz *et al.*, 2010).

Notably, aspartic acid residue (D160 in AmtB) is conserved in both prokaryotic and human Rh proteins (**Figure 1.11** D162/D177) (Javelle *et al.*, 2004; Lupo *et al.*, 2007; Gruswitz *et al.*, 2010). The functional studies revealed that mutation of this residue in $AmtB^{D160A}$, $RhCG^{D177N}$ and $RhAG^{D167N}$ resulted in loss of transport of MeA (Javelle *et al.*, 2004; Marini *et al.*, 2006). These observations strongly suggest that aspartic acid residue not only has a key structural role but might also be directly involved in transport of ammonium.

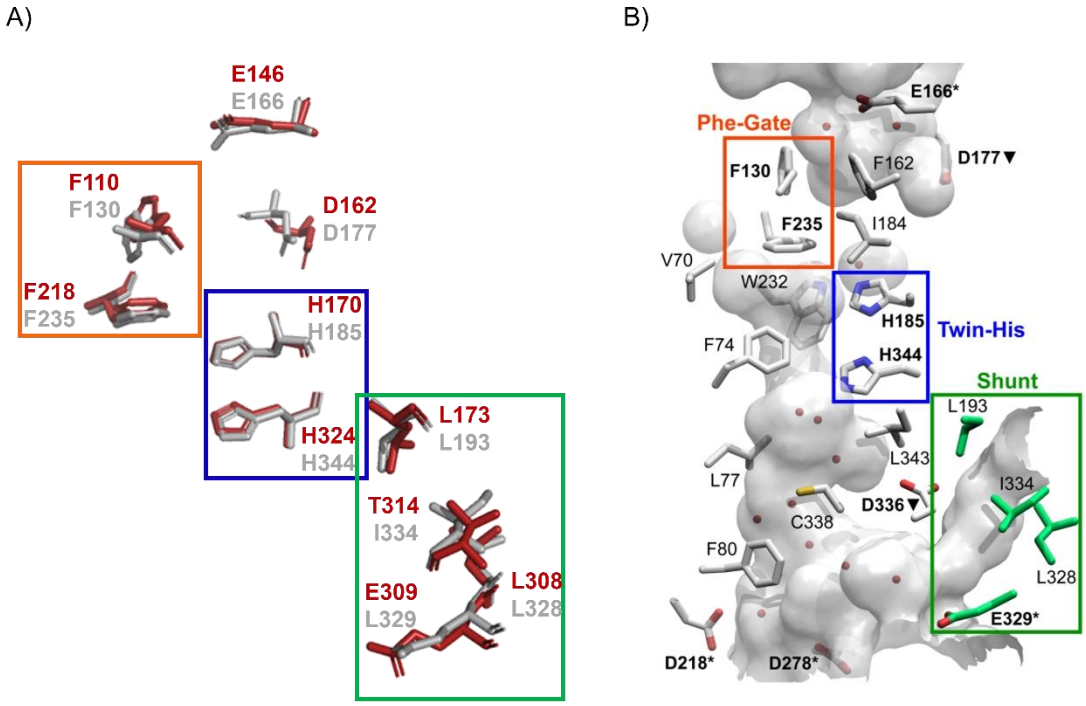

Figure 1.11 Translocation pathway of the Rh50. A) Residues from Rh50 from *Nitrosomonas europaea* (red) overlayed with residues from human RhCG (grey). B) Rh50 from human RhCG protein. Conserved segments are highlighted in red, blue, and green for Phe-gate, twin-His motif and Shunt, respectively. Residues denoted by an asterisk represents the potential binding site for ammonium (Figure B adapted from Grustitz *et al.*, 2010)

1.7.3 A Phenylalanine Gate

The phenylalanine gate is conserved, but the position of phe-rings is slightly different in Rh50 in comparison to that seen in AmtB (**Figure 1.12 B**). In *Ne*Rh50, first phenylalanine (F110) adopts an perpendicular orientation, permitting a water molecule to be 2 Å deeper along the channel entry path when compared to AmtB (Lupo *et al.*, 2007). For this reason it was proposed that the second phenylalanine (F218) in Rh50 might serve as a potential steric barrier (Li *et al.*, 2007).

The Phe-gate (F130/F235) in RhCG retains a similar positioning to that one seen in Rh50, where outer phenylalanine (F130) does not obstruct the RhCG pore (**Figure 1.13 B**). Interestingly, mutational studies demonstrated that F235V substitution in RhCG reduced NH_3 transport (Zidi-Yahiaoui *et al.*, 2006), suggesting that the inner phenyl ring could be critical in the transport mechanism. In addition, corresponding residue in AmtB was proved to be essential for its activity (Javelle *et al.*, 2008). These observations corroborate with the suggestion that F218 could serve as a potential steric barrier in Rh50 (Li *et al.*, 2007).

1.7.4 Twin-Histidine Motif

As previously discussed, the twin-His motif is conserved and protrudes into the centre of the hydrophobic pore (**Figure 1.13 C)**. In Rh50, H170 and H324, adopt a coplanar orientation which may stabilize an H^+ ion between them. However, $N\varepsilon_2$ atoms of both histidine residues form hydrogen bonds to neighbouring water molecules, while in AmtB only the second histidine was seen to form hydrogen-bonding partner (Li *et al.*, 2007). Additionally, residual electron density peaks observed in in the lumen AmtB (**section 1.6.1.3**) corresponding to ammonia or water molecules, were not identified in *Ne*Rh50 (Lupo *et al.*, 2007). Lastly, the opening above the second histidine in *Ne*Rh50 is occupied by two water molecules, whereas in AmtB this space is occupied by T273 residue which structurally aligns with glycine residue which is highly conserved in Rh proteins. This was proposed to create a larger pore entrance in the *Ne*Rh50 (Lupo *et al.*, 2007).

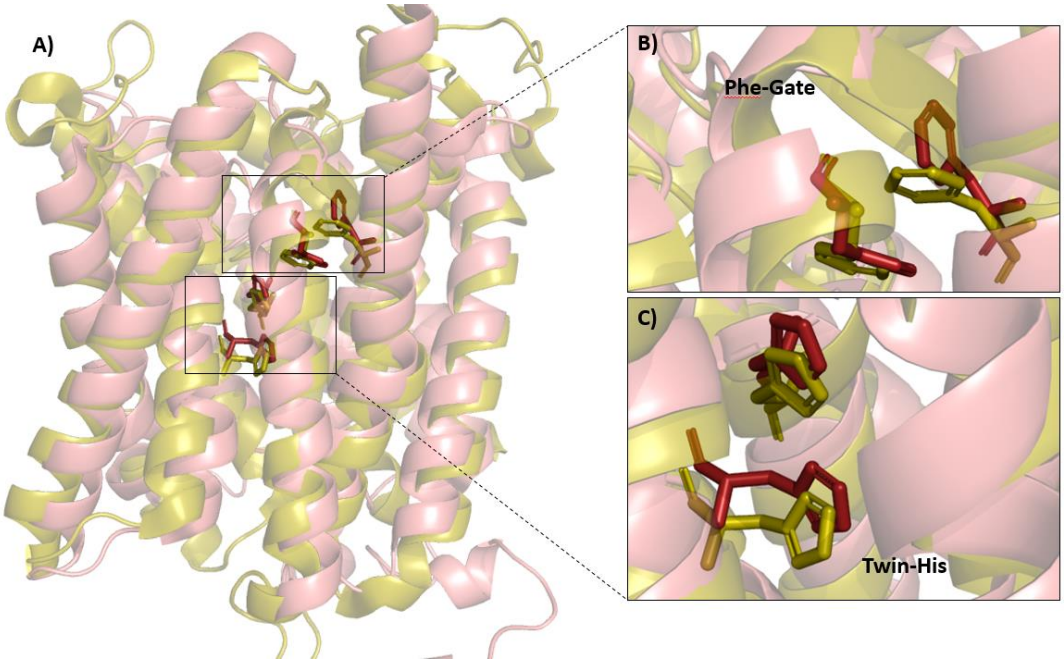

Figure 1.12 Comparison of AmtB from *E. coli* and Rh50 from *N. europea.* *A)* Overlay of a single monomer of *Ec*AmtB (olive) and *Ne*Rh50 (red) as inserted into the membrane with conserved phenylalanine and histidine residues displayed in the same colour as their respective monomer. **B)** Enlarged view of tilt in the Phe-gate and **C)** the twin-His motif in *Ec*AmtB compared to that in *Ne*Rh50.

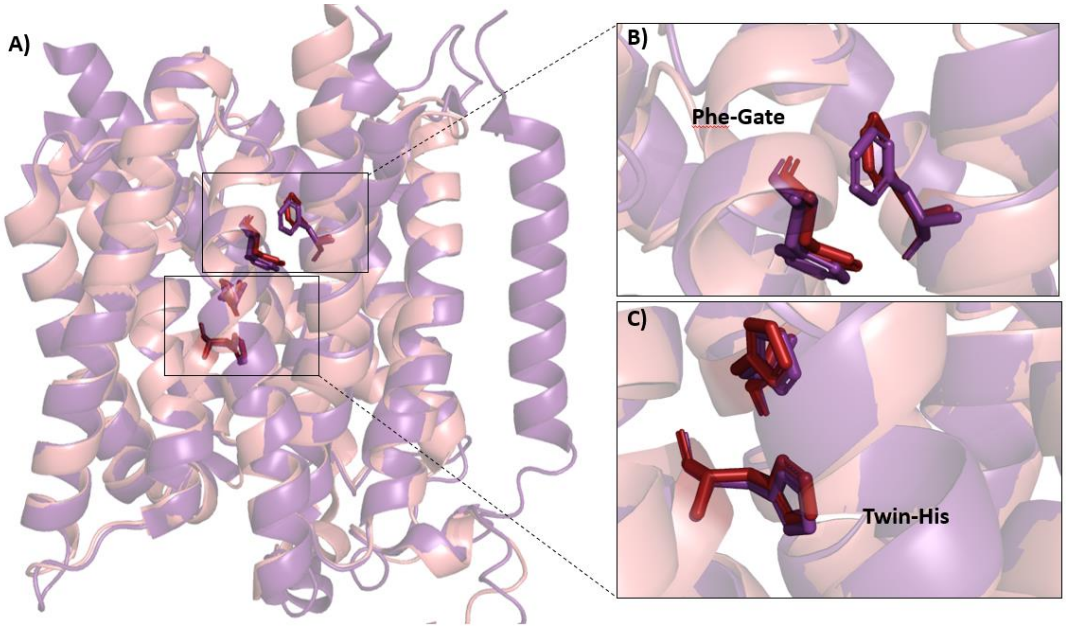

Figure 1.13 Comparison of the Rh50 from *Nitrosomonas europaea* and RhCG from human. A) Overlay of a single monomer of *Ne*Rh50 (red) and *Hs*RhCG (purple) as inserted into the membrane with conserved phenylalanine and histidine residues displayed in the same colour as their respective monomer. **B)** Enlarged view of tilt in the phenylalanine motif and **C)** the twin-His motif in *Ne*RH50 compared to that in *Hs*RhCG.

1.7.5 A Cytoplasmic Vestibule

The cytoplasmic vestibules of AmtB and Rh proteins are very similar. The clear asymmetry between the periplasmic and cytoplasmic vestibules seen in AmtB is minimal in Rh proteins due to lack of a binding site though. Interestingly a cytoplasmic CO_2 binding pocket has been identified in *Ne*Rh50 (Li *et al.*, 2007). It is formed by residues L58, F61, D201, S204, M205, I260, V261, A264, and N265, which are fairly conserved in non-transporting Rh30 proteins; its role, however, is still unclear. A CO_2 binding site present in prokaryotic Rh50 structure, is not present in the human Rh glycoproteins (Gruswitz *et al.*, 2010). In RhCG Q283 replaces an alanine at the equivalent position in *Ne*Rh50. This glutamate side chain occupies the proposed CO_2 site and is conserved in all the human Rh glycoproteins (Gruswitz *et al.*, 2010).

Interestingly, Rh proteins share a common feature not seen in Amt or Mep proteins: a “shunt” present on the cytoplasmic site (**Figure 1.11 B)**. While shunt has been observed in the structure of *Ne*Rh50, isoleucine I324 in RhCG is replaced by threonine in Rh50 (T304) (**Figure 1.11 A**). Nevertheless, this common to the Rh sub-family feature suggests its importance for these proteins (Gruswitz *et al.*, 2010). The authors proposed that it may function as an alternative pathway for NH_4^+ binding and transport across the membrane (Gruswitz *et al.*, 2010). However, its function is still unclear and has not been validated to date.

1.7.6 Functional Characterisation of Rhesus Protein

As the most distant member of the family, Rh have been proposed to have distinct functions to Amt/Mep proteins. However, yeast complementation assays (Marini *et al.*, 2000a; Weidinger *et al.*, 2007) and functional studies proved that Rh proteins facilitate ammonium transport (Zidi-Yahiaoui *et al.*, 2005; Benjelloun *et al.*, 2005), suggesting that the mechanism across the entire superfamily could be conserved to some extent. But the attempts to elucidate the mechanism, and substrate translocated provided conflicting results. The X-ray crystallographic structures of both, bacterial and human rhesus, suggested transport of ammonia (NH_3) (Lupo *et al.*, 2007; Gruswitz *et al.*, 2010) but electrogenic transport of NH_4^+ has also been noted (Nakhoul *et al.*, 2005; Caner *et al.*, 2015). In contrast to transporting Rh50 proteins, non-transporting Rh30 have different arrangement of residues. The pseudo-symmetrical histidine residues in the conductance pore are not conserved, therefore it was concluded that they do not function as ammonia channels and instead act as antigens on the surface of erythrocytes (Merrick *et al.*, 2006).

In this section, each of the proposed mechanisms of ammonium transport via bacterial and human Rh50 proteins will be reviewed. The transport mechanism for each protein discussed was summarised and presented in **Table 1.2**.

1.7.7 Rh50 Protein from **Nitrosomonas europaea**

The chemolithoautotroph *N. europaea* gains all its energy from the oxidation of ammonia to nitrate. A general assumption was that ammonia (NH_3) rather than ammonium (NH_4^+) is the substrate for ammonia oxidation in *N. europaea* (Suzuki, Dular and Kwok, 1974). It was suggested by Chain *et al* that an ammonium transporter is present in *N. europaea* and mediates a passive uptake at low pH (Chain *et al.*, 2003). In addition, a PII signal transduction protein which regulates the activity of ammonium transporters in response to nitrogen status is absent in *N. europaea.* This further implied that *N. europaea* mediates passive ammonium uptake (Chain *et al.*, 2003). Contrary to this, in natural environments *N. europaea* competes with many bacteria such as *E. coli* or *B. subtilis* which possess highly efficient ammonium transport proteins.

Therefore, passive ammonium uptake would be insufficient to compete with other bacteria. Additionally, high ammonium uptake rates were noted in *N. europaea.* It has also been seen to accumulate ammonium during ammonia oxidation process (Schmidt *et al.*, 2004). Those suggested an active ammonium transport system.

Soon after, it was revealed that the genome of *N. europaea* codes for a single gene (*rh1*) belonging to the family of the Amt/Mep/Rh ammonium transporters (Huang and Peng, 2005). First functional and physiological evidence for Rh50 involvement in ammonium transport came from a study demonstrating that the methylammonium (MeA) transport activity of *N. europaea* is correlated with the Rh50 expression transcription level (Weidinger *et al.*, 2007). A similar observation was made by another group which demonstrated decreased uptake rate of MeA in Rh50 KO strain vs the WT *N. europaea* (Cherif-Zahar *et al.*, 2007).

Interestingly it appears that AOB have developed a survival strategy at the molecular level by regulating transcription levels. Under starvation conditions (deprivation of NH_3 and CO_2), nearly 70% of *N. europaea* genes are downregulated. AMO and HAO levels are maintained, while genes related to oxidative stress and transcription of Rh50 are upregulated (Wei *et al.*, 2006, Beyer *et al.,* 2009). This suggests that Rh50 might be involved in the survival strategy of *N. europaea*, where it can sustain prolonged starvation periods, while preparing for the ammonia uptake and oxidation when it becomes available (Bollmann, Bär-Gilissen and Laanbroek, 2002).

While many studies supported the notion that Rh50 is involved in ammonium translocation in *N. europaea,* the understanding of the actual mechanism was lacking. The first insight into the mechanism of Rh50 was provided via complementation studies. When expressed in *S. cerevisiae*, it mediated pH-dependent MeA transport, and was concluded that neutral NH_3 is the transported species (or NH_4^+/H^+ exchange) (Cherif-Zahar *et al.*, 2007;Weidinger *et al.*, 2007). Resolution of the crystal structure of *Ne*Rh50 further supported the notion that it might mediate transport of uncharged species. The presence of a highly hydrophobic pore preventing charge

translocation, suggested that Rh50 acts as a gas for NH_3 and/or CO_2 (Lupo *et al.*, 2007; Li *et al.*, 2007). It was concluded to be highly representative of all Rh proteins, therefore it was widely assumed that human Rh proteins would also act as ammonia (NH_3) channels.

1.7.8 Human Rh50 Proteins

In 2000, RhAG found in erythrocytes, was identified as a distant relative of existing Amt/Mep ammonium transporters, through sequence similarity (Marini *et al.*, 1997b). Soon after, RhBG and RhCG glycoproteins were found in essentially all tissues involved in ammonia transport and metabolism (Liu *et al.*, 2000; Liu *et al.*, 2001). However, the understanding of their true substrate or mechanism was lacking.

1.7.8.1 RhAG Protein

In 2000, Marini *et al.* provided first the evidence that RhAG mediates transport of ammonium through the yeast growth complementation assay (Marini *et al.*, 2000a). Work by Stewart and colleagues showed that specific mutations (**Table 1.3**) in RhAG, which are linked with overhydrated hereditary stomatocytosis (OStH), affect the ability of the protein to transport amines (NH_3/NH_4^+ and MeA/MeA^+), further supporting RhAG role in ammonium transport (Stewart *et al.*, 2011). Ever since, many studies have tried to elucidate the mechanism and substrate translocated by RhAG. When expressed in *Xenopus oocyte* ammonium uptake was noted to be affected by a H^+ gradient suggesting electroneutral NH_4^+/H^+ exchange (Westhoff *et al.*, 2002), but a stopped-flow analysis study found RhAG to act as a channel (Ripoche *et al.*, 2004). At last, RhAG was proposed to transport both NH_3 and NH_4^+ (Benjelloun *et al.*, 2005; Stewart *et al.*, 2011; Caner *et al.*, 2015).

1.7.8.2 RhBG Protein

It is now well known that efficient ammonium excretion is essential to maintain the pH homeostasis in humans, as the elevated concentrations of ammonium can lead to a wide variety of clinical problems (Auron and Brophy, 2012). But the mechanisms by which this homeostasis is achieved is still a debated topic.

Most studies reported that NH_4^+ transport in RhBG is coupled to the H^+ gradient, resulting in electroneutral NH_4^+/H^+ exchange (Ludewig, 2004), or simple channelling of uncharged NH_3 species (Zidi-Yahiaoui *et al.*, 2005) as previously seen in RhAG (Ripoche *et al.*, 2004). In contrast, conflicting results have been observed by Naukhul *et al* where electrogenic NH_4^+ transport was measured in *Xenopus* oocytes expressing Rhbg by two electrode voltage-clamp and ion-selective microelectrodes (Nakhoul *et al.*, 2005; Nakhoul *et al.*, 2006).

It is difficult to explain these conflicting results. The reported affinity of RhBG to NH_4^+ is 2–4 mM, while NH_4^+ concentrations in the renal medulla varies between 2.5 and 9 mM. RhBG is expressed at the basolateral membrane (Quentin *et al.*, 2003) and the electrochemical gradient for NH_4^+ is consistent with electrogenic influx of NH_4^+, although electroneutral NH_3 transport may still occur.

1.7.8.3 RhCG Protein

Just like other Rh homologs, functional characterisation of RhCG provided conflicting evidence. A voltage-clamp experiments by Bakouh *el al* suggested RhCG may transport both, NH_3 and NH_4^+ (Bakouh *et al.*, 2004). In contrary, a study by Caner *et al* demonstrating lack of pH recovery and the absence of inward currents in oocytes expressing Rhcg argued that it acts predominantly as a NH_3 transporter (Caner *et al.*, 2015). Deletion of Rhcg was found to decrease NH_3 permeability without any change in NH_4^+ permeability in apical plasma membrane in the collecting duct of mice (Biver *et al.*, 2008). In addition, the work using stopped-flow spectrophotometry to measure changes in pH in HEK-293 cells expressing RhCG or in erythrocyte vesicles and liposomes

containing RhCG concluded that it was an electroneutral (NH_3) channel (Zidi-Yahiaoui *et al.*, 2006; Mouro-Chanteloup *et al.*, 2010).

To understand this, the localization of RhCG should be considered. RhCG are expressed at the apical membrane of the collecting duct (Quentin *et al.*, 2003), where electroneutral NH_3 or NH_4^+/H^+ transport is likely. This also suggests that mechanisms of RhCG may be different from that of basolateral RhBG and erythrocytic RhAG.

1.7.8.4 Bidirectionality of Rh Proteins

In 2000, Marini *et al.* provided the first evidence that RhAG and RhCG mediate bidirectional transport of ammonium through the yeast growth complementation assay (Marini *et al.*, 2000a). Methylammonium (MeA) is toxic to *S. cerevisiae* and can inhibit growth at external concentrations of 100 mM or higher. However, *S. cerevisiae* yeast mutant complemented with RhAG and RhCG grew on glutamic acid and MeA supplemented media even at the toxic MeA concentration range (< 100mM) (Marini *et al.*, 2000a). This provided initial support for the exporting ability of Rh proteins. Experiments utilising the catabolism of arginine to ammonium provided further support. When yeast cells expressing RhAG were grown on arginine, ammonium was excreted at a distinctly higher rate when compared with cells not expressing the human protein (Marini *et al.*, 2000a). A later study by Hemker *et al* revealed that Rh null RBC (not expressing Rh complex) had twice lowered exporting efficiency in comparison to normal RBC. Based on these results authors concluded that the Rh complex is involved in the export of ammonium from RBC (Hemker *et al.*, 2003). Later, Rh50 from *N. europaea* was also observed to provide resistance to toxic methylammonium concentrations, leading to a similar conclusion as for human Rh proteins (Weidinger *et al.*, 2007).

While mentioned studies provide initial support that Rh proteins mediate the export of the substrate, none of them investigated the mechanism which governs this unique ability.

1.7.8.5 Rh Proteins and CO_2 Transport

In parallel to NH_3 transport, Rh proteins were also proposed to be responsible for facilitating CO_2 transport across the plasma membrane. Analysis of evolutionary conservation and diversification supported that Rh transports neutral NH_3 but also suggested they might be involved in CO_2 waste disposal as a means of maintaining an appropriate pH homeostasis (Huang and Peng, 2005). The first report claiming Rh involvement in CO_2 transport came from studying expression of the *RH1* gene in the green alga *Chlamydomonas reinhardtii* (Soupene *et al.*, 2002). The authors showed that expression of *RH1* was higher for cells grown in air supplemented with 3% CO_2 and concluded that Rh1 and Rh proteins are a long-sought gas channels for CO_2 (Soupene *et al.*, 2002). A subsequent study provided further evidence for the claim by showing that inhibiting expression of the Rh reduces the responses to extracellular CO_2 in *Chlamydomonas reinhardtii* (Soupene, Inwood and Kustu, 2004). In another study a direct ammonia–CO_2 competition experiments affected both ammonia and CO_2 excretion in *Danio rerio* zebrafish, suggesting that Rh proteins may serve as channels for both CO_2 and NH_3 (Perry *et al.*, 2010). Identification of a potential CO_2 binding pocket in the *Ne*Rh50 crystal structure, further suggested that Rhesus proteins might act as gas channels for NH_3 and/or CO_2 (Li *et al.*, 2007). These findings prompted the investigation of human Rhesus proteins and their involvement in CO_2 transport (Endeward, 2006; Endeward *et al.*, 2008). Analysis of red blood cell ghost membrane vesicles deficient in RhAG expression and knockout mice displaying well-characterized protein defects, showed that even a small drop in the production of this protein significantly reduces CO_2 exchange (Endeward, 2006; Endeward *et al.*, 2008). It was found that, RhAG accounts for ~50% of CO_2 transport (Endeward, 2008). Another study supported the view that RhAG represents a channel for extrarenal transport of NH_3 and CO_2 molecules based on changes in surface pH in *Xenopus* oocytes expressing RhAG and aquaporin AQP1 (Musa-Aziz *et al.*, 2009). However, RhAG demonstrated 4-fold greater preference for passage of NH_3 versus CO_2 in comparison to AQP1, leaving the results rather open ended (Musa-Aziz *et al.*, 2009).

At the same time, experimental characterisation *Ne*Rh50 *in vivo* provided no evidence of a CO_2-dependent growth effect in a KO mutant (Cherif-Zahar *et al.*, 2007). Another argument against Rh involvement in CO_2 was presented in a later report monitoring transmembrane CO_2 flux by imposing a CO_2 concentration gradient across planar lipid bilayers and detecting the resulting small pH shift in the immediate membrane vicinity. The study concluded that protein facilitated transport of CO_2 through biological membranes is highly improbable (Missner *et al.*, 2008). In addition, CO_2 binding pocket was not detected in the crystal structure of human RhCG, which was proposed to be representative for all Rh homologues (Gruswitz *et al.*, 2010). Finally, a recent study showed that during long equilibration molecular dynamics (MD) simulations the CO_2 molecules do not show any tendency to diffuse across the periplasmic vestibule of neither bacterial of human Rh50 protein (Hoyhtya, 2020).

1.7.9 Summary of Rh Functional Studies

Functional studies carried out in different heterologous systems provided insights into the Rh-mediated ammonium transport mechanisms, but the transported substrate (CO_2/NH_3 or NH_4^+) remained a controversial topic. Very often the same or similar technique would provide conflicting evidence (**Table 1.2**). While it is possible that Rh from different organisms, or within organisms, can differ functionally, all previously mentioned studies used heterologous systems where presence of endogenous transporters or acid-base regulating proteins might have interfered with the NH_4^+ transport. Additionally, the lipid environment might have handicapped the activity of the protein as well as influence the membrane permeability to NH_3 (Mirandela *et al.*, 2018) producing conflicting results.

The lack of functional assays characterising variants with substitutions in conserved residues forming translocation pathway in human Rh also hinders the understanding of the mechanism of these proteins. Therefore, a reliable *in vitro* system is needed to characterise the mechanism and substrate translocated by the Rh proteins.

Table 1.2 Transport mechanism in Rh50 proteins

Protein	Mechanism/ Substrate	Supporting evidence	References
*Ne*Rh50	NH_3 transport	(i) Electroneutral transport (ii) pH dependent	(Weidinger *et al.*, 2007;Lupo *et al.*, 2007)
	CO_2 transport	(i) Presence of CO_2 binding pocket in crystal structure	(Li *et al.*, 2007)
*Hs*RhAG	NH_3 transport	(i) Rapid alkalisation of pHi at inwardly orientated substrate gradient	(Ripoche *et al.*, 2004)
	NH_4^+/H^+ exchange	(ii) Electroneutral transport (iii) Stimulated by rising extracellular/ lowering intracellular pH	(Westhoff *et al.*, 2002)
	NH_4^+ transport	(i) Electrogenic transport	(Caner *et al.*, 2015)
	CO_2 transport	(i) Intracellular pH changes (ii) Surface pH changes (iii) Ammonia-CO_2 competition experiments (iv) Translational knockdowns of Rh proteins	(Endeward *et al.*, 2008;Musa-Aziz *et al.*, 2009;Perry *et al.*, 2010)
*Hs*RhBG	NH_3 transport	(i) Electroneutral transport (ii) Rapid kinetics of the pHi changes	(Zidi-Yahiaoui *et al.*, 2005)
	NH_4^+/H^+ exchange	(i) Electroneutral transport (ii) Intracellular pH change	(Ludewig, 2004)
	NH_4^+ transport	(i) Electrogenic transport	(Nakhoul *et al.*, 2005;Nakhoul *et al.*, 2006;Caner *et al.*, 2015)
*Hs*RhCG	NH_3 transport	(i) Electroneutral transport (ii) pH change stopped-flow spectrophotometry	(Mouro-Chanteloup *et al.*, 2010)
	NH_4^+ transport	(i) Electrogenic transport	(Bakouh *et al.*, 2004)

1.8 A New Model for Electrogenic Ammonium Transport

It remains a matter of debate whether it is the neutral (NH_3) or the charged (NH_4^+) form of the substrate that is transported by Amt/Mep and Rh proteins. All crystal structures elucidated so far reveal a hydrophobic pore which prevents the translocation of charged ammonium (NH_4^+), suggesting that both protein families transport neutral ammonia (NH_3) (Khademi *et al.*, 2004; Andrade *et al.*, 2005; Lupo *et al.*, 2007; Gruswitz *et al.*, 2010). However, functional studies paint a more complex picture.

Despite the presence of the hydrophobic pore, the measurement of electric current provides strong evidence that AMT proteins transport NH_4^+ (Ludewig, von Wirén and Frommer, 2002; Wacker *et al.*, 2014; Mirandela *et al.*, 2018). In the case of Rh proteins, the debate is more open. They were reported to transport neutral NH_3 (Ludewig, 2004; Ripoche *et al.*, 2004; Mouro-Chanteloup *et al.*, 2010), as well as ionic NH_4^+ species (Hemker *et al.*, 2003; Nakhoul *et al.*, 2005). Some argued that both, NH_3 and NH_4^+ forms are translocated (Bakouh *et al.*, 2004; Benjelloun *et al.*, 2005). Lastly, Rh proteins were suggested to function as CO_2 channels (Kustu and Inwood, 2006; Endeward *et al.*, 2008; Musa-Aziz *et al.*, 2009).

The conflict between the crystal structures, which would clearly prevent charge translocation, and functional observations of electrogenic transport fuelled the controversies concerning the transport mechanism of Rh and Amt/Mep. The question of how a charge can travel through a hydrophobic pore remained unanswered.

1.8.1 A Two-Lane Mechanism of Electrogenic Ammonium Transport

Previously reported electrogenic ammonium transport in AmtB protein from *E. coli* was recently confirmed in our lab (Mirandela *et al.*, 2018; Williamson *et al.*, 2020). Inspired by the evidence suggesting NH_4^+ deprotonation upon binding to the protein (Ariz *et al.*, 2018) and extended molecular dynamic simulation (MDS), we identified a potential proton conduction route (Williamson *et al.*, 2020) and validated the model via the Solid Supported

Membrane Electrophysiology (SSME) *in vitro* assay (Bazzone, Barthmes and Fendler, 2017). A detailed description of our model mechanisms for electrogenic ammonium transport in *Ec*AmtB will be discussed in detail in **Chapter 4** (**Section 4.1.1**). Crucially the translocation pathway and residues involved in our model mechanisms are highly conserved in all known structures of Rh and Amt/Mep family of ammonium transporters (Lupo *et al.*, 2007; Gruswitz *et al.*, 2010; van den Berg *et al.*, 2016). This suggests that proposed mechanism could be conserved across the family, enabling us to finally elucidate the nature of transported species in Rh protein and shed a light on Rh malfunction leading to multiple diseases.

1.8.2 Bacterial Rh50 as a Model to Study Rh Proteins

The characterisation of human transport systems is often very difficult, as the proteins are very large and integral membrane proteins of this size are notoriously very challenging to handle (Lacapère *et al.*, 2007). The common features between Rh50 from *N. europaea* and human Rh proteins imply a conserved function, thus presenting Rh50 as a perfect candidate for the model. Structurally defined region of Rh50 and RhAG shares 36.3%/64.9% sequence identity/similarity (Lupo *et al.*, 2007), suggesting that architecture and structure of bacterial Rh50 is highly representative of all Rh proteins. Additionally, the residues in which mutations in the human orthologues leads to diseases, are conserved in the bacterial homologues (**Table 1.3**). Human RhAG models based on crystal structures of human RhCG (Gruswitz *et al.*, 2010), *Ne*Rh50 (Lupo *et al.*, 2007; Li *et al.*, 2007), and *Ec*AmtB (Khademi *et al.*, 2004; Zheng *et al.*, 2004) place mutant residues (**Table 1.3**) in the juxta-cytoplasmic portion of the second transmembrane domain (Stewart *et al.*, 2011). Finally, the unique exporting ability has also been observed in *Ne*Rh50 (Weidinger *et al.*, 2007), further justifying the choice of the bacterial Rh50 transporter as a tractable model system in the context of human Rh physiopathology.

Table 1.3 Mutations associated with human pathophysiology

Human protein	Mutation	Associated disease	Mutation in Bacterial homologue	References
*Hs*RhAG	I61R	OHSt	*Ne*Rh50 I51R	(Li *et al.*, 2007)
*Hs*RhAG	F65S	OHSt	*Ne*Rh50 F55S	
*Hs*RhCG	R202C	Metabolic acidosis	*Ec*AmtB R207C	(Merrick *et al.*, 2006)

**Hs*: *Homo sapiens*, *Ec*: *Escherichia coli*, *Ne*: *Nitrosomonas europaea*

1.9 Aims of the PhD project

High structural and functional similarity between the bacterial Rh50 and human Rh transporters makes it a perfect and tractable model system which will help us to understand the Rh mutations resulting in human physiopathology. In addition, this work has important environmental implications as AOB were found to be important in the treatment of wastewater and were proposed to have a potential for the bioremediation of sites contaminated with chlorinated aliphatic hydrocarbons (Juliette, Hyman and Arp, 1993; Keener and Arp, 1994). Despite extensive studies focusing on the ability of *N. europaea* to utilise ammonia, the mechanism in which ammonium enters cells is not known (Arp, Sayavedra-Soto and Hommes, 2002). Finally, this research provides an opportunity to investigate whether there is a universal mechanism for ammonium transport across the Rh and Amt/Mep family of transmembrane proteins.

In this context, the overall aim of this PhD project is to establish the mechanism of *Ne*Rh50-mediated transport at the molecular level, using a combinatorial approach (*in vivo* yeast complementation assays, and in vitro electrophysiology assays). Solid supported membrane electrophysiology (SSME) will be utilised as a tool for probing the mechanistic detail of ammonium transport (detailed in Section 2.6). Once SSME measurements are established and validated, the mechanism of *Ne*Rh50 will be investigated. The specific aims are to:

1. Characterise the kinetics, energetics, and specificity of *Ne*Rh50.
2. Decipher whether the mechanism present in *Ec*AmtB is conserved in *Ne*Rh50.
3. Understand the mechanism underlying *Ne*Rh50 bidirectionality.

Chapter 2

Chapter 2: Materials and Methods

2.1 Molecular Biology

2.1.1 Strains and Media Preparation

A list of all strains and media compositions used throughout this work can be found in **Table 2.1** and **Table 2.2,** respectively.

All media and buffers were filtered through a 0.22 µm pore filter and autoclaved at 121°C for 15 minutes to sterilise.

2.1.2 Chemically Competent Cells

A single colony of *E. coli* was used to inoculate 5 mL of LB media in a sterile 20 mL universal and incubated overnight at 37°C at 250 rpm. 1 mL of the culture was used to inoculate 100 mL of sterile LB in a 250 mL Erlenmeyer flask and subsequently incubated at 37°C until the OD_{600} reached 0.5.

The culture was transferred to sterile 50 mL centrifuge tubes and rested on ice for 10 minutes to halt the growth. The cells were harvested by centrifugation at 4000 *g* at 4°C for 10 minutes, gently resuspended in 10 mL of ice-cold sterile 0.1 M CaCl and rested on ice for a further 20 minutes. The centrifugation was repeated, and the cells resuspended in 5 mL of ice-cold sterile 0.1 M CaCl + 15% glycerol (w/v). The competent cells were dispensed in 100 µL aliquots, flash-frozen in liquid nitrogen and stored at - 80°C.

2.1.3 Heat-Shock Transformation of E. coli

0.1 µg of plasmid DNA was added to 50 µL of thawed chemically competent cells and incubated on ice for 30 minutes. The cells were heat-shocked at 42°C for 45 seconds and transferred to ice for 2 minutes. 900 µL of sterile LB was immediately added and the cells incubated at 37°C for at least 1 hour. 100 µL on culture was spread on selective LB agar plates.

Table 2.1 Genotype of *E. coli* bacterial strains used.

Strain	Genotype	Reference
E. coli		
DH5α	F^{-}φ80lacZΔM15 Δ(lacZYA-argF) U169 recA1 endA1 hsdR17 (r_K^-, m_K^+) phoA supE44 λ^{-}thi-1 gyrA96 relA1	(Hanahan, 1983)
C43 (DE3)	F- ompT gal dcm lon hsdSB (rB -mB – λ (DE3)	(Miroux and Walker, 1996)
GT1000	*Rbs lacZ::IS gyrA hutCK ΔglnKamtB*	(Coutts *et al.*, 2002)
S. cerevisiae		
31019b	MATa ura3 mep1Δ mep2Δ::LEU2 mep3Δ::KanMX2	(Marini *et al.*, 1997a)
228	mep1Δ mep2Δ mep3Δ trk1Δ trk2Δ leu2	(ten Hoopen *et al.*, 2010)

Table 2.2 Media used in this study

Name of medium	Composition	Reference
Luria-Bertani	1% (w/v) Tryptone 0.5% (w/v) Yeast Extract 0.5% (w/v) NaCl	(Sambrook, Fritsch and Maniatis, 1989; Bertani, 1951)
ZY	1% (w/v) N-Z Amine 0.5% (w/v) Yeast Extract	(Studier, 2005)
50x5052	270 mM Glycerol 1.4 M Glucose 300 mM α-Lactose	(Studier, 2005)
20xNPS	0.5M $(NH_4)_2SO_4$ 1M KH_2PO_4 1M Na_2HPO_4	(Studier, 2005)
M9 Minimum Media	0.2% (v/v) Glucose 0.2mg/ml Glutamine 1mM $MgSO_4$	(Elbing and Brent, 2002)
M9 Medium Salts	0.6% (w/v) Na_2HPO_4 0.3% (w/v) KH_2PO_4 0.05% (w/v) NaCl	(Elbing and Brent, 2002)
Carbenicillin	34µg/ml (1:1000 dilution)	
Chloramphenicol	34µg/ml (1:1000 dilution)	

2.1.4 Plasmid Purification

Cells were grown overnight in 5 mL of LB supplemented with the appropriate antibiotic and plasmids purified with a Wizard® Plus SV Miniprep DNA purification system (Promega Corporation), according to the manufacturer's instructions. Briefly, cells were pelleted via centrifugation and chemically lysed under alkaline conditions. Cellular debris was separated via centrifugation and DNA subsequently bound to a provided Promega silica membrane column. RNA and protein contaminants were washed off with a high salt buffer, and the DNA eluted in nuclease-free water. DNA concentration was quantified using Nanodrop 2000.

2.1.5 Random Mutagenesis

Random mutagenesis of *amtB,* from *E. coli* and *mep2,* from *S. cerevisiae* was performed using XL1 –Red *E. coli* cells (Muteeb and Sen, 2010), according to manufacturer's instructions with minor changes. Following transformation, ≤100 µL of the transformation mixture was plated on 10 separate LB plates containing carbenicillin or chloramphenicol (**Table 2.2**) for *amtB* and *mep2,* respectively, using a sterile spreader. Plates were incubated at 37°C for 24–30 hours and harvested using 1 mL of pre-warmed LB (**Table 2.2**) and a sterile scraper. Suspended cells were pulled together in a sterile 50 mL falcon tube and grown for a maximum of 2 hours at 37°C in presence of antibiotic. Plasmids were purified using QIAGEN Maxi Kit according to the provided instructions (Qiagen). DNA concentration was subsequently quantified using Nanodrop 2000.

2.1.6 Site Directed Mutagenesis

Site-directed mutagenesis of *rh50* gene was performed using the QuikChange Lightning Site-Directed Mutagenesis Kit (Agilent Technologies), according to manufacturer's instruction. Following a PCR mutagenesis, the product was incubated with DpnI restriction digest enzyme for at least 1 hour at 37°C, and transformed into chemically competent *E. coli* cells, DH5α (**Table 2.1**). DNA

was purified using Wizard® Plus SV Miniprep DNA purification system (Promega Corporation), and each construct was checked by Sanger sequencing (Eurofins Genomics). The primers used for the mutagenesis are listed in **Table 2.3** and the template was the *rh50* gene cloned into the plasmid pAD7 (**Table 2.4**).

Table 2.3 Primers used in this study

Primer	Direction	Sequence
Mutagenesis:		
NeRh50 P55S	Reverse	CATTCTGGCCATGCTGCTGGTCGGT**AG**CGGTTTTTTAATGG
NeRh50 H170A	Forward	CTGCCGGATCGATCGCTATCGCT**GC**TTTTGGTGCATATTT
NeRh50 H170E	Forward	TGCCGGATCGATCGCTATC**GAG**GCTTTTGGTGCATATTTT
NeRh50 H170D	Forward	CCGGATCGATCGCTATC**G**ATGCTTTTGGTGCATAT
NeRh50 D162A	Forward	ACTGAAGGATTCCAGG**C**TTCTGCCGGATCGATC
NeRh50 H324A	Forward	CTGCGGGGTACACAATCTG**GC**TGGATTACCAGGATTATTG
NeRh50 H324E	Forward	CTGCGGGGTACACAATCTG**GAG**GGATTACCAGGATTATTGG
NeRh50 H324D	Forward	GCGGGGTACACAATCTG**G**ATGGATTACCAGG
Expression in yeast		
*Ec*AmtB XhoI	Forward	AGTC**CTCGAG**ATGAAGATAGCGACGATAAAA
*Ec*AmtB BamHI	Reverse	AGTC**GGATCC**TCACGCGTTATAGGCATTCTC
*Ne*Rh50 XhoI	Forward	ATGC**CTCGAG**ATGAGTAAACACCTATGTTTCACTGC
*Ne*Rh50 BamHI	Reverse	ATGC**GGATCC**TAGCTATCCTTCTGACTTGGCACTC
P5'*Ne*Rh50	Forward	GCC**ACTAGT**ATGAGTAAACACCTATGTTTC
P3'*Ne*Rh50	Reverse	GCC**GAATTC**CTATCCTTCTGACTTGGCAC

**Nucleotides in bold have been changed to introduce the mutations/restriction sites, Escherichia coli (Ec), Nitrosomonas europaea (Ne)*

Table 2.4 Plasmids used in the study

Plasmid	Description	Reference
pET22b (+)	High copy bacterial expression vector	Novagen
pZheng		(Zheng *et al.*, 2004)
pDR195	pET22b-AmtB(His)$_6$	(Rentsch *et al.*, 1995)
p426MET25	High copy yeast expression vector High copy shuttle expression vector	(Mumberg, Müller and Funk, 1994)
pAD7	pESV2-Rh50(His)$_6$	(Cherif-Z *et al.*, 2007)
pADA1	pESV2-Rh50(His)$_6^{D162A}$	This study
pADA2	pESV2-Rh50(His)$_6^{H170A}$	This study
pADA3	pESV2-Rh50(His)$_6^{H170E}$	This study
pADA4	pESV2-Rh50(His)$_6^{H170D}$	This study
pADA5	pESV2-Rh50(His)$_6^{H170AH318A}$	This study
pADA5	pESV2-Rh50(His)$_6^{H170DH318E}$	This study
pADA6	pESV2-Rh50(His)$_6^{H318A}$	This study
pADA7	pESV2-Rh50(His)$_6^{H170E}$	This study
pADA8	pESV2-Rh50(His)$_6^{F55S}$	This study
pADA9	pDR195-Rh50^{D162A}	This study
pADA10	pDR195-Rh50^{H170A}	This study
pADA11	pDR195-Rh50^{H170E}	This study
pADA12	pDR195-Rh50^{H170D}	This study
pADA13	pDR195-Rh50^{H170AH318A}	This study
pADA14	pDR195-Rh50^{H170DH318E}	This study
pADA15	pDR195-Rh50^{H318A}	This study
pADA16	pDR195-Rh50^{H170E}	This study
pADA17	pDR195-Rh50^{F55S}	This study

2.2 Protein Expression in Yeast and Complementation Test

2.2.1 Sub-cloning for Yeast Overexpression

Rh50 protein was expressed in *Saccharomyces cerevisiae* yeast using p426Met25 vector (**Table 2.4**) allowing controlled expression of the protein by the yeast methionine repressible MET25 promoter. Both, AmtB and Rh50 were expressed using pDR195 plasmid (Rentsch *et al.*, 1995). In this plasmid, protein expression is controlled by the promoter of PMA1, a housekeeping plasma membrane ATPase gene.

20 ng of plasmid DNA from each construct was amplified by PCR reaction using Q5 High Fidelity DNA Polymerase (NEB), according to the manufacturer's instructions. The primers (**Table 2.3**) were designed to add XhoI and BamHI restriction sites to the end of *rh50* and *amtB.* After the PCR, 1 µg of amplified DNA products and 2 µg of pDR195 vector (**Table 2.4**) were digested with XhoI and BamHI (Promega Corporation) (5 units of enzyme/µg of DNA) for 2 hours at 37°C. Digested DNA samples were run on 2% agarose gels in TAE buffer (**Table 2.5**) at 100V*cm^{-1} for 1 hour. DNA was extracted from the gel using the kit Wizard® SV Gel and PCR clean-up system (Promega Corporation), according to the provided protocol.

For ligation, 50 ng of digested insert DNA was mixed with linearised pDR195 to an insert:vector molar ratio of 5:1. The ligations were carried out in a reaction volume of 10 µL and incubated overnight at 4°C to increase ligation efficiency. Finally, 10 µL of the ligation reaction was transformed into *E. coli* DH5α *via* heat-shock transformation (see section 2.1.3).

2.2.2 AmtB and Rh50 Expression in Yeast and Complementation Test

The sequence coding Rh50 gene was amplified from *Nitrosomonas europaea* genomic DNA (kind gift from Daniel J. Arp and Norman G. Hommes, Department of Botany and Plant Pathology, Oregon State University, Corvallis, USA) using the primers P5'*Ne*Rh and P3'*Ne*Rh (**Table 2.3**) and subsequently cloned into the SpeI and EcoRI restriction sites of p426Met25 vector (**Table 2.4**). AmtB was amplified using *amtB* cloned into pET22b(+) (**Table 2.3**) as a template, the primers AmtB XhoI and AmtB BamHI and sub-

cloned into the plasmid pDR195 (**Table 2.4**). Likewise, Rh50 was amplified using *rh50* cloned into pAD7 vector (**Table 2.3**) as a template, the primers Rh50 XhoI and Rh50 BamHI and sub-cloned into the plasmid pDR195 (**Table 2.4**).

The yeast strain 31019b (*MATa ura3 mep1Δ mep2Δ::LEU2 mep3Δ::KanMX2*) and 228 (mep1Δ mep2Δ mep3Δ trk1Δ trk2Δ leu2) (Marini *et al.*, 1997a; ten Hoopen *et al.*, 2010). Plasmids were transformed into these strains as described previously (Gietz *et al.*, 1992) and grown in a minimal buffered (pH 6.1) medium with 3% glucose as the carbon source and, 0.1% (7 mM) glutamate or various $(NH_4)_2SO_4$ concentrations as the sole nitrogen sources. For growth tests on limiting potassium concentrations, a minimal buffered (pH 6.1) medium deprived of potassium salts was used.

2.3 Protein Overexpression and Purification

2.3.1 Specific Growth Analysis of WT Rh50 and Rh50 variants

The Rh50 protein from *Nitrosomonas europaea* cloned into pAD7 vector (**Table 2.4**) was heterologously expressed in GT 1000 Δ(*glnK,amtB*) *E. coli* strain (**Table 2.1**). A hexa-histidine tag was engineered at the C- terminus of *Ne*Rh50 with gene expression controlled by the nitrogen promoter of the *E.coli glnK amtB* operon and using M9 media containing glutamine as a sole N-source. Each plasmid was transformed into GT 1000 *E. coli* strain, plated on selective LB media, and grown overnight at 37°C. Single colony was grown overnight at 37°C in 10 mL of LB media. Following morning cultures were normalised to an OD_{600} of 0.04 using M9 media supplemented with either 20mM NH_4^+ or 0.2mg/mL glutamine (inducer for a promotor of histidine tagged protein overexpression) as a sole nitrogen source, or in LB as a positive control for growth. The working volume was 0.2 mL. Each of media was plated also in duplicate as a negative control. The growth curves based on absorbance readings (600 nm) were carried out in 96-well plates (Tpp, Trasadingen, CH) and shaken continuously at 30°C in the Synergy™ Microplate Reader (BioTech). The optical density was measured every 10 minutes for up to 24 hours.

Data was collected and analysed in Excel Microsoft; the standard error was determined for each set of values/ time point. The natural logarithm (LN) of each value was determined before plotting the averaged LN values against time. The specific growth rate μ h^{-1} of a culture was calculated manually using the following formula: $\ln N_t - \ln N_0 = \mu (t-t_0)$, with N_t and N_0 as the culture concentrations at timepoints t and t_0, respectively, that mark the time in hours at the end and start of exponential phase. Statistical significance between two sets of determined growth rates was conducted with Tukey HSD test, using the following tool: https://www.statskingdom.com/index.html. **Table 2.2** lists compositions of all the media used.

2.3.2 Overexpression

*Ne*Rh50-$(His)_6$ cloned into the pAD7 vector (**Table 2.4**) was overexpressed and overproduced in GT 1000 strain. A single transformant colony containing pAD7- *Ne*Rh50-$(His)_6$ was used to inoculate 1 L of LB and incubated at 37°C for 6 hours (**Table 2.2**). Following incubation 12 L of the M9 media (**Table 2.2**) (Elbing and Brent, 2002) were inoculated at OD_{600} 0.02 and grown at 30°C, 210 rpm in presence of antibiotic for 19 hours.

*Ec*AmtB-$(His)_6$ cloned into the pET22b(+) vector (**Table 2.4**) was overexpressed and overproduced in C43(DE3) strain as described previously (Zheng *et al.*, 2004). Briefly, a single transformant colony containing pET22b-AmtB-$(His)_6$ was used to inoculate 1 L of LB and incubated at 37°C for 6 hours (**Table 2.2**). Following incubation 4 L of the auto induction medium ZYP-5052 (**Table 2.2**), were inoculated at OD_{600} 0.02 and grown at 30°C, 210 rpm in presence of antibiotic for 19 hours.

Cells were harvested by centrifugation at 7439 *g,* 4°C for 30 minutes (JLA 9.100, Beckman Avanti JXN-26) and suspended in resuspension buffer (**Table 2.5**) to ratio of 1g:10mL.

2.3.3 Membrane Preparation

The membrane was isolated as described previously (Blakey *et al.*, 2002). Cells were broken by passing the cell suspension three times through a French

Press (20 kPSI) followed by centrifugation at 27,000 *g*, 4°C for 30 minutes (JA 25-50, Beckman Avanti JXN-26) to pellet intact cells. Collected supernatant was centrifuged at 205,000 *g*, 4°C for 1 hour (TI45, Beckman Optima XPN-100) to pellet the inner membrane. Membrane pellet was stored at -20°C.

2.3.4 Immobilised Metal Affinity Chromatography

*Ec*AmtB and *Ne*Rh50 were purified following the same protocol with one exception. Detergent used for AmtB was N-deodecyl-β-D-maltopyranoside (DDM - 0.03% w/w), whereas for Rh50 n-Dodecyl-N, N-Dimethylamine-N-Oxide (LDAO - 0.09% w/w).

The membrane was solubilised using solubilisation buffer (**Table 2.5**) to a ratio of 1g:10mL. Appropriate detergent (**Table 2.5**) was added dropwise to a final concentration of 2% and incubated for 2 hours at 4°C under gentle agitation. Solubilised membrane was diluted 2-fold with IMAC buffer A (**Table 2.5**) and non-solubilised material was removed by centrifugation at 27,000 *g*, 4°C for 45 minutes (TI45, Beckman Optima XPN-100).

The sample was loaded on an IMAC column (Hitrap HP 1mL, Ge Healthcare) previously coated with cobalt and equilibrated with IMAC Buffer A containing appropriate detergent (**Table 2.5**). The his-tag at the C-terminal of protein binds to cobalt present on matrix of IMAC column via coordination bond allowing ÄKTA Pure FPLC system to purify the protein of interest. After sample loading was complete, non-specifically bound proteins were eluted by washing the column in 10 column volumes (CV) of IMAC B containing 40 mM imidazole. Imidazole acts as a competitive inhibitor which displaces the protein bound to cobalt (Bornhorst and Falke, 2000). The protein was eluted from IMAC column by imidazole gradient, gradually increasing from 40 mM to 500 mM over 20 column volumes present (**Table 2.5**). Protein was eluted into 2mL 96 well plate fraction collector and the absorbance at 280nm was monitored during the purification.

Elution fractions were loaded on a sodium dodecyl sulfate polyacrylamide (SDS-PAGE) gel and western blot were performed to monitor the presence of protein (Section 2.3.8 and 2.3.9).

2.3.5 IMAC Column Regeneration

IMAC column was regenerated by sequentially passing 5 column volume (CV) of water, stripping solution, water, cobalt solution and finally 20% ethanol. The composition of named solutions can be found in (**Table 2.5**).

2.3.6 Size Exclusion Chromatography

Elution fractions from IMAC containing protein were pooled concentrated to 5 mg/ml by subsequent centrifugation using MilliporeAmicon® Pro Affinity Concentration Kit Ni-NTA with 100 kDa Amicon® Ultra-0.5 Device. Size exclusion chromatography (SEC) allows the separation of proteins according to their hydrodynamic property. SEC was performed in SEC buffer containing appropriate detergent (**Table 2.5**) using Superdex S200 10/300 GL increase (Ge Healthcare) using ÄKTA Pure FPLC system. To confirm the presence and access purity of the protein in the sample, elution fractions were analysed on SDS-PAGE gel (**Table 2.5**). The sample was concentrated again to 5 mg/mL and kept at 4°C.

Table 2.5 Compositions of solutions used in IMAC and SEC purification

Name of the buffer	Composition
Resuspension buffer	50 mM Tris-HCl pH8 500 mM NaCl 10% (v/v) Glycerol 160 µM phenylmethylsulphonyl fluoride 10 µg/ml DNase
Solubilisation buffer	50 mM Tris-HCl pH8 500 mM NaCl 10% (v/v) Glycerol 2% DDM or 2% LDAO
IMAC A buffer	50 mM Tris- HCl pH8 500 mM NaCl 10% (v/v) Glycerol 0.03% DDM or 0.09% LDAO
IMAC B buffer	50 mM Tris- HCl pH8 500 mM NaCl 10% (v/v) Glycerol 500 mM Imidazole 0.03% DDM or 0.09% LDAO
SEC buffer	50 mM Tris-HCl pH7.8 100 mM NaCl 0.03% DDM or 0.09% LDAO
Stripping solution	100 mM EDTA 500 mM NaCl 100 mM $CoCl_2$
Cobalt solution	100 mM potassium phosphate pH7.6
Liposome buffer	300 mM KCl

2.3.7 Determination of Protein Concentration

Protein concentration was determined by measuring absorbance at 280nm related to the presence of aromatic amino acids such as tryptophan, tyrosine and cysteine. The molar extinction coefficient depends upon the relative concentrations of these amino-acids and was determined basing on the amino-acids sequence and the ExPASy ProtParam informatics tool (Wilkins *et al.*, 1999). The absorbance was measured using Nano-drop 2000/2000c spectrophotometer (ThermoFisher Scientific) and the concentration was calculated using Beer-Lambert law.

$$C = \frac{A}{\varepsilon * b}$$

A = absorbance

ε = molar absorptivity

b = length of light path

C = concentration

The amino acid sequences and extinction coefficients used are provided in **Table 2.6**.

Table 2.6 Amino Acid Sequence and Properties of Proteins in This Study

Protein	Amino Acid Sequence	MW (kDA)	ε (M-1cm-1)	Ref
*Ne*Rh50	MSKHLCFTAFSSIALFLLCFS SWASAVAPAENEARLVAQYN YSINILAMLLVGFGFLMVFVR RYGFSATTGTYLVVATGLPLY ILLRANGIFGHALTPHSVDAVI YAEFAVATGLIAMGAVLGRLR VFQYALLALFIVPVYLLNEWL VLDNASGLTEGFQDSAGSIAI HAFGAYFGLGVSIALTTAAQR AQPIESDATSDRFSMLGSMV LWLFWPSFATAIVPFEQMPQ TIVNTLLALCGATLATYFLSAL FHKGKASIVDMANAALAGGV AIGSVCNIVGPVGAFVIGLLG GAISVVGFVFIQPMLESKAKTI DTCGVHNLHGLPGLLGGFSA ILIVPGIAVAQLTGIGITLALALI GGVIAGALIKLTGTTKQAYED SHEFIHLAGPEDEHKAERLVL EAKTEIQGLKNRIDAAVLSAK SEG	44.6	38515	Uniprot Q82X47
*Ec*AmtB	MKIATIKTGLASLAMLPGLVM AAPAVADKADNAFMMICTAL VLFMTIPGIALFYGGLIRGKNV LSMLTQVTVTFALVCILWVVY GYSLAFGEGNNFFGNINWLM LKNIELTAVMGSIYQYIHVAFQ GSFACITVGLIVGALAERIRFS AVLIFVVVWLTLSYIPIAHMVW GGGLLASHGALDFAGGTVVH INAAIAGLVGAYLIGKRVGFG KEAFKPHNLPMVFTGTAILYI GWFGFNAGSAGTANEIAALA FVNTVVATAAAILGWIFGEWA LRGKPSLLGACSGAIAGLVGV TPACGYIGVGGALIIGVVAGL AGLWGVTMLKRLLRVDDPCD VFGVHGVCGIVGCIMTGIFAA SSLGGVGFAEGVTMGHQLLV QLESIAITIVWSGVVAFIGYKL ADLTVGLRVPEEQEREGLDV NSHGENAYNA	44.4	66390	Uniprot: C3TLL2

2.3.8 SDS-PAGE

Sodium dodecyl sulfate polyacrylamide gel electrophoresis (SDS-PAGE) was used to monitor the presence of the protein in elution fractions and to assess the purity of the sample.

For SDS PAGE, polyacrylamide gels were prepared and mounted using a Mini-Protean (Bio-Rad) system. Clamp, gel plates and spaces of the system were assembled into the gel stand. Resolving and stacking gel mix was setup, 10% ammonium persulphate and TEMED were added to the gel mix. The resolving gel mix was poured directly into the assembly gel plates and distilled isopropanol was added above the resolving gel mix in plates to keep the surface wet and straight. The gel plates were left at room temperature for 40 min until they solidified. Next, the stacking gel mix was prepared. The mix was poured above the resolving gel (after removing the isopropanol) and the appropriate comb was added. The gel was allowed to solidify at room temperature for 40 min. A running buffer was added to SDS-PAGE after the gel was setup.

Unless otherwise stated, samples were mixed with loading buffer, loaded onto the gel and run at 150V*cm^{-1} for 60 minutes in running buffer. The gel was then stained with Coomassie Blue for 30 minutes and de-stained for 15 minutes. **Table 2.7** lists compositions of all the buffers used.

2.3.9 Western Blot

The samples were mixed with the loading blue buffer, loaded onto SDS page gel, and run at 150V*cm^{-1} for 60 minutes in running buffer as described before. Gel was then equilibrated in transfer buffer for 10 minutes. A 0.45µm polyvinylidene difluoride (PVDF) (ThermoFisher SCIENTIFIC) membrane was activated by immersion in 100% methanol for 1 minute followed by equilibrating it in the transfer buffer for 10 minutes.

Transfer was carried out at 4 mA/cm^3 of the surface area of the membrane: here 221 mA for 30 minutes at 221 mA using semi-dry transfer system (Biometra FastBlot). After completion of the run, the membrane was released and blocked by incubation in a TBS-T 5% non-fat milk buffer for 1 h at room temperature, shaking. Then, the membrane was incubated with 0.1 µg/mL His epitope tag anti-mouse primary mAB antibody (GenScript) in TBS-T 5% non-fat milk buffer. The membrane was washed three times with TBS-T. The membrane was incubated with 0.1µg/mL ALEXA FLOUR 790 goat anti-mouse IgG (H+L) secondary antibody (ThermoFisher SCIENTIFIC) in TBS containing 5% non-fat milk at room temperature for 2 hours, shaking. Finally, the membrane was washed three times with TBS-T and the fluorescent bands were detected in the membrane by Li-COR Odyssey Infrared Imager, USA. **Table 2.7** lists compositions of all the buffers used.

Table 2.7 SDS PAGE and Western Blot Buffers

Name of the buffer	Composition
SDS-PAGE	
SDS-PAGE Resolving gel	32.5% (v/v) 30% (v/v) Acrylamide 25% (v/v) solution 2 SDS-PAGE 1% (v/v) of 10% APS 0.1% (v/v) TEMED
SDS-PAGE Stacking gel	15% (v/v) 30% Acrylamide 30% (v/v) solution 3 SDS-PAGE 60% (v) H2O 1% (v/v) of 10% APS 0.1% (v/v) TEMED
Solution 2 SDS - PAGE	1.5M Tris-HCl pH8.8 0.3% (w/v) SDS
Solution 3 SDS -PAGE	0.5M Tris-HCl pH6.8 0.3% (w/v) SDS
10x Running Buffer pH 8.3	3% (w/v) Tris-base 14.4% (w/v) Glycine 1% (w/v) SDS
Loading blue 5x	10% (w/v) SDS 30% (v/v) Glycerol 0.02% (w/v) Bromophenol Blue 250mM Tris-HCl pH6.8 5% (v/v) β-mercaptoethanol
Staining Buffer	0.1% (w/v) Coomassie Brilliant Blue 50% (v/v) Methanol 10% (v/v) Acetic acid
Destaining Buffer	40% (v/v) Methanol 10% (v/v) Acetic acid 50% (v/v) Distilled water

Western Blots

Transfer Buffer	0.3% (w/v) Tris-base pH 8.3 1.44% (w/v) Glycine 20% (v/v) Methanol 1% (w/v) SDS
TBS	50 mM Tris- HCl pH7.5 150 mM NaCl
TBS-T	50 mM Tris- HCl pH7.5 150 mM NaCl 0.1% (v/v) Tween 20
TBS-T 5% Milk	50 mM Tris- HCl pH7.5 150 mM NaCl 0.1% (v/v) Tween 20 5% (w/v) non-fat milk

Agarose Gels

1-2% agarose gel	1-2% (w/v) Agarose TAE buffer 1 µg/mL Ethidium bromide
TAE Buffer	40 mM Tris-HCl 20mM acetic acid 1 mM EDTA

2.4 Proteoliposomes Preparation

2.4.1 Lipids Preparation

E. coli polar lipids and 1-Palmitoyl-2-oleoylphosphatidylcholine (POPC) (Mirandela *et al.*, 2018) were mixed at 2:1 ratio and dried using nitrogen gas and vacuum desiccation. Lipids were subsequently rehydrated in 3 mL liposome buffer (**Table 2.5**) at 5mg/mL. The mixture of multilamellar liposomes was extruded through a 100 nm pore filer using a Mini-extruder (Avanti Polar Lipids) to achieve a unimodal size distribution of unilamellar liposomes.

2.4.2 R_{sat} and R_{sol} Determination

To destabilise the liposomes for optimal protein insertion, Triton X-100 detergent was used. The addition of detergent disrupts lipid-lipid interactions, which results in a more permeable bilayer which is more receptive to protein insertion. As the liposomes are saturated with detergent, the liposome solution becomes increasingly turbid until Rsat is reach, then the turbidity decreases until the lipids solubilise completely (Rsol). (Rigaud, Paternostre and Bluzat, 1988; Rigaud, 2002). To determine Rsat/Rsol (**Figure 3.4, Section 3.4.1**), 1 µL Triton X-100 at 25% was successively added to 500 µL of liposomes (5mg/5mL), and the absorbance at 400nm, 500nm, 550nm and 600nm was measured using Nano-drop 2000/2000c spectrophotometer (ThermoFisher Scientific). Rsat value was used to estimate the final volume of Triton X-100 needed for protein insertion.

2.4.3 Insertion of the Membrane Protein into the Liposome

Detergent/lipid mixture was incubated at 300 rpm, 25°C for 5 minutes on orbital shaker. Following incubation, the protein was added at a lipid: protein ratio (LPR) of 5:1, 10:1, 50:1 and incubated at 300 rpm, 4°C for further 30 minutes. The same procedure was used to prepare protein-free liposomes by replacing the protein with SEC buffer (**Table 2.5**).

Detergent was removed by incubating with BioBeads SM2-Adsorbent Media, BIO-RAD (~0.2 g BioBeads/500 µL reconstitution mixture) at 4°C on a rotating wheel for 2 hours, followed by BioBead replacement and overnight incubation at 4°C under rotation.

2.4.4 Proteoliposomes Wash by Ultra-centrifugation

Subsequently the proteoliposomes were subjected to three successive washes by ultracentrifugation at 200,000 *g*, 4°C for 1 hour (Ti 90, Beckman Optima XPN-100), using liposome buffer. Finally, the proteoliposomes were suspended in liposome buffer (5 mg/mL of lipids), aliquoted in 50 µL, and stored at -80°C. (**Table 2.5**).

The quantity of protein inserted in liposomes was assessed via SDS-PAGE analysis (**Figure 3.5**). 15 µL of proteoliposomes (5mg/ml) containing each variant at a LPR of 5:1, 10:1, or 50:1 (w/w) were run on 10% SDS-PAGE gels alongside proteoliposomes containing WT Rh50 at LPR 5, demonstrating that the quantity of protein inserted is similar for all variants and varied according to LPR.

The size distribution of proteoliposomes was measured via dynamic light scattering (DLS) using a Zetasizer Nano ZS (Malvern Instruments). This showed that the proteoliposomes had an average diameter of 110 nm (**Figure 3.6**).

2.4.5 Orientation of the Rh50 Protein in the Liposome

Following successful Rh50 protein insertion into artificial liposomes the orientation of the protein in the liposome was established via proteolysis analysis using trypsin. Liposomes containing Rh50 were digested with sequencing grade modified trypsin (Promega) at 20:1 (w/w) protein:trypsin ratio for 30 minutes at 37°C, according to manufacturer's instructions. The samples were mixed with the loading blue buffer, loaded onto two identical SDS page gels and run at 150V*cm^{-1} for 60 minutes in running buffer as

described before **(Section 2.3.8).** One gel was then stained with Coomassie Blue for 30 minutes and de-stained for 15 minutes. Second gel was prepared for western blotting as described before (**Section 2.3.9**).

2.5 Preparation of Rh50 Vesicles Directly from *E. coli* Membrane

Purification of membrane protein of eukaryotic origins in heterologous systems is very difficult and often not possible (Lacapère *et al.*, 2007; Carpenter *et al.*, 2008). To overcome this problem, the vesicles can be prepared directly from the membrane, from the organism of choice, as described before with minor modifications (Kaback, 1974; Kaback *et al.*, 1977).

2.5.1 Peptidoglycan Removal

Protein of interest was overexpressed and harvested as previously described in **2.3.2 Overexpression** section.

The pellet was resuspended in 30 mM Tris pH 8 containing 20% sucrose using homogeniser and the content was transferred into 100 ml flask. EDTA (pH 7.0) and lysozyme (Worthington, crystalline) are added to final concentrations of 10 mM and 0.5 mg/mL, respectively, and the suspensions were incubated for 30 minutes at room temperature on the orbital shaker. EDTA and alkaline pH exposes the rigid peptidoglycan layer to lysozyme (muramidase) an N-acetylhexosamidase, which weakens it.

2.5.2 Spheroplast Formation

To prepare the membrane and create the spheroplasts the lysed cells were centrifuged at 16,000 *g* for 30 min (JA 25-50, Beckman Avanti JXN-26). The pellet was resuspended in a small volume of 0.1 M potassium phosphate pH6.6 containing 20% sucrose, 20 mM MgSO4, DNase/RNase at 100 µ/ml using a glass homogeniser. The homogenized, concentrated spheroplast suspension is poured directly into 300-500 volumes of 50 mM potassium phosphate buffer, pH 6.6, which has been equilibrated to 37°C. The lysate is incubated for 15 minutes at 37°C with vigorous swirling. Potassium EDTA at pH 7.0, is then added to 10 mM final concentration, and the incubation is

continued for 15 minutes. During this time, the turbidity of the suspension decreases and the viscosity increases. To decrease the viscosity, magnesium sulphate is added to a final concentration of 15 mM and incubated for another 15 minutes at 37°C. During this step the membrane reanneals by an unknown mechanism, yielding closed, empty membrane vesicles (Kaback, 1974).

2.5.3 Isolation of Membranes

The lysates are centrifuged at 16000 *g* for 30 min (JLA 9.100, Beckman Avanti JXN-26) and resuspended by homogenisation in 10 mL of 0.1 M potassium phosphate buffer, pH 6.6, containing 10 mM EDTA at 0°C.

2.5.4 Removal of Cell Debris

Cell debris was removed by two centrifugations at 800 *g* for 30 min (JA 25-50, Beckman Avanti JXN-26). The low-speed centrifugation removes the whole cells and partially lysed cells. The yellowish, milky, supernatant fluid is carefully decanted and centrifuged at 45,000 *g* for 45 min at 4ºC (Ti 90, Beckman Optima XPN-100), until the pellet is clear.

2.5.5 Washing of Isolated Membranes

Obtained pellet, containing protein vesicles, was subjected to three successive washes by ultracentrifugation at 45 000 *g*, 4°C for 45 min, in liposome buffer **(Table 2.5 Compositions of solutions used).** After the last wash, the membranes were resuspended in liposome buffer, at a concentration of 5-10 mg/mL, aliquoted in 50µL, and stored at -80°C. Composition of buffers used for membrane preparation is listed in **Table 2.8**.

Table 2.8 Buffers used for membrane preparation

Tris Buffers	30 mM Tris-HCl pH 8 20 % sucrose (+ 10 mM EDTA; 0.5 mg/ml Lysosyme)
Potassium Phosphate Stock Solution	1 M KH_2PO_4 1 M K_2HPO_4 pH 6.6
Potassium Phosphate Buffers	0.1 M potassium phosphate pH 6.6 20 % sucrose 100 µ/ml DNase/RNaes 20 mM $MgSO_4$ 50 mM potassium phosphate pH6.6 (+ 10 mM EDTA; 15 mM $MgSO_4$) 0.1 M potassium phosphate pH 6.6, 10 mM EDTA

2.6 Solid Supported Membrane Electrophysiology (SSME)

The basis of this technique is a gold-coated sensor chip with an alkylmercaptane monolayer on top (**Figure 2.1**). The SSM is formed by adding lipid and rinsing the electrode with buffer. The SSM on the sensor chip is the measuring electrode which is coated with the membrane preparation containing the protein of interest.

2.6.1 Sensors Preparation

Gold-coated sensors chips (Nanion Technologies, Munich-Germany) are the basis of this technique and were prepared as previously described (Bazzone, Barthmes and Fendler, 2017). Briefly, sensors were coated with 50µL of thiol (1-octadecanethiol in isopropanol 0.5mM solution) and incubated for 1 hour at 4°C. Solution was removed and sensors were rinsed three times with 10mL 2-propanol and 10mL deionised water. Dry sensors were subsequently coated with 1.5µL of 1,2-diphytanol-*sn*-glycerol-3-phosphocholin solution and 100µL of non-activated (NA) buffer (**Table 2.9**) was immediately added to form solid supported membrane (SSM). The SSM on the sensor chip is the measuring electrode. Proteoliposomes/protein-free liposomes or membrane vesicles were defrosted and sonicated (U300H Ultrawave Precision) at 35W for ~10 seconds, diluted 10-fold in NA buffer pH 7 (unless stated otherwise) and 10 µL of solution was applied to the SSM on the sensor. Sensors were then centrifuged at 2500 *g* for 30 minutes and stored at 4°C for a maximum of 48h before electrophysiological measurements. For the measurements the sensor is placed inside a Faraday cage and connected to a fluidic system which allows fast solution exchange.

2.6.2 Single Solution Exchange

For functional measurements at a fixed concentration, a single solution exchange configuration was used where Non-Activating (NA), Activating (A) and NA buffers were injected on the sensor over constant osmolarity at a 200µl/s flow rate (Bazzone, Barthmes and Fendler, 2017). The activating solution contains the substrate (at a desired concentration) of the transporter immobilized on the SSM. Therefore, the NA-A solution exchange generates a substrate concentration gradient which drives the electrogenic transport reaction leading to an increase of the potential inside the adsorbed proteoliposomes/vesicles (**Figure 2.1 B**). Due to capacitive coupling, this leads to a charging current in the external measuring circuit (on-signal) (**Figure 2.1 D**), which is recorded by the amplifier. The subsequent switch to non-activating solution generates the opposite substrate concentration gradient and therefore restores initial conditions. A transient current with opposite sign is recorded (off-signal, not shown).

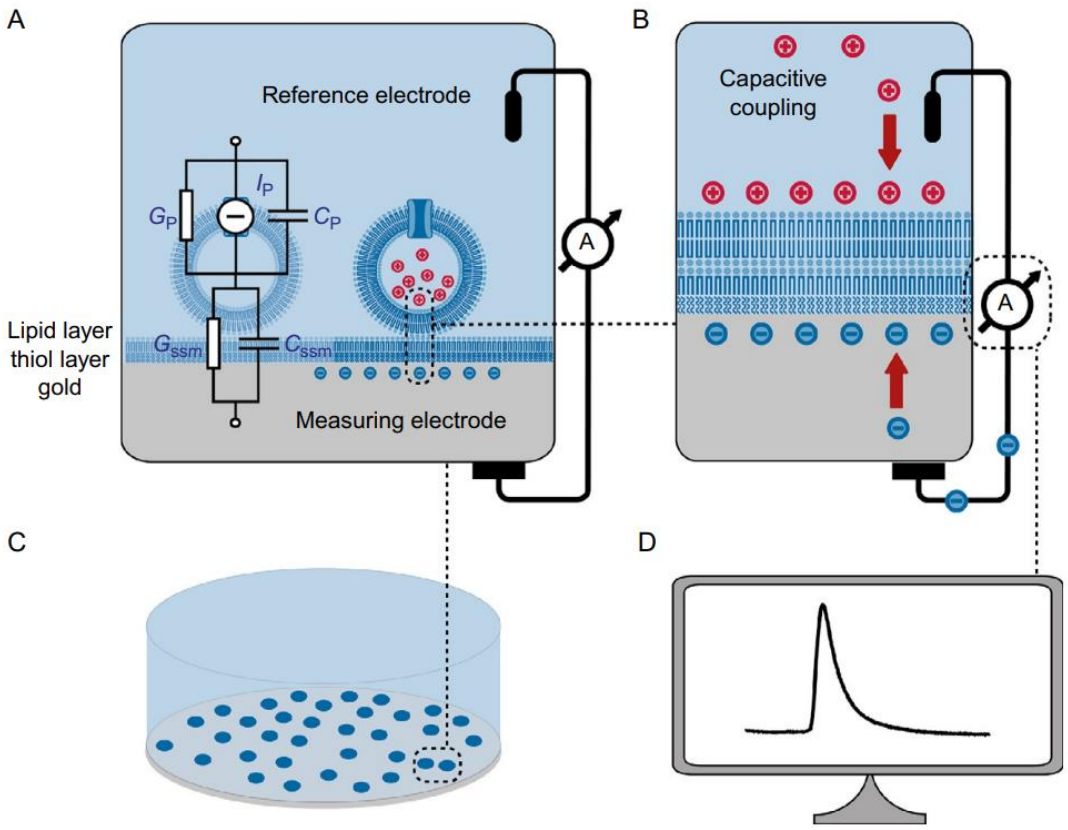

Figure 2.1 Measurement principles of SSM-based electrophysiology. (A) Adsorbed proteoliposomes on the SSM. The compound membrane forms a capacitively coupled system. Both membranes proteoliposomes (P) and SSM can be described using their capacitance C and conductance G. Electrogenic transport charges the proteoliposomal membrane which is accompanied by the charging of the measuring electrode. B) Expansion of the interface of the SSM and the proteoliposomal membrane. Charging of the membranes leads to a current flow in the external measuring circuit which is recorded by the amplifier (A). C) Millions of proteoliposomes adsorbed to the SSM contribute to the measured current. D) Currents measured at the SSM are in general transient currents. Figure from Bazzone, Barthmes and Fendler, 2017.

Table 2.9 Solid Supported Membrane Electrophysiology solutions

Substrate	Activating	Non-Activating
Ammonium	100 mM KPho	100 mM KPho
	100 mM KCl	300 mM KCl
	200 mM NH_4Cl	
Potassium	100 mM NaPho	100 mM NaPho
	100 mM NaCl	300 mM NaCl
	200 mM KCl	

**All solutions adjusted to pH 7 using KOH or NaOH solutions.*
KPho: potassium phosphate buffer, NaPho sodium phosphate buffer.

2.6.3 Double Solution Exchange

A pH gradient was generated by sequential passage of 200 µL of (NA) solution and (A) to establish the outside proteoliposomal pH, followed by a 15-minute incubation time in resting (R) NA solution. This incubation adjusts the inner proteoliposomal pH to the pH of R creating a pH gradient at the start of each measurement as visualised in **Figure 2.2** (Bazzone *et al.*, 2016). Using this approach, both inwardly and outwardly H^+ orientated gradients were set-up. The same programme was applied to check whether *Ec*AmtB and *Ne*Rh50 can translocate the H^+ into the cell in absence of the substrate. **Table 2.9** lists compositions of the solutions used.

The measurements were carried out in triplicate, from two independent purification batches, with 3 measurements recorded for each sensor at room temperature using a SURFE^{2}R N1 apparatus (Nanion Technologies) (Bazzone, Barthmes and Fendler, 2017). Protein-free liposomes (liposomes not containing the protein) or membrane vesicles not expressing the protein or interest were used as a control. Prior to measurements, the quality of the sensor was checked by measuring the capacitance (15–30nF) and conductance (<5nS). Sensors out-with above ranges were discarded.

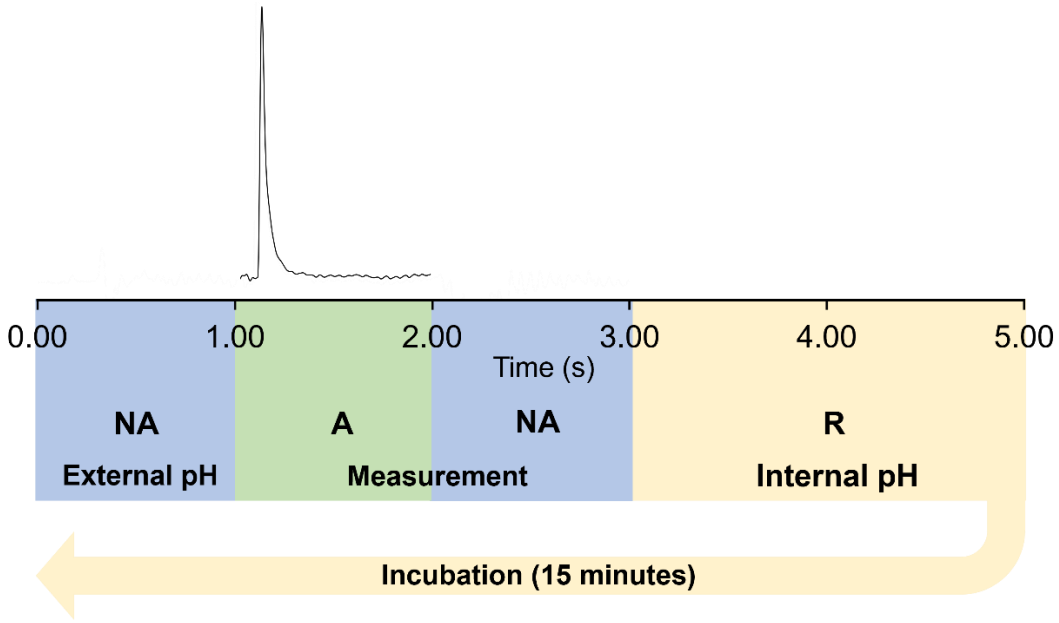

Figure 2.2. Schematic representation of the double solutions exchange protocol for SSME measurement. The bottom bar shows the flowtime sequence of each solution. The incubation time of 15 minutes adjusts the intraliposomal pH to the pH of resting solution (R). Following the incubation, the pulse of non-activating (NA) solution establishes a pH gradient (NA → R). After 1s the activating (A) solution provides ammonium and initiates a symport activity under pH gradient conditions and the transient current is recorded (Bazzone et. al., 2016).

2.6.4 Data Representation and Analysis

Solid Supported Membrane Electrophysiology (SSME) measures the charge translocation across a membrane in an electric circuit manner. SSME records this as a transient current which provides two information, namely a pre-steady and a steady state current. The former represents the interaction between the protein and the substrate, whilst the latter represents translocation cycle, which is the interaction and the transport of the substrate (Bazzone, Barthmes and Fendler, 2017).

2.6.4.1 Decay Time

To differentiate the signal which arise from substrate-protein interaction, from signal reflecting full transport cycles, the decay time of the transient current, which is proportional to the velocity of the complete transport cycle, was analysed (Bazzone, Barthmes and Fendler, 2017). The decay time of the transient current was calculated by fitting the raw data with one-phase exponential decay function (equation below) between the maximum height of the peak and the baseline using OriginPro 2018 (OriginLab).

$$\boldsymbol{y = y_0 + A_1 e^{-x/t_1}}$$

The fit was obtained using the Levenberg-Marquardt iteration algorithm, where x and y represent coordinates on the respective axis, y0 represents the offset at a given point, A represents the amplitude, and t is the time constant.

2.6.4.2 Kinetics

The measurements were carried out using ammonium/methylammonium concentration ranging between 98 µM to 200 mM. The maximum amplitude measured at each concentration was fitted according to Michaelis-Menten equation. The kinetic parameters (K_m, V_{max}) were calculated using Graphpad Prism v6 software.

Chapter 3

Chapter 3: Purification of WT *Ne*Rh50 and Development of an Assay for Functional Characterisation.

3.1 Introduction

A prevalent view was that Amt proteins acts as electrogenic transporters for NH_4^+ ammonium, whereas Rh proteins acts as passive channels for NH_3 (ammonia) or/and CO_2 (Huang and Peng, 2005). From a functional perspective the two modes of transport significantly differ. Transporters involve selective binding of the substrate and undergo a series of conformational changes to transfer the bound solute across the membrane against its electrochemical gradient. Channels, on the other hand, facilitate the translocation of the substrate down the electrochemical gradient, involving little interaction between the substrate and the protein and no conformational changes (Wirén and Merrick, 2004; Andrade and Einsle, 2007).

While Amt/Mep and Rh were divided into two categories of proteins, transporters and channels, respectively, there are no significant differences in the crystal structures of Amt and Rh proteins, that can clearly account for these functional differences (Khademi *et al.*, 2004; Lupo *et al.*, 2007; Gruswitz *et al.*, 2010). As extensively described in the introduction of this thesis, the so called “translocation pore” is highly conserved within the family, and the presence of the hydrophobic pore in its centre strongly suggest that all members of Amt/Mep/Rh family would only allow transport of neutral species (Khademi *et al.*, 2004; Andrade *et al.*, 2005; Lupo *et al.*, 2007; Pflüger *et al.*, 2018). However, multiple studies proved that Amt proteins are supporting electrogenic transport (Wacker *et al.*, 2014; Williamson *et al.*, 2020). Why have Amts and Rh been differentiated into two groups (transporters and channels) with supposedly different mechanisms and substrates?

3.1.1 Human Rh Proteins

Since Marini *et al* provided first evidence that human Rh mediates transport of ammonia using yeast growth complementation assay (Marini *et al.*, 2000a), many studies focused on deciphering the mechanism and substrate translocated (NH_4^+ vs NH_3). Throughout the decades of research scientists reported that human rhesus proteins facilitate translocation of neutral NH_3 (Ludewig, 2004; Ripoche *et al.*, 2004; Mouro-Chanteloup *et al.*, 2010), as well as ionic NH_4^+ species (Hemker *et al.*, 2003; Nakhoul *et al.*, 2005). Some argued that both, NH_3 and NH_4^+, forms are translocated in parallel (Bakouh *et al.*, 2004; Benjelloun *et al.*, 2005). Lastly, it was proposed that Rh proteins might play a role in CO_2 transport too (Kustu and Inwood, 2006;Endeward *et al.*, 2008; Musa-Aziz *et al.*, 2009). For more detailed analysis and in-depth discussion of research carried out on each of human rhesus proteins refer to **Chapter 1** (**Section 1.7.6**). While all the functional studies provided insights into the Rh-mediated ammonium transport mechanisms, the transported substrate (CO_2/NH_3 or NH_4^+) remained a controversial topic. While it is possible that Rh proteins can differ functionally, all mentioned above studies used heterologous systems, where presence of endogenous transporters or acid-base regulating proteins might have interfered with the NH_4^+ transport. The lack of suitable assays for functional characterisation hinders the understanding of ammonia translocation by human Rh proteins. In addition, the characterisation of human transport systems is often very difficult, as the proteins are very large and integral membrane proteins very challenging to handle (Lacapère *et al.*, 2007). Thus, it is timely to explore new and more reliable approaches and systems to investigate the mechanism of Rhesus proteins.

3.1.2 Bacterial Rh50 Protein from **Nitrosomonas europaea**

The ammonium oxidizing (AMO) bacteria *N. europaea* is capable of ammonium uptake at high rates and can accumulate ammonia during ammonia oxidation to an internal concentration of about 1 M (Schmidt *et al.*, 2004). These suggests the presence of active ammonium transport system. However, the first complete genome sequence revealed that *N. europaea*

does not possess any *amt* genes. Instead, it was found that it possesses *rh* genes named *rh50* (Huang and Peng, 2005). An unwashed transport assay, demonstrated that the uptake rate of ammonium analogue, methylammonium MeA) in *rh50*-knock out (KO) cells was five times lower in comparison to WT *N. europaea* cells (Cherif-Zahar *et al.*, 2007). The restoration of ammonium-dependent growth to a yeast *Δmep* mutant by Rh50 was more effective at higher pH values, which provided initial evidence to support that Rh50 translocate NH_3 rather than NH_4^+ (Cherif-Zahar *et al.*, 2007; Weidinger *et al.*, 2007). This was first experimental data proving that Rh50 protein is involved in ammonium uptake and has functionally replaced Amts in *N. europaea*. However, just like in case of human Rh, the actual mechanism of bacterial Rh50 in translocating ammonium into the cell was not understood at the time.

Soon afterwards, the Rh50 protein was purified, and its structure solved (Lupo *et al.*, 2007; Li *et al.*, 2007). Like other ammonium transporters, crystal structure of *N. europaea* Rh50 also revealed the presence of the hydrophobic pore in the centre of the transporter suggesting transport of the neutral NH_3 species (Lupo *et al.*, 2007; Li *et al.*, 2007). It was revealed that structurally defined region Rh50 and RhAG share 64.9% sequence similarity (Lupo *et al.*, 2007), suggesting that architecture and structure of bacterial rhesus is highly representative of all Rh proteins. The common features between bacterial Rh50 and human Rh proteins imply a conserved function and mechanism across enormously distant phylogenies. Furthermore, sequencing analysis provided evidence that Rh50 clusters more closely with human Rh proteins, as opposed to Rh50 from other organisms (Huang and Peng, 2005), justifying the choice even more **(Figure 1.4).**

3.2 Aims and Objectives:

Following Monod's famous dictum, "Anything found to be true of *E. coli* must also be true of elephants" we want to investigate the mechanism of Rh50 protein from *Nitrosomonas europaea,* one of the simplest organisms to have Rh proteins which seems to have functionally replaced Amts. The common features between bacterial and human Rh proteins present Rh50 as a perfect candidate for the model system to investigate the mechanism of ammonium transport in all Rh proteins. The residues, which mutations in the human orthologues leads to diseases, are conserved in the bacterial homologues, further justifying the choice of bacterial Rh50 transporter as a tractable model system in the context of human Rh physiopathology.

Therefore, in this chapter, we will fully disclose the purification process of Rh50 protein from *N. europaea* and develop an electrophysiology assay to characterise the transport mechanism of Rh50 (**Chapter 4 and 5**). The primary technique used to achieve this was Solid-Supported Membrane Electrophysiology (SSME) which has been successfully utilised by our group in characterising the activity of AmtB ammonium transporter from *E. coli.*

The aims were to:

1. Optimise the overexpression and purification of *Ne*Rh50.
2. Insert Rh50 into liposomes and characterise the proteoliposomes obtained (size, protein orientation).
3. Develop an assay to measure the activity Rh50 using solid supported membrane electrophysiology (SSME).

3.3 Purification of *Ne*Rh50

3.3.1 Over-expression of Rh50

Rh50, cloned into the plasmid pAD7 (**Table 2.4**) was heterologously expressed in *E. coli* strain GT 1000 (Δ*glnK,amtB)* with a hexa-histidine tag at its C terminus. In pAD7, Rh50 expression is controlled by the native promoter of the *E. coli glnK amtB* operon, activated by α-glutamine (N-source) in M9 media. The choice of pAD7 background for heterologous overexpression of Rh50 was motivated by the finding that overexpression of Rh50 in *E. coli* using a pET derivative produces unstable protein (unpublished data, Dr. Arnaud Javelle). The strain GT 1000 (*ΔglnK,amtB)* was used to avoid the potential formation of heterooligomer composed of AmtB and Rh50 protein.

Before proceeding with a large-scale over-expression, we first wanted to estimate if the presence of the pAD7 plasmid is toxic to the GT 1000 strain. Specific growth rate comparison of the GT 1000 vs GT 1000 containing pAD7 in LB media revealed no significant difference (0.483 ± 0.05 h^{-1} for GT 1000 and 0.478 ± 0.05 h^{-1} for GT 1000 containing the construct, p = 0.81) (**Figure 3.1 A**). These results indicate that the presence of pAD7 is not inducting toxicity to GT 1000 *E. coli* strain.

Next, we wanted to establish whether the overexpression of Rh50 induce toxicity to the cells. The overexpression of Rh50 is induced in the presence of glutamine but repressed in the presence of ammonium. Therefore, the growth analysis of the GT 1000 containing pAD7 in M9 media supplemented with either 0.2 mg/mL glutamine or 1.07 mg/mL NH_4^+ as sole nitrogen source was carried out. There were no significant differences in the specific growth rates of GT 1000 in M9 media supplemented with NH_4^+ or α-glutamine (0.31 ± 0.006 h^{-1} and 0.31 ± 0.007 h^{-1}, respectively, p = 0.9) (**Figure 3.1 B**). This suggests that the overexpression of histidine tagged Rh50 protein is not toxic to the cells.

Taken together, these results indicate that the large-scale overexpression can be carried out. It will also allow for comparison of growth between GT 1000 strain overexpressing variant of the Rh50 protein to the WT Rh50 in the future (**Chapter 4 and 5**).

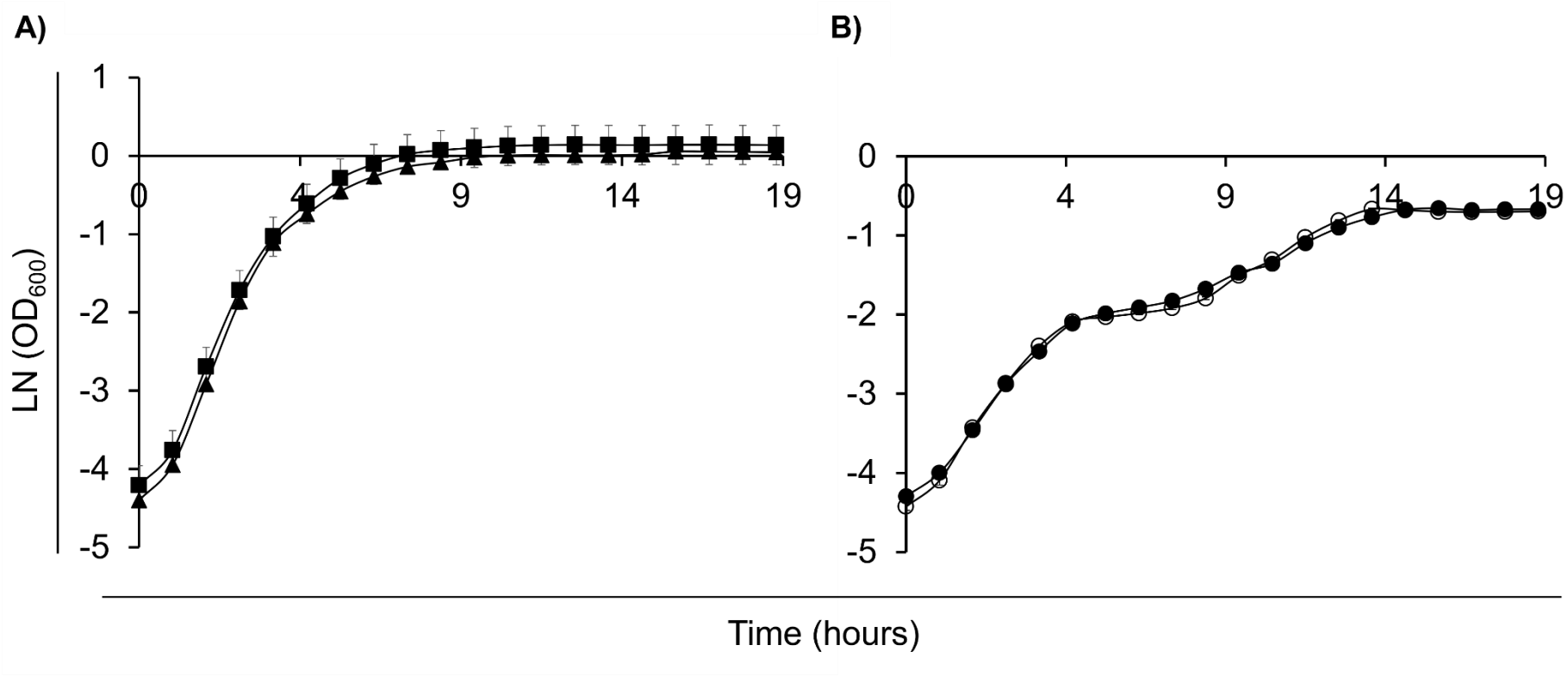

Figure 3.1 Specific growth rate analysis. A) GT 1000 strain (▲) and GT 1000 + pAD-7 (■) grown in LB. B) GT1000+ pAD7 in M9 minimal medium supplemented either with 1.07 mg/mL NH_4^+ (○) or 0.2 mg/mL glutamine (●) a s a sole nitrogen source (±SD, n=3, p value achieved with Tukey HSD test).

3.3.2 Immobilised Metal Affinity Chromatography

For Rh50 purification, the membrane fraction of *E. coli* containing Rh50 was isolated and solubilised in 2% LDAO, before being diluted to a final concentration 1% LDAO. Following ultracentrifugation, the sample was loaded onto a 1 mL Histrap column with cobalt coated Sepharose. The column was washed with 10 mL with IMAC buffer containing 40 mM imidazole to wash away non-specifically bound proteins. Rh50 was eluted using an imidazole gradient, rising from 40-500 mM over 20 mL. The absorbance at 280 nm on the chromatograph shows that Rh50 bound to the cobalt coated column, elutes between 100 and 200 mM of imidazole (**Figure 3.2 A**).

To confirm that the eluted sample is indeed the protein of interest, the elution fraction was analysed via western blot using anti-His antibodies. A major fluorescent band of ~34 kDa, corresponding to Rh50 monomer (M) (theoretical molecular weight for Rh50 monomer is ~ 43 kDa) was detected (**Figure 3.2 B**). A small amount of the Rh50 ran as a higher-molecular-mass species (~ 74 kDa) that most certainly correspond to Rh50 trimer (T). To estimate the purity of the sample, the membrane solution (MS), flow through (FT), wash (W), and the elution fractions across the peak were analysed by SDS-PAGE Coomassie Blue-stained gel. Similarly, the monomer is observed at ~ 34 kDa, while the trimer at ~ 74 kDa (**Figure 3.2 C**), It should be noted, that the anomalous migration of membrane proteins on SDS-PAGE is common and is likely due to partial unfolding of the hydrophobic domain of the protein in SDS (Rath *et al.*, 2009).

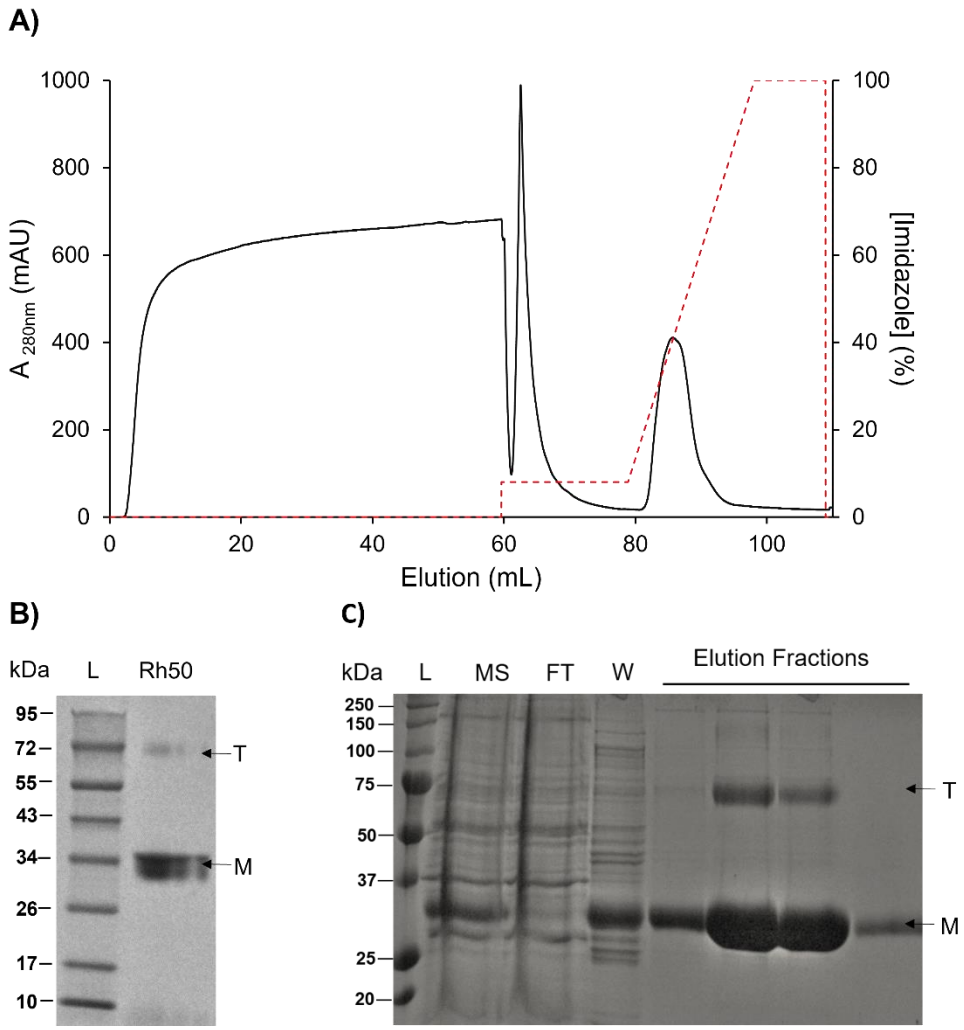

Figure 3.2 Purification of WT Rh50 A) IMAC profile of the wash and elution of *Ne*Rh50 from solubilised *E. coli* membrane. The solid black line represents A 280nm and the dotted red line represents the concentration of imidazole as a percentage (100% = 500 mM). B) Western Blot analysis of elution fraction using anti-His antibody. C) 12.5% SDS-PAGE Coomassie Blue-stained gel. Ladder (L); Membrane solution (MS), flow through (FT), wash (W), and elution fractions across the peak, Trimer (T), Monomer (M).

3.3.3 Size Exclusion Chromatography

After the IMAC, the elution fractions containing Rh50 were pooled together and concentrated to 5 mg/mL. The sample was injected (300 µL) on a Superdex S200 10/300 size exclusion chromatography (SEC) column. Throughout the purification process, the protein was continuously monitored by absorbance at 280 nm. Rh50 eluted as a single peak without any protein present in the void-volume indicating that the protein did not aggregate. While the protein elutes as a single peak, a small shoulder appears around 12 mL elution volume. This could be due to a presence of two different conformations of the protein in the sample. Nevertheless, the fractions of the elution peak analysed via SDS-PAGE revealed that the sample was pure, and as before, the Rh50 monomer appeared at ~34kDa (**Figure 3.3 inset)**

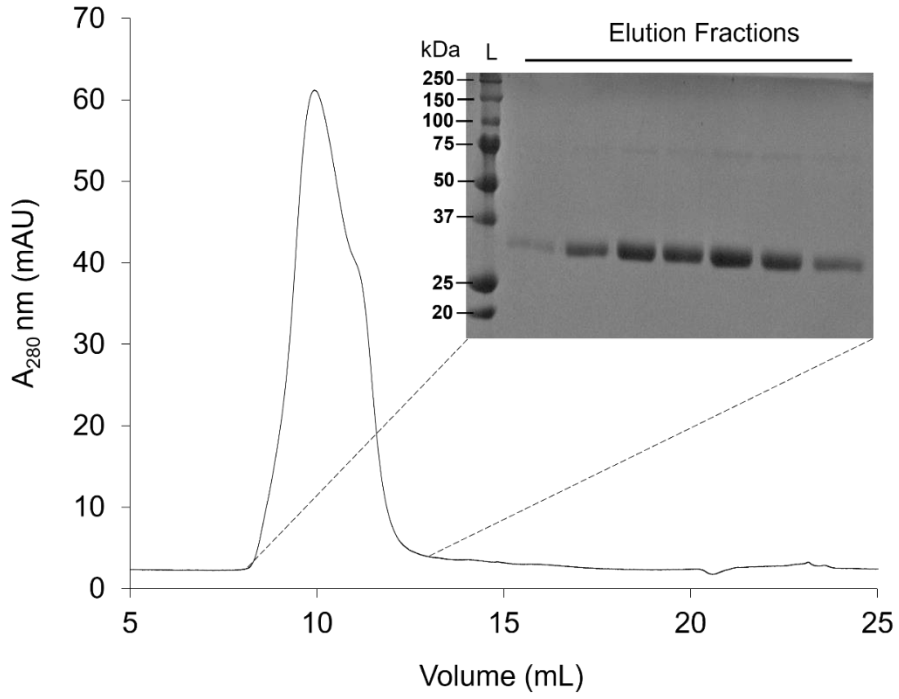

Figure 3.3 Size Exclusion Chromatography of *Ne*Rh50: Chromatogram of *Ne*Rh50 solubilised in 0.09% LDAO and injected onto a Superdex 200 increase (10/300) column. Inset: 12.5% SDS-PAGE Coomassie Blue-stained gel of fractions within the elution peak.

3.4 Proteoliposome Formation and Characterisation

3.4.1 Destabilisation of the liposomes: Rsat and Rsol Coefficients

A mixture of *E. coli* polar lipids and 1-palmitoyl-2-oleoyl-sn-glycero-3-phosphocholine (POPC) at a 2:1 ratio (wt/wt) was used to prepare liposomes. Functional studies on AmtB from *E. coli* from our lab proved AmtB is correctly inserted in this lipids mixture and it completes a full transport cycle (Mirandela *et al.*, 2018). We therefore followed the same conditions to prepare liposomes for Rh50 insertion to make comparisons between AmtB and Rh50 possible in the future.

To facilitate the optimal insertion of Rh50, the liposomes must be destabilised with a detergent. Such insertion occurs when the liposomes are at the onset of solubilisation and are saturated with detergent (Rsat). Any further addition of detergent results in total solubilisation of the liposomes reaching the onset of solubilisation (Rsol) (Rigaud, Paternostre and Bluzat, 1988; Rigaud, 2002).

To determine Rsat/Rsol, 1 µL of 25% Triton X-100 was added to 500 µL of liposomes (5mg/5mL) stepwise, and the absorbance at 400nm, 500nm, 550nm and 600nm was measured to track the change in liposome stability. The liposomes become increasingly saturated with detergent and swell, increasing the turbidity of the solution and in turn, its absorbance (**Figure 3.4**). After Rsat, the absorbance decreased with the addition of detergent due to total solubilisation of the liposomes, reaching a baseline after 9 µL of 25% Triton X-100 was added (**Figure 3.4**). The optimum amount of Triton X-100 for protein insertion was found to be 2.4 µL of Triton X-100 at 25% (w/v) per mg of lipid.

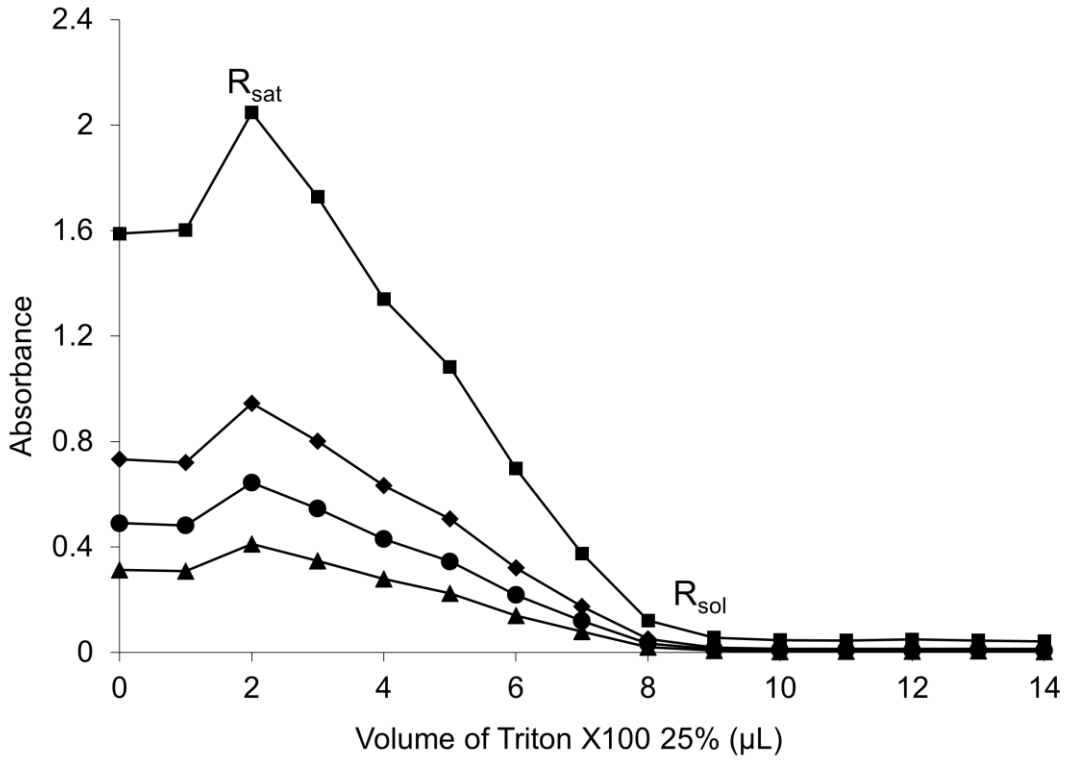

Figure 3.4 Determination of Triton X-100 volume needed for protein insertion. The detergent/lipid ratio between the onset of solubilisation (Rsat) and the total solubilisation (Rsol) constants was established via sequential addition of 25% Triton X-100 to liposomes (5mg/5mL). The absorbance of liposome/Triton X-100 mixture at 400nm (■), 500nm (♦), 550nm (●) and 600nm (▲) was measured using Nano-drop 2000/2000c spectrophotometer (ThermoFisher Scientific). R_{sat} value was used to estimate the final volume of Triton X-100 needed for protein insertion.

3.4.2 Insertion of Rh50 into proteoliposomes

Rh50 solubilised in LDAO (5 mg/mL) was mixed with the triton X100-distabilised liposomes. To allow for the insertion of Rh50 into the lipid bilayer, Triton X-100 surfactant and LDAO detergent were removed using hydrophobic beads (SM2 Biobeads). Following an overnight incubation with SM2 Biobeads, the proteoliposomes were subjected to three washing steps. An aliquot of the supernatant from each wash step was analysed on an SDS-PAGE gel. As shown in **Figure 3.5 A** no protein was observed in any of the wash fractions, while a single band corresponding to Rh50 was visible in the proteoliposome fraction.

Additionally, the quantity of protein inserted in liposomes at different Lipid to Protein Ratios (LPRs) was assessed via SDS-PAGE analysis. Proteoliposomes (5mg/ml) containing Rh50 at a LPR of 5:1, 10:1, or 50:1 (w/w) were run on SDS-PAGE demonstrating that the quantity of protein inserted is proportional to LPR (**Figure 3.5 B**). Taken together, these results show that Rh50 is successfully inserted into the liposomes.

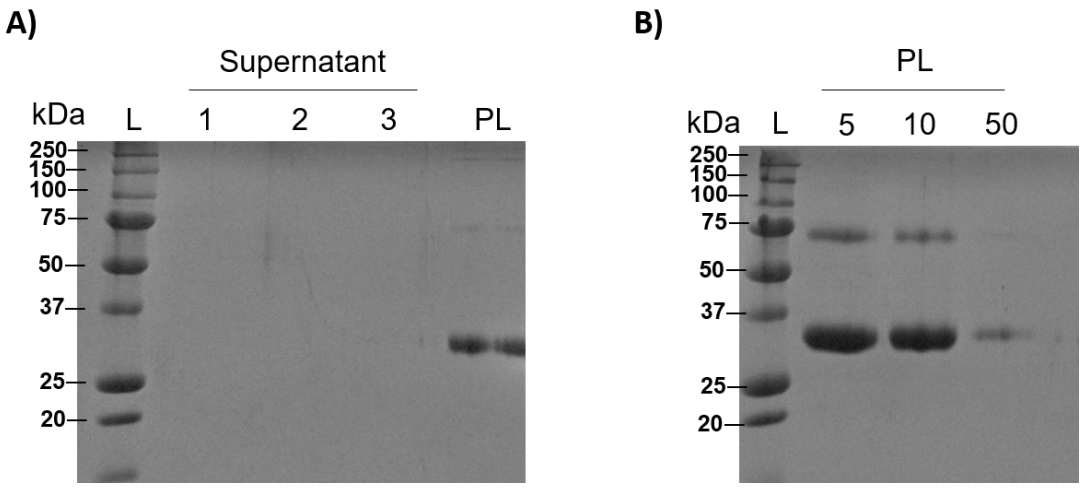

Figure 3.5 Insertion of Rh50 into Liposomes. A) 12.5% SDS-PAGE Coomassie Blue-stained gel monitoring the wash protocol. The lines correspond to L=Ladder, 1-3 supernatant from each wash step, PL = a proteoliposomes at LPR 5. B) 12.5% SDS-PAGE Coomassie Blue-stained gel monitoring the quantity of protein inserted into liposomes. The lines correspond to L=Ladder, and PL = proteoliposomes at LPR 5, LPR10, and LPR50.

3.4.3 Size Distribution of Proteoliposomes

The transient current observed via SSME is due to the accumulation of charge within the liposome and is therefore dependent on the volume of the liposomes. Hence, to allow the direct comparison of the transient current observed in liposomes/proteoliposomes at different LPRs, it is important to check that all samples contain liposomes of the same size.

The size of the liposomes and proteoliposomes was determined by dynamic light scattering (DLS). DLS allows to determine the size of liposomes by recording their motion in the solution via light scattering detectors set at certain angles. Here, an auto-correlation function was applied to derive the particle size distribution. The DLS analysis confirmed that the empty liposomes and proteoliposomes followed a unimodal size distribution, with a mean diameter of ~110 nm (**Figure 3.6**). This indicates that the insertion of Rh50 does not affect the size distribution, nor does it lead to liposomes aggregation.

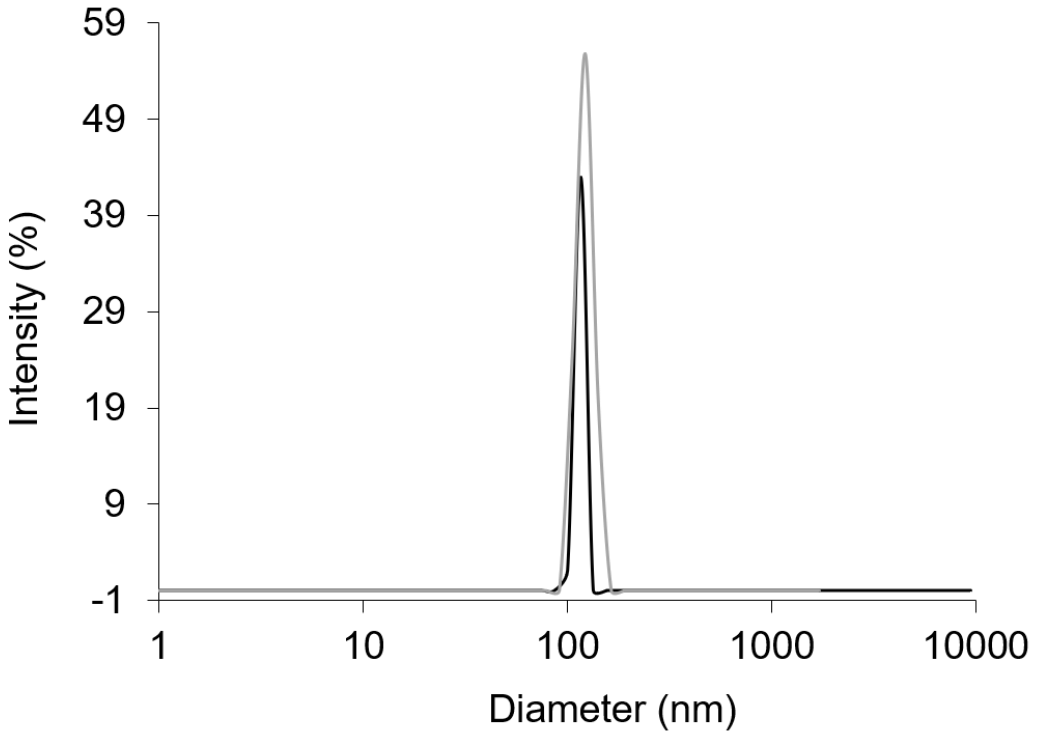

Figure 3.6 DLS analysis of Rh50 inserted into liposomes: Comparison of size distribution of empty polar/POPC 2/1 liposomes (grey) and Rh50 Polar/POPC 2/1 proteoliposomes LPR 10 (black) via DLS analysis.

3.4.4 Orientation of Rh50 in the Liposome

Following successful Rh50 protein insertion into artificial liposomes, the orientation of the protein inserted into the liposome was clarified via proteolysis analysis using trypsin. Briefly, trypsin is a serine protease which cleaves at the carboxylic side of lysine and arginine residues. Rh50 possesses a long C-terminal tail (**Figure 3.7**), and if the protein is inserted inside out (IO), where C- terminal tail is located outside of the liposome, it will be cleaved off by the trypsin (**Figure 3.8 A**). This in turn should change the apparent molecular weight of the protein, and thus how it migrates through the SDS-PAGE gel. Right-Side-Out (RSO) orientation would protect the C-terminal tail from the trypsin lysis.

The samples were digested with sequencing grade modified trypsin at 20:1 (w/w) protein:trypsin ratio for 30 minutes at 37°C. In the case of mixed population orientation of Rh50 in the liposome, trypsin will only cut the exposed C terminal off when the protein is in IO orientation (**Figure 3.8 A**). As seen in **Figure 3.8 B** there is a clear drop in protein size following trypsin digest. To further investigate the orientation of the protein, the same sample were analysed by western blot using anti-His antibody. If there was a mixed IO and RSO orientation of Rh50 in the liposome, less fluorescent emission would be expected in trypsin digested sample because the histidine tag at the C-terminus of IO orientated protein would be cleaved off. **Figure 3.8 C** shows a clear difference in the fluorescence emission in control versus trypsin treated proteoliposome.

As a control and to determine the efficiency of the lysis reaction, the liposomes were solubilised using detergent and subjected to trypsin lysis. In presence of 1.25% Triton X-100 or 1% DDM no fluorescence was detected, indicating that all the His-tagged C-termini of Rh50 protein were cleaved-off, confirming efficiency of lysis via trypsin. Taken together, these results show that Rh50 insertion into liposome is a mixture of IO/RSO.

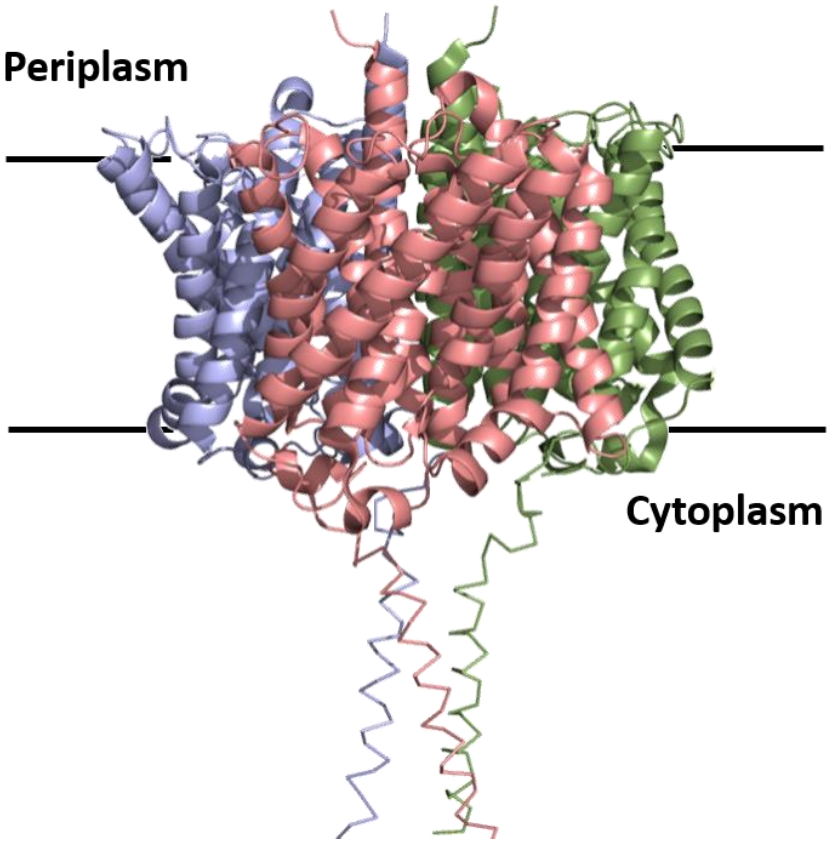

Figure 3.7 Crystal structure of *Ne*Rh50. The ribbon representation shows a side view with the approximate bilayer boundaries indicated. The C-terminal segments showing only backbone density are shown as Cα traces.

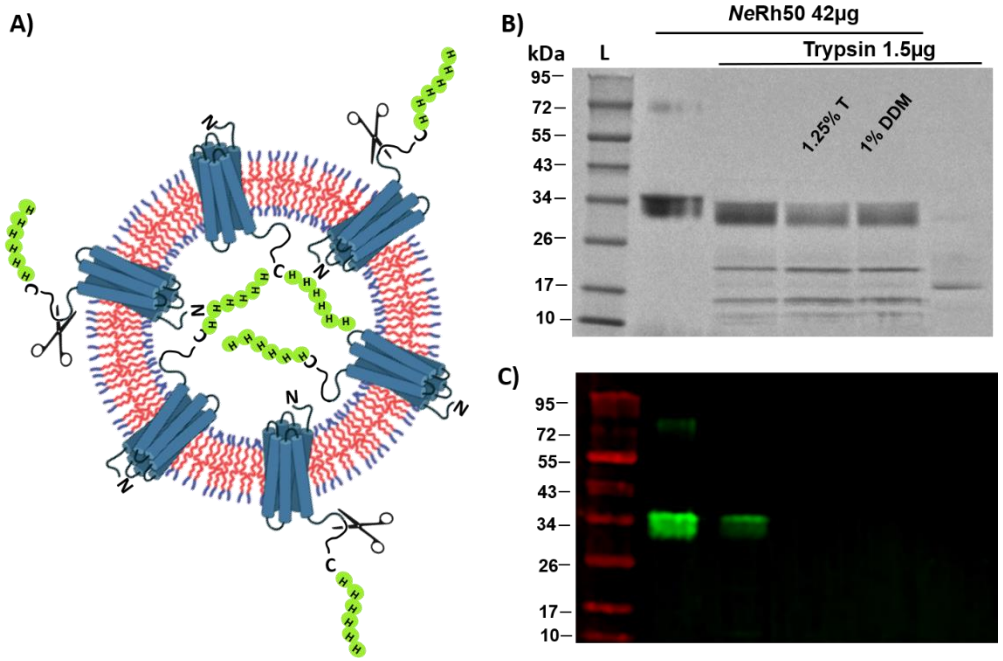

Figure 3.8 Rh50 orientation in the liposome. A) Schematic representation of the liposome and randomly orientated Rh50 protein. B) Coomassie stained SDS-PAGE gel illustrating the drop in protein size following trypsin digestion. C) Western Blot analysis illustrating concentration drop of Rh50 in the liposome following trypsin digestion. L – ladder, T- Triton x-100, DDM- n-Dodecyl β-D-maltoside.

3.5 Optimisation of SSME Procedures and Buffers

Next, we focused on determination of the optimum condition for Solid-Supported Membrane Electrophysiology (SSME) and establishing the standard procedure which will be used throughout this PhD thesis. More detailed description of SSME can be found in **Chapter 2, Section 2.6.** Briefly, the charge translocation across a membrane measured via Solid-Supported Membrane Electrophysiology (SSME) resembles an enclosed electric circuit with the reference electrode and measurement electrode. Both membranes proteoliposomes and SSM can be described using their capacitance C and conductance G. Electrogenic transport charges the proteoliposomal membrane which is accompanied by the charging of the measuring electrode.

The current measured by the SSME is recorded as a transient current because the charge displacement inside the proteoliposomes creates an outwardly orientated negative membrane potential that progressively inhibits the transport cycle. Therefore, a typical SSME trace possesses a rapid increase of the current followed by an exponential decrease characterised by a decay time. This fast increase of current provides two information, namely a pre-steady and a steady state current. The former represents the interaction between the protein and transport substrate and the latter represents both binding and transport of the substrate. A measurement of an active transporter represents a combination of both. The decay time measures the velocity at which the membrane potential is created.

3.5.1 Composition of Buffers

Before proceeding with characterisation of Rh50, the optimum condition for SSME measurements were developed using AmtB ammonium transporter. We will thereafter show that the same experimental conditions can be used to characterise the activity of Rh50. Using standardised condition to measure the activity of AmtB and Rh50 is important as it will ensure the reproducibility of the measurements and will allow for direct comparison of the activity of both proteins in the future.

Firstly, experimental condition which will allow to record a reproducible transient current with a good amplitude, in the nA range, must be established. To determine the influence of the buffer composition on the amplitude of SSME measurements, a range of buffers composed of different salts were tested. Ammonium transport was first determined using buffers containing 100 mM Tris only on proteoliposomes containing AmtB at a lipid to protein ratio (LPR) 10. A 200 mM NH_4^+ pulse with solution containing 100 mM Tris elicited a transient current with a maximum amplitude reaching ~ 9.5 nA (**Figure 3.9 A**). To confirm that the observed current is AmtB specific, the measurement was repeated on an empty liposome. SSME measured the transient current with a maximum amplitude reaching ~ 6 nA, on an empty liposome (**Figure 3.9 A**). This artefactual current measured in empty liposomes is due to the unspecific interaction of ammonium with the hydrophilic lipid headgroups.

3.5.2 Salts are Important to Reduce Non-specific Binding

As described by Bazzone and colleagues, the composition of the buffers for SSM-based electrophysiology is important to reduce solution exchange artefacts. Bazzone *et al* proposed that these unspecific interactions can be reduced by keeping the composition of activated (A) and non-activated (NA) solutions as similar as possible, including their ionic composition, pH, and temperature. In addition high background salt, such as KCl can help to reduce artefacts (Bazzone, Barthmes and Fendler, 2017).

Therefore, the influence of presence of KCl in the buffer on measurements was investigated by rinsing the same set of sensors with 100mM Tris + 100mM KCl buffer. After 200 mM NH_4^+ pulse with solution containing 100mM Tris +

100mM KCl the amplitude reached ~ 2.0 nA (**Figure 3.9 B**). This is a ~ 5 - fold reduction in the amplitude in comparison to the peak produced with Tris only buffer. To confirm that the current is AmtB specific, the same condition was tested on an empty liposome. While not as high as with Tris only buffer, the amplitude reached ~ 0.5 nA on an empty liposome (**Figure 3.9 B**). This indicated that presence of KCl reduces, but not completely abolishes the unspecific interaction.

Finally, we used different salts and altered their concentrations in the activating (A) and non-activating (NA) buffers for a better compensation of activating compound in the A buffer. Precise composition of buffers is detailed in **Table 2.9**. The same set of sensors were rinsed and tested with new buffers containing 100mM Potassium phosphate salts (KPhO) and 100mM KCl. 200mM NH_4^+ induced the maximum amplitude which reached ~ 3.3 nA on the liposomes containing AmtB at an LPR 10, while no current was recorded on an empty liposome (**Figure 3.9 C**). This indicated that the conditions are satisfactory in terms of height of the amplitude as well abolishment of the artefacts (unspecific binding) when 100mM KCl and 100mM KPhO were the main components of the buffer.

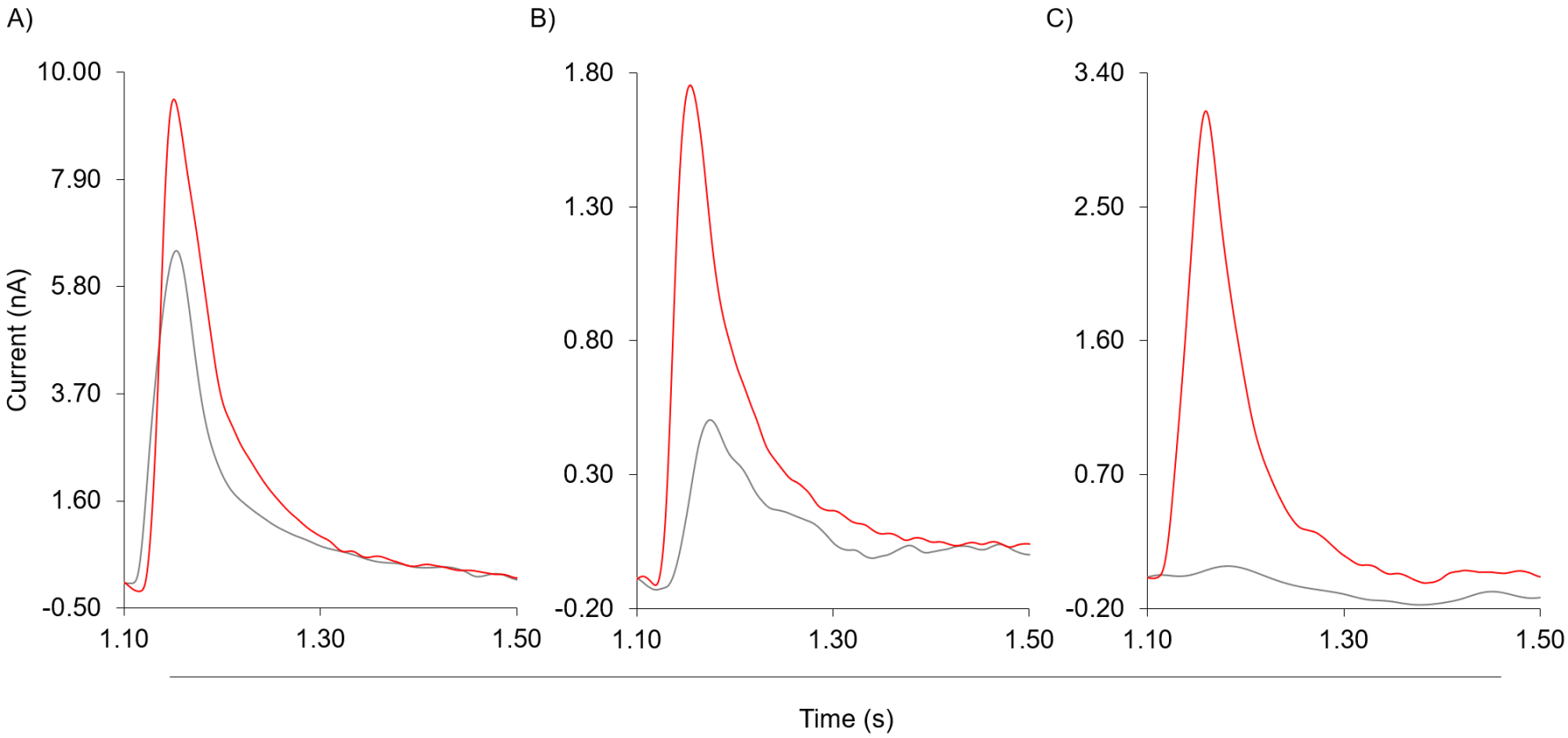

Figure 3.9 Importance of SSME buffer composition. Transient current measured in AmtB reconstituted into polar/popc 2/1 proteoliposomes at an LPR10 (red) and in empty liposome (grey) after pulse of 200mM NH_4^+ in A) 100mM Tris buffer, B) 100mM Tris+ 100mM KCl buffer, C) 100mM KPhO+100mM KCl buffer.

3.5.3 Checking the Transport at Different LPRs

To fully confirm that the conditions are satisfactory and that the transient current corresponds to the translocation of ammonium into proteoliposomes, the relation between the decay time and the protein density in the liposomes was investigated. The decay should be directly proportional to the protein density in the liposomes if the current represents a complete transport cycle, while it should be independent if the current reflects a simple interaction between the substrate and the protein (Zuber *et al.*, 2005). Therefore, to fully confirm that the 100mM KPhO and 100mM KCl buffers are suitable for the SSME analysis the decay (*k* value) was measured following 200mM NH_4^+ in AmtB at different LPR ratios. As seen in **Figure 3.10** the higher the protein density in the liposome (LPR 5) the higher the amplitude of the peak as well as the *k* value. Reduction of protein concentration in the liposomes, reduces the peak as well as the *k* value. This indicates that the 100mM KPhO and 100mM KCl buffers are suitable for the SSME analysis.

Taken together, these results allowed us to establish suitable SSME conditions to measure AmtB activity.

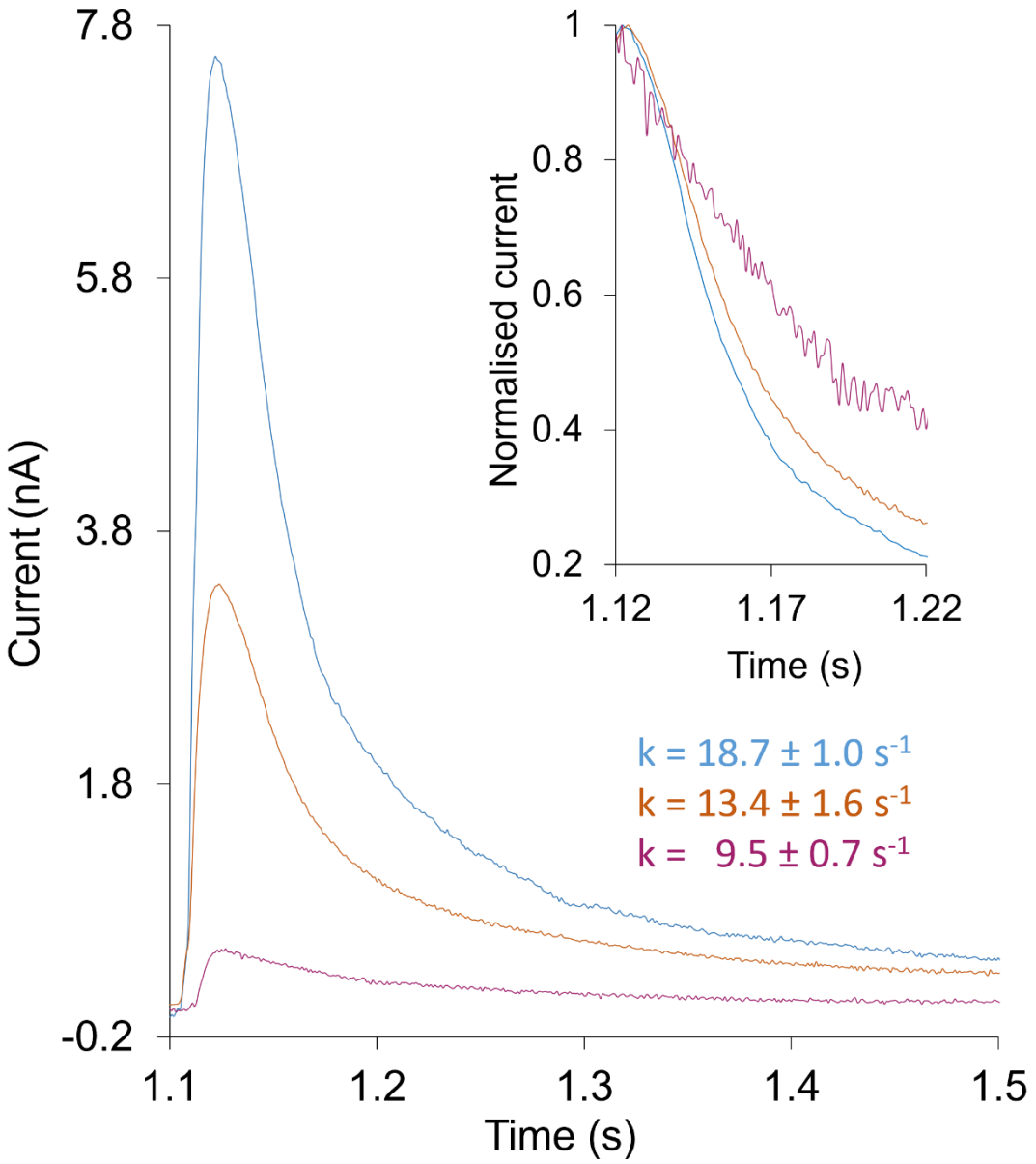

Figure 3.10 Characterisation of *Ec*AmtB activity. Transient current measured after a 200 mM ammonium pulse on proteoliposomes containing AmtB at a LPR5 5 (blue) 10 (orange) or 50 (magenta). **Insert**: Normalised current measured in proteoliposomes containing AmtB at a LPR50 (magenta), 10 (orange) or 5 (blue).

3.6 Activity of Rh50 is Electrogenic

Despite reports suggesting electroneutral nature of the Rh50, we were determined to subject the Rh50 protein to SSME analysis due to the strong conservation of the translocation pathway within the Amt/Mep/Rh family and electrogenic activity of its multiple members (**Figure 1.8**) (Wacker *et al.*, 2014; Mirandela *et al.*, 2018; Williamson *et al.*, 2020). Successful optimisation of the SSME assay using AmtB allowed us to compose buffers which accurately reflects the transport activity of the protein. Therefore, the same conditions to characterise the activity of the Rh50 protein were used for comparison purposes (**Chapter 4, Section 4.10**).

A 200 mM NH_4^+ pulse on polar/POPC 2/1 liposomes containing Rh50 at LPR 5 elicited a transient current that reached a mean maximum amplitude of ~2 nA which decays back to the baseline (**Figure 3.11 A**). To confirm that the observed current is due to transport activity, Rh50 was reconstituted into proteoliposomes at various LPRs of 5:1, 10:1, and 50:1 (**Figure 3.11 B**). Empty liposomes were also prepared and used as a negative control (**Figure 3.11 A**). As previously mentioned, (Section 3.5.3), an increase in the concentration of protein is expected to result in a maximum capacity being reached faster and in turn, would decay faster. In case where the protein was not able to complete the full translocation cycle but simply interact with the substrate, the decay rate would not change between different LPRs (Zuber *et al.*, 2005). As shown in **Figure 3.11 B**, the higher the protein density in the proteoliposomes, the higher maximum amplitude (transient current) while the empty liposome does not induce any observable current **Figure 3.11 A**. In addition, the decay rate is also depended on protein concentration, increasing from $24.22 \pm 0.97^{s-1}$ for LPR 50, to $33.47 \pm 1.62^{s-1}$ for LPR 10, to $44.08 \pm 3.93^{s-1}$ for LPR 5, proving that the protein is completing a full translocation cycle, and it is not just a substrate protein interaction.

Taken together these results demonstrates that the activity of Rh50 is electrogenic.

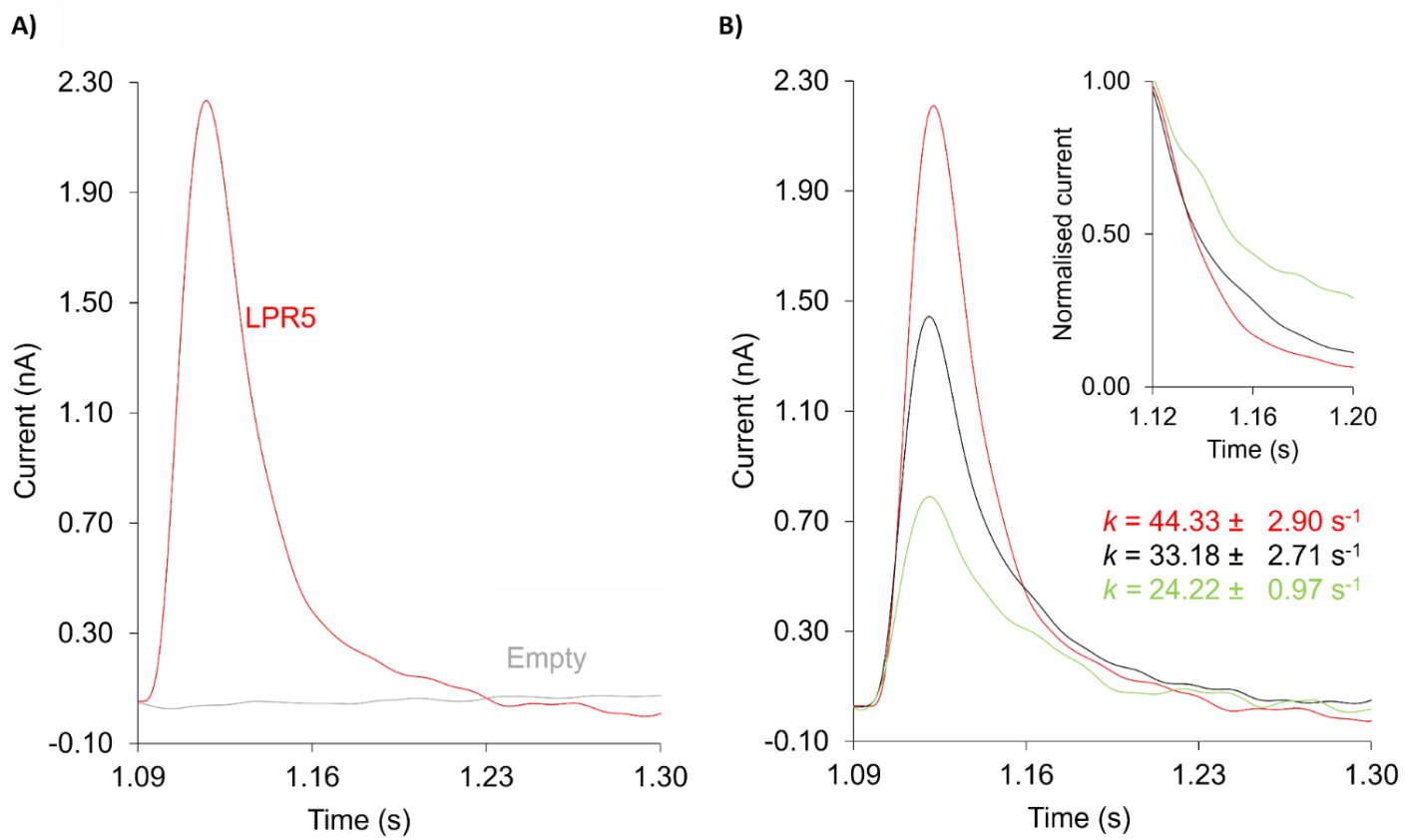

Figure 3.11 Characterisation of *Ne*Rh50 Activity: A) Transient currents following a 200 mM pulse of NH_4^+ in empty Polar/POPC 2/1 liposomes (grey) or with Rh50 reconstituted into Polar/POPC 2/1 proteoliposomes at a LPR of 5 (red) B) Transient currents following a 200 mM NH_4^+ pulse with Rh50 reconstituted into Polar/POPC 2/1 proteoliposomes at a LPR of 5 (red), 10 (black), or 50 (green).

3.7 Discussion

This chapter provides step by step guidance for successful heterologous expression of Rh50 from *Nitrosomonas europaea* using GT 1000 *E. coli* overexpression system and subsequent IMAC/SEC purification. Here we present that the obtained protein elutes as a single peak and can be successfully inserted into liposomes at different LPRs without affecting the size distribution of liposomes or leading to their aggregation. We estimated that the protein inserts at mixed, RSO and ISO, orientation in the liposome. Finally, the assay to measure the activity Rh50 using solid supported membrane electrophysiology (SSME) was successfully developed and tested on AmtB protein from *E. coli*.

3.7.1 Assay Development

As presented in results section of this chapter, special attention is required for the preparation of buffers for SSM-based electrophysiology. Here we show that the interactions between the compound membrane and the buffer components can generate large solution exchange artefacts. This may be due to the interaction of the ions with lipid headgroups which can overlay the transporter signal (Garcia-Celma *et al.*, 2007). We reduced named artefacts by increasing the dielectric charge of the buffer by adding K^+. It is also crucial to prepare non-activating and activating solutions and adjust their pH at the same time. This method has been proved successful in the past in reducing Na^+ artefacts in assays with NhaA, the main Na^+/H^+ antiporter in *Escherichia coli*, indispensable for adaptation to high salinity, for challenging Li^+ toxicity, and for growth at alkaline pH (in the presence of Na^+) (Zuber *et al.*, 2005). Another example for a successful artefact compensation strategy was developed by Wacker *et al* with transporter Amt, where the measurement was performed with different concentration ratios NH_4Cl/NaCl and at a constant total osmolarity in the activating and no-nactivating solutions (Wacker *et al.*, 2014). Working with low-affinity transporters, which need high substrate concentration pulse, generally require more attention concerning artefact controls when setting up the buffer systems (Bazzone, Barthmes and Fendler,

2017). For this reason, we included a crucial negative control in the form of liposome without the transporter of interest.

3.7.2 Rh50 is an Electrogenic Ammonium Transporter

It had been widely accepted that Rh50 from *Nitrosomonas europaea* is supporting electroneutral transport of NH_3 (Cherif-Zahar *et al.*, 2007; Weidinger *et al.*, 2007). Resolution of the crystal structure of Rh50, and specifically the presence of highly hydrophobic pore, further supported the notion that it might mediate transport of uncharged species (Lupo *et al.*, 2007; Li *et al.*, 2007). Based on structural similarities and close clustering of Rh50 and human rhesus proteins, Rh50 was concluded to be highly representative of all Rh proteins, therefore it was widely assumed that human Rh proteins will also act as ammonia (NH_3) channels. In contrary, results in this chapter demonstrate that Rh50 is in fact electrogenic, disputing above assumption. Here, we present that the transient current is measured in proteoliposomes containing Rh50, while no signal is measured in empty liposomes. The decay rate of the observed current is LPR-dependent, confirming that the transient current represents translocation of ammonium and not simply a protein-substrate interaction.

3.7.3 How is the Charge Translocated?

The electrogenic NH_4^+ transport via Rh50 implies either: direct translocation of NH_4^+; facilitated symport of NH_3 and H^+, or deprotonation of NH_4^+ into NH_3 and H^+, allowing their separate transport through the protein. An *in vivo* experimental data performed in yeast demonstrated for the first time that that the translocation of NH_4^+ was associated with deprotonation (Ariz *et al.*, 2018), ruling out the hypothesis of a direct NH_4^+ translocation. As already discussed, the hydrophobicity of the pore would not allow charge passage raising the question of how the proton is translocated by the protein. The authors proposed that after NH_4^+ deprotonation, H^+ and NH_3 could be translocated via different route, explaining the electrogenicity of the transport (Ariz *et al.*, 2018).

However, the mechanism whereby H^+ and NH_3 travel through the protein remained unclear. The idea of deprotonation and a separate translocation of NH_3 and H^+ has recently been pursued by our lab using AmtB from *E. coli* as a model system. We proposed and experimentally validated a new mechanism of selective and electrogenic transport in AmtB which will be presented and described in the introduction of chapter 4. Most importantly, the residues involved in the mechanism are highly conserved across the Amt/Mep/Rh family (Williamson *et al.*, 2020). Therefore, I have extensively characterised and studied the mechanism of the WT Rh50 in the context of our newest findings and presented the results in Chapter 4.

Chapter 4

Chapter 4: Model transport mechanism and functional analysis of Wild Type *Ne*Rh50

Some of the results presented in this chapter are the subject of a paper published in *eLife* in July 2020

Williamson G*, Tamburrino G*, **Bizior A***, Boeckstaens M, Dias Mirandela G, Bage M, Pisliakov A, Ives CM, Terras E, Hoskisson PA, Marini AM, Zachariae U, Javelle., (2020). 'A two-lane mechanism for selective biological ammonium transport'. *eLife* ;9. DOI: https://doi.org/10.7554/eLife.57183

***** Equally contributed

4.1 Introduction

The controversy around the substrate transported by Amt/Mep/Rh proteins (NH_4^+ vs. NH_3) as well as the mechanism of the transport (transporter or channel), has been an ongoing debate for decades. It was hoped that high-quality crystal structures would shed light on the long-standing debate about the mechanism of ammonium transporters. The structure of the *E. coli* ammonium transporter AmtB is well characterised with over 20 high-resolution structures, including numerous variants, deposited in the Protein Data Bank (PDB) (Khademi *et al.*, 2004; Zheng *et al.*, 2004; Javelle *et al.*, 2006; Javelle *et al.*, 2008). The hydrophobicity of the AmtB pore, as well as the lack in the conformation change in presence or absence of ammonium, suggested that the substrate is translocated in a channel-like manner (Khademi *et al.*, 2004; Zheng *et al.*, 2004). Based on this, and the hydrophobicity of the main pore in the translocation pathway, it was widely accepted that the mechanism of the transport was electroneutral (NH_3) for the majority of the family (Khademi *et al.*, 2004; Andrade *et al.*, 2005; Lupo *et al.*, 2007). However, Wacker *et al* demonstrated, for the first time, electrogenic transport in Amt1 from *Archaeoglobus fulgidus*, suggesting net charge translocation (Wacker *et al.*, 2014). This was a huge milestone and a ground-breaking finding, but it presented the research field with more confusion and a seemingly unsolvable paradox: how can a charge travel through the hydrophobic pore?

4.1.1 A two-lane Mechanism for Electrogenic Ammonium Transport in AmtB

To answer this question, our group have extensively studied and characterised the activity of *Ec*AmtB and selected variants using SSME technology and reported a direct observation of selective, electrogenic ammonium transport mediated by *Ec*AmtB (Mirandela *et al.*, 2018; Williamson *et al.*, 2020).

Our *in vitro* results, combined with *in silico* Molecular Dynamic Simulations (MDS) and *in vivo* yeast complementation assays enabled us to propose a mechanism for the electrogenic ammonium transport in AmtB (Mirandela *et al.*, 2018; Williamson *et al.*, 2020). We reason that NH_4^+ undergoes deprotonation upon binding to the extracellular side of the pore (S1) near the residue D160, allowing passage of uncharged NH_3 molecules through the centre of the hydrophobic channel. A parallel passage of H^+ into the cytoplasm is enabled by the previously undiscovered polar conduction route formed by two water wires (WWs) which span across the membrane (**Figure 4.1**). The WWs, linked by the histidine in position 168, form an aqueous chain while preventing the formation of a continuous water channel in the pore of the protein. The high conductivity of H^+ via the WWs has been described as a hopping mechanism by which H^+ jumps from H_3O^+ to a neighbouring water molecule, finally being released into the cytoplasm (DeCoursey and Cherny, 1997; Lishchuk, Lokotosh and Malomuzh, 2005). This parallel passage of NH_3 and H^+ is followed by the subsequent re-protonation in the cytoplasm allowing the organism to utilise ammonium for biosynthetic purposes (Javelle *et al.*, 2007; Williamson *et al.*, 2020).

The residues involved in our model are conserved across the entire family (Williamson *et al.*, 2020) suggesting that the mechanistic details could be shared, or to some extent preserved in the Amt/Mep/Rh family. In addition, the evidence supporting the importance of NH_4^+ deprotonation as a major step in ammonium transport across the whole family, including Rh protein, has been reported (Ariz et al., 2018). After establishing that SSME is a suitable way of characterising the activity of Rh50, and proving that its activity is electrogenic, we have pursued the idea of a conserved mechanism in Rh50.

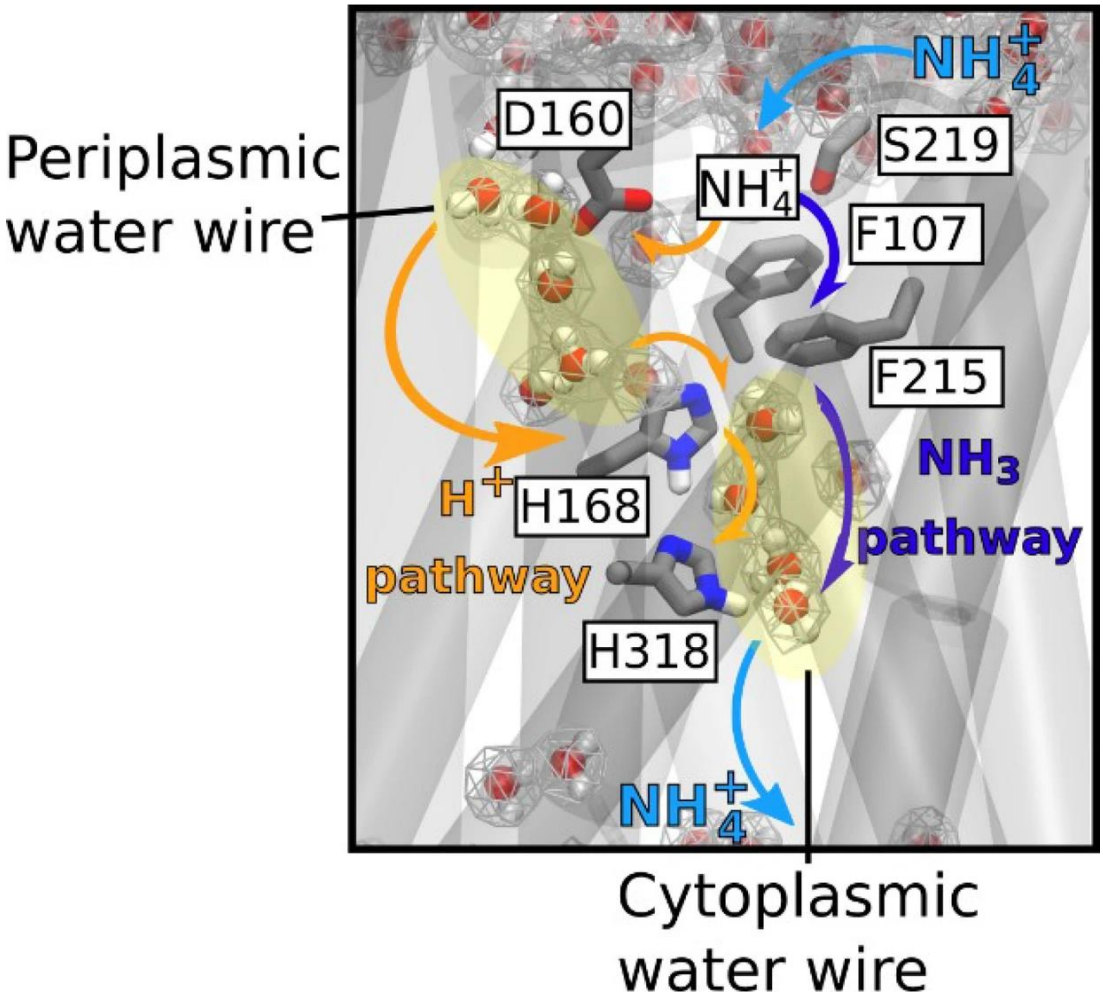

Figure 4.1 Mechanism of electrogenic NH_4^+ translocation in AmtB. NH_4^+ ion binds to the periplasmic binding site (S1) followed by de-protonation and the H^+ transport polar conduction route (indicated by yellow arrow). Electroneutral NH_3 is directly transported through the hydrophobic pore to the cytoplasm (indicated by dark blue arrow) and subsequently re-protonated to NH_4^+. Adapted from Williamson *et al*., 2020.

4.2 Aims and Objectives:

To this end we have successfully purified Rh50 protein, inserted it into the liposomes and established that its activity is electrogenic (**Chapter 3**). In this chapter, we will fully characterise the activity of WT Rh50 and a variant with a mutation in the periplasmic face of the protein to establish its relevance to a potential deprotonation mechanism in the protein. Finally, we will compare the activity of Rh50 to the activity of AmtB protein. Apart from deciphering the mechanism of Rh50 protein in the context of Rh protein pathophysiology, and physiology of *Nitrosomonas europaea,* this research provides an opportunity to investigate whether there is a universal mechanism for ammonium transport across the Rh and Amt/Mep family of transmembrane proteins.

In parallel to the *in vitro* SSME experiments, we also conducted *in vivo* yeast complementation experiments with help of our collaborators, Dr Ana Sofia Brito, Prof. Mélanie Boeckstaens and Prof. Anna-Maria Marini (Free University of Brussels, Belgium).

The aims were to:

1 Characterise the activity of WT Rh50 *in vitro* via SSME.

2 Purify and characterise the activity of Rh50 variant *in vivo* via SSME.

3 Compare the activity of Rh50 to AmtB.

4.3 Activity of Rh50 is Selective Towards Ammonium

After confirming that the activity of Rh50 is electrogenic (**Chapter 3, Section 3.6**) we sought to determine if there are any other substrates that Rh50 protein can translocate. To assess Rh50 specificity, the SSME measurements were repeated using K^+ as a substrate. The size and ionic radii of K^+ (0.152nm) is similar to the one of NH_4^+ ion (0.151nm) (Sidey, 2016;Shannon, 1976), therefore if Rh50 was not specific to ammonium, a similar current would be expected in presence of K^+. Following a 200 mM pulse of K^+, no observable current was recorded (**Figure 4.2 A**), demonstrating that Rh50 electrogenic activity is highly selective towards NH_4^+.

Methylammonium (MeA/ $CH_3NH_3^+$) has been widely used as an analogue of ammonium (NH_4^+) to study the transport in bacteria and fungi (Javelle *et al.*, 2007). This is due to very short half-life of the radiolabelled ^{13}N (~ 9 min) making impractical to use [^{13}N] Ammonium as a radioactive tracer to measure ammonium transport (Javelle *et al.*, 2007). For this reason, [^{14}C] Methylammonium has been widely used as a radioactive tracer for ammonium. We decided to clarify if MeA is a suitable analogue for ammonium transport analysis in Rh50 using SSME. A 200 mM pulse of methylammonium elicits a current of only 0.9 ± 0.2nA, a ~ 2-fold reduction compared to 200mM ammonium 2.03 ± 0.14 nA (**Figure 4.2 A**), while decay constant is also ~2-fold lower. Next, the kinetics of the transport of ammonium and MeA were investigated by measuring transient currents in LPR 5 following an ammonium/MeA pulse ranging from 0.1-200 mM. The peak amplitudes of these currents were recorded and fit according to the Michaelis-Menten equation. This analysis revealed that the Km for MeA (278.7 ± 77.11 mM) was ~2.2 fold higher than that of ammonium (124.3 ± 35.85 mM) (**Figure 4.2 B**), indicating that Rh has a higher affinity for ammonium in comparison to methylammonium.

These results demonstrate that Rh50 is a highly selective and electrogenic transporter and that MeA is a poor substrate for elucidating mechanistic details of Rh50 activity. While Rh50 clearly discriminates between ammonium and methylammonium it does so to a lesser degree in comparison to AmtB. It has

been shown that the AmtB conduction rate drops by ~80% when tested with MeA in comparison to ammonium (Mirandela *et al.*, 2018), while in Rh50 drops by ~50%. The differences between both transporters will be further investigated in Chapter 4 (**Section 4.10**).

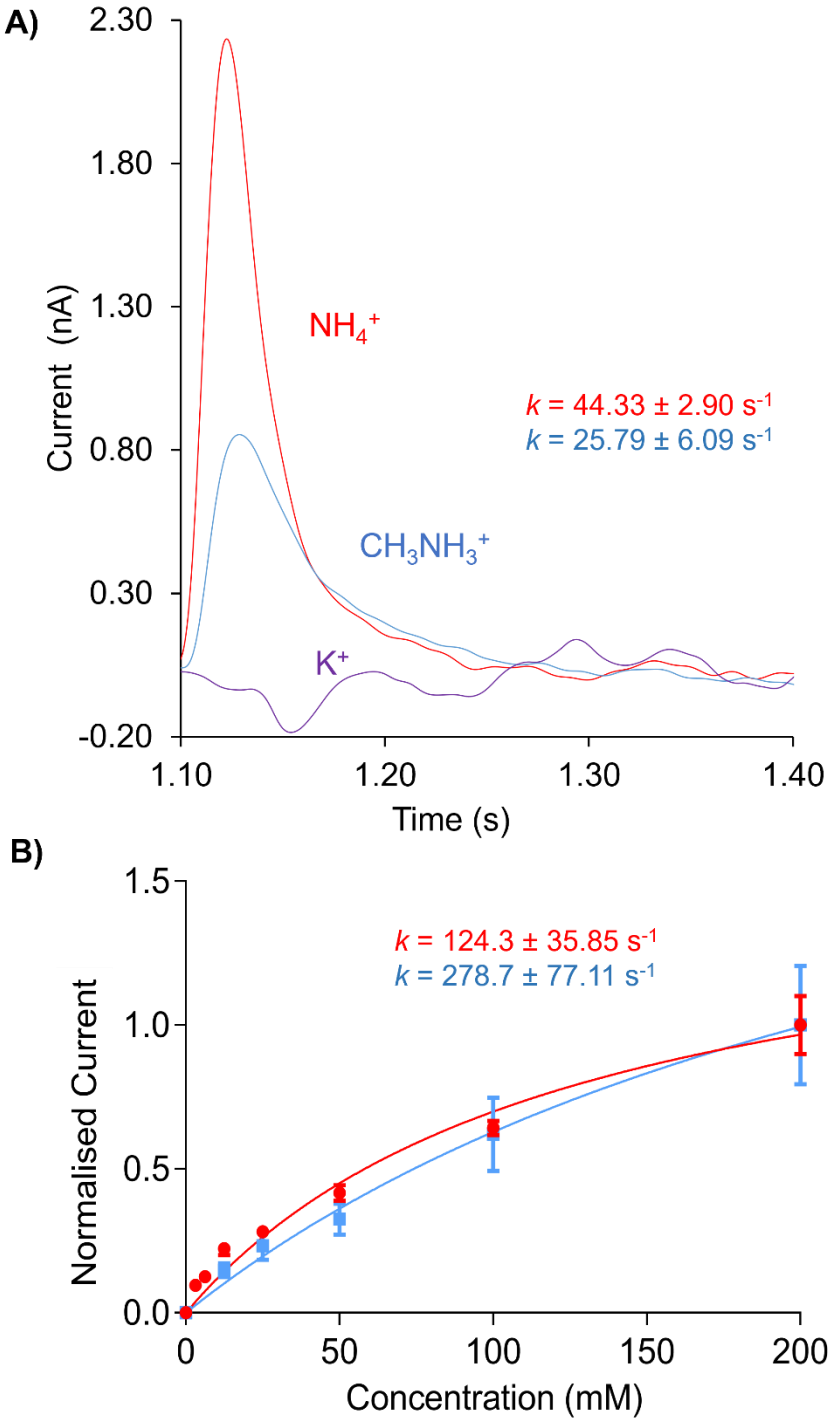

Figure 4.2 Selectivity of Rh50: A) Transient currents following a 200 mM pulse of NH_4^+ (red), $CH_3NH_3^+$ (blue), K^+ (purple) with Rh50 reconstituted into Polar/POPC 2/1 proteoliposomes at a LPR5 B) Kinetics for Rh50 at LPR 5 using NH_4^+ (red) or $CH_3NH_3^+$ (blue). Maximum amplitudes have been normalised to 1.0 for comparison.

4.4 *In-vivo* Characterisation of the Rh50

4.4.1 Rh50 is an Ammonium Transporter in vivo

To develop a paralleled approach to characterise the activity of Rh50 *in vivo*, we took advantage of a clear ammonium-dependent growth phenotype of *Saccharomyces cerevisiae* lacking all three MEP genes. Three genes, MEP1, MEP2, and MEP3, mediate ammonium transport in *S. cerevisiae*. They are all subject to nitrogen catabolite repression and encode proteins that differ in their affinities for ammonium (Boeckstaens, André and Marini, 2008). Any of these alone is sufficient for cell growth on low concentrations of ammonium, but deletion of all three, mep1–3 renders cells non-viable on medium containing 1–5 mM ammonium as the sole nitrogen source (Marini *et al.*, 1997a). We reasoned that if Rh50 were to function as an ammonium transporter, its expression in yeast *Δmep1–3* cells may complement the transport defect.

To investigate it, Rh50 was expressed from the pDR195 plasmid in the *S. cerevisiae* strain 31019b (*ΔMEP1-3*). The plasmid pDR195 allows to express Rh50 under the control of the ATPase promoter (Rentsch *et al.*, 1995). It can be seen in **Figure 4.3** that the *ΔMEP1-3* mutant yeast strain only shows a minimal growth on 3 mM ammonium as a sole nitrogen source. However, when the yeast expressed Rh50, growth was restored on media supplemented with as low as 1mM of ammonium as a sole nitrogen source.

This growth phenotype analysis showed that expression *in trans* of Rh50 is non-toxic to cells and in fact can replace the indigenous yeast MEP1-3 transporters to support the growth on ammonium as a sole nitrogen source (**Figure 4.3**).

4.4.2 Rh50 Prevents MeA Induced Toxicity in Yeast

Methylammonium (MeA) is toxic to *S. cerevisiae* and can inhibit growth at external concentrations of 100 mM or higher. This is because the glutamine synthetase converts MeA it into methyl glutamine, which cannot enter the nitrogen cycle and blocks the activity of glutamine synthetase. Without this enzyme, ammonium uptake is restricted, in turn preventing the cellular growth (Marini *et al.*, 1994; Marini *et al.*, 1997a). As such, it would be expected that expression of Rh50 would inhibit growth of *S. cerevisiae* on media supplemented with MeA. Surprisingly, *S. cerevisiae* complemented with Rh50 grew on glutamic acid and MeA supplemented media even at the toxic MeA concentration range (< 100mM) **Figure 4.3**. This implies that the mutant yeast complemented with Rh50 can grow on toxic MeA levels in presence of glutamic acid. These results suggests that Rhesus protein from *N. europaea* can export toxic MeA from the cells and use an alternative nitrogen source to support the growth.

Taken together Rh50 not only promote ammonium import but it is highly likely that it also promotes ammonium export, hence potentially work bi-directionally as opposed to other ammonium transporters form Amt/Mep family.

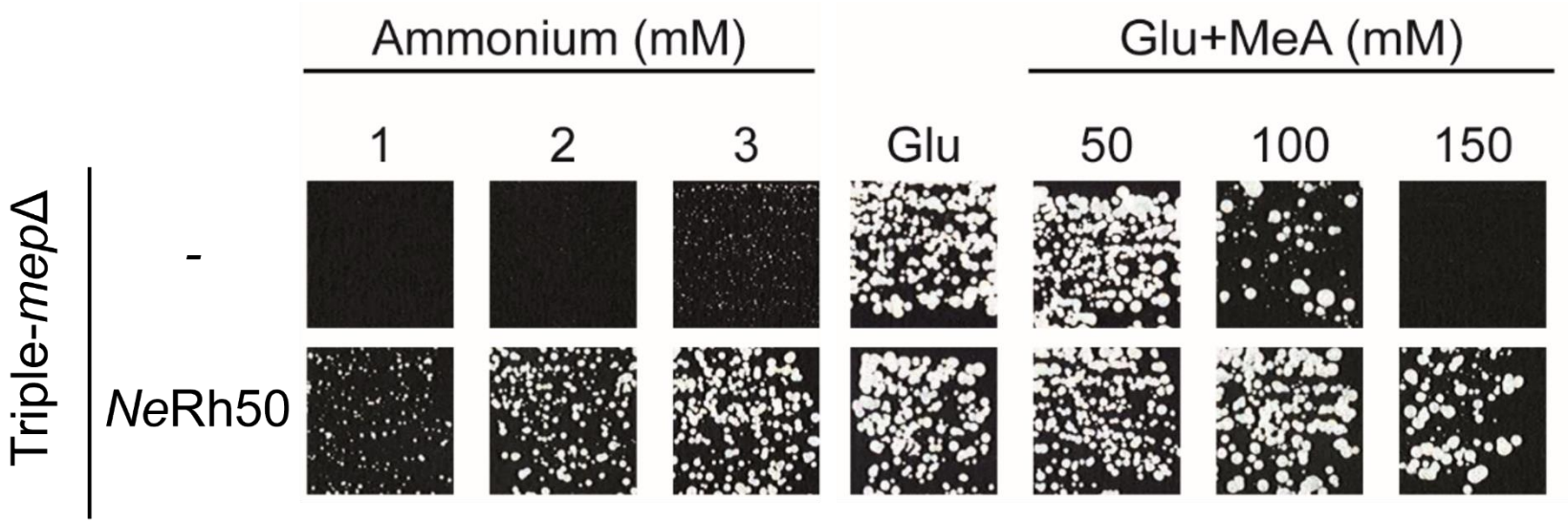

Figure 4.3 Rh50 complement the yeast cells deficient in ammonium transport. Yeast complementation after 5 days of growth on minimal media supplemented with either: (Left to right) 1 - 3 mM ammonium, glutamic acid (Glu), glutamic acid and 50 - 150 mM Methylammonium (Glu+MeA).

4.5 Effect of the pH on Rh50 Activity

4.5.1 Rh50 Activity is pH Dependent

To further characterise the activity of Rh50, the effect of the pH on its transport activity was investigated. To do this Rh50 activity was measured in a pH 5 - 8 range using SSME. First, to assess whether the exposure of Rh50 to various pH conditions affects the protein stability in the liposome, the activity of Rh50 at pH 7 before and after exposure to pH 5, 6 and 8 were compared. This is an essential step which will ensure that the signal change is not due to irreversible transporter inactivation, but indeed due to the pH change.

The results show that the average amplitude of transient current was comparable at pH 7 before and after exposure to pH 5 - 8 (**Figure 4.4**). In addition, there was no appreciable difference in the *k* value between the measurements (**Figure 4.4 inset**). These results confirmed that the exposure of Rh50 to acidic or basic pH do not affect the protein stability inserted in artificial liposomes.

Once this was clarified, the activity at pH 5, pH 6, pH 8 was characterised. A shift in the amplitude was observed at different pH conditions (**Figure 4.5**). It was found to be lowest at acidic pH 5 (0.6±0.23nA) and pH 6 (0.90±0.19nA) and was higher at neutral pH 7 (1.1±0.31nA) and basic pH 8 (1.2±1.29). In addition, the *k* value was clearly different between the two most extremes pH values (33.23 ± 3.96 s^{-1} at pH 5 and 23.68 ± 7.57 s^{-1} at pH 8) (**Figure 4.5 inset**).

Taken together, these results show that Rh50 is active in the pH 5-8 range, but it is clearly less efficient at acidic pH 5. Both, the amplitude of the transient current, corresponding to substrate-protein interaction and transport, and the *k* value, corresponding to Rh50 activity and translocation aspects of transport, were affected by a lower pH. Since the transport efficiency increase with the pH, it can be concluded that the transport of ammonium is pH dependent.

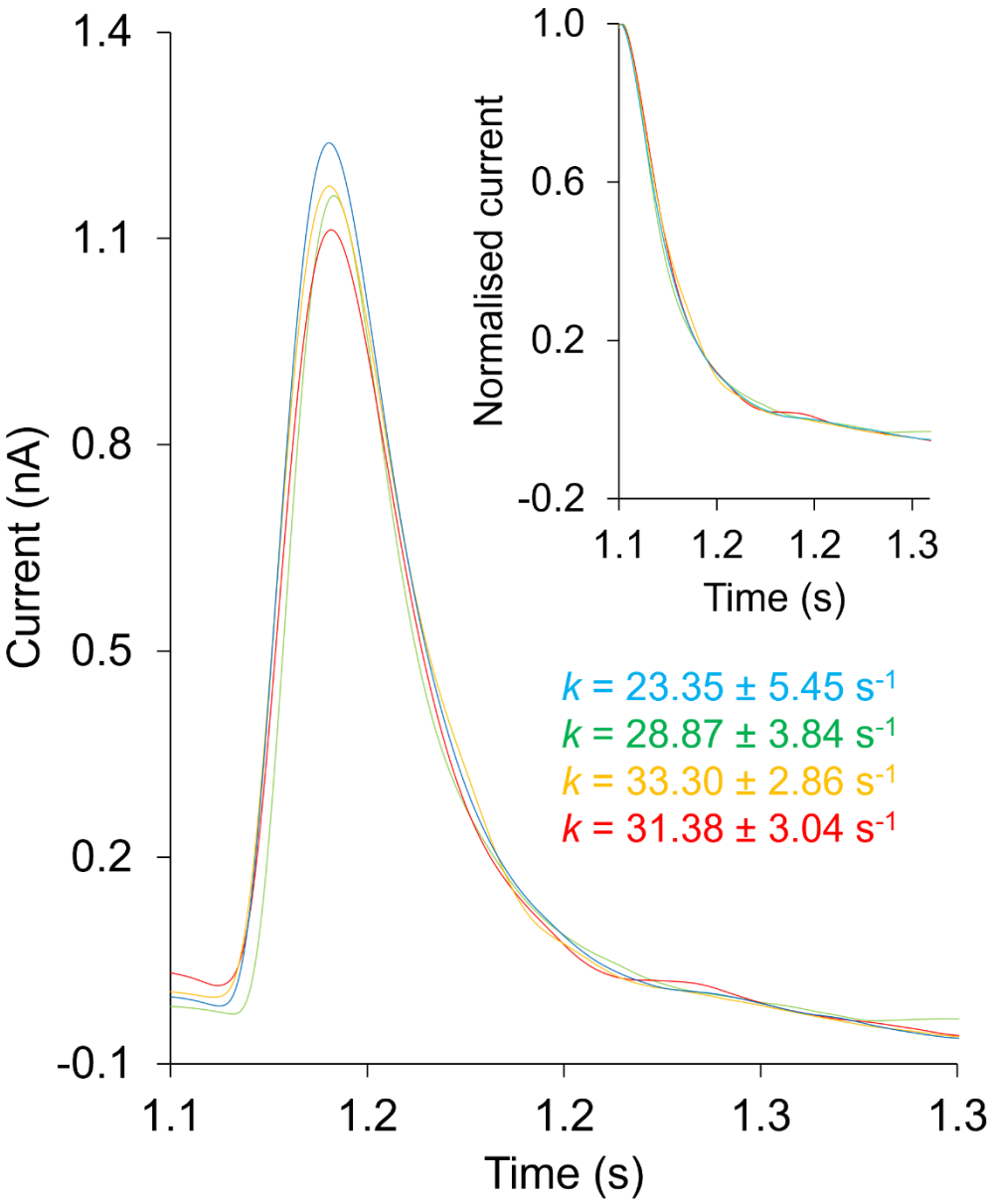

Figure 4.4 Rh50 following exposure various pH. Transient current was measured after 200 mM ammonium pulse in proteoliposomes containing Rh50 at an LPR10 at pH 7 (green), pH 7 after pH 5 (red), pH 7 after pH 6 (yellow), pH 7 after pH 8 (blue). Inset: Maximum amplitude has been normalised to 1.0 for comparison

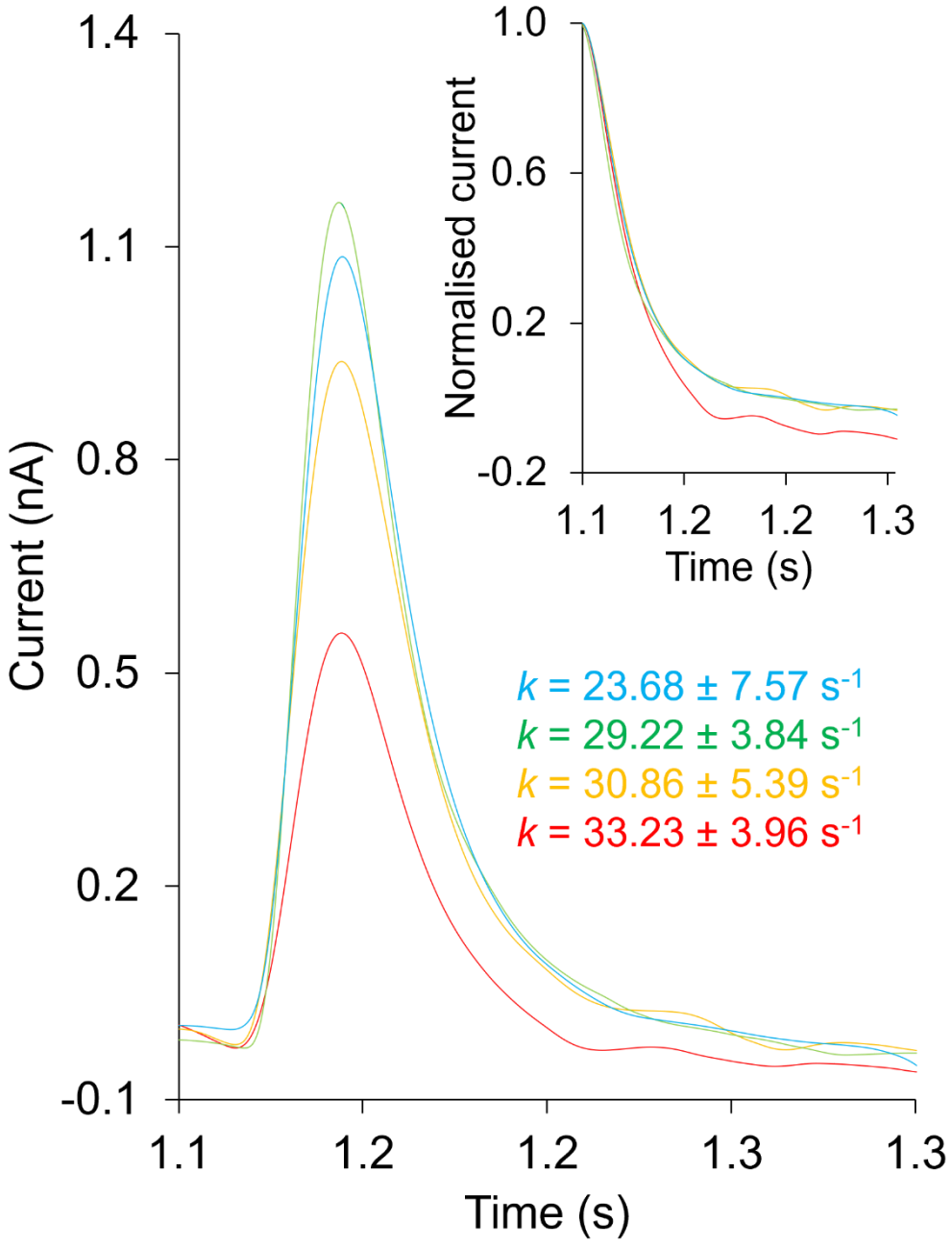

Figure 4.5 Rh50 pH dependence. Transient current measured after 200mM ammonium pulse in proteoliposomes containing Rh50 at an LPR10 at pH 7 (green), pH 5 (red), pH 6 (yellow), pH 8 (blue). Inset: Maximum amplitude has been normalised to 1.0 for comparison

4.6 A Proton Gradient Does Not Affect the Activity of Rh50

Driven by the finding that the Rh50 is indeed electrogenic, we aimed to determine whether the transport is proton gradient dependent which may indicate a symport (NH_4^+/H^+) mechanism.

To test it, the activity of Rh50 was characterised under inward proton gradient conditions in the presence of NH_4^+**.** If the co-transport of a proton and NH_4^+ (NH_4^+/H^+ symport) was indeed the occurring mechanism, there should be an observable difference in Rh50 activity when a proton gradient is applied. There was no appreciable difference in the amplitude or *k* value of the transient current measured after a 200 mM ammonium pulse at static pH 6.5 or under an inwardly orientated proton gradient (**Figure 4.6**). This indicates that the simultaneous NH_4^+ and H^+ symport could be excluded.

We also tested if protons could pass through the protein in absence of the substrate (ammonium): if so, an inward proton gradient would be expected to yield a current on the SSME. As shown in **Figure 4.6**, no current was measured in absence of substrate at inwardly orientated proton gradient, excluding the possibility of protons being translocated in absence of substrate.

These results indicates that Rh50 is not a proton symporter, and that the proton cannot be translocated on its own. In contrast, they strongly suggest that the current recorded by SSME is due to the translocation of a proton coming from NH_4^+ deprotonation, as it has been previously suggested for AmtB from *E. coli* (**Figure 4.1**) (Williamson *et al.*, 2020).

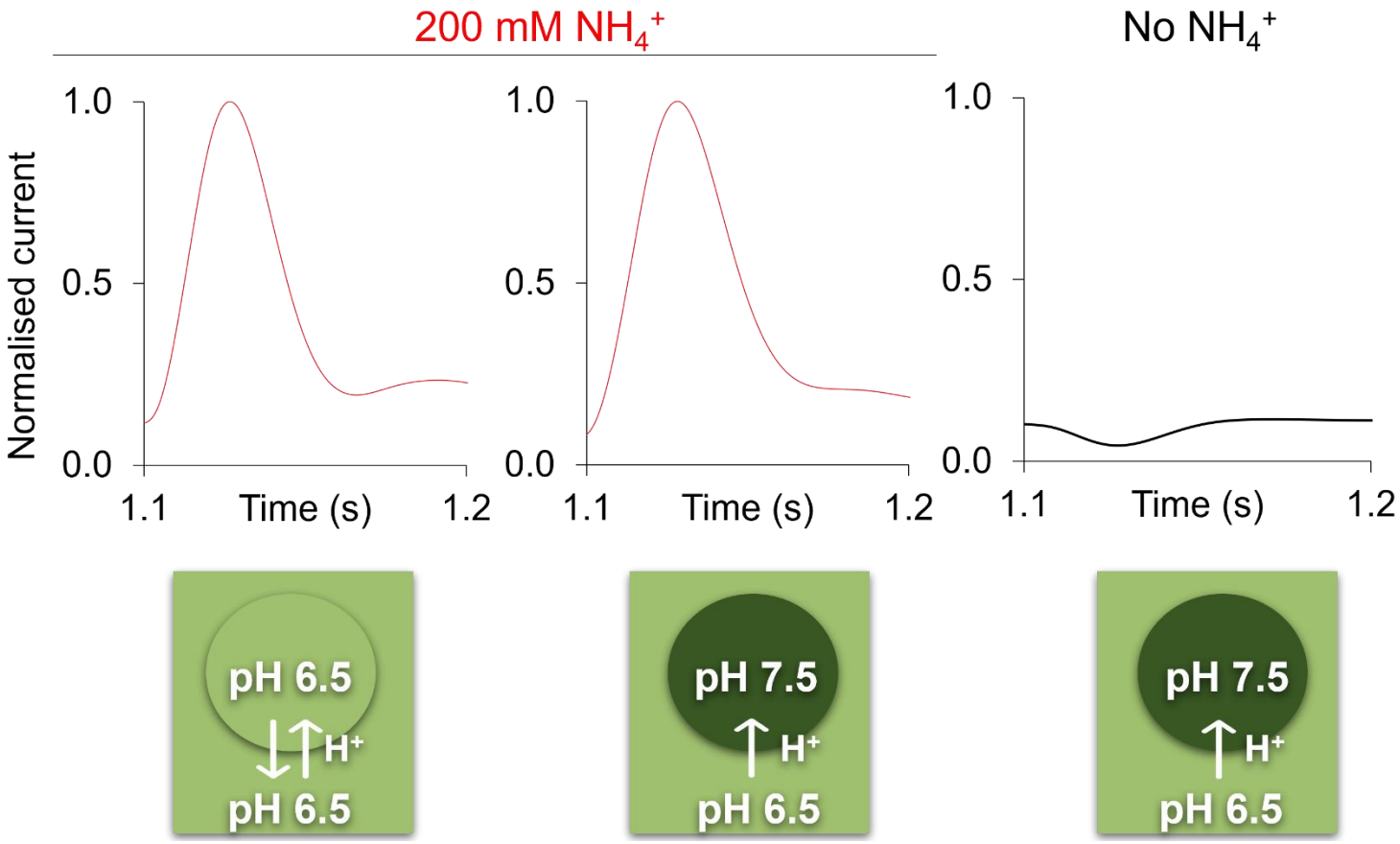

Figure 4.6 Effect of a proton gradient on Rh50 activity. The transient currents were measured following 200mM NH_4^+ pulse in proteoliposomes containing Rh50 at an LPR10 at static pH (left) or under an inwardly directed pH in the presence (centre) or absence (right) of ammonium. The pH of the buffer used are indicated inside circles and squares symbolizing the inside and outside of proteoliposomes, respectively; white arrow indicates H^+ movement.

4.7 Deprotonation in Rh50

Results in this chapter demonstrate that Rh50 is not a symporter and that NH_4^+ could be deprotonated before the entrance to the hydrophobic pore. However, the specific deprotonation place and residues involved are yet to be unravelled. We will now investigate a potential deprotonation site in Rh50 protein and propose a potential candidate for the role.

The mechanism of electrogenic transport in AmtB proposed by our lab relies on recruitment of NH_4^+ at the periplasmic face of the protein, deprotonation, and a separate transfer of NH_3 and H^+ (Williamson *et al.*, 2020). The periplasmic vestibule and the ammonium ion binding site identified in Amt structures is shaped by three highly conserved residues (F107, T148, and S219 in *Ec*AmtB) (Khademi *et al.*, 2004; Zheng *et al.*, 2004; Andrade *et al.*, 2005; Pflüger *et al.*, 2018). Of those, only the F residue is conserved in the Rh family (F110 in Rh50, F130 in RhCG) (Lupo *et al.*, 2007; Li *et al.*, 2007; Gruswitz *et al.*, 2010). For this reason, the Rh proteins are believed to possess a different mechanism for ammonia recruitment in comparison to other ammonia transporters.

At the bottom of the periplasmic vestibule, A144 of AmtB is replaced by a conserved glutamic acid in RhCG (E166) and Rh50 (E146), which appears to be a prime candidate for a charged substrate recruitment site. Recent MD simulation on human RhCG suggest that NH_4^+ makes hydrogen bonds with residue E166 and that the “Phenylalanine gate” (Phe-gate) could be a potential recruitment site for NH_3 molecule (Hoyhtya, 2020). Following this logic, the deprotonation must occur somewhere close to the E166 residue and the Phe-gate. Aspartic acid (D182 in RhCG, D162 in Rh50) residue is positioned very closely to the glutamic acid in Rh proteins (**Figure 4.10 A**), and is conserved across the entire family (Williamson *et al.*, 2020). In addition, aspartic acid (D160) residue has been previously proposed to be involved in deprotonation mechanism in *Ec*AmtB (Javelle et al., 2004; Khademi et al., 2004; Ishikita and Knapp, 2007). It has also been proved crucial for our proposed mechanism in AmtB (Williamson *et al.*, 2020). To investigate the role of D162 in Rh50 we

substituted this residue with alanine, purified the variant protein and performed *in vivo* yeast complementation and *in vitro* SSME analysis.

4.8 Overexpression and Purification of Rh50 Variant

4.8.1 Overexpression of D162A

Site-directed mutagenesis of *rh50* gene was performed and checked by Sanger sequencing (Eurofins Genomics). The primers used for the mutagenesis are listed in (**Table 2.3**) and the template was the *rh50* gene cloned into the plasmid pAD7 (**Table 2.4**) (Cherif-Zahar *et al.*, 2007).

As before, the Rh50 variant was heterologously expressed in *E. coli* strain GT 1000 (Δ*glnK,amtB)* with a hexa-histidine tag at its C terminus. It has already been established that the presence of the pAD7 plasmid is not toxic to the GT 1000 strain and that overexpression of the WT Rh50 does not induce toxicity to the cells (**Chapter 3, Section 3.3.1**). However, it is not possible to predict how altering conserved residues in Rh50 may affect the activity of the protein activity and hence, the growth of GT 1000 strain. Therefore, before proceeding with a large-scale overexpression, we performed a growth curve analysis of the GT 1000 strain expressing D162A variant and compared it to the growth of the GT 1000 strain expressing the WT protein.

As before, the overexpression of protein was induced in the presence of glutamine, therefore, the growth analysis of the GT 1000 containing pAD7 in M9 media supplemented with 0.2 mg/mL α-glutamine as sole nitrogen source was carried out. There were no significant differences in the specific growth rates of GT 1000 expressing WT or D162A variant (0.212 0.03 ± h^{-1} and 0.215 ± 0.04 h^{-1}, respectively, p = 0.75) (**Figure 4.7**). This suggests that the overexpression of histidine tagged Rh50 protein variant is not toxic to the cells and that the large-scale overexpression can be carried out.

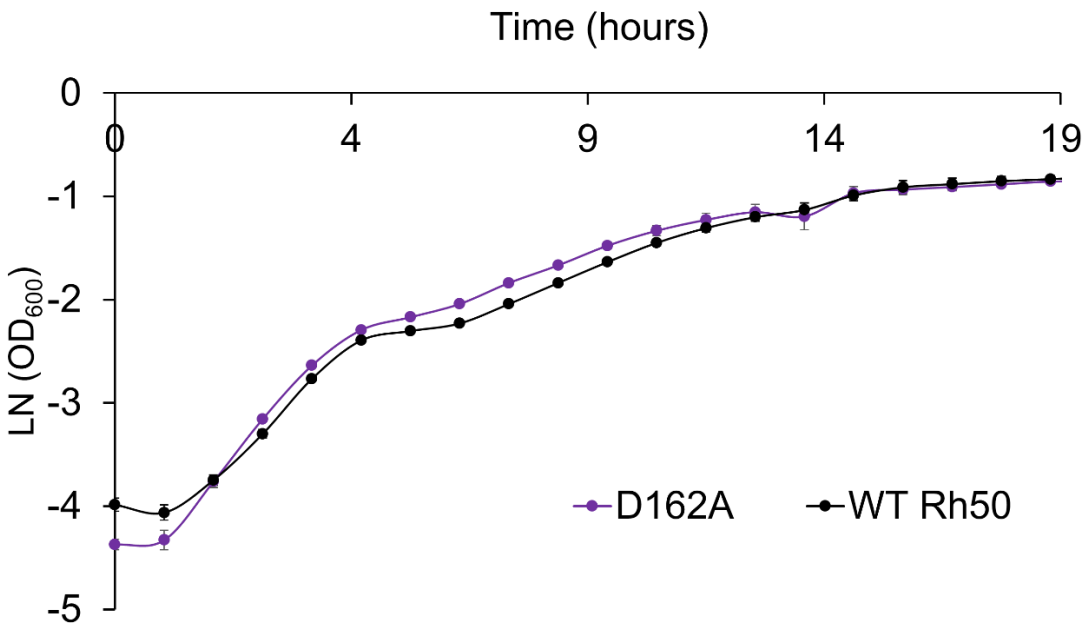

Figure 4.7 Specific growth rate analysis of Rh50^{D162A} variant. GT 1000 + pAD7 expressing either WT Rh50 (black ●) or Rh50^{D162A} (purple ●) in M9 minimal medium supplemented with 0.2 mg/mL glutamine a s a sole nitrogen source (±SD, n=3, p value obtained with Tukey HSD test).

4.8.2 D162A Variant Purify and Insert Correctly

Rh50 variant was overexpressed, purified, and reconstituted in liposomes following the procedure established for wild-type Rh50. However, it is possible that the mutation introduced could destabilise the protein, interfere with its folding, or impact the reconstitution of the protein into the liposomes. To ensure that D162A variant is stable, the protein was analysed by Size Exclusion Chromatography and compared to the WT (**Figure 4.8 A**). The D162A variant eluted as a single peak from the SEC column and over the same elution volume as the WT protein, indicating that it retains the same hydrodynamic properties. To further verify the stability of the protein and whether the insertion into proteoliposomes was successful, SDS-PAGE was used to monitor the wash step following reconstitution. All wash fractions were protein-free, with bands only present in the proteoliposomes lane (**Figure 4.8 B**). The size of the bands matched the expected size of a WT Rh50 monomer (~ 34 kDa), and the trimer (~ 74 kDa). All above indicates that D162A variant was successfully inserted into liposomes. This confirms viability of SSME measurements and variants comparison to the WT.

After the IMAC purification step, the sample was pure and in addition, there were no differences observed between IMAC vs SEC insertion into proteoliposomes, confirming that the SEC purification step is not necessary for the insertion into the liposome. Therefore, insertion of proteins into liposomes was carried out straight after IMAC purification, while SEC was performed for analytical purposes and to confirm the stability of the sample.

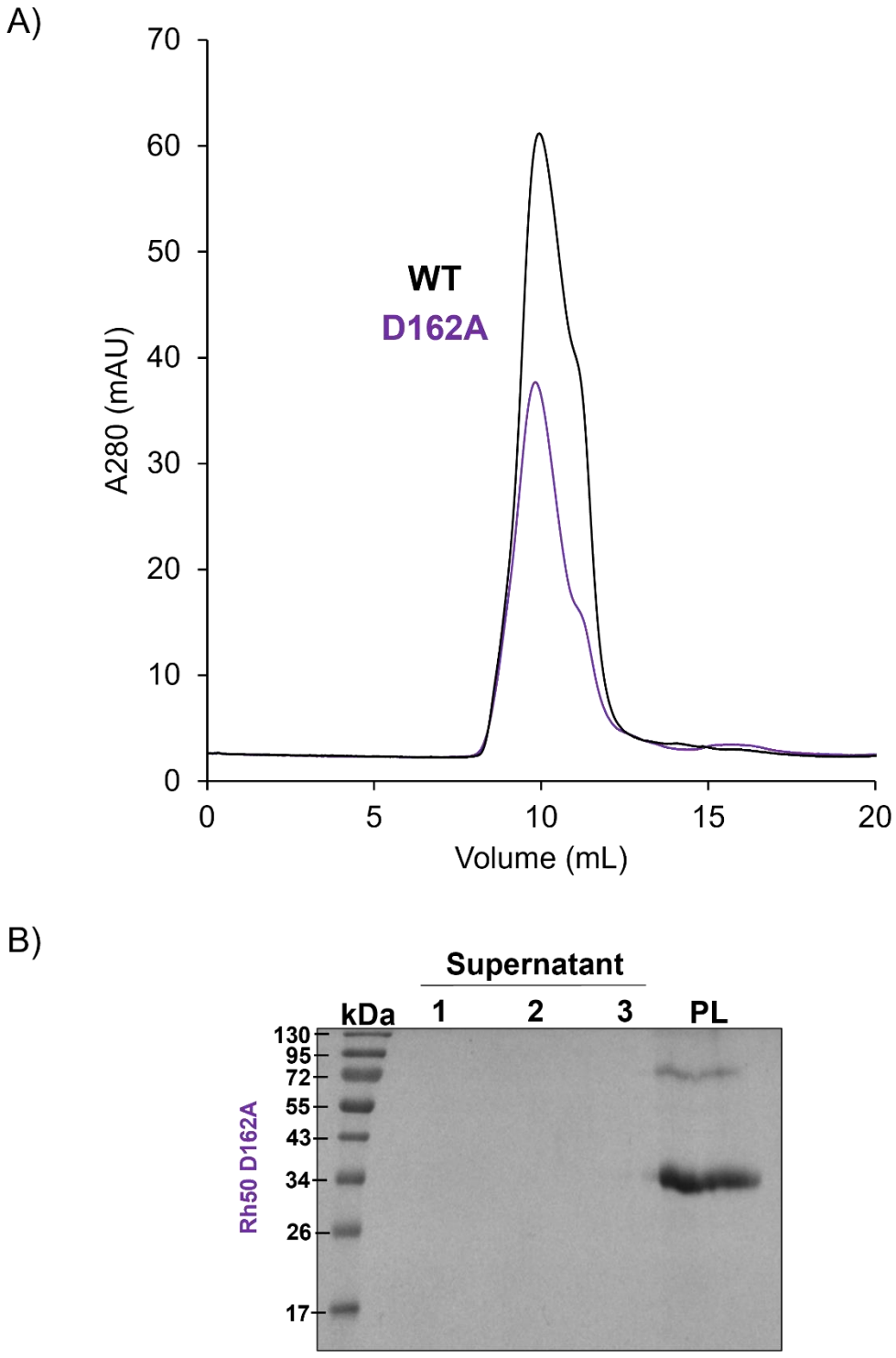

Figure 4.8 D162A Rh50 variant SEC verification and insertion into proteoliposomes. A) Chromatogram of Rh50: WT (black) and D162A (purple) solubilised in 0.09% LDAO. B) 12.5% SDS-PAGE gel of supernatant from each wash step (1-3), and PL (sample) of Rh50 D162A.

4.8.3 Orientation of D162A Variant in the Liposomes

Following successful insertion of Rh50 protein variant into artificial liposomes, the orientation of the protein inserted into the liposome was clarified. This was achieved via proteolysis analysis using trypsin as described before (**Chapter 3, Section 3.4.4**). As seen in **Figure 4.9 A** there is a clear drop in protein size following trypsin digest on SDS-PAGE gel. In addition, a clear drop in the fluorescence emission in control vs trypsin treated proteoliposome was observed on western blot analysed by anti-His antibody **Figure 4.9 B**. This indicates that trypsin cleaved off the histidine tagged C-terminal tail of Rh50 variant inserted at the inside out (IO) orientation (where C- terminal tail is located outside of the liposome) resulting in a drop of the size as well as fluorescence. This indicates that, just like the WT Rh50, D162A variant inserts at a mixed IO and RSO orientation in liposomes.

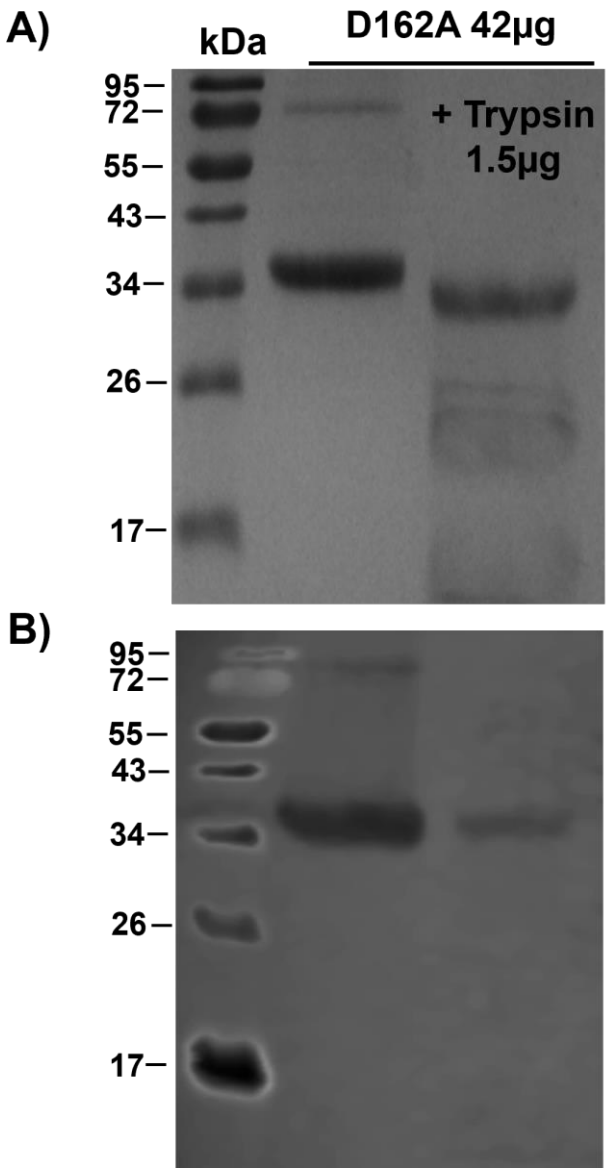

Figure 4.9 Rh50^{D162A} orientation in the liposome. A) Coomassie stained SDS-PAGE gel illustrating the drop in protein size following trypsin digestion. B) Western Blot analysis illustrating drop in fluorescence of Rh50^{D162A} in the liposome following trypsin digestion.

4.8.4 D162 is Essential for Rh50 Activity

A 200 mM ammonium pulse on $Rh50^{D162A}$ proteoliposome at an LPR 5 yielded a transient current with a maximum of 1.1 nA, a ~2-fold decrease in comparison to the WT (**Figure 4.10 B**). The observation of a current implies some residual activity, however the $Rh50^{D162A}$ variant failed to restore the growth in triple-*mepΔ S. cerevisiae* strain (**Figure 4.10 C**) on media supplemented with ammonium as a sole nitrogen source. This suggests that the variant cannot replace the function of endogenous ammonium transporters and is inactive.

Indeed, the comparison of currents obtained in our SSME measurements reveals that the rate of the decay time is unaffected at different LPR, suggesting that the current observed is due to binding rather than translocation event (**Figure 4.11 A**). In addition, the *Km* of $Rh50^{D160A}$ increased 2-fold compared to the WT indicating decreased affinity for the substrate, further suggesting that the protein variant only binds the substrate but does not translocate it (**Figure 4.11 B**). Therefore, whilst a protein-specific electrogenic interaction is taking place, likely at the unknown binding site, $Rh50^{D160A}$ is no longer able to complete a full translocation cycle of ammonium.

These results demonstrate an essential functional role for D162 in Rh50-mediated NH_4^+ transport. We propose that D162, like D160 in AmtB, could be involved in deprotonation step that precedes separate translocation of NH_3 and H^+. While deprotonation is a plausible event in Rh50, it is not known how the charge is translocated through to the cytoplasm.

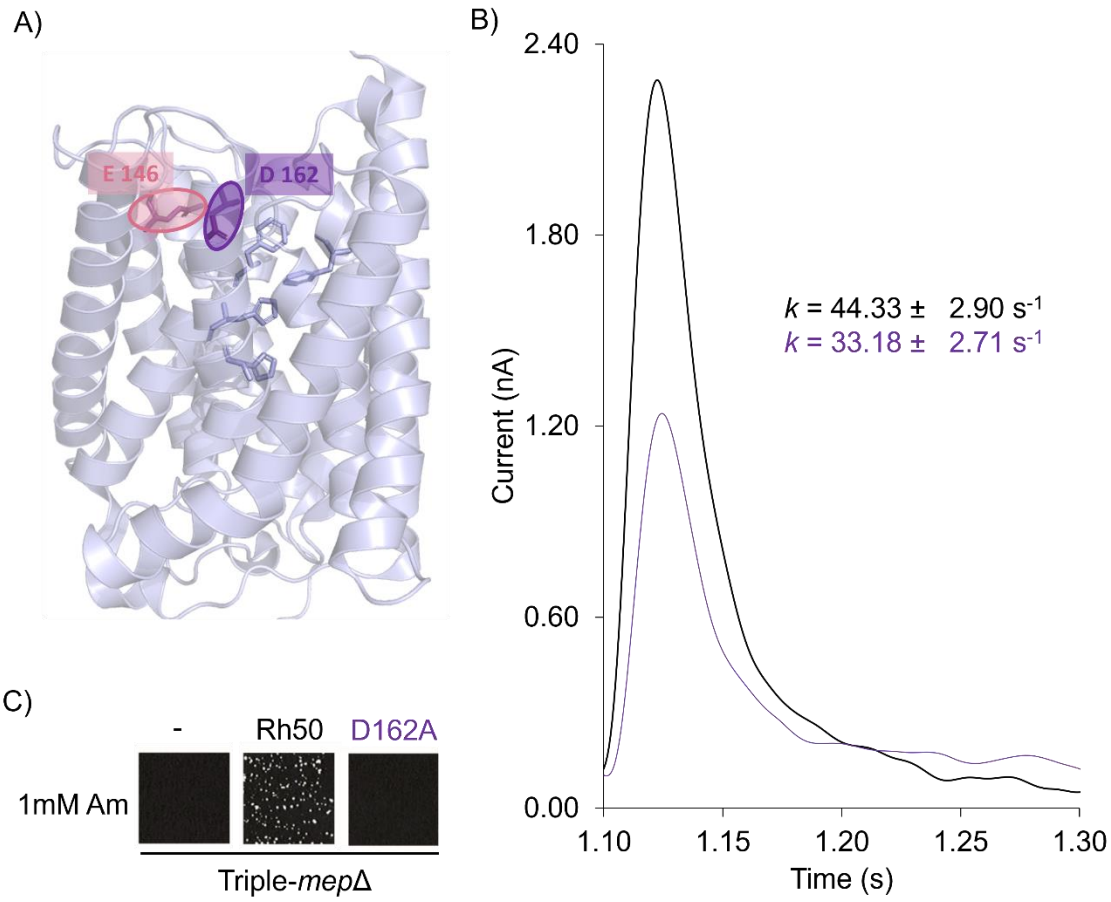

Figure 4.10 D162 is Essential for Rh50 activity. A) Crystal structure of monomer with key residues, D162 highlighted in purple and E146 in pink. D160 is highlighted in purple. B) Representative traces following a 200 mM ammonium pulse for WT Rh50 (black) and Rh50^{D162A} (purple) at LPR 5. C) Yeast complementation after 5 days of growth on minimal media supplemented with 1 mM ammonium (Am).

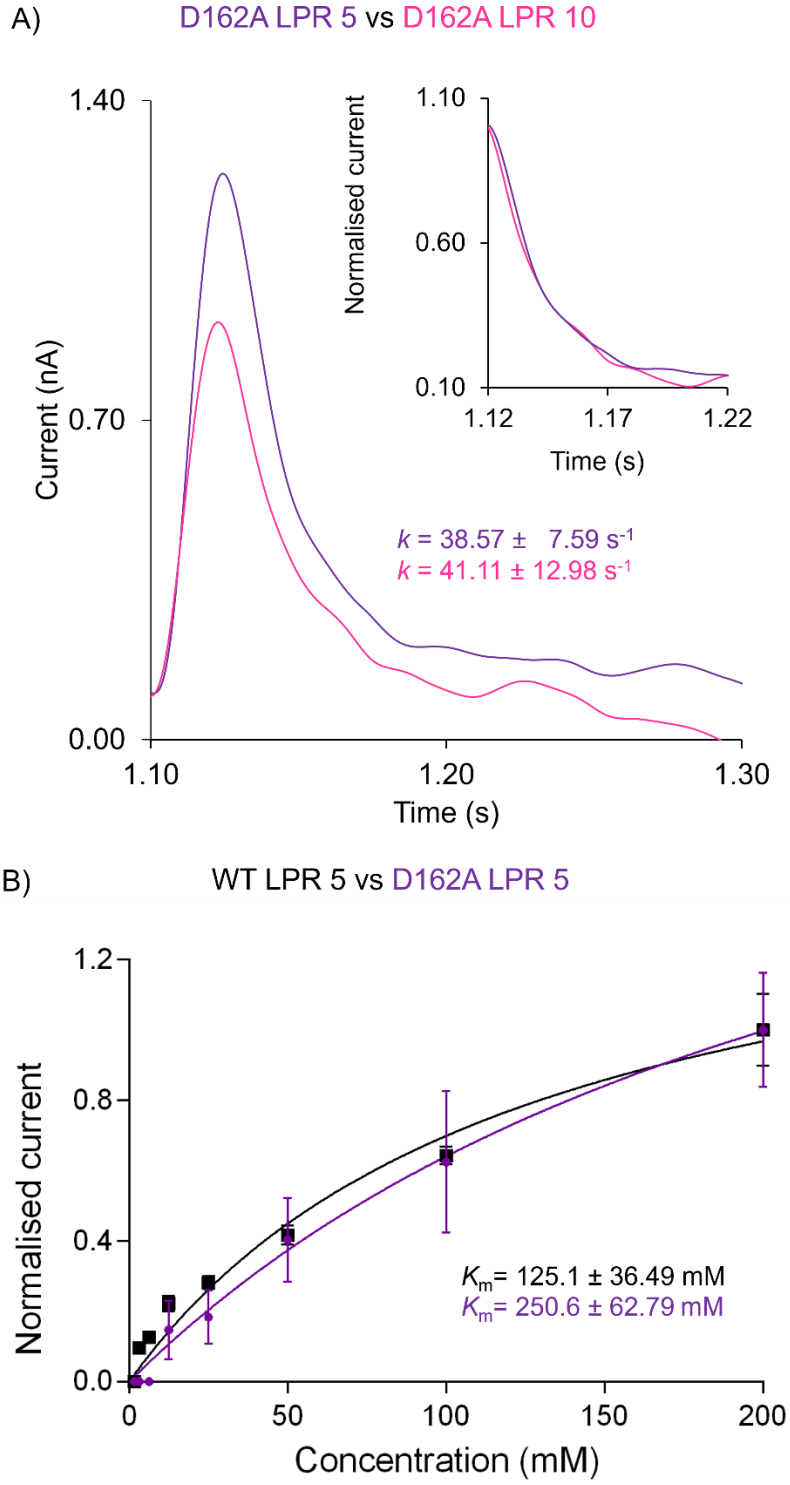

Figure 4.11 Rh50^{D162A} Activity is Abolished. A) Representative traces following a 200 mM ammonium pulse for Rh50^{D162A} at LPR 5 (purple) and LPR 10 (magenta). Inset: Maximum amplitude normalised to 1.0 for comparison. B) Kinetics for WT Rh50 (black) and Rh50^{D162A} (purple) at LPR 5 using NH_4^+. Maximum amplitudes have been normalised to 1.0 for comparison. Data points represent mean ± SD.

4.9 Importance of Water Wires in the Mechanism of Rh50

Following the deprotonation of NH_4^+ into NH_3 and H^+ the water wires were proven to be essential for the proton conduction during AmtB transport cycle (Williamson *et al.*, 2020) wherein H^+ has been ascribed to jump from H_3O^+ to a neighbouring water molecule in a process called Grotthuss mechanism (Cukierman, 2006). To decipher whether Rh50 relays on water wires to import the proton into the cytoplasm following deprotonation, the water (protium oxide, H_2O) in SSME buffers was substituted by heavy water (deuterium oxide, D_2O). There are several differences in chemical and physical properties between D_2O and H_2O. The most relevant for this study are: 1) reduced conductivity of deuterium D^+ in D_2O by ~ 1.5 in comparison to hydrogen H^+ in H_2O, 2) the molecular weight of D^+ is twice higher in comparison to H^+, and 3) D^+ binds more tightly in D_3O^+ than H^+ in H_3O (DeCoursey and Cherny, 1997). Therefore, a mechanism involving a single deuteron transfer should be impaired by ~ 30%. In AmtB the polar network of water identified by Molecular Dynamic Simulations (MDS) comprise of more than 3 water molecules, therefore AmtB activity was entirely abolished when tested in the presence of D_2O (Williamson *et al.*, 2020).

Driven by this finding we wanted to determine if Rh50 also makes use of water wires in transporting the H^+ into the cytoplasm. All buffers used to prepare the proteoliposomes and SSME sensors were prepared using D_2O instead of H_2O. A 200 mM ammonium pulse with D_2O buffers did not abolish the current entirely but decreased the activity of the Rh50 protein by ~ 60% (**Figure 4.12**).

As a control and to ensure that the loss of activity was not merely the result of damage to the protein, D_2O sensors were rinsed with H_2O based buffers. By doing so, the D_2O should be replaced with H_2O restoring electrogenic activity of the protein. Indeed, after rinsing the sensor prepared in D_2O with water-based buffers, Rh50 regained 100% of its activity measured by SSME (**Figure 4.12**), showing that the presence of D_2O did not affect the protein itself nor impact the integrity of the proteoliposome. The same measurements were repeated with MeA as a substrate, having a similar impact of the transport activity **Figure 4.13**.

To check if the current recorded is representing a full translocation cycle, or just substrate-protein binding, the proteoliposomes at an LPR 5, LPR 10 and LPR 50 were tested and compared. As shown in **Figure 4.14**, the higher the protein density in the proteoliposomes, the higher maximum amplitude. For each of the conditions (different LPRs), there is a ~60% reduction of the amplitude when H_2O measurements are compared to D_2O, indicating that this is not simply substrate-protein binding, but indeed a full translocation cycle. In addition, the decay rate is also dependent on protein concentration, increasing from 48.28 ± 8.65 $^{s-1}$ for LPR 10, to 55.64 ± 7.16 $^{s-1}$ for LPR 5, indicating that the transient current is protein specific. There was no visible current recorded for LPR 50.

These results clearly demonstrate that Rh50 relies on water wires to translocate the charge across the membrane, and that proton hopping remains its mechanistic feature. However, the observed current in presence of D_2O, indicates that it is not the only mechanism Rh50 relies on and that some charge translocation is occurring independently of this mechanism.

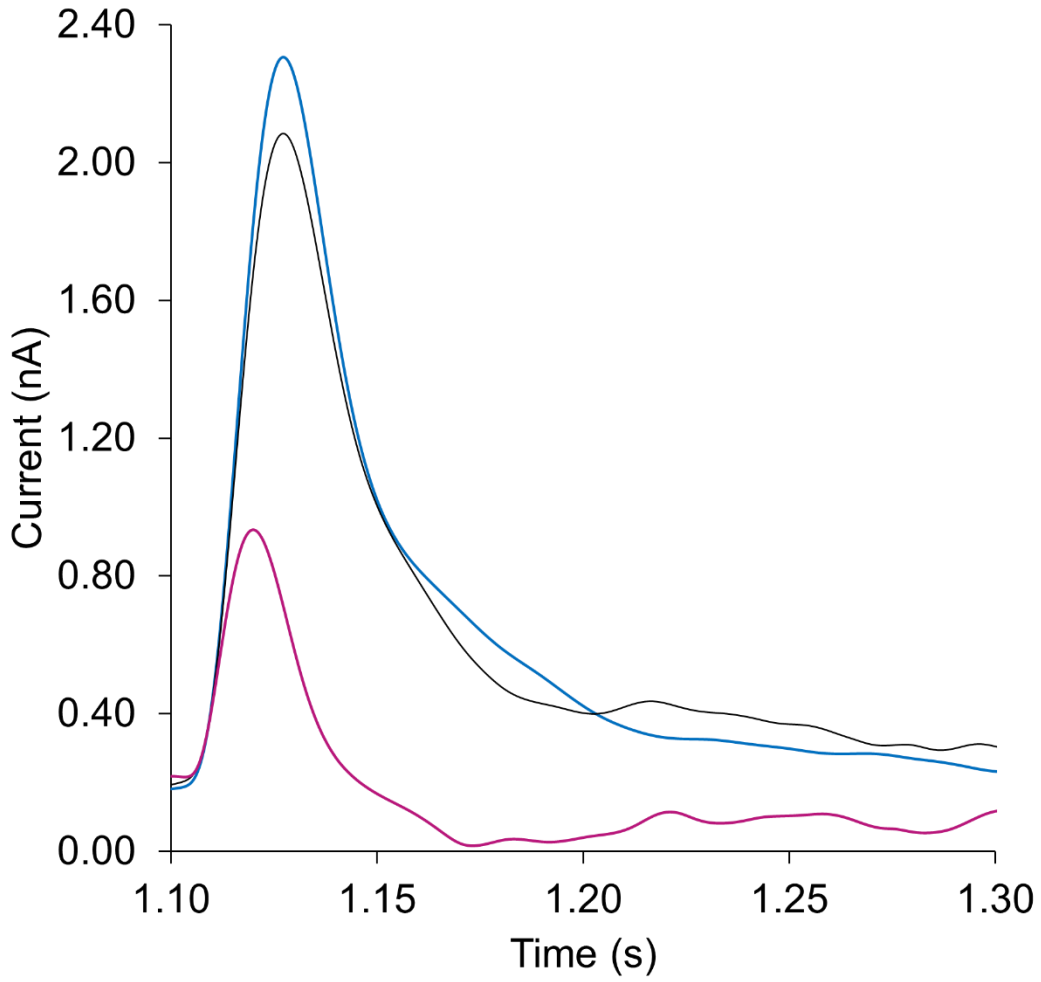

Figure 4.12 D_2O reduces electrogenic activity of Rh50. Transient currents measured following a 200 mM ammonium in proteoliposomes containing Rh50 at an LPR5 pulse on sensors prepared with solutions containing either H_2O (blue) or D_2O (magenta). Subsequently, the D_2O sensors were rinsed with H_2O-solutions and measured again (black).

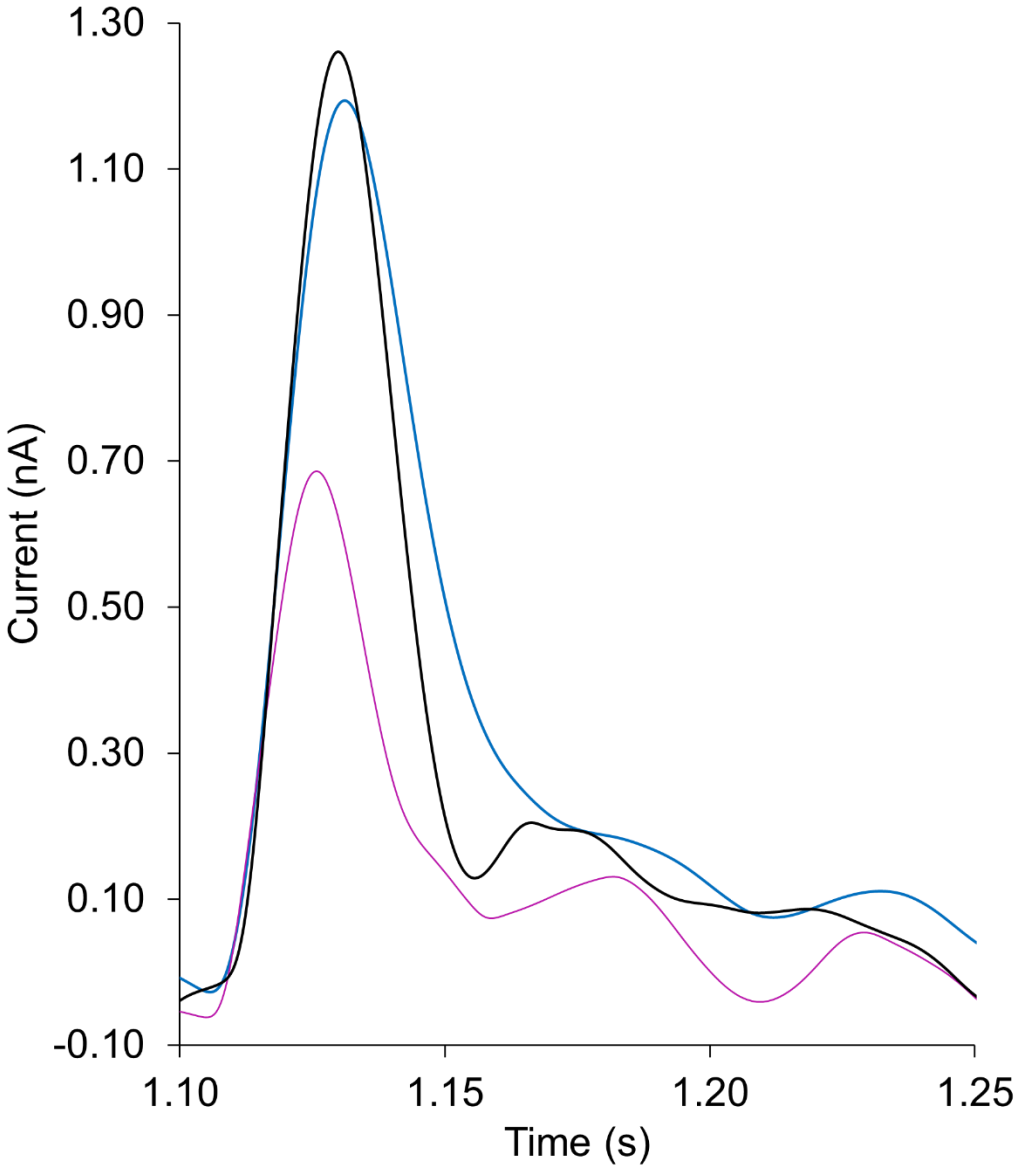

Figure 4.13 D_2O reduces electrogenic activity of Rh50. Transient currents measured following a 200 mM methylammonium pulse in proteoliposomes containing Rh50 at an LPR5 on sensors prepared with solutions containing either H_2O (blue) or D_2O (magenta). Subsequently, the D_2O sensors were rinsed with H_2O-solutions and measured again (black).

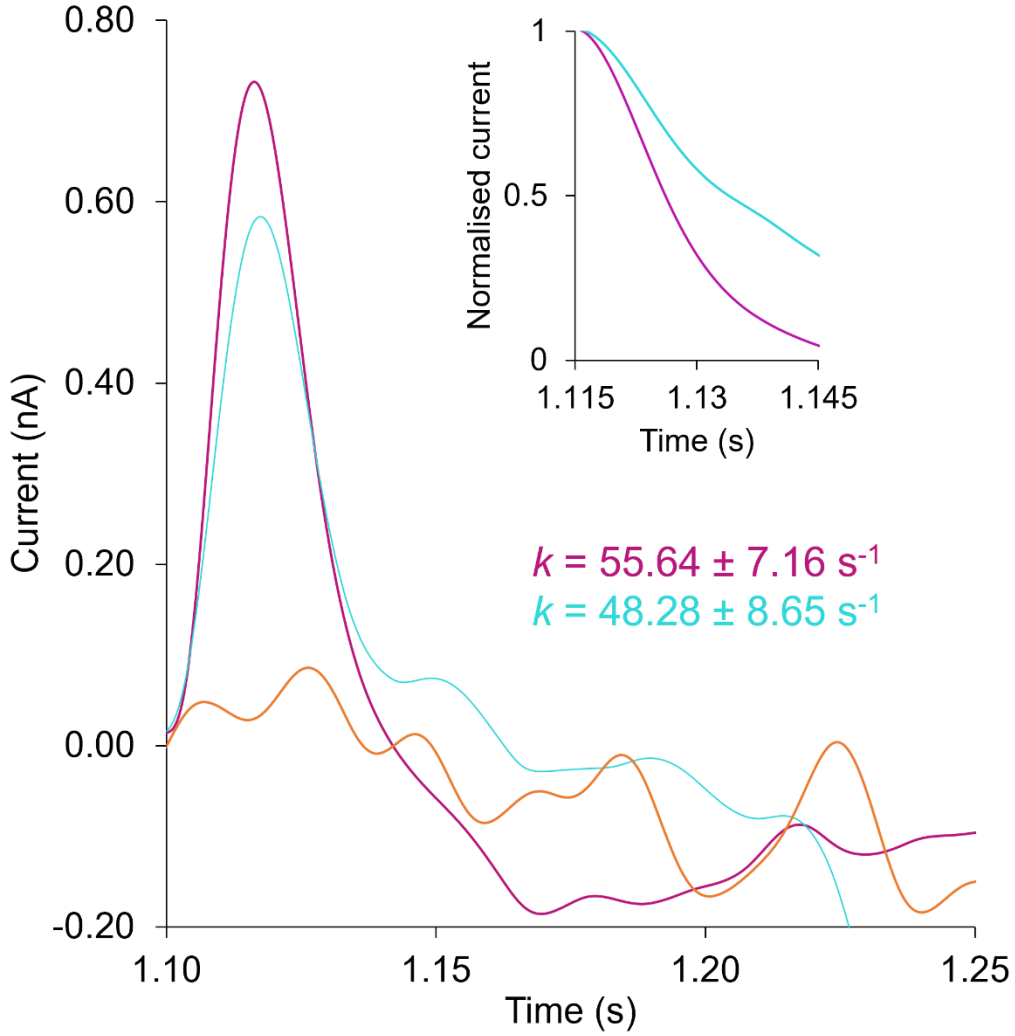

Figure 4.14 D_2O reduces electrogenic activity of Rh50. Transient currents measured following a 200 mM ammonium pulse in proteoliposomes containing Rh50 at an LPR5 (magenta), LPR10 (teal) and LPR50 (orange) on sensors prepared with D_2O based solutions.

4.10 Comparison of Rh50 and AmtB: Translocation and Affinity

The different results between AmtB and Rh50 protein, when tested with D_2O prepared buffers, suggest a difference in the transport mechanism. As mentioned, AmtB activity was entirely abolished when tested in the presence of D_2O suggesting a multistep process, while in the case of Rh50 the activity was reduced by ~ 60%. In addition, AmtB conduction rate drops by ~ 80% when tested with MeA in comparison to ammonium (Mirandela *et al.*, 2018), while in Rh50 it drops by ~ 50% (section 4.3). To elucidate the mechanistic difference between AmtB and Rh50 their translocation and affinity towards ammonium were investigated and compared.

A 200 mM NH_4^+ pulse on polar/POPC 2/1 liposomes containing either AmtB or Rh50 at an LPR 10 elicits a transient current that reaches a mean maximum amplitude of ~ 3.3 nA for AmtB and ~ 1 nA for Rh50 (**Figure 4.15 A**)**.** In addition, both proteins retain selectivity against potassium (for Rh50 see section 4.3, and for AmtB Williamson *et al.,* 2020). Next, the kinetics of ammonium were investigated by measuring transient currents for ammonium pulses ranging from 0.1 mM to 200 mM. It was revealed that the Km of AmtB for ammonium (0.8 ± 0.1 mM) was ~ 70-fold lower than the Km of Rh50 (55.68 ± 16.8 mM) (**Figure 4.15 B**). It should be noted that here we used proteoliposomes prepared at LPR10 for comparison between AmtB and Rh50, which could explain why the Km value is different for Rh50 from results presented above (**section 4.3**).

These results demonstrate that Rh50 activity and affinity for ammonium is lower in comparison to AmtB. Despite these differences, Rh50 activity is saturable, suggesting a transporter-like rather than channel-like activity as previously suggested (Lupo *et al.*, 2007; Weidinger *et al.*, 2007). However, further analysis, including characterisation of variant activity (**Chapter 5**) is necessary to clarify this point.

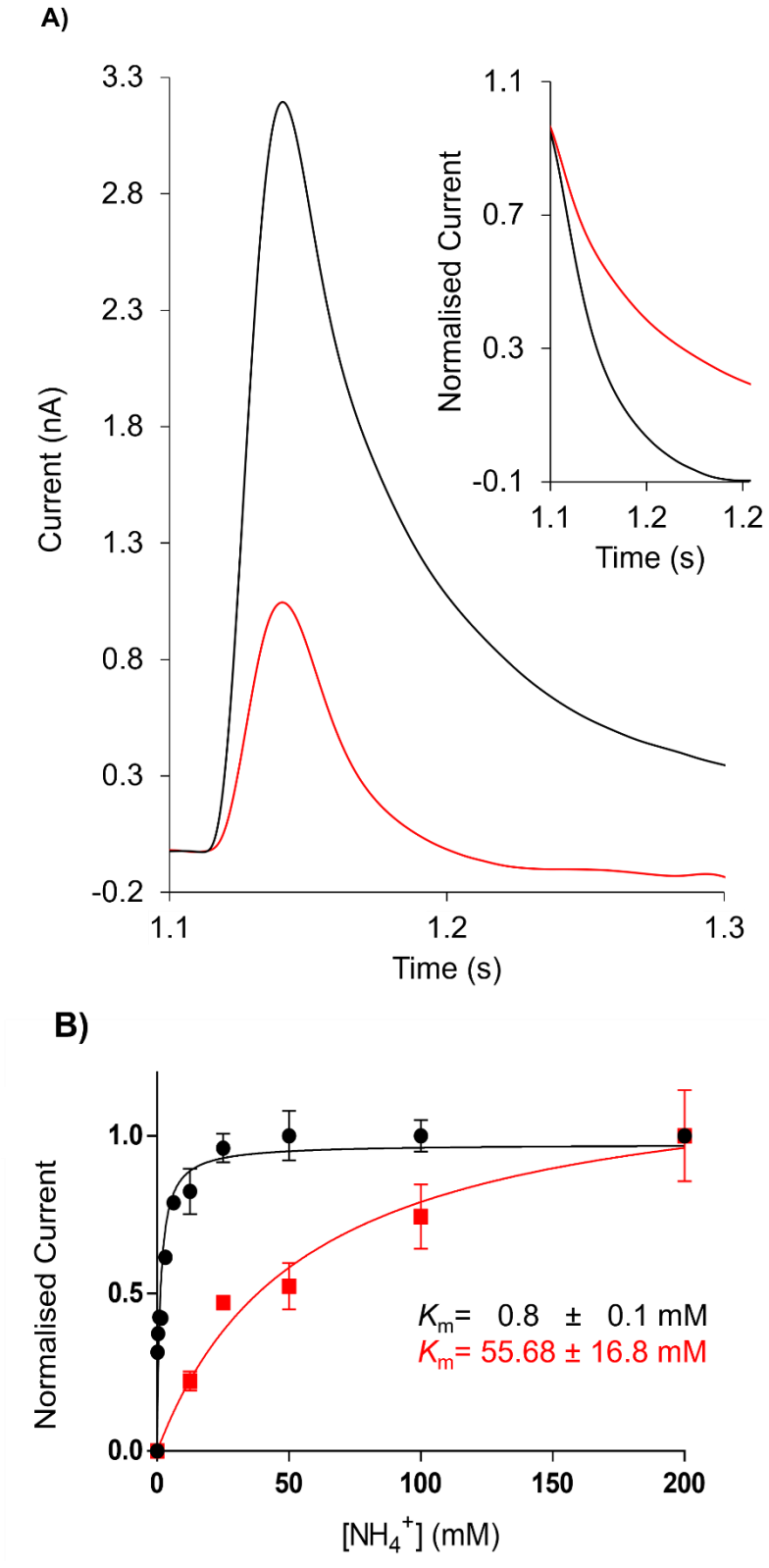

Figure 4.15 Comparison of AmtB and Rh50. A) Transient currents following a 200 mM pulse of NH_4^+ in AmtB (black) or Rh50 (red) reconstituted into Polar/POPC 2/1 proteoliposomes at a LPR of 10:1. Inset: Maximum amplitude has been normalised to 1.0 for comparison B) Kinetics for WT AmtB (black) and Rh50 (red) at LPR 10 using NH_4^+. Maximum amplitudes have been normalised to 1.0 for comparison.

4.11 Discussion

In the previous chapter (**Chapter 3**), we showed that a transient current is measured in proteoliposomes containing Rh50, while no signal is measured in empty liposomes. The decay rate is LPR-dependent, confirming that the transient current represents translocation of ammonium and not simply a protein-substrate interaction. In this chapter, a more in-depth characterisation of Rh50 transport was carried out. We show that the selectivity profile of Rh50 observed with SSME relates to the previously described selectivity of AmtB, where it is permeable to NH_4^+ but not K^+ (Javelle *et al.*, 2008; Mirandela *et al.*, 2018; Williamson *et al.*, 2020). In addition, Rh50 clearly discriminates between ammonium and methylammonium, as its conduction rate drops by ~50 % when tested with MeA in comparison to ammonium. These results demonstrate that Rh50 is ammonium-selective and electrogenic and that MeA is a poor substrate for elucidating mechanistic details of Rh50 activity. In addition, Rh50 activity is saturable, presenting affinity in a mM range, suggesting a transporter-like as opposed to previously suggested channel-like activity (Lupo *et al.*, 2007; Weidinger *et al.*, 2007; Cherif-Zahar *et al.*, 2007). It was also found that Rh50 is active in the pH 5-8 range, but it is clearly less efficient at acidic pH 5. Since the transport efficiency increase with the pH, it can be concluded that the transport of ammonium is pH dependent. This links the Rh50 activity with a natural environment in which *N. europaea* resides, such as soil, sewage, or freshwater where the pH tends to be neutral or basic (Chain *et al.*, 2003). In addition, RhAG mediate ammonia/ammonium transport in human RBCs was also found to be pH depended (pH optimum 7.4 ± 0.1) (Sudnitsyna *et al.*, 2016). This further highlights the similarities between bacterial and human Rh proteins, again justifying our choice of choosing bacterial Rh50 to study the mechanisms of Rh proteins in general.

4.11.1 Mechanism of Transport

As mentioned in the previous chapter electrogenic nature of Rh50 implies either: 1) direct translocation of NH_4^+, 2) Facilitated symport of NH_3 and H^+, or 3) Deprotonation of NH_4^+ into NH_3 and H^+, allowing their separate transport through the protein.

My results demonstrate that NH_4^+ /H^+ symport is unlikely, as a proton gradient does not increase the activity of Rh50. In addition, Rh50 is not able to translocate a proton in the absence of NH_4^+, suggesting that the current induced by Rh50 activity is generated by either a direct translocation of NH_4^+ or deprotonation of the substrate and subsequent H^+ translocation. Indeed, a study utilising relative depletion of ^{15}N compared to ^{14}N provided initial support to argue that deprotonation is a shared characteristic of Amt/Mep/Rh proteins (Ariz et al., 2018). However, the study did not consider where deprotonation happens, and which residues are involved. My results showing the electrogenic nature of Rh50 suggests that the proton is not exiting into the periplasmic space, and that it is likely to be accepted by a residue within Rh50. The very recent MD simulation on human RhCG suggested that NH_4^+ makes hydrogen bonds with residue E 166 positioned at the bottom of the periplasmic vestibule of the protein. Once NH_4^+ is near the E residue, another NH_4^+ approaches, potentially repelling the bound ammonium away. Based on the MD simulation authors suggested that the Phe-gate (**Figure 1.1358**) could be a potential recruitment site for NH_3 molecule, speculating that deprotonation must occur somewhere near the E 166 residue and the Phe-gate (Hoyhtya, 2020). Due to its proximity and high conservation across the family, D162 was investigated as a potential candidate for a proton acceptor in Rh50. It has been have demonstrated that D162 is strictly essential, as Rh50 activity is abolished when substituted to alanine. Thus, it seems clear that D162 plays an essential role in the translocation mechanism in Rh50, and whilst a specific role in deprotonation is yet to be proven the results here provide initial support.

The importance of the aspartic acid residue has also been proven for other members of the Amt/Mep and Rh family. Marini *et al* found that human $RhAG^{D167N}$ and $RhCG^{D177N}$ variants lost their ability to complement the

ammonium growth defect of triple-*mepΔ* yeast. Ammonium removal assays in liquid medium also proved the loss of activity for the D/N protein variants (Marini *et al.*, 2006). Replacement of the conserved aspartate in AmtB from *E. coli* resulted in a loss of activity in the protein (Javelle *et al.*, 2004; Williamson *et al.*, 2020) while studies on *Sc*Mep2 suggested an involvement of its D186 in ammonium recognition, further highlighting the functional importance of this residue (Marini *et al.*, 2006). Hence this highly conserved residue likely plays a preserved functional role in the transport mechanisms of Mep/Amt and Rh proteins in general, potentially as a proton acceptor.

4.11.2 Two Mechanisms Underpin Ammonium Translocation in Rh50

While deprotonation seems to be an important step in the transport mechanism in Rh50, the conductivity in presence of D_2O, detected in Rh50 proteoliposomes shows that the activity does not entirely depend on the translocation of the proton via water wires.

A recent MDS report suggests that water molecules are allowed 2 Å deeper along the channel entry path of the Rh50 pore (Hoyhtya, 2020). This is due to the unusual perpendicular orientation of the Rh50 Phe-gate as opposed to stacked orientation observed in other ammonium transporters (**Figure 1.12**). Such orientation allows the formation of hydrogen bonds between water and central histidine residues, in turn shortening the length of the hydrophobic pore to 11 Å (Hoyhtya, 2020). By contrast, the distance between the water molecules on both sides of the pore for AmtB is more than 20 Å (Khademi *et al.*, 2004; Hoyhtya, 2020). In addition, Hoyhtya *et al* observed that the bottom of the periplasmic vestibule is divided into two parts in the *Ne*Rh50 crystal structure, creating a narrow pathway. Moreover, the cytoplasmic exit of the pore is not guarded by phenylalanine rings as in *E. Coli* AmtB; Human RhCG and bacterial Rh50 have leucine and cysteine residues instead. These structural differences at the periplasmic and cytoplasmic exits may result in differences in the accessibility of water to the central pores of AmtB and Rh proteins. In bacterial Rh50 water molecules were free to create a water bridge between the pore entrance and the periplasmic vestibule allowing water

conduction from periplasm to the central pore (Hoyhtya, 2020). Therefore, some NH_4^+ could potentially slip though the channel along with the water molecules, bypassing deprotonation. This would explain why when D_2O is used in place of H_2O in SSME buffers there is only ~60% reduction in Rh50 activity. In AmtB the mechanism is believed to be purely relying on deprotonation and water wires for NH_3/H^+ translocation, and therefore the conductivity is entirely abolished when tested in D_2O (Williamson *et al.*, 2020). It is thus likely that two mechanisms proposed in **Figure 4.16** are present under our experimental conditions in the bacterial Rh50.

In the context of ion selectivity, this idea becomes more complicated. If NH_4^+ could potentially slip through the pore along with the water molecules, why K^+ would not be able to do so? Understanding the difference in the solvation strength of these ions is particularly important in determining ion selectivity, and, hence answering this question (Song and Corry, 2009). Both NH_4^+ and K^+ are known to exhibit very similar solvation properties in liquid water despite the fact that they possess rather different chemical compositions (Marcus, 2009). However, a study by Aydin *el al* revealed the marginally smaller solvation energy of NH_4^+ compared to that of K^+ based on first-principles molecular dynamics simulations. This suggests that NH_4^+ desolvates easier and, therefore, could migrate into nanopores or ion-exchange membranes (Aydin *et al.*, 2020). This coincides with our results showing that Rh50 is selective against K^+ ions, while still being able to transport charged NH_4^+. However, it is important to emphasize that the activation energy for ion transport through membranes also depends on the chemistry of the membranes. Additional interactions with membranes may play an important role due to the difference in the chemical composition between NH_4^+ and K^+, and further studies are required to determine this.

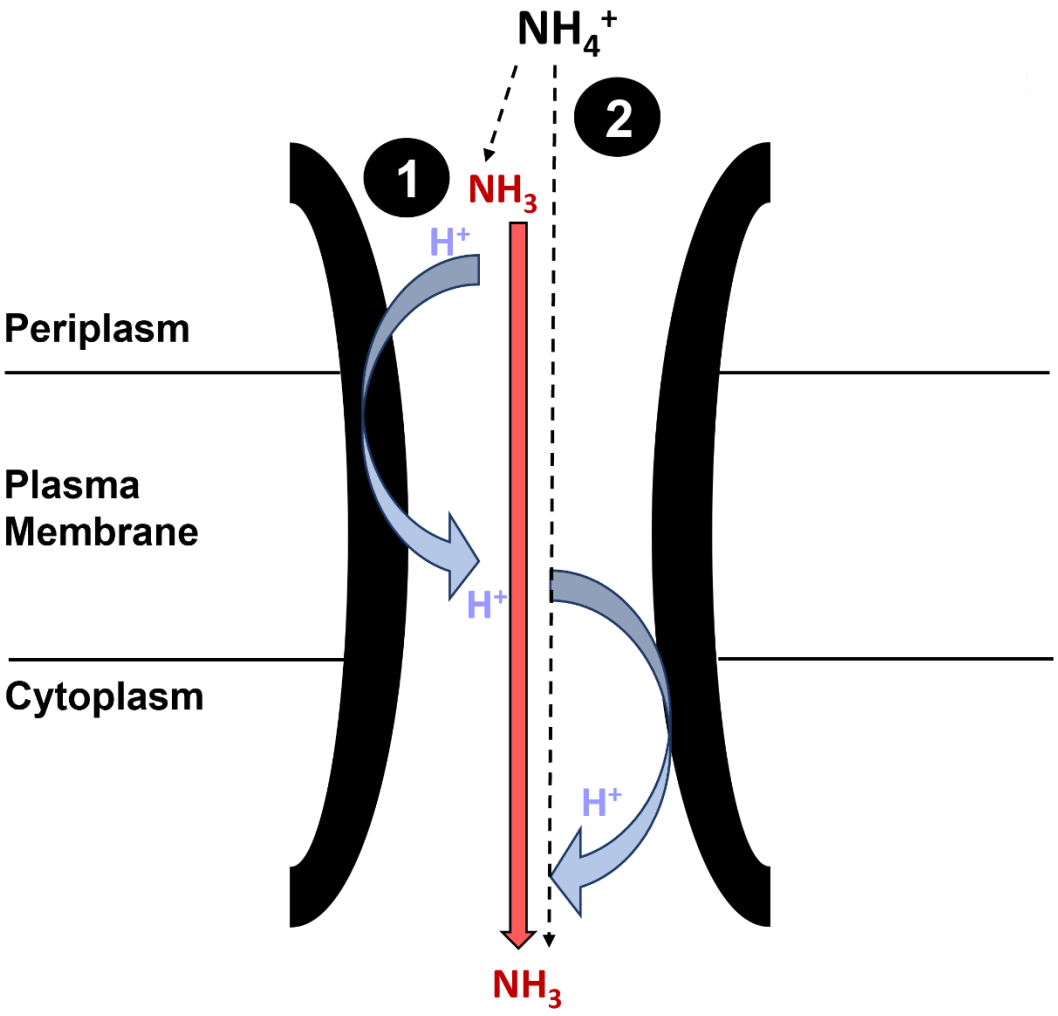

Figure 4.16 Hypothetical transport mechanisms of Rh50 protein. Mechanism I ensure separate NH_3 and H^+ translocation after NH_4^+ deprotonation as proposed for *Ec*AmtB. Mechanism II supports a direct translocation of a hydrated NH_4^+.

4.11.3 Rh50 is Not a Channel

It was previously shown that the restoration of ammonium-dependent growth to a yeast *Δmep* mutant by Rh50 was more effective at higher pH values, a result that is compatible either with facilitated transport of NH_3 through the channel or with a NH_4^+/H^+ exchanger. (Cherif-Zahar *et al.*, 2007; Weidinger *et al.*, 2007). Channel-like activity was also proposed to be a mechanistic feature of mammalian rhesus proteins. Using stopped-flow spectrofluorometric analysis on red blood cells (RBCs) and ghosts from human and mouse genetic variant subjected to ammonium pulse it was concluded that RhAG work as a channel for an NH_3 (Ripoche *et al.*, 2004). Using the same experimental approach on HEK cell expressing RhBG or on liposomes containing purified RhCG, both proteins were also concluded to act as channels for NH_3 (Zidi-Yahiaoui *et al.*, 2005).

Here, we report that the transport mechanism of Rh50 from *N. europaea* is electrogenic and that the kinetics of both, AmtB and Rh50 proteins are saturable, presenting an affinity in the mM range (0.8 ± 0.1 mM vs 55.68 ± 16.8 mM for AmtB and Rh50, respectively). This suggests a transporter-like as opposed to channel-like activity. Moreover, we propose, that this could also be true for the rest of the Rh proteins, as the bacterial Rh50 is thought to be highly representative of all Rh proteins (Lupo *et al.*, 2007). The lower affinity measured on Rh50 compared to AmtB could be explained by the lack of any obvious binding site in Rh50, as described before in Chapter 1 (**Section 1.7.2**). The low ammonium affinity of Rh proteins could also be explained by the protein adaptation to the environment of the organisms/tissues in which they are expressed. *N. europaea* can often be found in ammonium rich environments such as sewage and waste waters. Similarly, human Rh proteins are expressed in tissues which contains high ammonium concentration like erythrocytes, liver, or kidneys (Zidi-Yahiaoui *et al.*, 2005). Therefore, there is no need for a high affinity binding site to scavenge ammonium from the environment in Rh protein. Lastly, the lack of obvious binding site could also be reason why Rh50 discriminates between ammonium and MeA to a lesser extend in comparison to AmtB.

4.11.4 Rh50 Functions Bidirectionally

Results in this chapter show that the expression of Rh50 in a yeast *triple-mep⊿* strain protect the cells from MeA toxicity which provides preliminary evidence that Rh50 promote MeA export from the cell. Using the same technique similar results were previously obtained for Rh50 (Weidinger *et al.*, 2007) and for human RhAG and RhCG proteins (Marini *et al.*, 2000a). In addition, when yeast cells expressing RhAG were grown on arginine, under which conditions catabolism leads to ammonium production, ammonium was excreted at a distinctly higher rate compared with cells not expressing the human protein (Marini *et al.*, 2000a). Another study revealed that Rh null RBC, expressing no Rh complex, had twice lowered exporting efficiency in comparison to normal RBC. Based on these results authors concluded that the Rh complex is involved in the export of ammonium from RBC (Hemker *et al.*, 2003).

This unique ammonium exporting function of the Rh proteins could serve as a protection for RBC in an environment with high ammonium levels. The ammonium concentration is reported to be three times higher inside erythrocytes than in plasma, therefore a tentative hypothesis would be that RhAG, in the Rh complex, promotes export of ammonium accumulated into erythrocytes. If Rh proteins are absent, haemolysis might occur, as noticed in Rh null individuals (Endeward *et al.*, 2006). RhAG may also promote erythrocyte mediated retention of ammonium from the plasma and its release to detoxifying organs such as the liver and brain (Dejong, Deutz and Soeters, 1996). Other ammonium transporting human rhesus proteins RhCG and RhBG are expressed in tissues responsible for ammonia metabolism including liver and kidneys (Liu *et al.*, 2000). More specifically, RhBG and RhCG are expressed on epithelium of the kidney cells involved in ammonium secretion including connecting tubules and collecting ducts (Quentin *et al.*, 2003). Indeed, excretion of excess ammonium ions is crucial in maintaining the systemic acid-base balance (Pitts, 1971). Therefore, it makes sense for Rh proteins to develop strategy providing cells and tissues with protection against ammonium toxicity via excretion or retention of the substrate. For *N. europaea,* it would also be logical to control ammonia import/exit due to its natural habitats which are waste waters rich in ammonia. Indeed, a study on *Aedes*

aegypti, which mostly occupies sewage contaminated water, demonstrated that the larvae owe its resistance to lethal ammonia concentrations to Rh proteins. It was proposed that the larvae can efficiently excrete ammonium against a steep concentration gradient by upregulating expression of rhesus protein within a “physiological triad” of organs (Durant and Donini, 2019).

This unique ability of Rh proteins to excrete ammonium could be due to the water accessibility into the central part of the pore which has not been reported in other ammonium transporters. Unlike AmtB, the Rh protein pores allow water molecules (Hoyhtya, 2020). We, therefore, reason that there could be a relationship between the less hydrophobic nature of the central pore of Rh proteins and their bidirectionality, allowing hydrated NH_4^+ to travel across the pore of Rh. To further investigate the coexistence of these two mechanisms we have purified and characterised variants of *Ne*Rh50 with altered hydrophobicity of the pore. The results are presented in Chapter 5.

Chapter 5

Chapter 5: The Importance of Twin-His Motif and Hydrophobicity of the Pore on the Mechanism of Rh50

5.1 Introduction

Crystal structures of various family members of Amt/Mep/Rh revealed a trimeric organization with a narrow pore present in each monomer (Khademi *et al.*, 2004; Andrade *et al.*, 2005; Lupo *et al.*, 2007; Gruswitz *et al.*, 2010). Unusually conserved two histidine residues, forming the so-called twin-His motif, protrude into the centre of the pore which is otherwise entirely lined by hydrophobic residues. This remarkable conservation of two histidines in this position suggests a strong evolutionary pressure to retain them, and hence their vital role in transport. The only variation in the twin-His motif in members of the Amt/Mep/Rh family is in several fungal Mep transporters where the first histidine (H170 in Rh50 and H168 in AmtB) is replaced by glutamic acid (E) residue (Javelle *et al.*, 2006), and the complete absence of the twin-His motif in human rhesus RhD and RhCE proteins, which have lost transporter functionality (Burton and Anstee, 2008). However, the precise role of twin-His has been a controversial topic for many years. From the analysis of the first crystal structure of AmtB, interactions of twin-His with ammonia was noted, implying that it might be involved in ammonium ion deprotonation (Khademi *et al.*, 2004). However, as aforementioned, in a number of fungal ammonium transporter proteins the first histidine is replaced by glutamic acid residue, what goes against this hypothesis (Javelle *et al.*, 2006). Further structural and mutagenesis studies linked the efficiency of transport with the conserved presence of the twin-His motif (Merrick *et al.*, 2006) which hinted that they might play a key role in allowing the substrate to cross the central part of the channel. This was supported by findings from our lab where we presented a new model for electrogenic ammonium translocation, in which twin-His motif is essential in maintaining a pathway for the translocation of H^+ following NH_4^+ deprotonation **(Chapter 4, section 4.1.1)** (Williamson *et al.*, 2020). The protonation pattern of the twin-His motif has also been proposed to play a role in the hydration of the AmtB protein (Ishikita and Knapp, 2007) and thus serving as a selectivity filter blocking the passage of small cations (Na^+ and

K^+) (Khademi *et al.*, 2004; Zheng *et al.*, 2004). This again has been confirmed experimentally in our lab. Tampering with the hydrophobicity of the pore alters the selectivity of the protein as the result of a mechanistic switch from a transporter-like activity to a channel-like activity in AmtB (Williamson *et al.*, 2022).

The conservation of the twin-His site in the bacterial and human Rh proteins may suggest a similar role(s). Due to how conserved this structure is across the entire family, we want to experimentally determine the functional role of the twin-His motif in Rh proteins.

5.2 Aims and Objectives:

In previous chapters we successfully characterized the activity of WT Rh50 protein. We established that it supports electrogenic transport and does not rely on symport mechanism but rather a deprotonation of NH_4^+. We demonstrated an essential functional role for D162 in Rh50-mediated NH_4^+ transport and proposed its involvement in a deprotonation step that precedes separate translocation of NH_3 and H^+. We also proposed that a direct transport of protonated NH_4^+ molecule might also be happening in parallel to deprotonation, resulting in two mechanisms coexisting together (**Chapter 4, Section 4.11.2**). But how exactly the charge is translocated, either following deprotonation or via direct translocation of the ion, is yet to be unravelled.

In this chapter, we will investigate the importance of a highly conserved twin-His motif and the impact of altering the hydrophobicity of the pore on the Rh50 mechanism. These results will shine light on the possible routes for the charge translocation and further explore the possibility of coexistence of two mechanisms in Rh50. To do this we will utilise *in vitro* SSME measurements and *in vivo* yeast complementation assays. As stated in previous **Chapter 4**, *in vivo* yeast complementation experiments were achieved with the help of our collaborators, Dr. Ana Sofia Brito, Prof. Mélanie Boeckstaens and Prof. Anna-Maria Marini (Free University of Brussels, Belgium).

The aims of this chapter were to investigate the hydrophobicity of the pore and the importance of twin-His motif in:

1. The activity of Rh50 protein.
2. The mechanism of substrate translocation.
3. The selectivity of Rh50 protein.
4. The bidirectionality of the transport.

5.3 Overexpression and Purification of Rh50 Histidine Variants

To better understand the functional role of H170 and H324, we constructed seven variants of Rh50, replacing the histidines with polar and charged amino acids, with the purpose of either increasing or decreasing the hydrophobicity of the pore. Protein variants studied in this chapter are listed in

Table 5.1.

As before, the Rh50 variants were heterologously expressed in *E. coli* strain GT 1000 (Δ*glnK,amtB)* with a hexa-histidine tag at its C terminus. There were no significant differences in the specific growth rates of GT 1000 expressing WT or histine variants suggesting that their overexpression is not toxic to the cells and that large-scale overexpression can be carried out (**Figure 5.1**).

All Rh50 variants were overexpressed, purified, and reconstituted in liposomes following the procedure established for wild-type Rh50 (**Chapter 3, Section 3.3.1**) and D162A variant (**Chapter 4, section 4.8**). Variants eluted from the SEC column over the same column volume (mL) as the WT, indicating that they retain the same hydrodynamic properties (**Figure 5.2**). The shoulder appearing in the gel filtration trace of RH50^{H170AH324A} is possible due to a presence of two different conformations of the protein in the sample. However, the SDS-PAGE analysis of samples inserted into liposomes showed that wash fractions were protein free, with bands corresponding to expected size of a Rh50 monomer (~ 34 kDa), and the trimer (~ 74 kDa) present only in the proteoliposomes lane (**Figure 5.3**). This indicates that while some variants might have more than one conformation in the sample, they remain undamaged by the process and all inserts properly into liposomes.

Table 5.1 Histidine variants investigated in this chapter

Residue changed	Variant	Impact on the Protein	References
		Increasing hydrophobicity of the Pore	
H170	A170	Increased hydration around A168 in *Ec*AmtB	(Javelle *et al.*, 2006;Wang *et al.*, 2013;Williamson *et al.*, 2022)
H324	A324	*Ec*AmtB^{H168A} and AmtB^{H318A} loose selectivity	
H170/H324	A170/A324	*Ec*AmtB^{H168AH318A} is inactive	
		Decreasing Hydrophobicity of the Pore	
H170	E170	Increased hydration pattern in *Ec*AmtB^{H168E}	
H170	D170	E replaces first H naturally in *Sc*Mep1 and 3 *Sc*Mep2^{H194E} variant switches from sensor/transporter to transporter only *Ec*AmtB^{H168E} and *Ec*AmtB^{H168D} are hyperactive	(Javelle *et al.*, 2006;Boeckstaens, André and Marini, 2008;Williamson *et al.*, 2022)
H324	E324	*Ec*AmtB^{H318E} is inactive	
H170/H324	D170/E324	*Ec*AmtB ^{H168DH318E} loses selectivity	

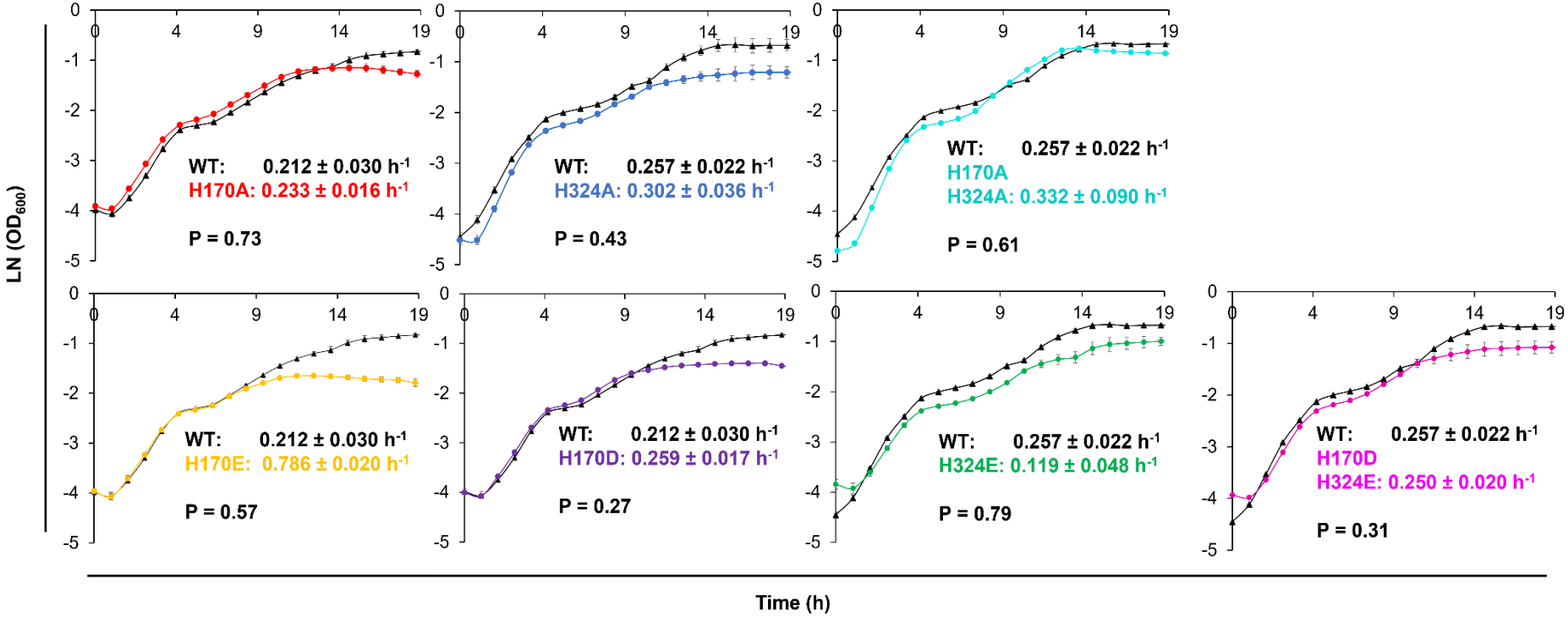

Figure 5.1 Specific growth rate of Rh50 histidine variants. GT 1000 + pAD7 expressing either WT Rh50 or Rh50 histidine variant in M9 minimal medium supplemented with 0.2 mg/mL glutamine a s a sole nitrogen source (±SD, n=3, p value obtained using Tukey HSD test).

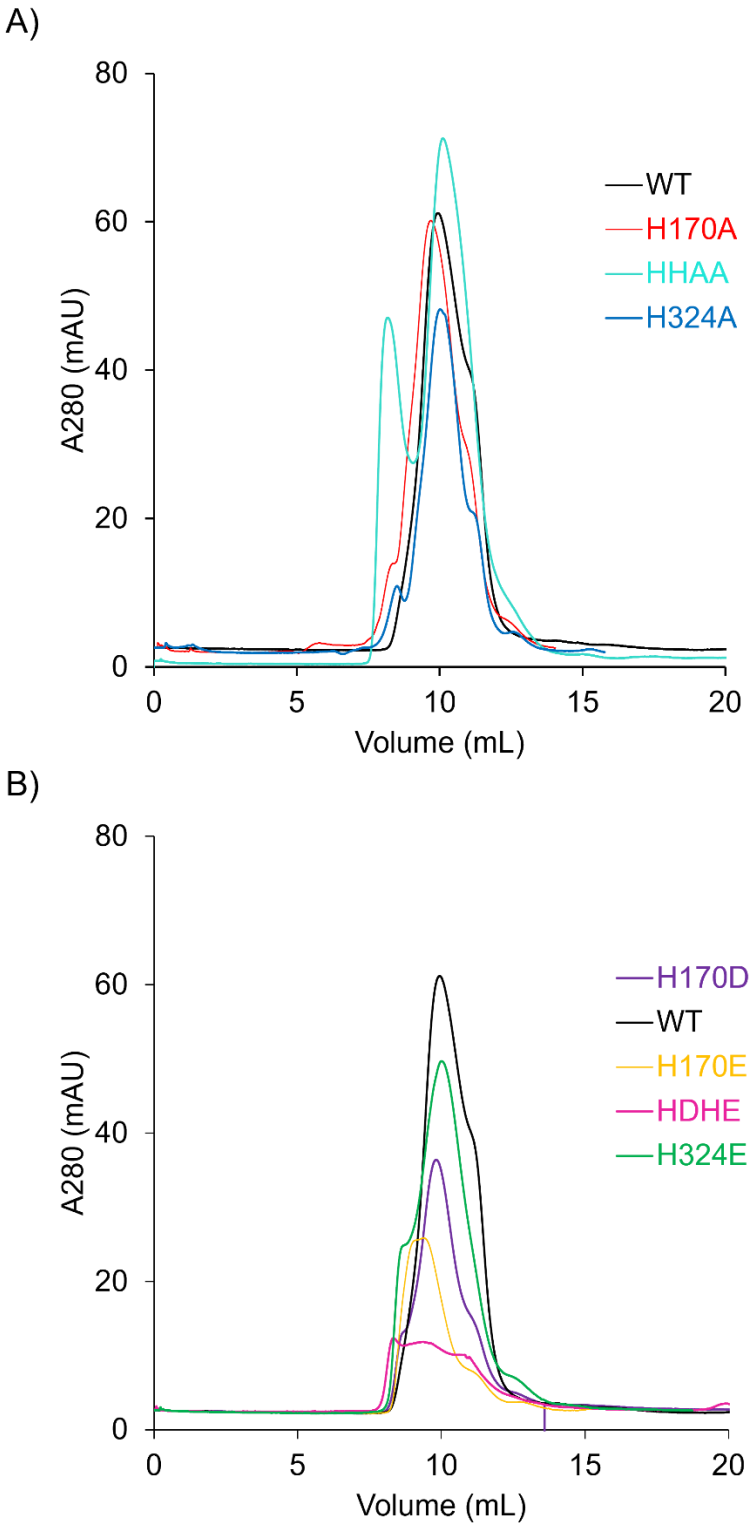

Figure 5.2 Rh50 variants SEC verification. A) Chromatogram of Rh50: WT Rh50 (black), $Rh50^{H170AH324A}$ (teal), $Rh50^{H170A}$ (red), and $Rh50^{H324A}$ (blue), solubilised in 0.09% LDAO. B) Chromatogram of Rh50: WT Rh50 (black), $Rh50^{H170D}$ (purple), $Rh50^{H170E}$ (yellow), $Rh50^{H324E}$ (green) and $Rh50^{H170DH324E}$ (magenta)solubilised in 0.09% LDAO.

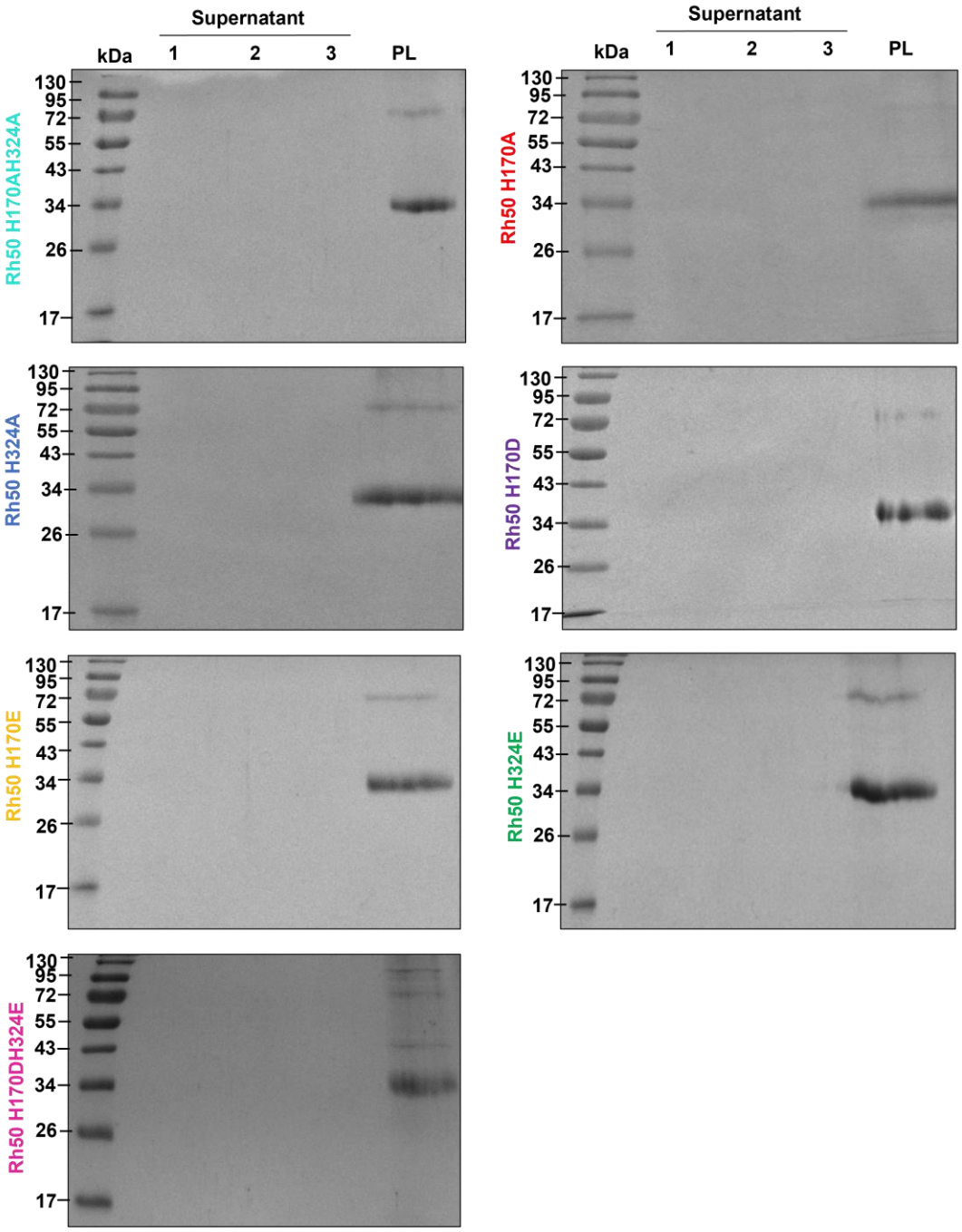

Figure 5.3 Insertion of Rh50 histidine variant into proteoliposome. 12.5% SDS gel monitoring the wash protocol. Left to right: kDA ladder, supernatant 1-3, PL = proteoliposome of either $Rh50^{H170AH324A}$ (teal), $Rh50^{H170A}$ (red), $Rh50^{H324A}$ (blue), $Rh50^{H170D}$ (purple), $Rh50^{H170E}$ (yellow), $Rh50^{H324E}$ (green) and $Rh50^{H170DH324E}$ (magenta)

5.3.1 Orientation of the twin-His Variants

Following successful insertion of Rh50 protein variants into artificial liposomes, the orientation of the protein inserted into the liposome was investigated. This was achieved via proteolysis analysis using trypsin as described before (**Chapter 3, Section 3.4.4**). As seen in **Figure 5.4** there is a clear drop in protein size following trypsin digest on SDS-PAGE gel (blue box). In addition, a clear drop in the fluorescence emission in control vs trypsin treated proteoliposome was observed on western blot analysed by anti-His antibody (**Figure 5.4**, green box). This indicates that trypsin cleaved off a long C-terminal tail of Rh50 variants inserted at inside out (IO) orientation, where C-terminal tail is located outside of the liposome, resulting in a drop of the size as well as fluorescence. This proves that, just like the WT Rh50, all histidine variants insert at a mixed Inside Out (IO) and Right Side Out (RSO) orientation in liposomes.

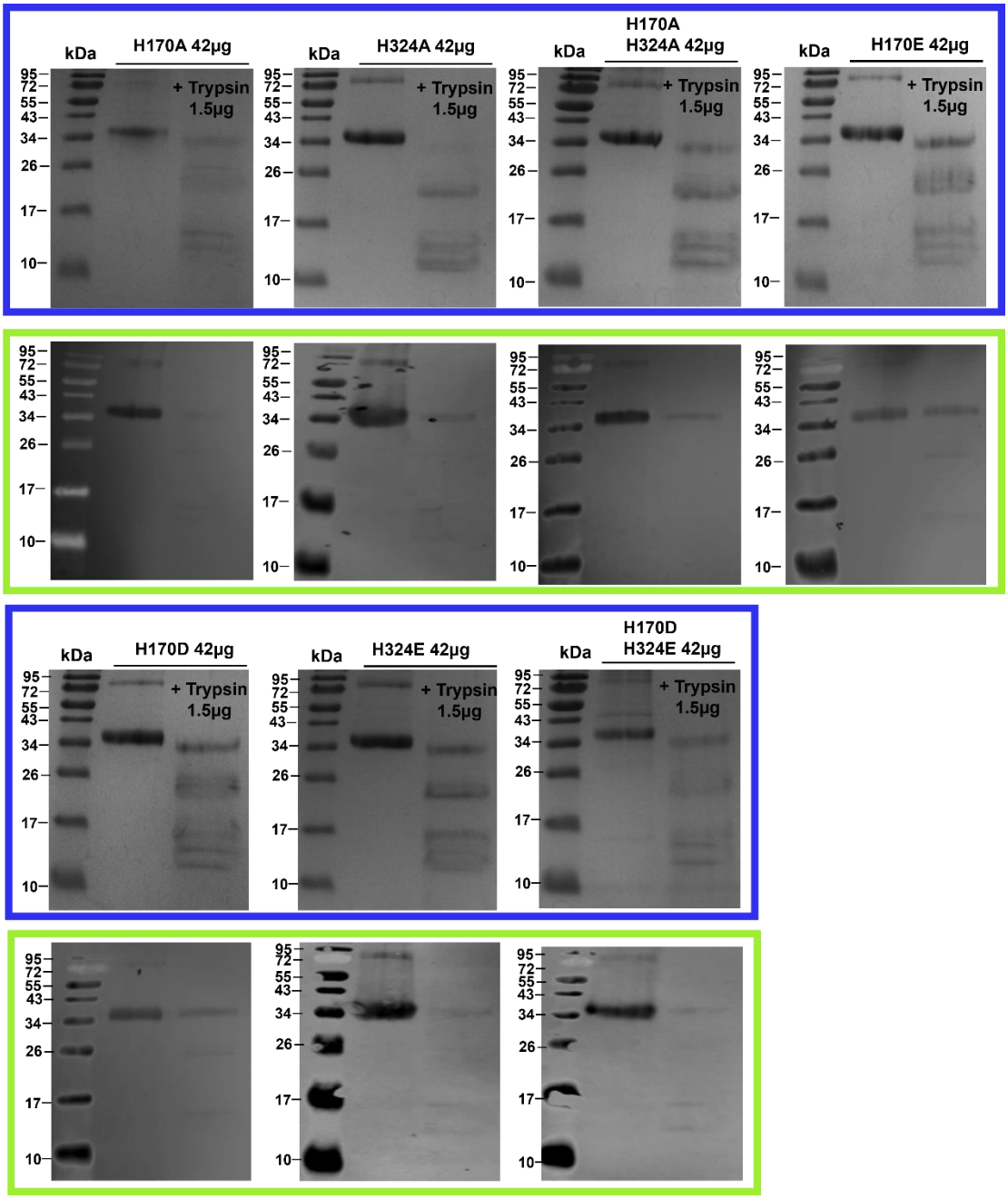

Figure 5.4 Rh50 histidine variants orientation in the liposome. Coomassie stained SDS-PAGE gel illustrating the drop in protein size following trypsin digestion (blue box) with corresponding Western Blot analysis underneath illustrating drop in fluorescence (neon green) following trypsin digestion.

5.4 The Importance of the twin–His in Rh50 Activity

The remarkable conservation of the two pore histidines led to the hypothesis that they play a key role in allowing the substrate to cross the central part of the channel. Our lab presented a new model in which twin-His motif is essential in maintaining a dynamic polar pathway spanning the pore of *Ec*AmtB which allows translocation of H^+ (Williamson *et al.*, 2020). Atomistic molecular dynamics (MD) simulations of AmtB in mixed lipid bilayers revealed two water wires: cytoplasmic water wire (CWW) and periplasmic water wire (PWW). The former spans from residue D160 near the S1 region to the central twin-His motif, while the latter connects the twin-His motif to the cytoplasmic side of the pore (Lamoureux, Klein and Bernèche, 2007; Williamson *et al.*, 2020). Twin-His is therefore essential in forming this molecular bridge allowing the H^+ (following deprotonation) to be transported across (more detailed description **Chapter 4, Section 4.1.1**).

In Rh proteins, the precise function of twin-His, whether to serve as proton acceptors for an entering ammonium ion, or more simply, to shape the pore and balance its polarity, has remained unanswered and no experimental data is available to confirm their role. Our SEC analysis and reconstitution SDS-gels show that all variants appear intact and correctly folded, thus histidine residues are not merely for structural purposes. This suggests they are rather required for the activity of the protein. In attempt to decipher the importance of the twin-His motif in Rh50, we investigated the mechanisms of Rh50 histidine variants with a residue substitution which either increase or decrease the hydrophobicity of the pore (

Table 5.1).

5.4.1 Increasing the Hydrophobicity of the Pore

Previous molecular dynamic simulations on AmtB showed that although the overall structures of the variant channels are very similar to the wild type (WT), when the polar residue histidine is mutated to the hydrophobic residue alanine, the hydrophobicity of the pore becomes higher than that of the WT (Wang *et al.*, 2013). Due to high conservation of the pore across the Amt/Mep/Rh family this could also be true for Rh50 protein. Therefore, both histidines (H170 and H324) were substituted with alanine to determine how increasing the hydrophobicity of the pore impacts the activity of the protein.

We observed a drop in amplitude after a 200 mM ammonium pulse, in proteoliposomes containing $Rh50^{H170AH324A}$ vs WT (**Figure 5.5 B**). However, when expressed in triple-*mepΔ* yeast, $Rh50^{H170AH324A}$ did not support growth on media supplemented with ammonium as a sole nitrogen source (**Figure 5.5 C**). This suggests that the variant is not active. Indeed, the decay rates were not dependent on the LPR (**Table 5.2**) suggesting that residual current observed was merely the result of an interaction between NH_4^+ and Rh50 and not translocation.

It is not clear if the loss of activity is caused by the removal of both residues or if removal of just one of the histidines would have a similar effect. To distinguish the difference in their roles, each of the histidine residues was individually substituted with alanine. A 200 mM ammonium pulse elicited a transient current in both histidine variants. For $Rh50^{H170A}$ we did not observe a significant difference in current in our SSME recordings in comparison to the WT, and triple-*mepΔ* yeast cells expressing $Rh50^{H170A}$ displayed growth in the presence of low ammonium concentrations (**Figure 5.6 C**). $Rh50^{H170A}$ activity was LPR-dependent (**Figure 5.7 A**), suggesting it is an active transporter and the current observed is due to both binding and translocation of the substrate. NH_4^+ translocation activity was saturable in the concentration range [12.5-200 mM] and followed the Michaelis-Menten kinetics model presenting with similar affinity for the substrate as the WT, suggesting that it behaves in a transporter-like manner (**Figure 5.7 B**).

Similarly, Rh50^{H324A} produced a transient current following a 200 mM ammonium pulse, with a maximum amplitude ~2-fold lower than that of the WT (**Figure 5.6 B**). However, unlike Rh50^{H170A}, Rh50^{H324A} failed to support the growth in triple-*mepΔ* yeast, on the media supplemented with ammonium (**Figure 5.6 C**), indicating that Rh50^{H324A} is inactive. Indeed, the decay rate of the transient current was not LPR dependent for Rh50^{H324A} (**Table 5.2**), suggesting that the variant is unable to transport ammonium, and the current observed is only the results of substrate binding, and not the translocation event.

Taken together, the data suggests that increasing the hydrophobicity of the pore is only tolerated if the first histidine is substituted by alanine. It is not entirely clear if histidine in position 324 is more crucial for activity of the protein, but the above data seem to imply that.

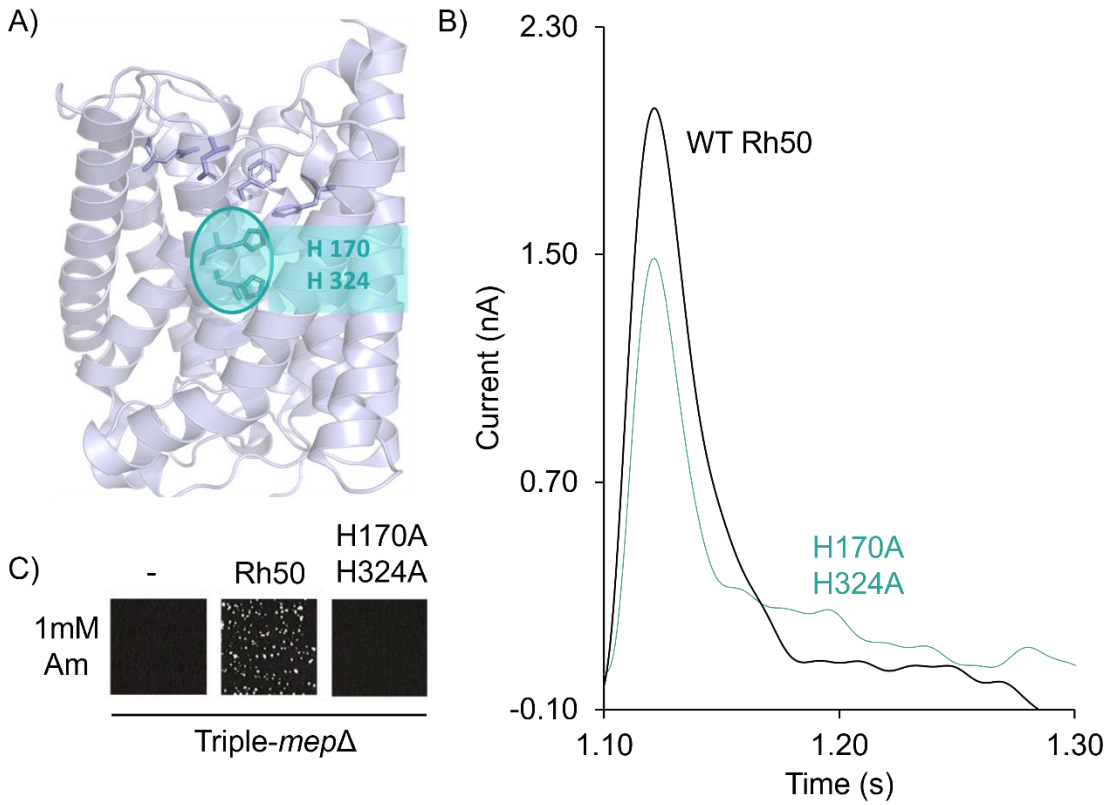

Figure 5.5 Twin-His is Essential for Rh50 activity. A) Cartoon representation of Rh50 monomer, highlighting substituted H170 and H324 residues. B) Representative traces following a 200 mM ammonium pulse for WT Rh50 (black) and Rh50^{H170AH324A} (cyan) at LPR 5. C) Yeast complementation after 5 days of growth on minimal media supplemented with 1 mM ammonium (Am).

Table 5.2 Decay time constants (s^{-1}) of transient currents triggered after an ammonium, methylammonium or potassium pulse of 200 mM measured by SSME.

	NH4+		MeA	K^+
Protein	LPR5	LPR10	LPR5	LPR5
WT	44.3 ± 2.7	33.2 ± 2.7	25.8 ± 6.1	NC
H170A	36.1 ± 6.8	28.1 ± 4.9	21.4 ± 2.6	NC
H170D	33.2 ± 2.6	25.5 ± 9.6	21.4 ± 4.4	NC
H170E	24.0 ± 4.9	14.3 ± 3.4	15.7 ± 4.9	NC
H324A	25.0 ± 2.7	20.9 ± 0.8	43.3 ± 6.8	NC
H324E	20.3 ± 3.3	27.6 ± 7.0	27.8 ± 8.6	NC
H170A H324A	68.0 ± 1.7	58.8 ± 11.8	60.2 ± 25.3	NC
H170D H324E	29.4 ± 12.1	21.9 ± 4.5	21.5 ± 7.6	NC

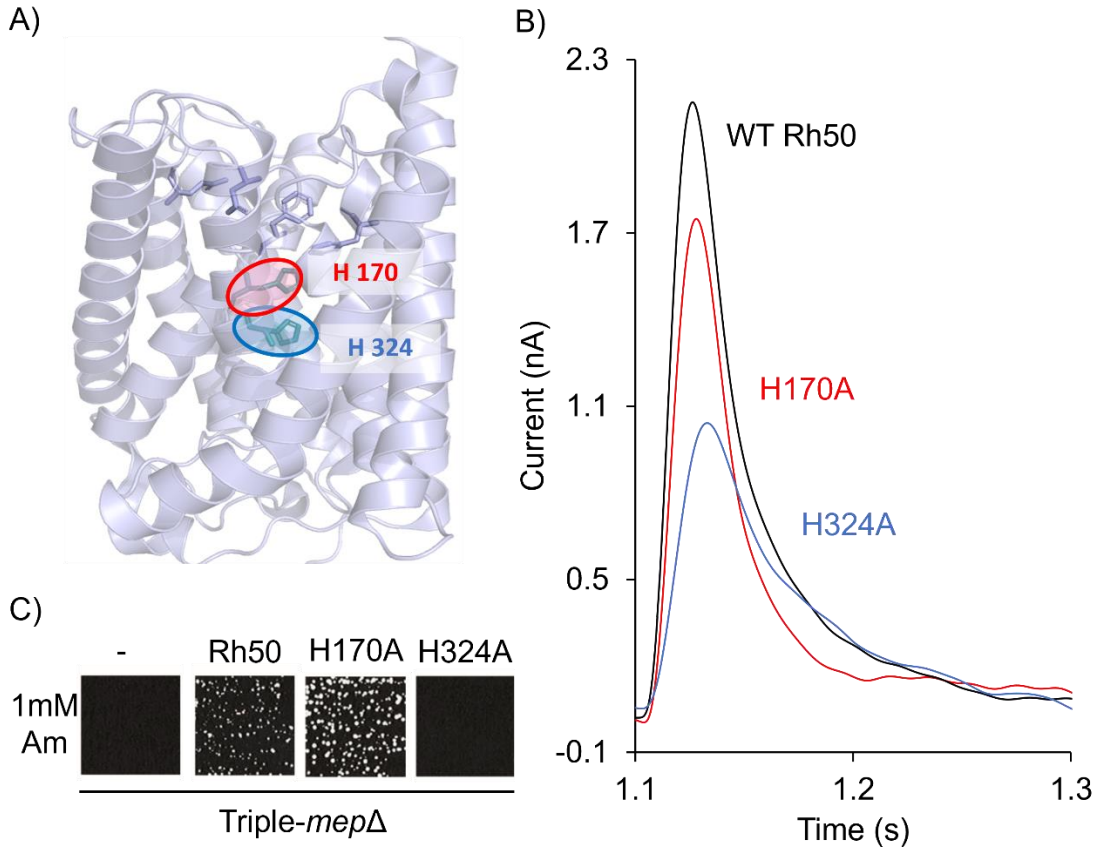

Figure 5.6 Impact of Increasing Hydrophobicity of the Pore on Rh50 activity. A) Cartoon representation of Rh50 monomer, highlighting substituted H170 and H324 residues. B) Representative traces following a 200 mM ammonium pulse for WT Rh50 (black) and $Rh50^{H170A}$ (red) $Rh50^{H324A}$ (blue) at LPR 5. C) Yeast complementation after 5 days of growth on minimal media supplemented with 1 mM ammonium (Am).

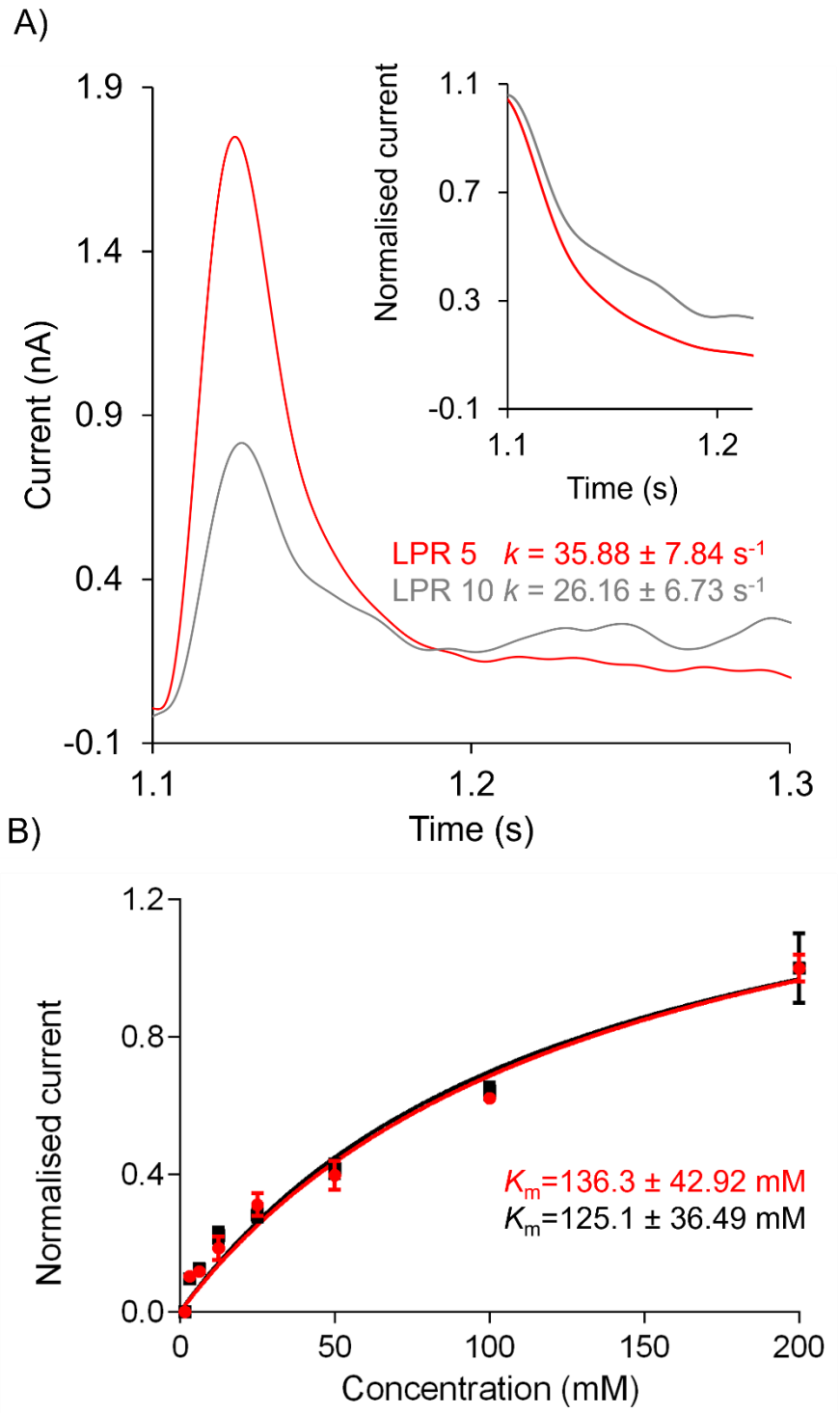

Figure 5.7 H170A is an active transporter. A) Representative traces of proteoliposomes containing $Rh50^{H170A}$ at LPR 5 (red) and LPR10 (grey) following a 200 mM ammonium pulse. Inset: Maximum amplitudes have been normalised to 1.0 for comparison. B) Kinetics for WT Rh50 (black) and $Rh50^{H170A}$ (red) at LPR 5 using NH_4^+. Data points represent mean ± SD.

5.4.2 Decreasing the Hydrophobicity of the Pore

The presence of charged species would be expected to decrease the hydrophobicity of the pore, and hence change its hydration pattern. We wanted to investigate how this change in hydration pattern would affect the activity of the protein. To do this we substituted histidine residues within the twin-His with charged species, either glutamic acid (E), or aspartic acid (D), or both, and tested the impact on the activity of Rh50. It is of interest to note, that in a number of fungal Mep proteins, a glutamic acid (E) residue replaces the first histidine and these proteins can also facilitate ammonium transport (Marini *et al.*, 1997a; Smith *et al.*, 2003; Biswas and Morschhäuser, 2005; Brito *et al.*, 2020). Therefore, we first looked at the effect of single acidic substitutions within the twin-His motif of Rh50, mimicking the glutamic acid substitution present in the fungal Mep1 and Mep3 - type transporters.

Following a 200 mM ammonium pulse we observed a current in our SSME recordings in proteoliposomes containing $Rh50^{H170E}$ (**Figure 5.8 B**). In addition, triple-*mepΔ* yeast cells expressing $Rh50^{H170E}$ display growth in the presence of low ammonium concentrations (**Figure 5.8 C**), suggesting that the variant is active. Indeed, $Rh50^{H170E}$ transport is LPR-dependent indicating that the current reflects a full translocation cycle (**Figure 5.9** A). NH_4^+ translocation activity is saturable in the concentration range [12.5-200 mM] and the variant protein retains similar affinity for the substrate to that of WT protein (*Km*= 67.71 ± 28.78 mM and K_m= 69.73 ± 18.67 mM, respectively) (**Figure 5.9 B**). Similarly, the current has been observed for $Rh50^{H170D}$ variant, and a triple-*mepΔ* yeast cells expressing $Rh50^{H170D}$ display growth in the presence of low ammonium concentrations (**Figure 5.8**). The transport is LPR-dependent, and the NH_4^+ translocation activity is saturable in the concentration range [12.5-200 mM] following the Michaelis-Menten model (**Figure 5.10**).

Taken together, these findings suggests that the additional charge in place of first histidine does not impact the translocation ability of Rh50. Given that some fungal Mep proteins have glutamic acid in place of their first histidine, it is not a surprising finding. However, whether those fungal Mep proteins containing the natural E substitution have gained a specific biochemical or physiological

function during evolution remains unclear (Javelle *et al.*, 2006). In addition, *E. coli* AmtB^{H168E} did not perturb the structure of the protein in previous studies (Javelle *et al.*, 2006). It was argued that E residue appears to occupy about the same space and can potentially make similar hydrogen-bonding interactions as the equivalent histidine residue (Winkler, 2006). Therefore, this could also be true for Rh50 protein.

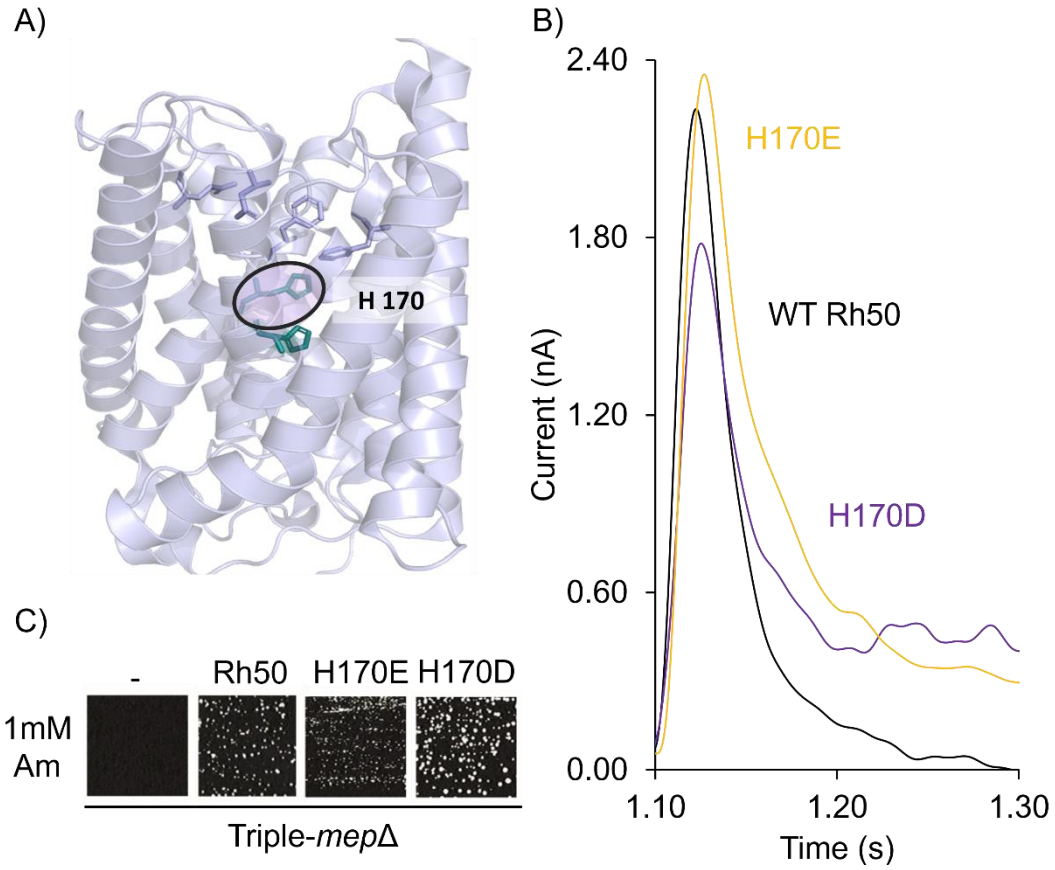

Figure 5.8 Impact of Increasing the Hydrophobicity of the Pore on Rh50 activity. A) Cartoon representation of Rh50 monomer, highlighting substituted H170 residue. B) Representative traces following a 200 mM ammonium pulse for WT Rh50 (black) and $Rh50^{H170E}$ (yellow) $Rh50^{H170D}$ (purple) at LPR 5. C) Yeast complementation after 5 days of growth on minimal media supplemented with 1 mM ammonium (Am).

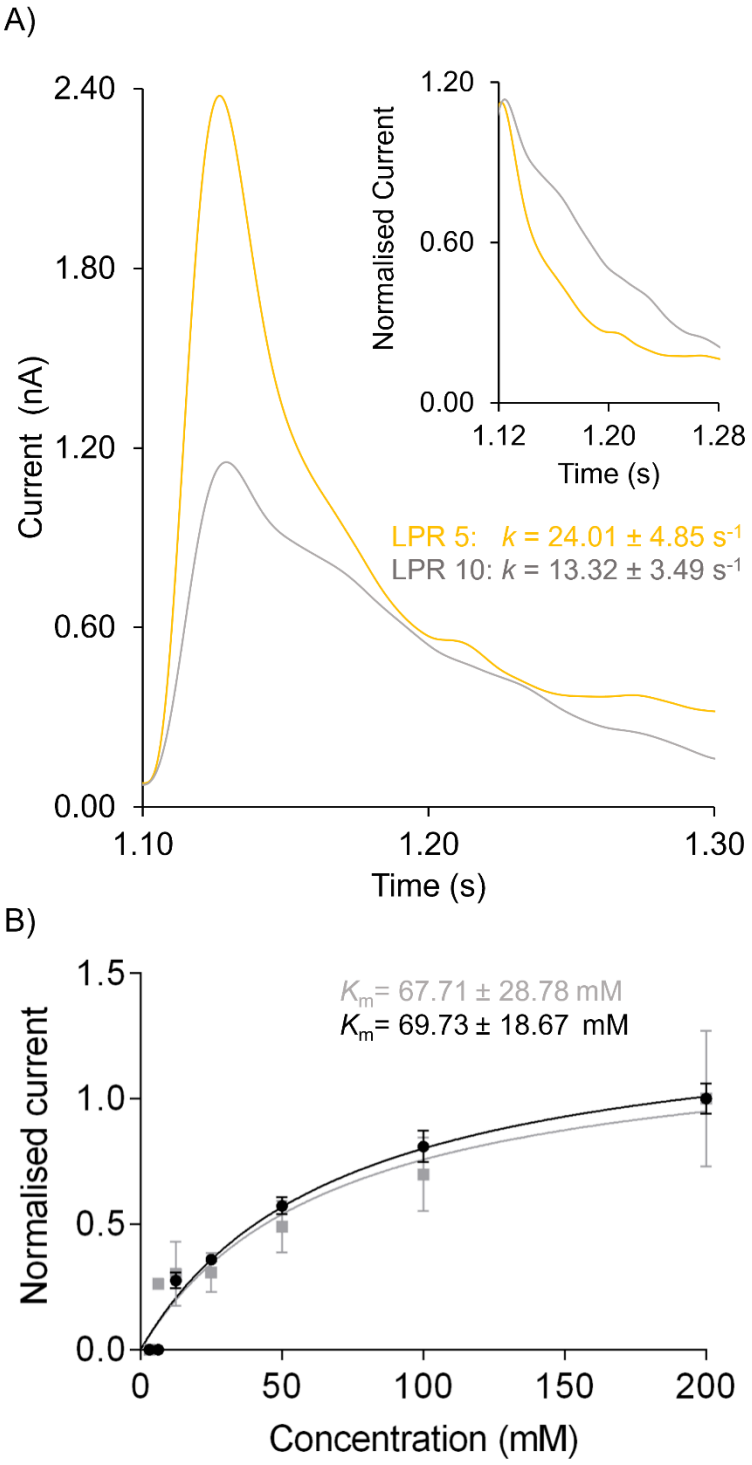

Figure 5.9 H170E is an active transporter. A) Representative traces of proteoliposomes containing Rh50^{H170E} at LPR 5 (yellow) and LPR10 (grey) following a 200 mM ammonium pulse. Inset: Maximum amplitudes have been normalised to 1.0 for comparison. B) Kinetics for WT Rh50 (black) and Rh50^{H170E} (grey) at LPR 10 using NH_4^+. Data points represent mean ± SD.

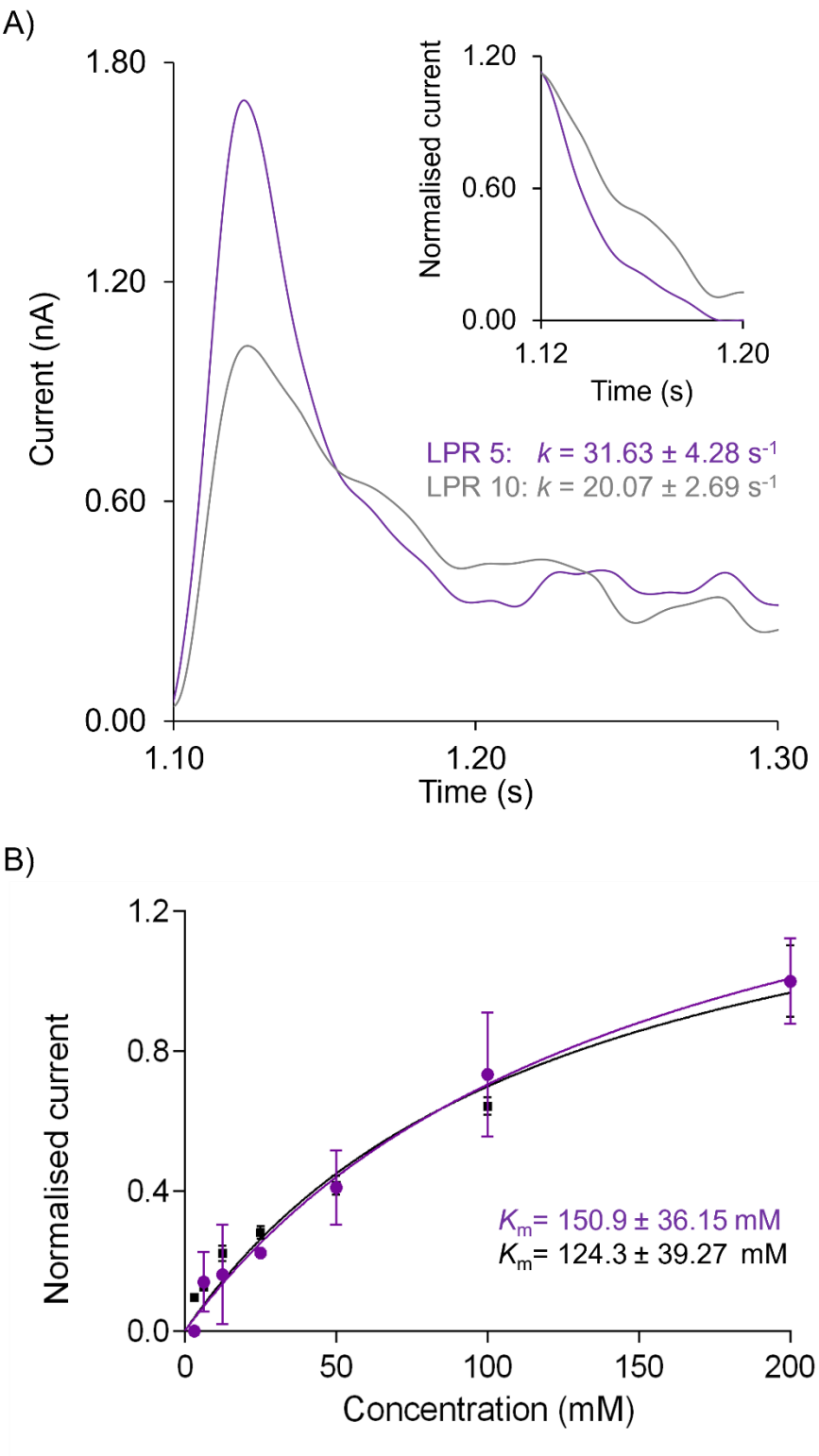

Figure 5.10 H170D is an active transporter. A) Representative traces of proteoliposomes containing Rh50^{H170D} at LPR 5 (purple) and LPR10 (grey) following a 200 mM ammonium pulse. Inset: Maximum amplitudes have been normalised to 1.0 for comparison. B) Kinetics for WT Rh50 (black) and Rh50^{H170D} (purple) at LPR 5 using NH_4^+. Data points represent mean ± SD.

Seeing that acidic substitutions of first histidine (H170) residue is tolerated by the protein, we wanted to further probe the impact of increasing the hydrophobicity of the pore on the activity of Rh50, by accessing the effect of a substitution of a second histidine (H324), or both histidine residues (twin-His) with acidic residues.

As with first histidine variants, a transient current was observed following a 200 mM ammonium pulse on proteoliposomes containing $Rh50^{H324E}$ as well as $Rh50^{H170DH324E}$, with a maximum amplitude ~2-fold lower for both variants in comparison to the WT (**Figure 5.11 B**). However, none of the $Rh50^{H324E}$ and $Rh50^{H170DH324E}$ variants were able to restore the growth of triple-*mepΔ* yeast, on the media supplemented with ammonium (**Figure 5.11 C**) indicating that both proteins are inactive. This was further confirmed by analysing the decay rates of transient currents, which show that the transports are not LPR dependent (**Table 5.2**). Taken together, these results suggests that $Rh50^{H324E}$ and $Rh50^{H170DH324E}$ both lose the translocation ability and are inactive.

These observations provide new insights into the roles of the two conserved histidine residues in Rh proteins. It becomes apparent from both *in vitro* and *in vivo* data that both histidine residues are not absolutely required for ammonia conduction. The substitution of histidine (H170) is well tolerated, while substitution of second histidine (H324) or both histidines leads to an inactive protein variant. This is not as surprising as second histidine is more conserved than the first one; as mentioned in a number of fungal Mep proteins, a glutamic acid (E) residue replaces first histidine, and these proteins can also facilitate ammonium transport (Marini *et al.*, 1997a; Smith *et al.*, 2003; Biswas and Morschhäuser, 2005). As for explanation of inactivity for second histidine variants; Lupo and colleagues observed that the opening above the second histidine in Rh50 is occupied by two water molecules, whereas in *Ec*AmtB this space is occupied by T273 residue which structurally aligns with highly conserved in Rh proteins glycine residue. This forms a larger pore entrance in the Rh50 (Lupo *et al.*, 2007). Perhaps, changing the hydration pattern by substitution of second histidine in Rh50, disrupts the pore entrance, in result abolishing the transporting abilities.

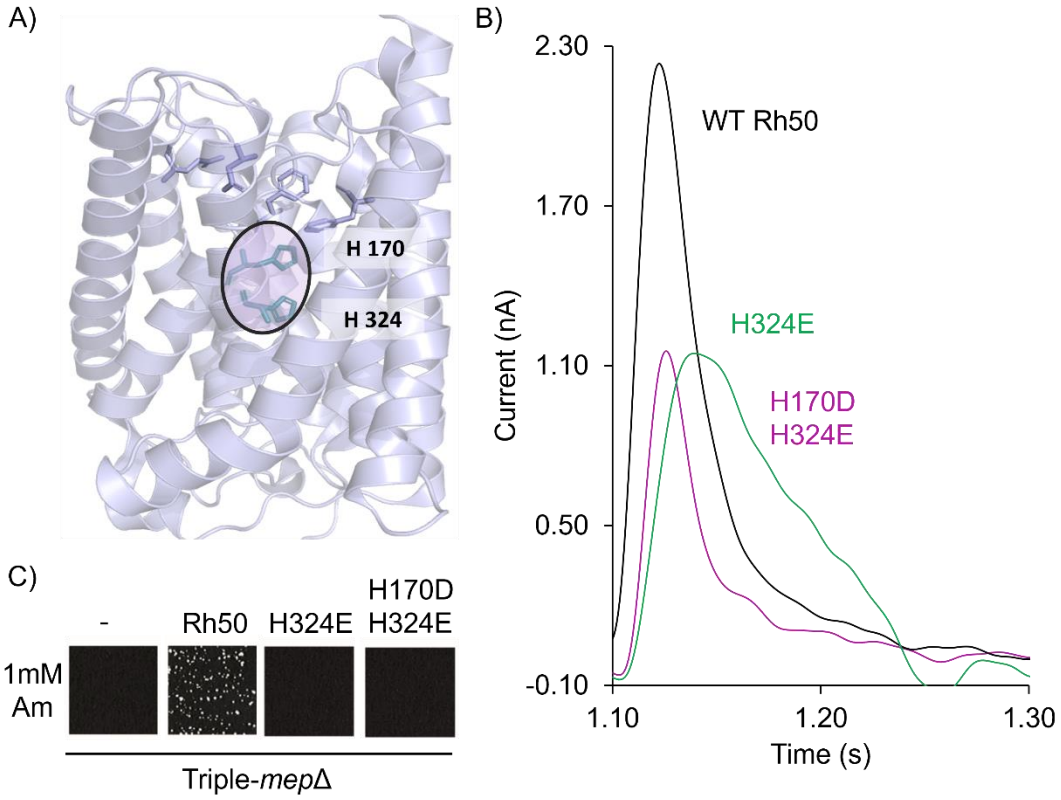

Figure 5.11 Second Histidine and Double Histidine Mutations are not Tolerated. A) Cartoon representation of Rh50 monomer, highlighting substituted residues. B) Representative traces following a 200 mM ammonium pulse for WT Rh50 (black) and Rh50^{H324E} (green) Rh50^{H170DH324E} (magenta) at LPR 5. C) Yeast complementation after 5 days of growth on minimal media supplemented with 1 mM ammonium (Am).

5.4.3 The Effect of Altering the Hydrophobicity of the Pore on Two Mechanisms in Rh50

The Mep proteins in yeast can be separated into two subfamilies according to whether the first of histidines is conserved, as in yeast *Sc*Mep2 (H194), or replaced by glutamate, as in *Sc*Mep1 (E181) and *Sc*Mep3 (E180) (Javelle *et al.*, 2006; Boeckstaens, André and Marini, 2008; Brito *et al.*, 2020). While all Mep proteins transport ammonium, Mep2 is thought to have an additional role in ammonium sensing involved in filamentation of pathogenic fungi (Lorenz and Heitman, 1998;Brito *et al.*, 2020). Mutagenesis studies revealed that that a change of H194 to E194 in *Sc*Mep2 leads to increased transporting properties, but a loss in the signal transduction leading to filamentation, thus simply switching to *Sc*Mep1/3-like transporter mechanistically (Boeckstaens, André and Marini, 2008, Williamson *et al.*, 2022).

In the previous chapter (**Chapter 4, Section 4.11.2**) we proposed coexistence of two mechanisms in Rh50. We hypothesise that under our experimental conditions the translocation of the substrate in Rh50 happens via:

1. Mechanism I: Separate translocation of ammonia and hydrogen ion following NH_4^+ deprotonation.
2. Mechanism II: Direct transport of hydrated NH_4^+ along with water molecules that are leaking through the pore.

In the context of loss of filamentation function in *Sc*Mep2^{H194E} protein variant, and the potential presence of two mechanisms in Rh50 we wanted to investigate how substitution of the first histidine (H170) with a charged residues would affect the dual transport of Rh50. To do this, we measured the conductivity of the active histidine variants (H170E and H170D) in presence of D_2O. As before (**Chapter 4, Section 4.9**), all buffers used to prepare the proteoliposomes and SSME buffers were prepared with D_2O instead of H_2O.

A 200 mM ammonium pulse with D_2O buffers on proteoliposomes containing either Rh50^{H170E} or Rh50^{H170D} did not produce any detectable current (**Figure 4.12**). The loss of current is consistent with transporters that use mechanism I, showing that this mechanism is in use here. The complete abolition of current suggests that mechanism II, which supports direct transport of ion, does not

contribute to the activity of those variants. This indicates that, just like in the case of *Sc*Mep2^{H194E}, there is a loos in one of two mechanism in Rh50^{H170E} and Rh50^{H170D}. Notably, the mechanism of those variants now is reminiscent of the WT AmtB (Williamson *et al.*, 2020), indicating that both Rh50^{H170E} and Rh50^{H170D} only rely on deprotonation mechanism for the substrate translocation. From crystal structures of Rh50, we know that Nε_2 atoms of both histidine residues form hydrogen bonds to neighbouring water molecules, while in AmtB only the second histidine was seen to form hydrogen-bonding partner (Li *et al.*, 2007). Perhaps E or D residues cannot make similar hydrogen-bonding interactions as the equivalent histidine residue after all, as proposed before (Winkler, 2006). The substitution of the first histidine in Rh50, potentially disrupts formation of hydrogen bonds in this position, seen in the WT Rh50. This would mean that hydrogen bonds can now only be formed by a second histidine, just like in AmtB, thus producing a an AmtB-like transporter, which only relies on mechanism I for substrate translocation. Potentially, by introducing those mutations, the water wires are stabilised/more organised, and there is no water leakage in and out of the pore of Rh50^{H170E} and Rh50^{H170D}, as proposed for the WT Rh50 (Hoyhtya, 2020), thus creating an AmtB-like transporter. Overall, these substitutions seem to have a different impact on AmtB vs Rh50. AmtB^{H168E} and AmtB^{H170D} variants were observed to have massive increase in activity (Williamson *et al.*, 2022), while in Rh50 activity was not affected nearly as much (section 5.4.2). This further highlights the differences between AmtB and Rh50.

We also wanted to determine if increasing the hydrophobicity of the pore will have the same effect on mechanism II, therefore we investigated the transport of Rh^{H170A} variant in the presence of D_2O. A 200 mM ammonium pulse with D_2O buffers (**Figure 4.12 C**) on proteoliposomes containing Rh50^{H170A} produced a minimal current of 0.31 nA ± 0.05. This indicates that both mechanisms are present in this variant, and that substitution with alanine has a different impact on the dual mechanism present in Rh50. Previous crystal structures (Javelle *et al.*, 2006) and MD simulations from our lab (Williamson *et al.*, 2020) revealed increased hydration in the area around AmtB^{H168A}. Substitution of this residue with alanine created a hydrophilic cavity filled with

water in AmtB (Javelle *et al.*, 2006). If this is also the case for $Rh50^{H170A}$, a direct translocation of NH_4^+ could be expected, or simply more water molecules would be allowed to slip through the pore. As we know from MDS by Hoyhtya *et al,* water molecules were observed to diffuse through pore of Rh50 in both directions (Hoyhtya, 2020), and introducing alanine in the position of histidine may enhance this diffusion. This could explain why we observe current on SSME in presence of D_2O with this variant. It is also possible, that the current observed with $RH50^{H170A}$ in presence of D2O could only represent interaction between the substrate and the protein, due to higher water accessibility in this variant, and not necessarily a full translocation cycle. To discriminate between the binding and the translocation cycle, it would be essential to test the activity of H170A at different LPRs in presence of D_2O to compare decays of currents. However, an already very low amplitude at LPR 5 makes it technically difficult.

To summarise, *in vitro* electrophysiology measurements in presence of D2O revealed that mechanism II no longer exist in H170E and H170D variants. While the current has been observed for H170A, indicating that both mechanisms are still present, we are unable to determine if its due to full translocation of ammonium or just a residual binding.

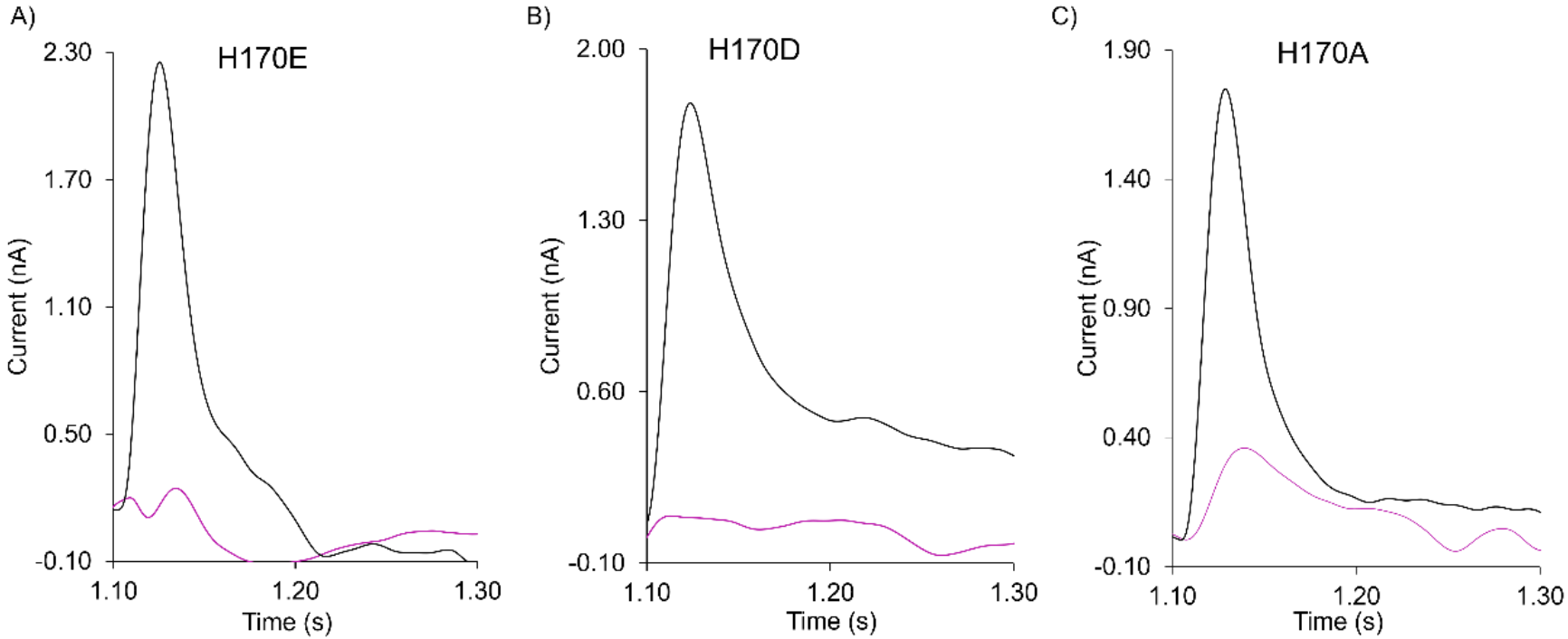

Figure 5.12 Activity of Rh50 Histidine variants in D_2O. Transient currents measured following a 200 mM ammonium pulse on sensors containing proteoliposomes A) $Rh50^{H170E}$ at an LPR5, B) $Rh50^{H170D}$ at an LPR5, C) $Rh50^{H170A}$ at an LPR5, prepared with solutions containing either H_2O (black) or D_2O (magenta).

5.4.4 Importance of twin-His in Selectivity

As mentioned, current detected with $Rh50^{H170A}$ variant in presence of D_2O might be due to increased water leakage into the Rh50 pore, allowing more NH_4^+ to pass through. If this is the case, we could expect other ions to be able to pass through the pore of this variant too. In addition, from our previous work on AmtB from *E. coli* we know that selectivity of the protein is governed by the twin-His motif. Selected AmtB histidine variants (including equivalent $AmtB^{H168A}$) were observed to lose selectivity *in vivo* and *in vitro* against monovalent ions including K^+ and Na^+ (Williamson *et al.*, 2022). Motivated by this finding we wanted to investigate if this is also the case for the Rh50. To do this we substituted ammonium with potassium in our SSME buffers.

A 200 mM K^+ pulse did not trigger transient current in any of the histidine variants, including $Rh50^{H170A}$ (**Figure 5.13 A Figure 5.13 B**). This implies that selectivity of Rh50 could be governed by a different mechanism to AmtB protein, highlighting yet another difference between AmtB and Rh50.

To see if the SSME electrophysiology results are also reflected in an *in vivo* setting, WT Rh50 and histidine protein variants were expressed in a *S. cerevisiae* strain lacking its three endogenous Mep (NH_4^+) and two Trk (K^+) transporters. This strain is unable to grow on media with a limited concentration of NH_4^+ as a nitrogen source and on K^+. As seen in **Figure 5.13 C** only the expression of $Rh50^{H170D/H324E}$ complemented this growth defect, whilst neither WT nor any other variants were able to do so.

While the growth of yeast expressing $Rh50^{H170D/H324E}$ variant is minimal, it clearly transports K^+ to a degree sufficient to support growth. It is rather a puzzling finding, as data in this chapter show that $Rh50^{H170D/H324E}$ is inactive both *in vivo* and *in vitro* in transporting ammonium (**Figure 5.11**)**.** We also did not observe any current on SSME in presence of potassium (**Figure 5.13 B**), therefore it is difficult to explain how it is suddenly able to transport potassium *in vivo*. We speculate that the variant might still slowly leak potassium ions over a prolonged period when expressed in yeast (over 5 days), but the transport could be so scarce that the variant appears inactive when measured over 1 millisecond on SSME. The lack of growth of yeast complemented with

$Rh50^{H170DH324E}$ variant on media supplemented with ammonium can be explained by a competition between the two ions. The media prepared for ammonium complementation assay contains 180 mM K^+, which could in turn interfere with NH_4^+ transport. Currently, our collaborators Dr. Ana Sofia Brito, Prof. Mélanie Boeckstaens and Prof. Anna-Maria Marini are exploring different media with lower potassium concentration to investigate this possibility. It is also possible that the H170D/H324E substitution might alter the structure of Rh50 and, possibly, that of the conducting pore, resulting in a strongly functionally altered protein which does not insert correctly into the membrane of the yeast. Thus, it is essential to perform subcellular yeast fractionation to determine if the variant of the protein is properly inserted into the periplasmic membrane following expression in the yeast.

To summarise, none of the active variants were able to translocate potassium *in vitro* or *in vivo*. This suggests that that the selectivity of the Rh50 protein might be governed by an additional mechanism in comparison to AmtB. This is consistent with the fact that water can travel in and out the pore in WT Rh50, activity not observed in AmtB (Hoyhtya, 2020). If the water can travel in and out of the pore in the WT Rh50 protein already, and the WT is clearly highly selective towards ammonium, an additional hurdle must be overcome in this protein for it to allow passage of other monovalent cations, such as potassium or sodium. We reason this must be linked with the differences in the hydrophobicity of the pore between Rh50 and AmtB.

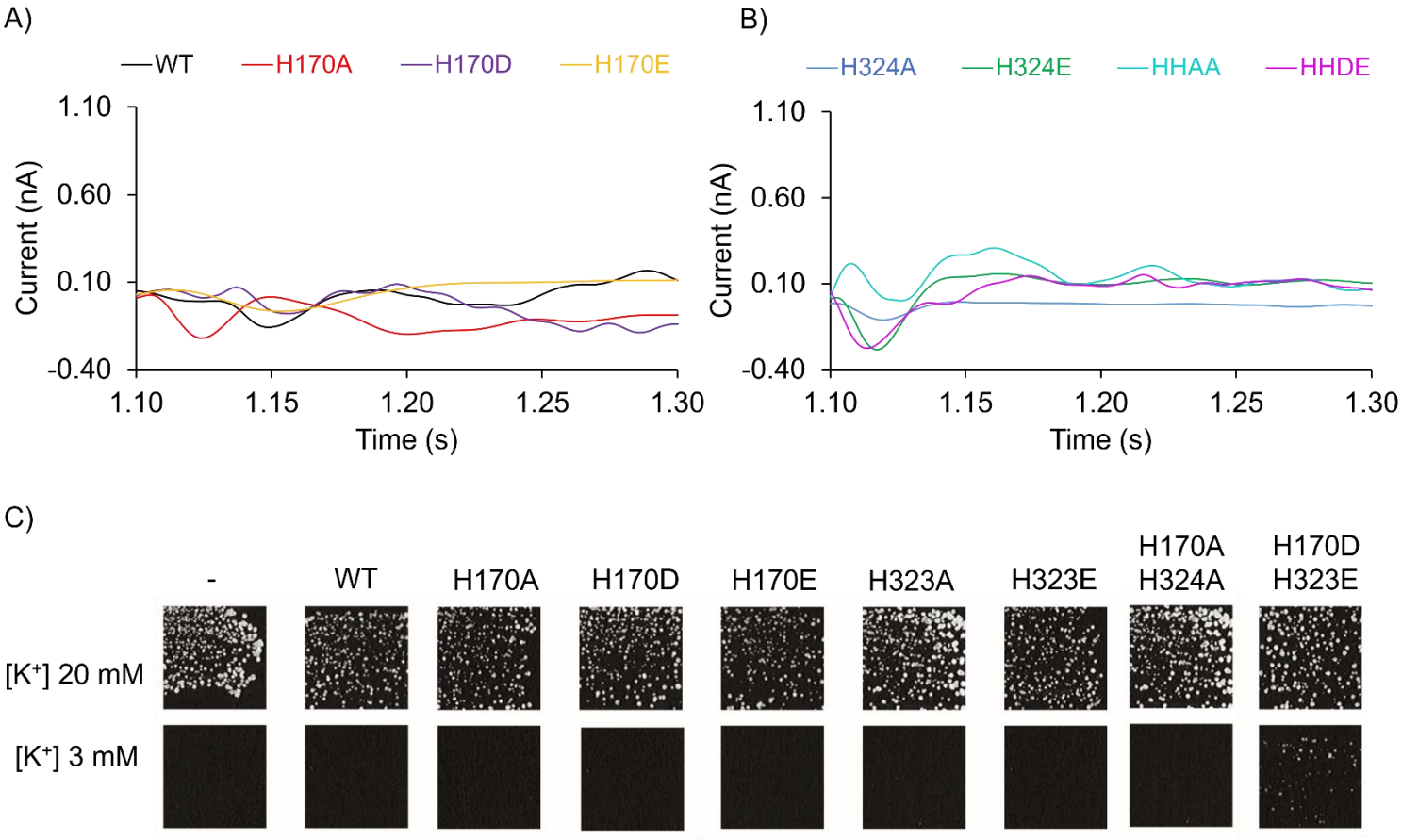

Figure 5.13 SSME and yeast complementation results. A) and B) Representative traces following a 200 mM potassium pulse for WT Rh50 and Rh50 variants at LPR 5, C) Yeast complementation test (strain #228, mep1Δ mep2Δ mep3Δ trk1Δ trk2Δ leu2 ura3) after 5 days of growth on minimal media supplemented with 3 mM or 20 mM KCl.

5.5 Altering the Hydrophobicity of the Pore vs Bidirectionality of Rh50

From previous studies, we know that methylammonium (MeA) is toxic to *Saccharomyces cerevisiae* yeast and can inhibit growth at external concentrations of 100 mM or higher. For more details about MeA induced toxicity please refer to **Chapter 4, Section 4.4.2.** We already established that *S. cerevisiae* grows on glutamic acid supplemented media (nitrogen source) in presence of toxic MeA concentration range (< 100mM) when complemented with the WT Rh50 (**Chapter 4, Section 4.4.2**). This presents preliminary evidence that Rh50 provides resistance to toxic methylammonium, most probably by counteracting its accumulation up to toxic levels. It is not clear how Rh50 achieves this, as we do not have a full understanding to what MeA resistance corresponds to at the physiological level. One of the possibilities is that the growth of the yeast on a MeA supplemented media creates the gradient towards the cytosol, and the resistance is achieved not directly through the Rh protein, but an unknown source of energy leading to export of the toxic substrate. Alternatively, there might be intracellular components helping cells to resist, such as through vacuole trapping (Interpersonal communication with Prof. Anna-Maria Marini). Another possibility is that Rh50 promotes export in addition to import of the substrate. This would mean that Rh50 works bidirectionally as opposed to other ammonium transporters form Amt/Mep family (Marini *et al.*, 1997b).

To pursue the idea of bidirectionality of Rh50 protein, we will now investigate whether the twin-His motif is involved in a potential exporting ability of the protein. To do this we made use of the methylammonium (MeA) induced toxicity to *Saccharomyces cerevisiae* cells in complementation assay. Before proceeding with yeast complementation, we wanted to make sure that twin-His variants retain the ability to transport methylammonium in the first place. To clarify this, we tested methylammonium transport *in vitro* using SSME first.

5.5.1 Methylammonium Transport in vitro

Transient currents were observed for all variants following a 200 mM MeA pulse (**Figure 5.14**). For $Rh50^{H170A}$, $Rh50^{H170D}$, and $Rh50^{H170E}$ variants, both the decay and amplitude of the observed currents are higher for ammonium, and lower for methylammonium at an LPR 5, mirroring results of WT Rh50 (**Table 5.2** decay and **Table 5.3** amplitude). This suggests that those variants are active in methylammonium transport. On the other hand, variants which lose transporting ability ($Rh50^{H324A}$, $Rh50^{H170AH324A}$, $Rh50^{H324E}$, and $Rh50^{H170DH324E}$) have comparable or higher maximum amplitudes for methylammonium in comparison to ammonium (**Table 5.3**). In addition, these variants have comparable decay values for methylammonium versus ammonium at LPR 5 (**Table 5.2**). This suggests that they are inactive, and the amplitude is a result of a protein-methylammonium interaction, as opposed to translocation.

In summary, variants active in ammonium translocation retain the ability to translocate methylammonium. Having this confirmed, we can proceed with the yeast complementation tests to see if these variants can still support the export of the toxic methylammonium *in vivo.*

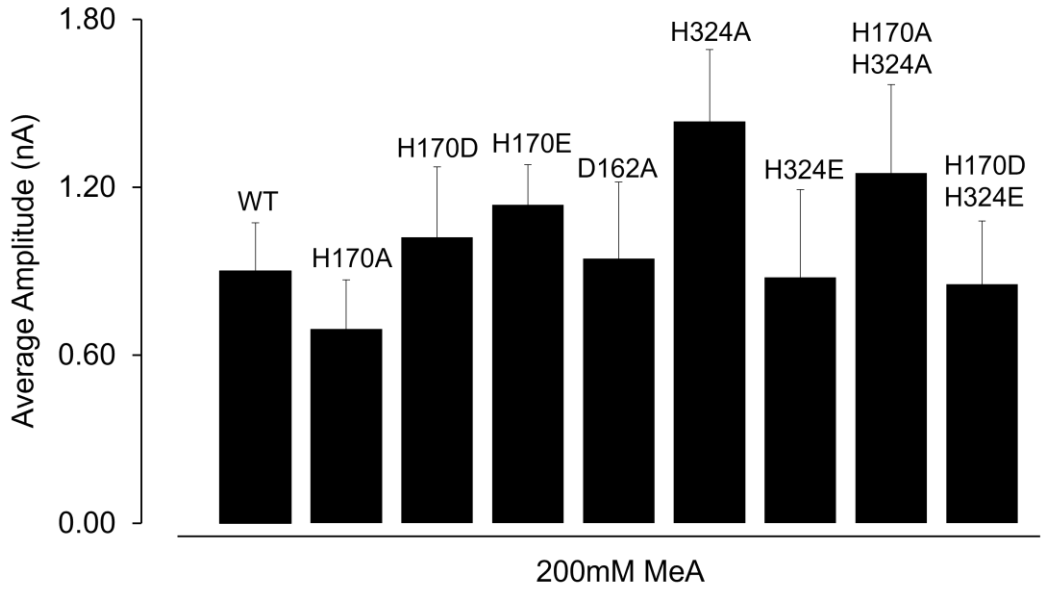

Figure 5.14 Methylammonium Transport in Rh50 Variants. Average of maximum amplitude of the transient current (nA) measured using SSME after a 200 mM MeA pulse. Bars represent mean measurements from four sensors with two measurements recorded for each sensor (means ± SD).

Table 5.3 Mean amplitudes of transient currents (nA) triggered after an ammonium or methylammonium pulse of 200 mM measured by SSME.

Protein	NH_4^+	MeA
WT	2.03 ± 0.14	0.90 ± 0.17
H170A	1.48 ± 0.44	0.69 ± 0.18
H170D	1.84 ± 0.41	1.02 ± 0.25
H170E	2.14 ± 0.45	1.13 ± 0.14
H324A	0.73 ± 0.16	1.44 ± 0.26
H324E	0.77 ± 0.19	0.88 ± 0.31
H170A H324A	1.54 ± 0.27	1.25 ± 0.32
H170D H324E	0.9 ± 0.19	0.85 ± 0.23

5.5.2 Yeast Complementation Assays

To clarify the involvement of the twin-His motif in bidirectionality of Rh50, *S. cerevisiae mepΔ3* mutant expressing histidine variants was plated on glutamic acid supplemented media in presence of toxic MeA and the results are presented in **Figure 5.15**.

All histidine variants were unable to support the growth of mutant yeast on media supplemented with toxic methylammonium concentrations **Figure 5.15**. While it is not so surprising for the variants that were inactive in ammonium and methylammonium transport *in vitro*, it is a valuable result for the active variants ($Rh50^{H170A}$, $Rh50^{H170E}$, $Rh50^{H170D}$). It provides evidence that twin-His motif, or first histidine (H170), is essential for maintaining the pathway for exporting the substrate in the yeast. Notably, when triple-*mepΔ* yeast is complemented with any of the first histidine variants, no growth is present even methylammonium concentrations as low as 50mM, while the toxicity is induced at concentrations of <100mM for the control **Figure 5.15**. To understand this, we compared the growth of the yeast complemented with these variants' vs WT Rh50 on ammonium supplemented media. The growth of variants appears more prominent in comparison to the WT. This could potentially mean that import of the substrate is enhanced *in vivo* in those variants. This in turn may lead to a faster accumulation of the toxic substrate, and in the absence of export, leading to cellular death, explaining the lack of growth in presence of only 50mM methylammonium.

Taken together, above data provides more evidence for bidirectionality in Rh50. *In vivo* complementation assays revealed that twin-His motif, or potentially H170, is essential for the exporting abilities of Rh50 protein. SSME results proved evidence suggesting that active variants (H170A, H170D, H170E) are capable of translocating methylammonium *in vitro,* therefore the lack of growth of yeast mutant complemented with these variants is not due to their inability to translocate methylammonium, but due to importance of first histidine residue in exporting the substrate. This indicates that the disruption of twin-His motif affects export of the substrate *in vivo* in Rh50 protein.

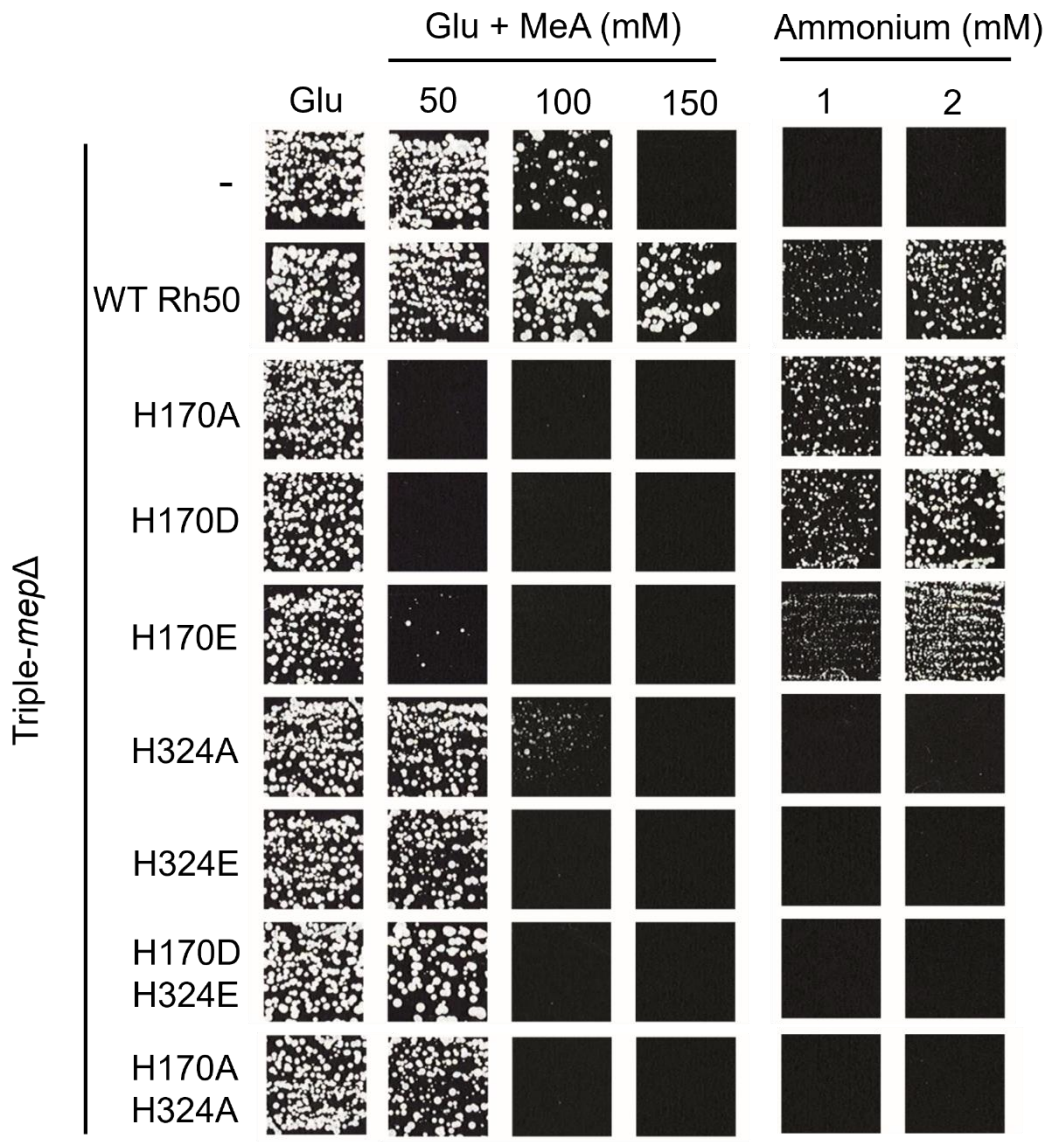

Figure 5.15 Export and import of substrate in Rh50 variants *in vivo*. Yeast complementation after 5 days of growth on minimal media supplemented with either: (Left to right) glutamic acid (Glu), glutamic acid and 50 - 150 mM Methylammonium (Glu+MeA), and 1 - 2 mM ammonium.

5.6 Discussion

In the previous chapter (**Chapter 4**), we analysed the activity of the WT Rh50 and provided a rationale for an electrogenic ammonium translocation by proposing the coexistence of two mechanisms in Rh50 protein. We also provided preliminary evidence supporting the notion that Rh50 is bidirectional. In this chapter, we further probe the mechanism of Rh50 protein by altering the hydrophobicity of the pore. Our studies revealed that substitution of histidine with either hydrophobic or charged residues in position 170 is tolerated and does not disrupt substrate translocation. Substitution of the second histidine (H324) was proved to be detrimental for the mechanism of the transport as none of the H324 or H170/H324 variants were active *in vitro* or *in vivo*. We also show that when charged residues replace histidine 170, the mechanism II is entirely abolished. Finally, we show that altering the hydrophobicity of the protein eliminates the exporting function of the protein.

5.6.1 The Twin-His Structure Is Not Essential for Optimum Substrate Conductance

The results in this chapter show that the substitution of the first histidine is well tolerated and still allows both *in vivo* and *in vitro* ammonium translocation. The second histidine and double variants were proved to be inactive. This suggests that twin-His structure is not essential for optimum substrate conduction but highlights a specific, yet still unknown, role of a second histidine (H324) in maintaining the transport. The fact that first His mutants still retain activity, while second His and double mutants are inactive could be explained by the different impact these substitutions have on the neighbouring water wires and water accessibility to the pore. As previously discussed, the twin-His motif is conserved and protrudes into the centre of the hydrophobic pore. In Rh50, H170 and H324, adopt a coplanar orientation which may stabilize an ion between them. In Rh50 $N\varepsilon_2$ atoms of both histidine residues form hydrogen bonds to neighbouring water molecules, while in AmtB only the second histidine was seen to form hydrogen-bonding partner (Li *et al.*, 2007). Notably, the opening above the second histidine in Rh50 is occupied by two water

molecules, whereas in AmtB this space is occupied by T273 residue which structurally aligns with highly conserved in Rh proteins glycine residue. This forms a larger pore entrance in the Rh50 (Lupo *et al.*, 2007). Therefore, this could mean that removal, specifically of second histidine, could change the hydration pattern of the pore and potentially create an even larger pore entrance. Clearly this change must lead to some sort of instability, either by leading to collapse of the pore, or altering the accessibility of the substrate, thus resulting in inactivation of translocation.

5.6.2 Mechanism of Rh50 Differs from the one of AmtB

The existing crystal structure for $AmtB^{H168A}$ revealed increased hydration around A168 (Javelle et al., 2006), which was suggested to allow passage of hydrated ions. This was indeed confirmed in our lab (Williamson *et al.*, 2020). Through the yeast complementation assays and SSME characterisation we showed that single mutations of twin-His to H168A in AmtB allow for a switch from a selective transporter to a non-selective channel-like transporter allowing passage to potassium and sodium ions (Williamson *et al.*, 2020). This does not seem to be the case for the Rh protein. $Rh50^{H170A}$ variant does not lose selectivity, and in fact, it retains similar properties to the WT Rh50, including substrate affinity. This could be explained by the difference in the hydration pattern of Rh50 in comparison to AmtB. A conserved phenylalanine in Rh proteins (F74 in RhCG, F55 in Rh50) occupies a large portion of the pore at the level of the two signature histidine residues, whereas the pore of AmtB is unobstructed (Baday *et al.*, 2013). Therefore, it could serve as an additional obstruction for potassium or sodium ions, aiding in selectivity of Rh proteins. Indeed, a mutation of the equivalent phenylalanine residue to a serine (F65S) in RhAG has been associated with overhydrated hereditary stomatocytosis (OHSt) of red cells, which is a hemolytic anemia characterized by monovalent cation leaks (Bruce *et al.*, 2009). Lastly, albeit lower in comparison to the WT Rh50, a current has been observed for $Rh50^{H170A}$ proteoliposome while tested with D_2O. Although, it is impossible for us to determine if the current observed

in $Rh50^{H170A}$ in presence of D_2O corresponds to full translocation cycle or only residual binding, due to a very low amplitude of the current.

Decreasing hydrophobicity of the Rh50 pore also revealed differences between Rh50 and AmtB. Existing crystal structures of $AmtB^{H168E}$ show that the region around E168 has increased organised hydration pattern, which could lead to more efficient transport of the substrate (Javelle *et al.*, 2006). Indeed, increased activity was observed on SSME for $AmtB^{H168E}$ and $AmtB^{H168D}$ previously in our lab (Williamson *et al.*, 2022). However, this is not the case for the $Rh50^{H170E}$ and $Rh50^{H170D}$, as neither of those variants exhibit hyperactivity *in vivo* nor *in vitro*. Interestingly, by introducing those mutations in Rh50 protein, we produce a protein variant which is mechanically reminiscent of WT AmtB. In the context of our model where we suggest that Rh50 might possess two mechanisms: MI NH_4^+ deprotonation, and MII a direct translocation of the NH_4^+. We observe a complete current abolishment in the presence of D_2O for $Rh50^{H170E}$ and $Rh50^{H170D}$ which indicates that only mechanism I (deprotonation of NH_4^+ and a separate translocation of NH_3 and H^+ via water wires) is present in those protein variants. Since both protein variants also retain selectivity, their mechanism is similar to WT AmtB. From crystal structures of Rh50, we know that Nε2 atoms of both histidine residues form hydrogen bonds with neighbouring water molecules, while in AmtB only second histidine was seen to form hydrogen-bonding partner (Li et al., 2007). It has been argued that E residue in place of H in the position 168 could to occupy about the same space and can potentially make similar hydrogen-bonding interactions in AmtB (Winkler, 2006). Perhaps it is not entirely accurate, or simply substitution of first histidine with an acidic residue has a different impact on Rh50. If that is the case, substitution of the first histidine in Rh50 (H170), potentially disrupts formation of the hydrogen bonds with neighbouring water molecules observed in the WT Rh50. This would mean that hydrogen bonds can only be formed by the second histidine, just like in AmtB, thus producing an AmtB-like transporter, which only relies on mechanism I for substrate translocation.

5.6.3 Bidirectionality of Rh50

While the second histidine (H324) might be essential in substrate conductance, either by stabilising the pore, or providing a route for substrate translocation, it seems obvious that the twin-His, or the fist histidine (H170) are important for the unique bidirectionality of the protein. All active histidine variants ($Rh50^{H170A}$, $Rh50^{H170E}$, $Rh50^{H170D}$) lost the exporting abilities and were unable to support the growth of mutant yeast on media supplemented with toxic methylammonium concentrations, even though electrophysiology measurements suggests that these variants are still able to translocate MeA *in vitro*. These results suggest that the lack of growth on MeA is not due to variants inability to translocate MeA, but rather due to loss of bidirectionality, which protects against toxicity. We reason that the unique ability of Rh proteins to excrete ammonium could be due to the water accessibility into the central part of the pore, and by altering the hydrophobicity of the pore we manage to eliminate the exporting ability of the protein. It cannot be left without comment, that there might be a pattern linking bidirectionality of Rh50 with the presence of two mechanisms. Indeed, $Rh50^{H170E}$ and $Rh50^{H170D}$ lost dual mechanism in our *in vitro* experimental conditions when tested in presence of D_2O. Although we are unable to discriminate if the current observed in presence of D_2O with $Rh50^{H170A}$ is due to translocation or just binding, this variant seems to have lost the ability to export the substrate *in vivo*.

Increased sensitivity of Rh50 variants to toxic MeA *in vivo* can also be an effect of increased import of the substrate in effect counteracting the export, or more simply decreased export ability. In either case, this would inevitably lead to increased sensitivity which might appear as the lack of excretion. However, it is difficult to draw any specific conclusions as we do not know which translocation mechanism is more efficient (import vs export). Currently, there is no method to assess import vs export of the substrate separately neither *in vivo* nor *in vitro*. In addition, as mentioned before, we do not have a full understanding to what MeA resistance corresponds to at the physiological level. The growth of the yeast on a MeA supplemented media creates the gradient towards the cytosol, and there is a possibility that the resistance could be achieved not directly through the Rh protein, but an unknown source of

energy leading to export of the toxic substrate. Alternatively, there might be intracellular components helping cells to resist, such as vacuole trapping (Interpersonal communication with Prof. Anna-Maria Marini). This, however, does not explain why yeast containing all its native transporters, or yeast mutant complemented with AmtB from *E. coli* experience MeA toxicity, while when complemented with WT Rh50 protein (or human Rh proteins) it is protected from such toxicity (Marini *et al.*, 2000a). To fully understand bidirectionality of Rh50, a method proving a direct assessment of Rh50 export *in vivo* and *in vitro* must be established. An example of *in vivo* characterisation could be ammonium excretion assays. However, to measure any appreciable difference in signal, the cells would have to be present in high concentrations, and therefore results obtained this way could be associated with problems and thus considered unreliable or even irrelevant when physiology of the organism is considered. While SSME provides a useful tool to study the mechanism of this membrane protein *in vitro*, the limitation of the assay in context of bidirectionality and dual mechanism is the (mixed) orientation of the protein inserted into the liposome (**Section 5.3.1**). To overcome this issue, our group is working towards developing a way of controlling the orientation of the protein, through making vesicles directly from the membrane of the organism used for overexpression of selected protein. This technique will enable assessment of bidirectionality and a direct investigation of the import/export separately, as well as its potential relevance to the presence of two mechanisms in the Rh50 protein *in vitro* using SSME. Preliminary data has been presented in the final Chapter 6 (**Section 6.3.1.3**) of this thesis.

Chapter 6

Chapter 6: Discussion and Future Work

6.1 Summary

Throughout my PhD, I characterised Rh50 protein from the bacterium *Nitrosomonas europaea* as a preliminary move towards enhancing our understanding of the mechanism of Rh proteins.

I successfully optimised the conditions for overexpression and purification of the protein and optimised the Solid Supported Membrane Electrophysiology (SSME) measurements for *in vitro* characterisation (**Chapter 3**). This permitted investigation into the activity, kinetics, and mechanism of WT Rh50 (**Chapter 4**) and revealed new insights into its mechanism. Overall, this work has provided evidence that Rh50 mediates electrogenic ammonium transport which conflicts to date observations in the field. With the help of our collaborators, I combined our *in vitro* SSME results with *in vivo* yeast complementation assays to investigate the role of deprotonation in the mechanism of Rh50 as well as the routes the charge takes to reach the cytoplasm. Assays exploiting the altered proton mobility between H_2O and D_2O revealed that proton is transferred along water wires via the Grotthuss reaction (mechanism I), a mechanism for electrogenic activity observed in AmtB (Williamson *et al.*, 2020). The same assay also revealed presence of another mechanism supporting a direct transfer of an ion (mechanism II), under our laboratory conditions. This motivated us to investigate potential transfer routes for the charge translocation across Rh50. Altering the conserved twin-His motif and thus hydrophobicity of the pore revealed new insight into functional importance of the motif in maintaining mechanism II. Through altering the hydrophobicity of the pore, we also provided further evidence of existence bidirectionality of Rh50, and we propose that two mechanisms could be linked with the bidirectionality of the protein (**Chapter 5**). While it still requires validation if the mechanism II could be responsible for export of the substrate and hence be directly linked with bidirectionality of the protein, the results here provide initial support. Further steps must now be taken to investigated what confers these properties to Rh50 and why they are not present in other ammonium transporters.

This research not only offers a new and crucial insights into the mechanism of other Rh proteins providing understanding of Rh related human pathophysiology, but also into the physiology of ammonia oxidising organisms possessing Rh proteins. Both AOA and AOB, including *N. europaea,* are the key contributors to ammonia oxidation, and their relative contribution to this process is one of the most important issues related to the nitrogen cycle. This study offers a way to understand how *N. europaea* acquires ammonium from the environment and in turn contributes to the nitrification processes.

6.2 General Discussion

Based on crystal structures and very indirect experimental assays it has been widely accepted that Rh50 from *Nitrosomonas europaea* is supporting electroneutral transport of NH_3 (Lupo *et al.*, 2007; Li *et al.*, 2007; Cherif-Zahar *et al.*, 2007). In contrast, my results demonstrate that Rh50 is in fact electrogenic, disputing above assumption. We show that Rh50 is highly selective towards NH_4^+, and that its activity is saturable, presenting affinity in a mM range, suggesting a transporter-like activity. While the kinetics are saturable, they actual values are somehow unexpected, averaging 124.3 ± 35.85 mM for ammonium and 278.7 ± 77.11 mM for methylammonium. In comparison to previous studies in which the Km value for the MeA uptake of *N. europaea* was 1.8 ± 0.2 mM (pH 7.25), these values appear very high (Weidinger et al., 2007). Human RhAG was also proved to transport the ammonia analog with apparent Km value of ~1.6 mM (Westhoff et al., 2002). While is it difficult to explain these highly contrasting affinity values, mentioned above studied used whole *Nitrosomonas europaea* cells or cells heterogously expressing the transporter of interest. It could be that the affinity of a whole cell towards the substrate differs to the system wherein the protein is purified and inserted into an artificial liposome. In addition, in both studies an ammonium analogue methylammonium was used as a guide to understand ammonia translocation via Rh proteins, which could potentially lead to different response of cells in turn affecting the result. Finally, both studies concluded

that the transport is electroneutral (NH_3 or NH_4^+ / H^+ exchange), which disagrees with data in this thesis. While unclear why the affinity values are this high under our experimental conditions, high affinity of Rh50 corroborates with the natural environment of its host. It has been found that AOB, such as *N. europaea* prefer areas with high ammonium concentrations, while ammonia oxidising archaea (AOA) prefer areas with low ammonium concentrations (Di *et al.,* 2009).

The data in this thesis also demonstrates the ammonium transport via Rh50 protein is pH dependent. This corroborates with the previous studies showing that the restoration of ammonium-dependent growth to a yeast mutant by Rh50 was more effective at higher pH values (Weidinger et al., 2007). However, the authors suggested that it is compatible either with facilitated transport of NH_3 through the channel or with a NH_4^+/H^+ exchanger. Since the pKa of the NH_4^+/NH_3 equilibrium is 9.25, more NH_3 should be available at higher pH values providing the main argument in favour of electroneutral transport hypothesis. However, *N. europaea* achieves high nitrification rates and is able to accumulate ammonia while residing environments such as soil, sewage, or freshwater where the pH tends to be neutral or basic (between 7 and 8) in which the ammonia (NH_3) concentration is low (Chain *et al.*, 2003). In addition, the pH value of the cytoplasm in active *N. europaea* cells is about pH 6.8 - 7.2 (Schmidt *et al.,* 2004), again a pH at which NH_4^+ is predominant. SSME data presented in this thesis, strongly oppose electroneutral transport driven by a pH. Both, the amplitude of the transient current was lower in more acidic pH, while in neutral and basic pH the amplitude of the transport, corresponding to both binding and translocation of the substrate, was increased. This could mean that at neutral pH an electrostatic interaction between the periplasmic face and the substrate (NH_4^+) is enhanced and/or favoured. This data corroborates with the natural habitat of the host which, as above mentioned, tend to be at neutral/basic pH. In terms of wider scope of the rhesus proteins research, these results also agree with the findings that ammonia/ammonium transport in human RBCs via RhAG is also pH influenced (Sudnitsyna *et al.*, 2016).

6.2.1 Mechanism of Rh50

The electrogenic NH_4^+ transport via Rh50 suggested either direct translocation of NH_4^+, facilitated symport of NH_3 and H^+, or deprotonation of NH_4^+ into NH_3 and H^+, allowing their separate transport through the protein. In our model mechanism in AmtB, we proposed that D160 is essential in maintaining the pathway for H^+ translocation and was pronounced important in deprotonation mechanism. Due to its proximity to the pore entrance and high conservation across the family, we investigated it as a potential candidate for a proton acceptor in Rh50. D162 appears strictly essential, as Rh50 activity is abolished when this aspartic acid is substituted to alanine. While deprotonation seems to be an important step in the transport mechanism in Rh50, the conductivity in the presence of D_2O imply that the activity does not entirely depend on the translocation of the proton via water wires. In molecular dynamic simulations on Rh50 water molecules were observed to create a water bridge between the pore entrance and the periplasmic vestibule allowing water conduction from periplasm to the central pore of bacterial Rh protein (Hoyhtya, 2020). Therefore, some NH_4^+ could potentially slip though the channel along with the water molecules, bypassing deprotonation, thus creating this dual mechanism in Rh50 protein.

In addition, bacterial Rh50 as well as human Rh proteins, have been proposed to facilitate CO_2 transport too. While in this study we mainly focus on Rh50 involvement in NH_4^+ translocation, this possibility could not be left undiscussed. The most recent molecular dynamic simulations of both *Ne*Rh50 and *Hs*RhCG, as well as *Ec*AmtB did not show any tendency of CO_2 molecules to diffuse through the periplasmic vestibule (Hoyhtya, 2020). This provides further evidence in favour of Rh proteins being sole ammonium transporters, as opposed to CO_2 transporters.

6.2.2 Mechanism of Rh50 Relies on Hydrophobicity of the Pore

Results in this thesis show that twin-His structure is not essential for optimum substrate conductance. Instead, hint at their importance in maintaining the hydrophobicity of the pore, which in turn have an impact on different aspects of the mechanism of the protein. While substitution of the first histidine is well tolerated, the second histidine or double variants proved to be inactive, suggesting that the second histidine (H324) is most likely essential for maintaining the transport. On the other hand, removal of the first histidine and its replacement with acidic residues, was proved to have a very specific impact on the transport. The direct translocation of the NH_4^+ ion (mechanism II) has been entirely abolished in those variants, resulting in protein variants solely relying on deprotonation mechanism (mechanism I) for the translocation of the substrate. Since both protein variants also retain selectivity, their mechanism is highly alike to the WT AmtB protein. We reason that the water bridge observed in MDS formed between the pore entrance and the periplasmic vestibule, allowing NH_4^+ to pass central pore of bacterial Rh50 protein with water molecules, is disturbed in those mutants (Hoyhtya, 2020). Therefore, resulting in loss of the mechanism II. We proposed that this is also a reason for the loss in bidirectionality in variants with substitution in position H170, as any change in this residue leads to a complete abolishment of the export *in vivo*.

While we still need more evidence to prove Rh exporting abilities, having this unique feature makes sense biologically for organisms and tissues expressing Rh proteins. The natural habitats of *N. europaea* include waste waters which are rich in ammonia. Therefore, the import/export function seems like a sensible feature for this organism to enable it control internal ammonia concentrations. The exporting function of the Rh proteins could serve as a protection for RBC in an environment with high ammonium levels. If Rh proteins are absent, haemolysis might occur, as noticed in Rh null individuals. In fact a study on Rh null RBC, not expressing Rh complex, had 2-fold lower exporting efficiency in comparison to normal RBC which suggested that Rh complex is involved in the export of ammonium from RBC (Hemker *et al.*, 2003). This could also be true for the other ammonium transporting human

rhesus proteins RhCG and RhBG which are expressed in tissues responsible for ammonia metabolism including liver and kidneys (Liu *et al.*, 2000). Therefore, it makes sense for Rh proteins to develop this strategy providing the cells with the protection against ammonium toxicity. However, while we know the specific tissues and localisation of each of the Rh protein expression, none of the studies investigated in which orientation these proteins are expressed in tissue specific cells. It is possible that the same protein can be inserted at Right Site Out (RSO) and Inside Out (ISO) in the same tissue. This must be clarified for us to have a better understanding of the way in which the transport is occurring, and if bidirectionality is really a feature that might be adapted by all Rh protein to fulfil their role.

6.3 Future Work

6.3.1 Rh50 Research

6.3.1.1 Ammonia Recruitment Site in Rh50

The periplasmic vestibule and the ammonium ion binding site identified in Amt structures is shaped by three highly conserved residues (F107, T148, and S219 in *Ec*AmtB) (Khademi *et al.*, 2004; Zheng *et al.*, 2004; Andrade *et al.*, 2005; Pflüger *et al.*, 2018). Of those only the phenylalanine residue is conserved in the Rh family, suggesting that Rh proteins have a different mechanism for ammonium recruitment from the rest of the family (Lupo *et al.*, 2007; Li *et al.*, 2007; Gruswitz *et al.*, 2010). At the bottom of the periplasmic vestibule, A144 of AmtB is replaced by a conserved glutamic acid in Rhesus proteins (*Hs*RhCG E166, and *Ne*Rh50 E146). Recent MD simulation on human RhCG suggest that NH_4^+ makes hydrogen bonds with E166, and the study proposed it to be a prime candidate for a charged substrate recruitment site (**Figure 6.1**) (Hoyhtya, 2020). Currently in our studies, even an inactive variant of Rh50 produces a current, which is due to residual binding between the substrate and the unknown binding site of the protein. If E146 is truly involved in the NH_4^+ recruitment and binding in Rh50, mutating this reside should abolish the binding, and thus the current on SSME. Therefore, we

propose to mutate this residue to another acidic residue, such as aspartic acid, and a hydrophobic residue alanine. $Rh50^{E146D}$ would allow us to ascertain if E146 is important due to electrostatic interactions between its carboxylic function and NH_4^+. If this were the case, it would be expected that a substitution of E for D would conserve the activity of Rh50, as the carboxylic function is retained, while $Rh50^{E146A}$ would be expected to lose its activity.

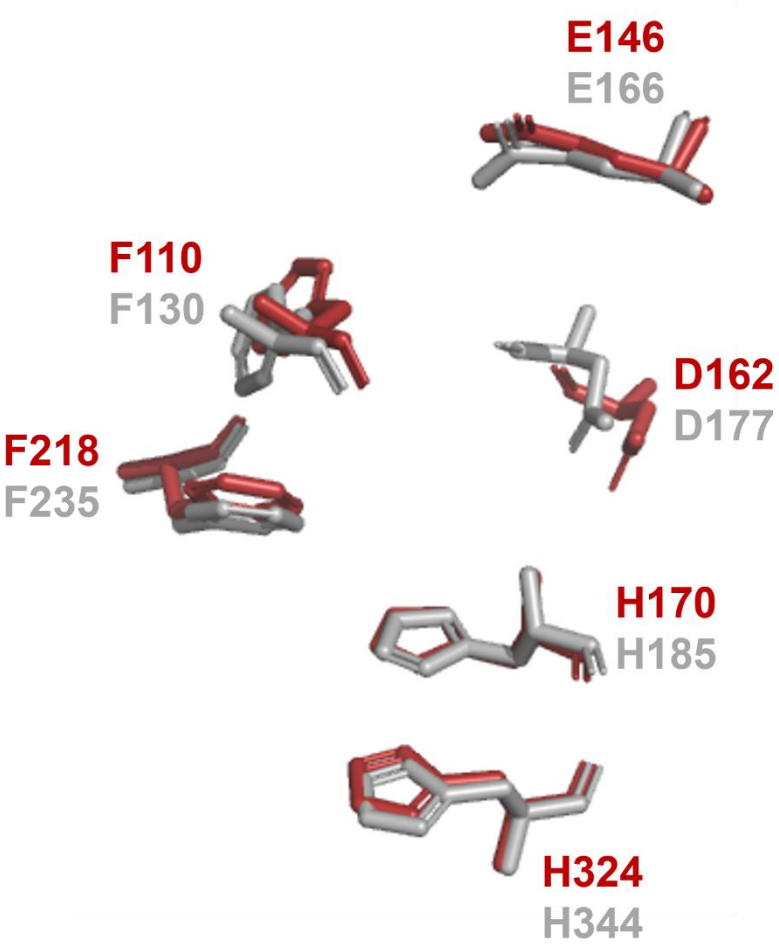

Figure 6.1 Conserved Residues in Rh Proteins. Residues in red are from Rh50 *Nitrosomonas europaea*, and residues in grey are from RhCG *Homo sapiens.*

6.3.1.2 Importance of Phenylalanine Gate

Following NH_4^+ recruitment, we proposed that a conserved aspartic acid residue (D162 Rh50) is involved in the substrate transfer, through either providing stability of the pore or deprotonation. Hoyhtya *el at* proposed that the "Phenylalanine gate" (Phe-gate) could be a potential recruitment site for NH_3 molecule following deprotonation (Hoyhtya, 2020). Of note, Rh proteins, have phenylalanines that create a right angle with each other with one in a vertical position while the other lies horizontal (**Figure 6.1**), while in Amts phenyl rings of Phe-gate are parallel. This difference suggests that the role of the phenyl gate is different between Rh proteins and AmtB. In experimental study, Javelle *et al* found that mutating both phenyls to alanine completely inhibit the activity of AmtB (Javelle *et al.*, 2008). On the other hand, studies in our lab suggests that this variant ($AmtB^{F107AF215A}$) still retains electrogenic activity (unpublished data, Dr. Gordon Williamson PhD thesis). Similar findings were noticed with a study on RhCG, showing that a double mutation keeps the protein almost as active as the WT (Zidi-Yahiaoui *et al.*, 2009). In the molecular dynamic simulations performed by Hoyhtya *et al* the phenylalanines are constantly moving and turning. They speculate that this might give the NH_3 molecule the opportunity to slip into the channel and navigate to the pocket with the structural water molecule (Hoyhtya, 2020). In the study they do not consider what happens to the proton following deprotonation but taking into consideration that the activity of Rh50 is electrogenic, we propose that H^+ travels via water wires like in AmtB. We also propose that some NH_4^+ slips through the pore with water molecules, independently of deprotonation. If the gate constantly moves and turns (Hoyhtya, 2020), such occurrence could be permitted. Therefore, it would be of interest to investigate the involvement of Phe-gate in the transport mechanism of Rh50 using *in vitro* SSME as well as *in vivo* yeast complementation.

6.3.1.3 Studying Bidirectionality and the Presence of Dual Mechanism

Our yeast complementation data suggested that Rh50 protein is capable of export as well as import, thus work bidirectionally. We also propose that there might be two mechanisms present in Rh50. However, we do not know if one mechanism could potentially be responsible for import and the other for export, or whether they are simply coexisting together. There is also a question of whether these two mechanisms can be linked with bidirectionality of Rh50. At present, there is no way of answering those question using either *in vivo* or *in vitro* methods. While SSME is a useful tool to study the mechanism of this membrane protein *in vitro*, the limitation of the assay is the mixed RSO and ISO orientation of the protein in the liposome. Therefore, it is impossible for us to discriminate import/export of the two mechanisms using our *in vitro* SSME measurements. Hence, means of controlling the orientation of the protein must be developed. Towards the end of my PhD, I utilised a way to produce vesicles containing the protein of interest straight from the membrane of the organism used for overexpression. More detailed description can be found in Chapter 2, section 2.5. Briefly, spheroplasts formed by treatment with the lysozyme-EDTA release their intracellular contents when placed in hypotonic media. The membrane reanneals yielding closed, empty membrane vesicles with proteins inserted at Right Site Out (RSO). Membranes prepared in this way have been shown to be physiologically active for integrated membrane functions such as amino acid and sugar transport, phospholipid biosynthesis, and electron transport (Kaback, 1974; Kaback *et al.*, 1977). We successfully made vesicles containing WT Rh50, from the membrane of GT 1000 (*ΔglnK,amtB*) overexpression strain. The strain GT 1000 was used to avoid the potential formation of heterooligomer composed of AmtB and Rh50 protein. In addition, we prepared an “empty” vesicle (made from membrane of GT 1000 overexpression strain, not expressing WT Rh50) which serves as a control for transport measurements (**Figure 6.2**). We confirmed that the size distribution of vesicles was comparable to the size of artificially made liposomes (**Figure 6.3**). This validates a direct comparison of transient charge displacement between empty vesicles, vesicles containing Rh50, and Rh50 proteoliposomes on SSME, providing us with a new way of tracking the

bidirectionality as well as existence of two mechanisms in Rh50 *in vitro* using SSME.

This work is currently being continued and expanded by Thomas Harris, a PhD student in the Javelle group. The main goal of his work will be to generate a collection of *Ne*Rh50 variants, including equivalents to mutants presented throughout this work. It is hoped that his work will provide insights into the mechanism of Rh50, especially its bidirectionality and provide more insights into coexistence of two mechanisms. Moreover, optimisation of this technique with *Ne*Rh50 and *Ec*AmtB is hoped to allow for our studies to be extended to eukaryotic ammonium transporters belonging to Amt/Mep/Rh family. Purification of eukaryotic membrane proteins is very challenging and costly. Therefore, utilising vesicles for SSME membrane protein characterisation is the best way forward to explore mechanism of mammalian Rh proteins or eukaryotic yeast Mep proteins using SURFE^{2}R in the future.

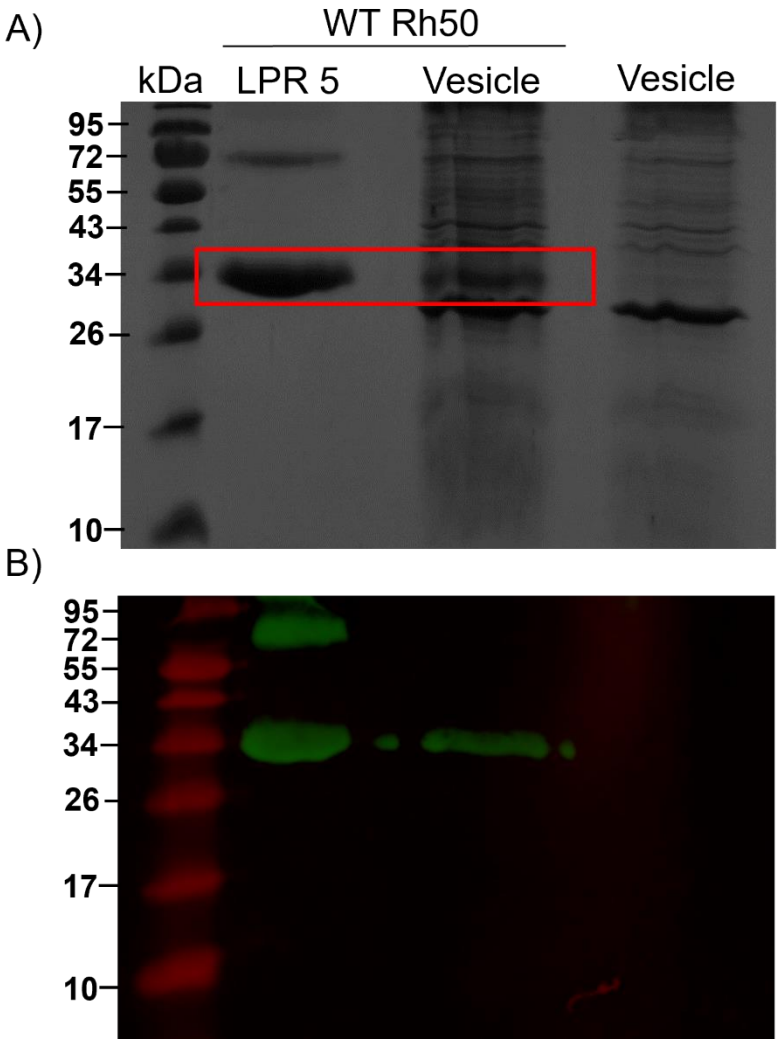

Figure 6.2 Vesicles containing WT Rh50. A) Coomassie Blue stained 12.5% SDS-PAGE showing WT Rh50 proteoliposome at an LPR 5, vesicle with WT Rh50 made from GT 1000 overexpression strain, and a vesicle made from GT 1000 overexpression strain not expressing WT Rh50. Red box highlights the clear presence of WT Rh50 dimer. B) Western Blot showing the presence of WT Rh50.

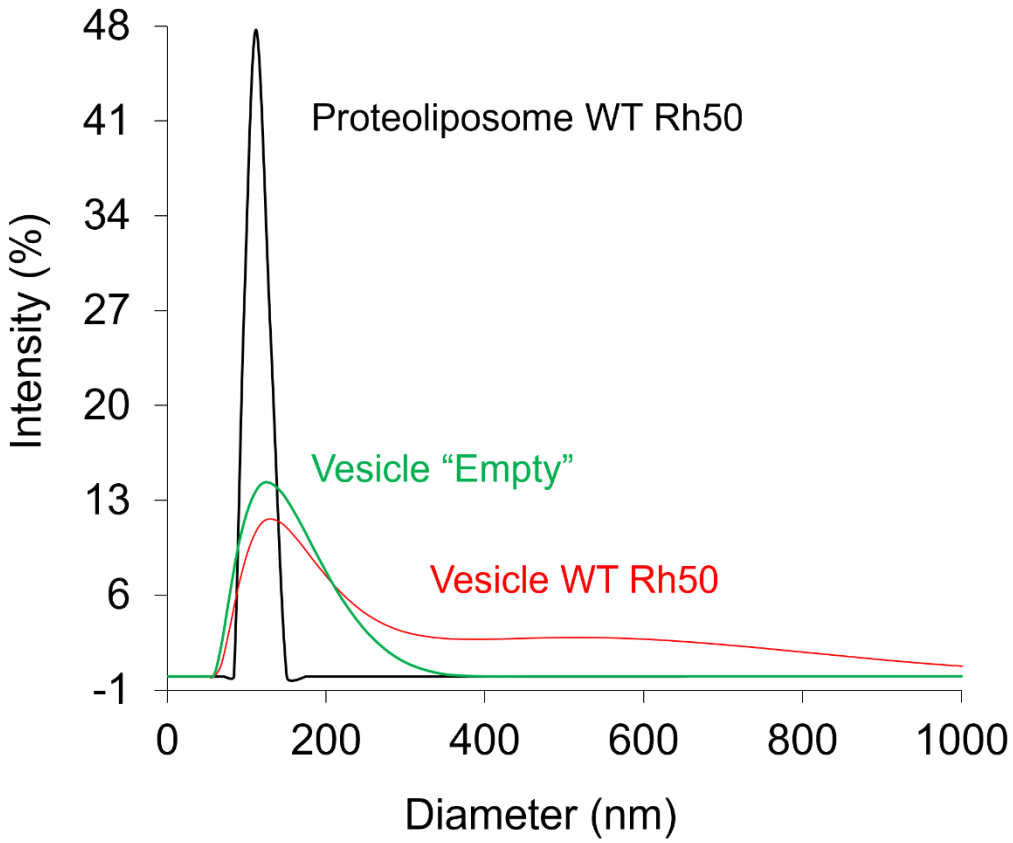

Figure 6.3 Size distribution of WT Rh50 vesicles. A) Comparison of size distribution of Rh50 polar/POPC 2/1 proteoliposome (black) and WT Rh50 vesicle made from GT 1000 membrane(red), “Empty” vesicle made form GT 1000 membrane (green) via DLS analysis.

6.3.1.4 Human Related Pathophysiology

The biological role of Rh proteins was proposed to be essential for detoxification in erythrocytes, maintaining pH balance, and reabsorption of ammonium through the renal tubule epithelial cells (Knepper *et al.*, 1991; Wright *et al.*, 2011). Consequently, mutations in Rh are associated with numerous pathologies. In RhAG protein, mutation of the phenylalanine residue to a serine (F65S) is associated with overhydrated hereditary stomatocytosis (OHSt) of red blood cells, which is a hemolytic anemia characterized by monovalent cation leaks (Bruce *et al.*, 2009; Stewart *et al.*, 2011). Modelling RhAG on pre-existing Rh50 structures revealed enlarged pore diameter for $RhAG^{F65S}$, which could permit the passage of hydrated Na^+ and K^+ ions (Bruce *et al.*, 2009). Indeed, expression in *Xenopus laevis* oocytes confirmed that the mutant RhAG proteins induced a large monovalent cation leak (Bruce *et al.*, 2009; Stewart *et al.*, 2011). In addition, molecular dynamic simulation on RhCG with the equivalent phenylalanine residue mutated to serine (F74S) revealed that water molecules occupy the pore in a large enough amount to potentially accommodate a cation (Baday *et al.*, 2013). This suggests that all Rh proteins should behave similarly in presence of this mutation. To clarify this, we mutated the equivalent residue in Rh50 (F55S) and subjected the variant to SSME analysis. Surprisingly, the transport was found to be independent of LPR, suggesting that the variant is inactive (**Figure 6.4 A**). Indeed, $Rh50^{F55S}$ fail to restore the growth in triple-*mepΔ* yeast, on the media supplemented with ammonium (**Figure 6.4 B**), further confirming it is inactive. We also clarified any potential conductivity in potassium transport. A 200 mM K^+ pulse did not trigger transient current (**Figure 6.5 A**) and no growth of *S. cerevisiae* strain lacking its three endogenous Mep (NH_4^+) and two Trk (K^+) transporters was observed when complemented with this variant (**Figure 6.5 B**).

Above results show that F55 residue is crucial for Rh50 activity, as substitution of this residue with serine leads to an inactive transporter. F55 could potentially play a key structural role in maintaining the pore of the Rh50. This contradicts previous findings that this mutation leads to leak of monovalent seen in $RhAG^{F65S}$. However, these results were based on a very indirect methods of

accessing the transport. In addition, expression of WT RhAG in *Xenopus laevis* oocytes also induced a monovalent cation leak, making us question the reliability of these results (Bruce *et al.*, 2009). It is of interest therefore, to find a more direct approach to measure transport in $RhAG^{F65S}$, such as SSME, to be able to directly compare the results we obtained for $Rh50^{F55S}$. The aforementioned vesicle method provides a perfect solution for this. It is also possible, that the hydration pattern may vary slightly between human and bacterial Rh protein, thus leading to observed discrepancies.

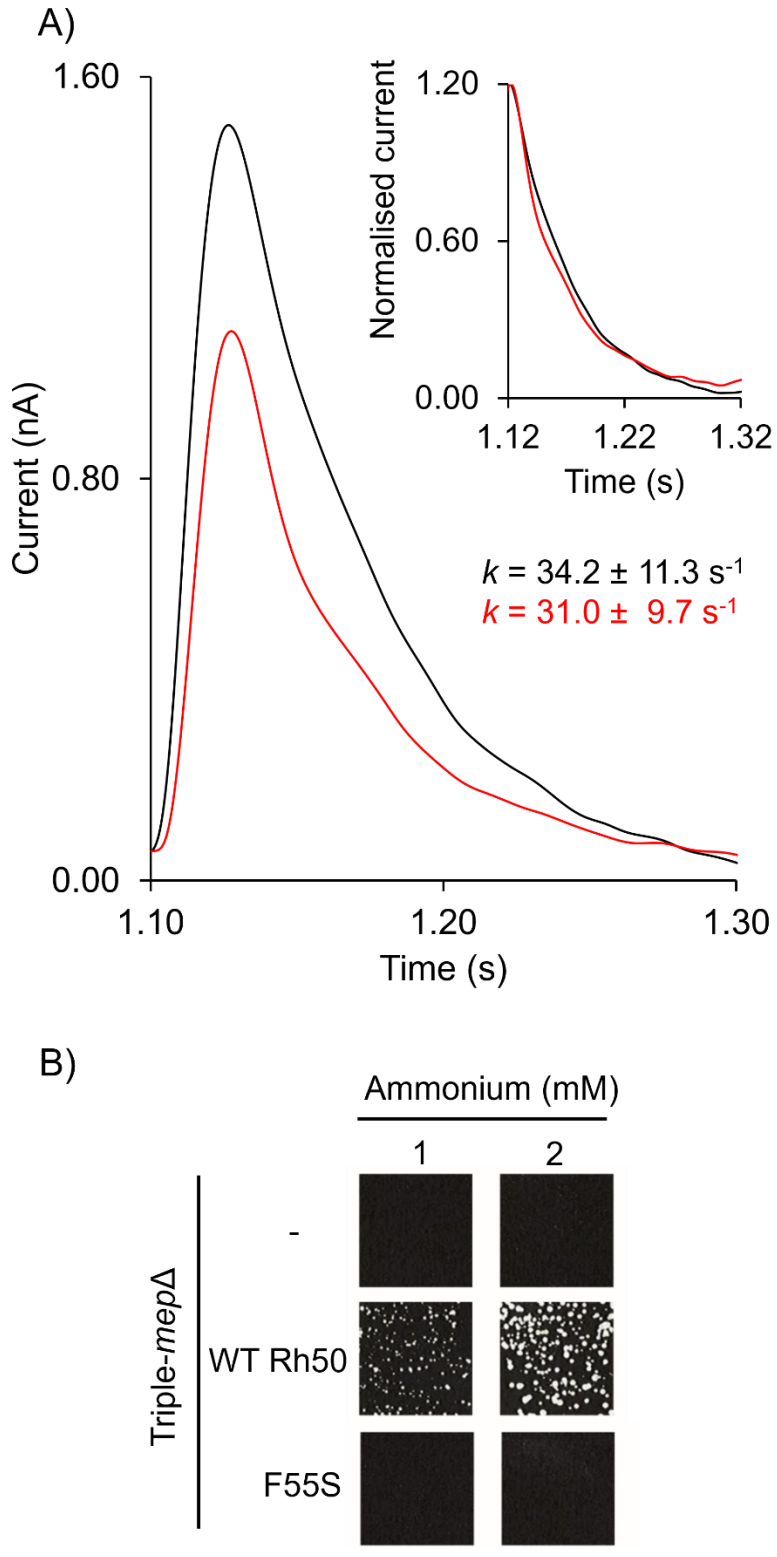

Figure 6.4 F55 is essential for Rh50 activity. A) Representative traces following a 200 mM ammonium pulse for Rh50^{F55S} (black) at LPR 5 and LPR 10 (red). B) Yeast complementation after 5 days of growth on minimal media supplemented with ammonium (Am).

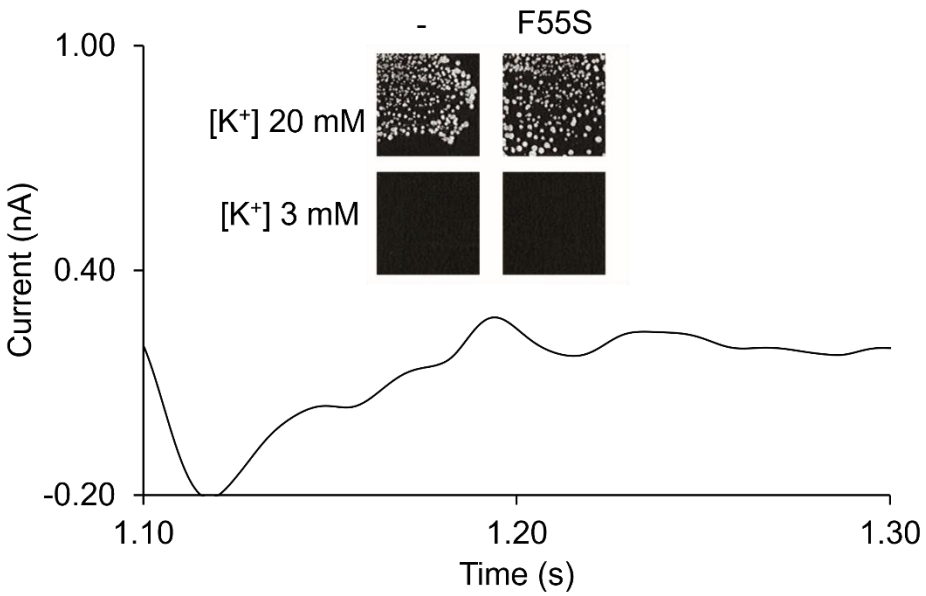

Figure 6.5 Rh50^{F55S} does not transport potassium. Representative trace following a 200 mM potassium pulse for Rh50^{F55S} variant at an LPR 5. Inset: Yeast complementation test (strain #228, mep1Δ mep2Δ mep3Δ trk1Δ trk2Δ leu2 ura3) after 5 days of growth on minimal media supplemented with 3 mM or 20 mM KCl.

6.3.1.5 Hydration Pattern of the Rh50 Protein

Data in this thesis highlights very important and unique patterns of Rh50 mechanism, which could be linked with the water accessibility into its pore. Indeed, previous molecular dynamic simulations and free energy calculations show that contrary to what is observed in AmtB, the upper part of the RhCG pore, at the level of Phe-gate (F130 F235 in RhCG, F110 F218 in Rh50), is partially hydrated, allowing a continuous chain of water molecules to form between the first histidine (H185 in RhCG) and the extracellular water bulk. In addition, unlike AmtB, the Rh protein allows water to leak into the central part of the pore (Hoyhtya, 2020). Yet, the residual electron density peaks observed in the lumen AmtB corresponding to ammonia or water molecules, were not identified in Rh50. Despite good resolution (1.3 Å and 1.85 Å) at which Rh50 crystals were resolved (Lupo *et al.*, 2007; Li *et al.*, 2007), there might be important interactions which cannot be captured via conventional crystallography. In addition, the only crystal structure available for Rh50 or human Rh proteins are the WT forms, and no available crystal structures for variants of Rh proteins. Gaining better resolution crystal structures of Rh50, as well as solving structures of protein variants would aid in understanding the hydration pattern and water accessibility into the pore of Rh proteins.

In attempt to reconcile this we propose to use a novel PanDDA analysis (Pan-Dataset Density Analysis) to identify and validate low occupation sites in Rh50. The PanDDA method analyses a series of datasets of the ground-state and the changed-state of the target protein, enabling it to eliminate the source of background noise yielding a far greater contrast at occupation site (Pearce *et al.*, 2017). Using this approach, the collection of a large data set (>50) from a batch of high quality Rh50 crystals would enable studying the hydration pattern at a higher quality. This method of acquisition generates a lot of images of the same crystal that can be overlayed, allowing for a better analysis of residual densities withing the crystal structure of the protein. A new data collection strategy and the ability of Diamond MX beamlines to collect the best data to the highest resolution would provide the best possible model of Rh50.

More structural information about Rh50 would allow us to clearly show the similarities between AmtB, such as the presence of water wires (PWW and CWW) and whether Rh50 relies on them to translocate the H^+. Simulations on the structure of RhCG have revealed the presence of a water chain linking the periplasmic vestibule to the twin-His motif (Baday *et al.*, 2015), but there is not mention of a water chain linking twin-His motif with a cytoplasmic vestibule in Rh proteins in literature. In addition, it will hopefully shed light on the existence of, proposed by us, a second mechanism allowing transfer of a hydrated NH_4^+. Our experimental results suggest that the mechanism II is abolished in $Rh50^{H170E}$ and $Rh50^{H170D}$ potentially due to lack hydrogen bonds with the neighbouring water molecules. Exporting ability *in vivo* is also killed in those variants as well as $Rh50^{H170A}$ variant. We also observed differences in results with $Rh50^{F55S}$ variant vs $RhAG^{F65S}$. Our SSME and yeast complementation data show that $Rh50^{F55S}$ is inactive, while previous studies suggests that $RhAG^{F65S}$ is still active and seems to lose selectivity towards ammonium (Bruce *et al.*, 2009). It is not clear if the conflicting data is the result of two different methods of assessments, SSME being more direct, or a difference in hydration pattern in Rh50 vs human Rh proteins. PanDDA analysis of all variants would allow the connection between Rh50 activity and pore hydration to be established and explored. Finally, it would allow for accessing the structural movement, particularly of the Phe-gate, in activity within the pore.

6.3.2 Amt/Mep/Rh Studies

6.3.2.1 Random Mutagenesis

Random mutagenesis is a useful technique to study the functions of different gene products. Propagation of the genes cloned in plasmids through a mutator strain, like *Escherichia coli* XL1-red, produces randomly mutagenized plasmid libraries. This method offers a very simple and economic way of introducing random point mutations throughout the gene with a high mutation rate. The whole process involves transformation of XL-1 red with a plasmid containing the desired gene and isolating the mutagenized plasmid library (detailed description in Chapter 2, section 2.1.5). A desired yeast strain can then be

transformed with mutagenised plasmid and screened for a phenotypic change. We want to utilise this technique to further study the mechanism of AmtB and Rh50. Using mutator strain and introducing random mutations into the gene coding for AmtB or Rh50 could produce a variant protein with gain of function in transporting monovalent cations (potassium or sodium), mechanistic switch (from transporter into channel like protein), or loss of function (bidirectionality in Rh proteins). Such protein could then be selected, purified, and studied *in vitro* using SSME. Since in our studies we did not see a similar selectivity mechanism in Rh50 in comparison to the AmtB, utilising this approach could lead us to discovering a Rh50 protein phenotype which loses selectivity towards ammonium and switches from transporter to a channel-like mechanism. In addition, it could shine light onto other members of Amt/Mep/Rh family and expand our research.

6.3.2.2 Revisiting Phylogenetics and Divergence of Amt/Mep/Rh Family

While still not clear, the evolutionary history of Rh and Amt/Mep family appears to be filled with expansion, contraction, gene loss and horizontal gene transfer (HGT). It was proposed that *Amt* genes were vertically transferred from parent to offspring, while *Mep* were horizontally transferred from a different species (McDonald, Dietrich and Lutzoni, 2012; McDonald and Ward, 2016). Rh family was proposed to have a common ancestor of prokaryotic origins due to presence of Rh homologs in bacteria (Huang and Peng, 2005). It was suggested that *N. europaea* acquired the Rh50 gene by HGT where it displaced Amt genes (Cherif-Zahar *et al.*, 2007; Matassi, 2017). While it has been proposed that there might be a universal mechanism across the family (Williamson *et al.*, 2020), some members of the family appear electrogenic and other electroneutral. Some appear to work bidirectionally, like Rh proteins, other seem to acquire additional sensing functions like in case of *Sc*Mep2 (Boeckstaens, André and Marini, 2008), or entirely switch for sensing functions like *Ks*Amt5 (Pflüger *et al.*, 2018). It is not clear how those proteins developed their distinct functions and acquired different mechanisms, as the understanding of the expansion (and reasons for it) of this family is scarce.

When the size and diversity of this family is taken into consideration, relatively little has been done to examine their phylogeny versus their role and mechanism in the past years. To reconcile this, Thomas Harris, a PhD student in the Javelle group, will undertake bioinformatic investigations into the phylogeny of this superfamily, as well as sub family investigations, to explore possible relationships between expansion and divergence of the family versus their function and mechanism. Having more information about their phylogeny and divergence is hoped to shine light onto gaps in knowledge about mechanism/s present in those proteins.

Chapter 7

References

Amlal, H., Paillard, M., and Bichara, M. (1994) 'NH_4^+ transport pathways in cells of medullary thick ascending limb of rat kidney. NH_4^+ conductance and $K^+/NH_4^+(H^+)$ antiport', *Journal of Biological Chemistry,* 269 (35), pp. 21962-21971.

Andrade, S. L., Dickmanns, A., Ficner, R. and Einsle, O. (2005) 'Crystal structure of the archaeal ammonium transporter Amt-1 from *Archaeoglobus fulgidus*', *Proceedings of the National Academy of Sciences*,102(42), pp. 14994–9

Andrade, S. L., and Einsle, O. (2007) 'The Amt/Mep/Rh family of ammonium transport proteins.', *Molecular membrane biology*, 24(5–6), pp. 357–365.

Ariz, I., Boeckstaens, M., Gouveia, C., Martins, A. P., Sanz-Luque, E., Fernández, E., Soveral, G., von Wirén, N., Marini, A. M., Aparicio-Tejo, P. M. and Cruz, C. (2018) 'Nitrogen isotope signature evidences ammonium deprotonation as a common transport mechanism for the AMT-Mep-Rh protein superfamily', *Science Advances*, 4(9), pp. eaar3599.

Arp, D.J., Sayavedra-Soto, L.A. and Hommes, N.G. (2002) 'Molecular biology and biochemistry of ammonia oxidation by *Nitrosomonas europaea*', *Archives of Microbiology,* 178 (4), pp. 250-255.

Ashkenazy,H., Abadi,S., Martz,E., Chay,O., Mayrose,I., Pupko,T. and Ben-Tal, N. (2016) 'ConSurf 2016: an improved methodology to estimate and visualize evolutionary conservation in macromolecules', *Nucleic Acids Research,* 44 (W1), pp. W344-350.

Auron, A. and Brophy, P.D. (2012) 'Hyperammonemia in review: pathophysiology, diagnosis, and treatment', *Pediatric Nephrology,* 27 (2), pp. 207-222.

Aydin, F., Zhan, C., Ritt, C., Epsztein, R., Elimelech, M., Schwegler, E. and Pham, T. A. (2020) 'Similarities and differences between potassium and ammonium ions in liquid water: a first-principles study', *Physical Chemistry Chemical Physics,* 22 (4), pp. 2540-2548.

Baday, S., Orabi, E. A., Wang, S., Lamoureux, G. and Bernèche, S. (2015) 'Mechanism of $NH_4(^+)$ Recruitment and NH_3 Transport in Rh Proteins', *Structure,* 23 (8), pp. 1550-1557.

Baday, S., Wang, S., Lamoureux, G. and Bernèche, S. (2013) 'Different Hydration Patterns in the Pores of AmtB and RhCG Could Determine Their Transport Mechanisms', *Biochemistry*, 52(40), pp. 7091–7098.

Bakouh, N., Benjelloun, F., Hulin, P., Brouillard, F., Edelman, A., Chérif-Zahar, B. and Planelles, G. (2004) 'NH_3 is involved in the NH_4^+ transport induced by the functional expression of the human Rh C glycoprotein', *Journal of Biological Chemistry,* 279 (16), pp. 15975-15983.

Bates, R.G. and Pinching, G.D. (1950) 'Dissociation Constant of Aqueous Ammonia at 0 to 50° from E. m. f. Studies of the Ammonium Salt of a Weak Acid', *Journal of the American Chemical Society,* 72 (3), pp. 1393-1396.

Bazzone, A., Barthmes, M. and Fendler, K. (2017) 'SSM-Based Electrophysiology for Transporter Research'. *Methods in Enzymology,* 594, pp. 31-83.

Bazzone, A., Madej, M.G., Kaback, H.R. and Fendler, K. (2016) 'pH Regulation of Electrogenic Sugar/H^+ Symport in MFS Sugar Permeases', *PLoS One,* 11 (5), pp. e0156392.

Behie, S.W. and Bidochka, M.J. (2014) 'Nutrient transfer in plant-fungal symbioses', *Trends in Plant Sciences,* 19 (11), pp. 734-740.

Benjelloun, F., Bakouh, N., Fritsch, J., Hulin, P., Lipecka, J., Edelman, A., Planelles, G., Thomas, S. R. and Chérif-Zahar, B. (2005) 'Expression of the human erythroid Rh glycoprotein (RhAG) enhances both NH_3 and NH_4^+ transport in HeLa cells', *Pflügers Archiv: European Journal of Physiology,* 450 (3), pp. 155-167.

Benko, P.V., Wood, T.C. and Segel, I.H. (1969) 'Multiplicity and regulation of amino acid transport in Penicillium chrysogenum',*Archives of Biochemistry and Biophysics,* 129 (2), pp. 498-508.

Bertani, G. ‘Studies on lysogenesis. I. The mode of phage liberation by lysogenic Escherichia coli.’, *Journal of Bacteriology*, 62(3), pp. 293–300.

Beyer, S., Gilch, S., Meyer, O., Schmidt, I. (2009) 'Transcription of genes coding for metabolic key functions in Nitrosomonas europaea during aerobic and anaerobic growth.', *Journal of Molecular Microbiolology and Biotechnology,* (16), pp. 187–197

Bishop, J.M., Verlander, J.W., Lee, H.W., Nelson, R.D., Weiner, A.J., Handlogten, M.E. and Weiner, I.D. (2010) 'Role of the Rhesus glycoprotein, Rh B glycoprotein, in renal ammonia excretion', *The American Journal of Physiology,* 299 (5), pp. F1065-1077.

Biswas, K. and Morschhäuser, J. (2005) ‘The Mep2p ammonium permease controls nitrogen starvation-induced filamentous growth in Candida albicans’, *Molecular Microbiology*, 56(3), pp. 649–669.

Biver, S., Belge, H., Bourgeois, S., Van Vooren, P., Nowik, M., Scohy, S., Houillier, P., Szpirer, J., Szpirer, C., Wagner, C. A., Devuyst, O. and Marini, A. M. (2008) 'A role for Rhesus factor Rhcg in renal ammonium excretion and male fertility.', *Nature*, 456(7220), pp. 339–343.

Blakey, D., Leech, A., Thomas, G. H., Coutts, G., Findlay, K. and Merrick, M. (2002) 'Purification of the Escherichia coli ammonium transporter AmtB reveals a trimeric stoichiometry', *Biochemical Journal*, 364(2), pp. 527–535.

Bock, E. and Wagner, M. (2006) 'Oxidation of Inorganic Nitrogen Compounds as an Energy Source', *The Prokaryotes,* pp. 457-495.

Bode, B.P. and Souba, W.W. (1994) 'Modulation of cellular proliferation alters glutamine transport and metabolism in human hepatoma cells', *Annals of Surgery,* 220 (4), pp. 411-422; discussion 422-414.

Boeckstaens, M., André, B. and Marini, A. M. (2008) 'Distinct transport mechanisms in yeast ammonium transport/sensor proteins of the Mep/Amt/Rh family and impact on filamentation.', *The Journal of Biological Chemistry*, 283(31), pp. 21362–70.

Bollmann, A., Bär-Gilissen, M.J. and Laanbroek, H.J. (2002) 'Growth at low ammonium concentrations and starvation response as potential factors involved in niche differentiation among ammonia-oxidizing bacteria', *Applied and Environmental Microbiology,* 68 (10), pp. 4751-4757.

Bornhorst, J.A. and Falke, J.J. (2000) 'Purification of proteins using polyhistidine affinity tags', *Methods in Enzymology,* 326, pp. 245-254.

Bourgeois, S., Meer, L., V. Wootla, B., Bloch-Faure, M., Chambrey, R., Shull, G.E., Gawenis, L.R. and Houillier, P. (2010) 'NHE4 is critical for the renal handling of ammonia in rodents', *Journal of Clinical Investigation,* 120 (6), pp. 1895-1904.

Brito, A. S., Neuhäuser, B., Wintjens, R., Marini, A. M. and Boeckstaens, M. (2020) 'Yeast filamentation signaling is connected to a specific substrate translocation mechanism of the Mep2 transceptor', *PLoS Genetics*, 16(2), pp.1- 32

Britto, D.T., Siddiqi, M.Y., Glass, A.D. and Kronzucker, H.J. (2001) 'Futile transmembrane $NH_4(^+)$ cycling: a cellular hypothesis to explain ammonium toxicity in plants',*Proceedings of the National Academy of Sciences of the United States of America,* 98 (7), pp. 4255-4258.

Bruce, L. J., Guizouarn, H., Burton, N. M., Gabillat, N., Poole, J., Flatt, J. F., Brady, R. L., Borgese, F., Delaunay, J. and Stewart, G. W. (2009) 'The monovalent cation leak in overhydrated stomatocytic red blood cells results from amino acid substitutions in the Rh-associated glycoprotein', *Blood*, 113(6), pp. 1350–7.

Burton, N.M. and Anstee, D.J. (2008) 'Structure, function and significance of Rh proteins in red cells', *Current Opinion in Hematology,* 15 (6), pp. 625-630.

Caner, T., Abdulnour-Nakhoul, S., Brown, K., Islam, M. T., Hamm, L. L. and Nakhoul, N. L. (2015) 'Mechanisms of ammonia and ammonium transport by rhesus-associated glycoproteins', *American Journal of Physiology. Cell physiology*. 309(11), pp. C747–C758.

Cartron, J.-P., Callebaut, I., Genetet, S., Le Van Kim, C., Zidi-Yahiaoui, N., Ripoche, P., Colin, Y. and Mouro-Chanteloup, I. (2009) ' Functional analysis of human RhCG: comparison with *E. coli* ammonium transporter reveals similarities in the pore and differences in the vestibule ', *American Journal of Physiology. Cell Physiology*, 297(3), pp. C537–C547.

Carpenter, E.P., Beis, K., Cameron, A.D. and Iwata,S. (2008) 'Overcoming the challenges of membrane protein crystallography', *Current Opinion in Structural Biolology,* 18 (5), pp. 581-586.

Chain, P., Lamerdin, J., Larimer, F., Regala, W., Lao, V., Land, M., Hauser, L., Hooper, A., Klotz, M., Norton, J., Sayavedra-Soto, L., Arciero, D., Hommes, N., Whittaker, M. and Arp, D. (2003) 'Complete genome sequence of the ammonia-oxidizing bacterium and obligate chemolithoautotroph *Nitrosomonas europaea*', *Journal of Bacteriology,* 185 (9), pp. 2759-2773.

Chen, B.S., Xu, Z.X., Xu, X., Cai, Y., Han, Y.L., Wang, J., Xia, S.H., Hu, H., Wei, F., Wu, M. and Wang, M.R. (2002) 'RhCG is downregulated in oesophageal squamous cell carcinomas, but expressed in multiple squamous epithelia', *European Journal of Cancer,* 38 (14), pp. 1927-1936.

Cherif-Zahar, B., Durand, A., Schmidt, I., Hamdaoui, N., Matic, I., Merrick, M. and Matassi, G. (2007) 'Evolution and functional characterization of the RH50 gene from the ammonia-oxidizing bacterium *Nitrosomonas europaea*', *Journal of Bacteriology*, 189(24), pp. 9090–9100.

Conroy, M. J., Jamieson, S. J., Blakey, D., Kaufmann, T., Engel, A., Fotiadis, D., Merrick, M. and Bullough, P. A. (2004) 'Electron and atomic force microscopy of the trimeric ammonium transporter AmtB', *EMBO Reports*, 5(12), pp. 1153–1158.

Coutts, G., Thomas, G., Blakey, D. and Merrick, M. (2002) 'Membrane sequestration of the signal transduction protein GlnK by the ammonium transporter AmtB', *The EMBO Journa*l, 21(4), pp. 536–545.

Cukierman, S. (2006) 'Et tu, Grotthuss! and other unfinished stories', *Biochimica et Biophysica Acta,* 1757 (8), pp. 876-885.

DeCoursey, T.E. and Cherny, V.V. (1997) 'Deuterium isotope effects on permeation and gating of proton channels in rat alveolar epithelium', *The Journal of General Physiology,* 109 (4), pp. 415-434.

Dejong, C.H., Deutz, N.E. and Soeters, P.B. (1996) 'Ammonia and glutamine metabolism during liver insufficiency: the role of kidney and brain in interorgan nitrogen exchange', *Scandinavian Journal of Gastroenterology,* 218 61-77.

Di, H. J., Cameron, K. C., Shen, J. P., Winefield, C. S., O'Callaghan, M., Bowatte, S. (2009). 'Nitrification driven by bacteria and not archaea in nitrogen-rich grassland soils', *Nature Geoscience.* 2, pp. 621–624.

Durant, A.C. and Donini, A. (2019) 'Development of Aedes aegypti (Diptera: Culicidae) mosquito larvae in high ammonia sewage in septic tanks causes alterations in ammonia excretion, ammonia transporter expression, and osmoregulation', *Scientific Reports,* 9 (1), pp. 19028.

Eladari, D., Cheval, L., Quentin, F., Bertrand, O., Mouro, I., Cherif-Zahar, B., Cartron, J. P., Paillard, M., Doucet, A. and Chambrey, R. (2002) 'Expression of RhCG, a new putative $NH(_3)/NH(_4)(^+)$ transporter, along the rat nephron', *Journal of the American Society of Nephrology,* 13 (8), pp. 1999-2008.

Elbing, , K. and Brent, R. (2002) 'Media Preparation and Bacteriological Tools', *Current Protocols in Molecular Biology*, 59(1), pp. 111-117.

Endeward, V., Cartron, J. P., Ripoche, P. and Gros, G. (2006) 'Red cell membrane CO_2 permeability in normal human blood and in blood deficient in various blood groups, and effect of DIDS', *Transfusion Clinique et Biologique*, 13 (1-2), pp. 123-127.

Endeward, V., Cartron, J. P., Ripoche, P. and Gros, G. (2008) 'RhAG protein of the Rhesus complex is a CO_2 channel in the human red cell membrane', *The FASEB Journal,* 22 (1), pp. 64-73.

Eng, C.H. and Abraham, R.T. (2010) 'Glutaminolysis yields a metabolic by-product that stimulates autophagy'. *Autophagy,* 6 (7), pp. 968-970.

Eyers, S.A., Ridgwell, K., Mawby, W. J. and Tanner, M. J. (1994) 'Topology and organization of human Rh (rhesus) blood group-related polypeptides.', *The Journal of Biological Chemistry*, 269(9), pp. 6417–6423.

Bergersen, F.J. (1965) 'Ammonia- An Early Stable Product of Nitrogen Fixation by Soybean Root Nodules', *Australian Journal of Biological Sciences*, 18 (6), pp.1-9

Garcia-Celma, J.J., Dueck, B., Stein, M., Schlueter, M., Meyer-Lipp, K., Leblanc, G. and Fendler, K. (2007) 'Specific anion and cation binding to lipid membranes investigated on a solid supported membrane'. *Langmuir,* 23 (20), pp. 10074-10080.

Gietz, D., St Jean, A., Woods, R. A. and Schiestl, R. H. (1992) 'Improved method for high efficiency transformation of intact yeast cells', *Nucleic Acids Research,* 20 (6), pp. 1425.

Gimeno, C.J., Ljungdahl, P.O., Styles, C.A. andFink, G.R. (1992) 'Unipolar cell divisions in the yeast *S. cerevisiae* lead to filamentous growth: regulation by starvation and RAS', *Cell,* 68 (6), pp. 1077-1090.

Good, D.W. and DuBose, T.D. (1987) 'Ammonia transport by early and late proximal convoluted tubule of the rat', *Journal of Clinical Investigationt,* 79 (3), pp. 684-691.

Gruswitz, F., Chaudhary, S., Ho, J. D., Schlessinger, A., Pezeshki, B., Ho, C.-M., Sali, A., Westhoff, C. M. and Stroud, R. M. (2010) 'Function of human Rh based on structure of RhCG at 2.1 Å', *Proceedings of the National Academy of Sciences,* 107(21), pp. 9638–9643

Hamm, L.L. and Simon, E.E. (1990) 'Ammonia transport in the proximal tubule', *Mineral and Electrolyte Metabolism,* 16 (5), pp. 283-290.

Hanahan, D. (1983) 'Studies on transformation of *Escherichia coli* with plasmids', *Journal of Molecular Biology,* 166 (4), pp. 557-580.

Handlogten, M.E., Hong, S.P., Westhoff, C.M. and Weiner, I.D., (2004) 'Basolateral ammonium transport by the mouse inner medullary collecting duct cell (mIMCD-3)', *The American Journal of Physiology - Renal Physiology,* 287 (4), pp. F628-638.

Handlogten, M.E., Hong, S.P., Westhoff, C.M., and Weiner, I.D. (2005) 'Apical ammonia transport by the mouse inner medullary collecting duct cell (mIMCD-3)', *The American Journal of Physiology - Renal Physiology,* 289 (2), pp. F347-358.

Hemker, M.B., Cheroutre, G., van Zwieten, R., Maaskant-van Wijk, P.A., Roos, D., Loos, J.A., van der Schoot, C.E. and von dem Borne, A.E., (2003) 'The Rh complex exports ammonium from human red blood cells', *British Journal of Haematology,* 122 (2), pp. 333-340.

Hooper, A.B., Bergmann, T. V., Arciero, D.J. and David M. (1997) 'Enzymology of the oxidation of ammonia to nitrite by bacteria', *Antonie Van Leeuwenhoek*, 71 (1-2), pp. 59–67.

Hoyhtya, H., Koster, H., Christiansen, M. and Akgun, U. (2020) Human RhCG Ammonia Conduction Mechanism, *Computational Molecular Bioscience*, 10, 81-94.

Huang, C.H., Chen, Y., Reid, M.E. and Seidl, C. (1998) 'Rhnull disease: the amorph type results from a novel double mutation in RhCe gene on D-negative background', *Blood,* 92 (2), pp. 664-671.

Huang, C.H. and Liu, P.Z. (2001) 'New insights into the Rh superfamily of genes and proteins in erythroid cells and nonerythroid tissues', *Blood Cells, Molecules and Diseases,* 27 (1), pp. 90-101.

Huang, C.H. and Peng, J. (2005) 'Evolutionary conservation and diversification of Rh family genes and proteins', *Proceedings of the National Academy of Sciences of the United States of America,* 102 (43), pp. 15512-15517.

Ishikita, H. and Knapp, E.W. (2007) 'Protonation states of ammonia/ammonium in the hydrophobic pore of ammonia transporter protein AmtB', *Journal of the American Chemical Society,* 129 (5), pp. 1210-1215.

Javelle, A., Severi, E., Thornton, J. and Merrick, M. (2004) 'Ammonium sensing in Escherichia coli. Role of the ammonium transporter AmtB and AmtB-GlnK complex formation', *Journal of Biological Chemistry*, 279(10), pp. 8530–8538.

Javelle, A., Thomas, G., Marini, A.M., Krämer, R. and Merrick, M. (2005) '*In vivo* functional characterization of the Escherichia coli ammonium channel AmtB: evidence for metabolic coupling of AmtB to glutamine synthetase', *Biochemical Journal,* 390 (1), pp. 215-222.

Javelle, A., Lupo, D., Zheng, L., Li, X. D., Winkler, F. K. and Merrick, M. (2006) 'An unusual twin-His arrangement in the pore of ammonia channels is essential for substrate conductance', *Journal of Biological Chemistry*, 281(51), pp. 39492–39498.

Javelle, A., Lupo, D., Li, X. D., Merrick, M., Chami, M., Ripoche, P. and Winkler, F. K. (2007) 'Structural and mechanistic aspects of Amt/Rh proteins', *Journal of Structural Biology*, 158(3), pp. 472–481.

Javelle, A., Lupo, D., Ripoche, P., Fulford, T., Merrick, M. and Winkler, F. K. (2008) 'Substrate binding, deprotonation, and selectivity at the periplasmic entrance of the *Escherichia coli* ammonia channel AmtB.', *Proceedings of the National Academy of Sciences*, 105(13), pp. 5040–5045.

Ji, Q., Hashmi, S., Liu, Z., Zhang, J., Chen, Y. and Huang, C. H. (2006) 'CeRh1 (*rhr-1*) is a dominant Rhesus gene essential for embryonic development and hypodermal function in *Caenorhabditis elegans*', *Proceedings of the National Academy of Sciences of the United States of America,* 103 (15), pp. 5881-5886.

Johansson, F.K., Brodd, J., Eklöf, C., Ferletta, M., Hesselager, G., Tiger, C.F., Uhrbom, L. and Westermark, B. (2004) 'Identification of candidate cancer-causing genes in mouse brain tumors by retroviral tagging', *Proceedings of the National Academy of Sciences of the United States of America,* 101 (31), pp. 11334-11337.

Juliette, L.Y., Hyman, M.R. and Arp, D.J. (1993) 'Mechanism-Based Inactivation of Ammonia Monooxygenase in *Nitrosomonas europaea* by Allylsulfide', *Applied Environmental Microbiology,* 59 (11), pp. 3728-3735.

Kaback, H.R. (1974) 'Transport studies in bacterial membrane vesicles', *Science,* 186 (4167), pp. 882-892.

Kaback, H.R., Ramos, S., Robertson, D.E., Stroobant, P. and Tokuda, H. (1977) 'Energetics and molecular biology of active transport in bacterial membrane vesicles', *Journal of Supramolecular Structure,* 7 (3-4), pp. 443-461.

Keener, W.K. and Arp, D.J. (1994) 'Transformations of Aromatic Compounds by *Nitrosomonas europaea*', *Applied Environmental Microbiology,* 60 (6), pp. 1914-1920.

Khademi, S., O'Connell 3rd, J., Remis, J., Robles-Colmenares, Y., Miercke, L. J. and Stroud, R. M. (2004) 'Mechanism of ammonia transport by Amt/MEP/Rh: structure of AmtB at 1.35 Å', *Science*, 305(5690), pp. 1587–1594.

Kikeri, D., Sun, A., Zeidel, M.L. and Hebert, S.C. (1989) 'Cell membranes impermeable to NH_3', *Nature,* 339 (6224), pp. 478-480.

Kitano, T. and Saitou, N. (2000) 'Evolutionary history of the Rh blood group-related genes in vertebrates', *Immunogenetics,* 51 (10), pp. 856-862.

Kleiner, D. (1981) 'The transport of NH_3 and NH_4^+ across biological membranes', *Biochimica et Biophysica Acta,* 639 (1), pp. 41-52.

Klenk, H.P. (1997) 'The complete genome sequence of the hyperthermophilic, sulphate-reducing archaeon *Archaeoglobus fulgidus*', *Nature,* 390 (6658), pp. 364-370.

Knepper, M.A., Desai, S.S., Hornbuckle, K. and Packer, R.K. (1991) 'Regulation of renal medullary ammonium accumulation', *Contributions to Nephrology,* 92 119-123.

Kustu, S. and Inwood, W. (2006) 'Biological gas channels for NH_3 and CO_2: evidence that Rh (Rhesus) proteins are CO_2 channels', *Transfusion Clinique et Biologique,* 13 (1-2), pp. 103-110.

Lacapère, J.J., Pebay-Peyroula, E., Neumann, J.M. and Etchebest, C. (2007) 'Determining membrane protein structures: still a challenge!', *Trends in Biochemical Sciences,* 32 (6), pp. 259-270.

Laing, C.M., Toye, A.M., Capasso, G. and Unwin, R.J. (2005) 'Renal tubular acidosis: developments in our understanding of the molecular basis', *The International Journal of Biochemistry & Cell Biology,* 37 (6), pp. 1151-1161.

Lamoureux, G., Klein, M.L. and Bernèche, S. (2007) 'A stable water chain in the hydrophobic pore of the AmtB ammonium transporter', *Biophysical Journal,* 92 (9), pp. L82-84.

Landsteiner, K. and Wiener, A.S. (1941) 'Studies on an agglutinogen (Rh) in human blood reacting with ani-rhesus sera and with human isoantibodies', *Journal of Experimental Medicine,* 74 (4), pp. 309-320.

Lee, I.R., Morrow, C.A. and Fraser, J.A. (2013) 'Nitrogen regulation of virulence in clinically prevalent fungal pathogens', *FEMS Microbiology Letters,* 345 (2), pp. 77-84.

Li, X., Jayachandran, S., Nguyen, H. H. T. and Chan, M. K. (2007) 'Structure of the *Nitrosomonas europaea* Rh protein', *Proceedings of the National Academy of Sciences*, 104(49), pp. 19279–19284

Lin, Y., Cao, Z. and Mo, Y. (2006) 'Molecular dynamics simulations on the *Escherichia coli* ammonia channel protein AmtB: mechanism of ammonia/ammonium transport', *Journal of the American Chemical Society,* 128 (33), pp. 10876-10884.

Lishchuk, S.V., Lokotosh, T.V. and Malomuzh, N.P. (2005) 'Properties of the H-bond network for two-dimensional lattice water model', *The Journal of Chemical Physics,* 122 (24), pp. 244504.

Liu, Z., Chen, Y., Mo, R., Hui, C., Cheng, J.F., Mohandas, N. and Huang, C.H. (2000) 'Characterization of human RhCG and mouse Rhcg as novel nonerythroid Rh glycoprotein homologues predominantly expressed in kidney and testis', *Journal of Biological Chemistry,* 275 (33), pp. 25641-25651.

Liu, Z., Peng, J., Mo, R., Hui, C. and Huang, C.H. (2001) 'Rh type B glycoprotein is a new member of the Rh superfamily and a putative ammonia transporter in mammals', *Journal of Biological Chemistry,* 276 (2), pp. 1424-1433.

Livingston, M. D., Bhargav, V. V., Turko, A. J., Wilson, J. M. and Wright, P. A. (2018) 'Widespread use of emersion and cutaneous ammonia excretion in *Aplocheiloid killifishes*', *Proceedings of the Royal Society B: Biological Sciences*, 285(1884)

Lo, H., Köhler, J. R., DiDomenico, B., Loebenberg, D., Cacciapuoti, A. and Fink, G. R. (2015) 'Nonfilamentous *C . albicans* Mutants Are Avirulent', *Cell,* 90, pp. 939–949

Loqué, D., Mora, S. I., Andrade, S. L., Pantoja, O. and Frommer, W. B. (2009) 'Pore mutations in ammonium transporter AMT1 with increased electrogenic ammonium transport activity', *Journal of Biological Chemistry*, 284(37), pp. 24988–24995

Lorenz, M.C. and Heitman, J. (1998) 'The MEP2 ammonium permease regulates pseudohyphal differentiation in *Saccharomyces cerevisiae*', *EMBO Journal,* 17 (5), pp. 1236-1247.

Ludewig, U., von Wirén, N. and Frommer, W.B. (2002) 'Uniport of NH_4^+ by the root hair plasma membrane ammonium transporter *Le*AMT1;1', *Journal of Biological Chemistry,* 277 (16), pp. 13548-13555.

Ludewig, U. (2004) 'Electroneutral ammonium transport by basolateral rhesus B glycoprotein', *The Journal of Physiology,* 559 (Pt 3), pp. 751-759.

Lupo, D., Li, X.-D., Durand, A., Tomizaki, T., Cherif-Zahar, B., Matassi, G., Merrick, M. and Winkler, F. K. (2007) 'The 1.3-Å resolution structure of *Nitrosomonas europaea* Rh50 and mechanistic implications for NH_3 transport by Rhesus family proteins', *Proceedings of the National Academy of Sciences*, 104(49), pp. 19303–19308

Luzhkov, V. B., Almlof, M., Nervall, M. and Aqvist, J. (2006) 'Computational study of the binding affinity and selectivity of the bacterial ammonium transporter AmtB.', *Biochemistry*, 45(36), pp. 10807–10814.

López-Pedrosa, A., González-Guerrero, M., Valderas, A., Azcón-Aguilar, C. and Ferrol, N. (2006) '*Gint*AMT1 encodes a functional high-affinity ammonium transporter that is expressed in the extraradical mycelium of *Glomus intraradices*', *Fungal Genetics and Biology,* 43 (2), pp. 102-110.

Marcus, Y. (2009) 'Effect of ions on the structure of water: structure making and breaking', *Chemical Reviews,* 109 (3), pp. 1346-1370.

Marini, A. M., Matassi, G., Raynal, V., Andre, B., Cartron, J. P. and Chérif-Zahar, B. (2000a) 'The human Rhesus-associated RhAG protein and a kidney homologue promote ammonium transport in yeast', *Nature Genetics*, 26(3), pp. 341–344

Marini, A. M., Springael, J. Y., Frommer, W. B. and André, B. (2000b) 'Cross-talk between ammonium transporters in yeast and interference by the soybean SAT1 protein', *Molecular Microbiology*, 35(2), pp. 378–385.

Marini, A. M., Vissers, S., Urrestarazu, A. and André, B. (1994) 'Cloning and expression of the *MEP1* gene encoding an ammonium transporter in Saccharomyces cerevisiae', *The EMBO Journal*, 13(15), pp. 3456–3463.

Marini, A. M., Soussi-Boudekou, S., Vissers, S. and André, B. (1997a) 'A family of ammonium transporters in Saccharomyces cerevisiae.', *Molecular and Cellular Biology*, 17(8), pp. 4282–4293.

Marini, A. M., Urrestarazu, A., Beauwens, R. and André, B. (1997b) 'The Rh (rhesus) blood group polypeptides are related to NH_4^+ transporters', *Trends in Biochemical Sciences*, 22(12), pp. 460–461.

Marini, A. M., Boeckstaens, M., Benjelloun, F., Chérif-Zahar, B. and André, B. (2006) ‘Structural involvement in substrate recognition of an essential aspartate residue conserved in Mep/Amt and Rh-type ammonium transporters’, *Current Genetics*, 49(6), pp. 364–374

Marino, R., Melillo, D., Di Filippo, M., Yamada, A., Pinto, M.R., De Santis, R., Brown, E.R. and Matassi, G. (2007) 'Ammonium channel expression is essential for brain development and function in the larva of *Ciona intestinalis*', *The Journal of Comparative Neurology,* 503 (1), pp. 135-147.

Matassi, G., Chérif-Zahar, B., Pesole, G., Raynal, V. and Cartron, J.P. (1999) 'The members of the RH gene family (RH50 and RH30) followed different evolutionary pathways', *Journal of Molecular Evolution,* 48 (2), pp. 151-159.

Matassi, G. (2017) 'Horizontal gene transfer drives the evolution of Rh50 permeases in prokaryotes', *BMC Evolutionary Biology,* 17 (1), pp. 2.

Mayer, M., Dynowski, M. and Ludewig, U. (2006) 'Ammonium ion transport by the AMT/Rh homologue *Le*AMT1;1', *Biochemical Journal,* 396 (3), pp. 431-437.

McDonald, T.R., Dietrich, F.S. and Lutzoni, F. (2012) 'Multiple horizontal gene transfers of ammonium transporters/ammonia permeases from prokaryotes to eukaryotes: toward a new functional and evolutionary classification', *Molecular Biology and Evolution,* 29 (1), pp. 51-60.

McDonald, T.R. and Ward, J.M. (2016) 'Evolution of Electrogenic Ammonium Transporters (AMTs)', *Frontiers in Plant Science,* 7 352.

Merrick, M., Javelle, A., Durand, A., Severi, E., Thornton, J., Avent, N.D., Conroy, M.J. and Bullough, P.A. (2006) 'The Escherichia coli AmtB protein as a model system for understanding ammonium transport by Amt and Rh proteins', *Transfusion Clinique et Biologique,* 13 (1-2), pp. 97-102.

Mirandela, G. D., Tamburrino, G., Hoskisson, P. A., Zachariae, U. and Javelle, A. (2019) ‘The lipid environment determines the activity of the *Escherichia coli* ammonium transporter AmtB’, *FASEB Journal*, 33(2), pp. 1989–1999.

Miroux, B. and Walker, J.E. (1996) 'Over-production of proteins in *Escherichia coli:* mutant hosts that allow synthesis of some membrane proteins and globular proteins at high levels', *J. of Molecular Biology,* 260 (3), pp. 289-298.

Missner, A., Kügler, P., Saparov, S.M., Sommer, K., Mathai, J.C., Zeidel, M.L. and Pohl, P. (2008) 'Carbon dioxide transport through membranes', *J Biol Chem,* 283 (37), pp. 25340-25347.

Mouro-Chanteloup, I., Cochet, S., Chami, M., Genetet, S., Zidi-Yahiaoui, N., Engel, A., Colin, Y., Bertrand, O. and Ripoche, P. (2010) 'Functional reconstitution into liposomes of purified human RhCG ammonia channel', *PLoS One,* 5 (1), pp. e8921.

Mumberg, D., Müller, R. and Funk, M. (1994) 'Regulatable promoters of *Saccharomyces cerevisiae*: comparison of transcriptional activity and their use for heterologous expression', *Nucleic Acids Research,* 22 (25), pp. 5767-5768.

Musa-Aziz, R., Chen, L., M. Pelletier, M.F. and Boron, W.F. (2009) 'Relative CO_2/NH_3 selectivities of AQP1, AQP4, AQP5, AmtB, and RhAG', *Proceedings of the National Academy of Sciences of the United States of America,* 106 (13), pp. 5406-5411.

Muteeb, G. and Sen, R. (2010) 'Random mutagenesis using a mutator strain', *Methods in Molcular Biology,* 634 411-419.

Nagami, G.T. (1989) 'Ammonia production and secretion by the proximal tubule', *American Journal of Kidney Diseases,* 14 (4), pp. 258-261.

Nakada, T. Westhoff, C. M. Kato, A. Hirose, S. (2007) 'Ammonia secretion from fish gill depends on a set of Rh glycoproteins'. *FASEB Journal,* 21 (4), pp. 1067-1074.

Nakhoul, N.L., DeJong, H., Abdulnour-Nakhoul, S. M., Boulpaep, E. L., Herring-Smith, K. and Hamm, L. L. (2005) 'Characteristics of renal Rhbg as an NH4(+) transporter', *Amercian Journal of Physiology: Renal Physiology,* 288 (1), pp. F170-181.

Nakhoul, N. L. Schmidt, E. Abdulnour-Nakhoul, S. M. Hamm, L. L. (2006) 'Electrogenic ammonium transport by renal Rhbg', *Transfusion Clinique et Biologique,* 13 (1-2), pp. 147-153.

Neuhäuser, B., Dynowski, M., Mayer, M. and Ludewig, U. (2007) 'Regulation of NH_4^+ Transport by Essential Cross Talk between AMT Monomers through the Carboxyl Tails', *Plant Physiology*, 143(4), pp. 1651–1659.

Neuhäuser, B., Dynowski, M. and Ludewig, U. (2009) 'Channel-like NH_3 flux by ammonium transporter *At*AMT2.', *FEBS letters,* 583(17), pp. 2833–2838.

Neuhäuser, B., Dynowski, M. and Ludewig, U. (2014) 'Switching substrate specificity of AMT/MEP/ Rh proteins', *Channels*, 8(6), pp. 496–502.

Norberg, A., Forsgren, L., Holmberg, D. and Holmberg, M. (2006) 'Exclusion of the juvenile myoclonic epilepsy gene *EFHC1* as the cause of migraine on chromosome 6, but association to two rare polymorphisms in *MEP1A* and RHAG', *Neuroscience Letters,* 396 (2), pp. 137-142.

Nygaard, T.P., Rovira, C., Peters, G.H. and Jensen, M. (2006) 'Ammonium recruitment and ammonia transport by E. coli ammonia channel AmtB'. *Biophysical Journal,* 91 (12), pp. 4401-4412.

Pearce, N. M., Krojer, T., Bradley, A. R., Collins, P., Nowak, R. P., Talon, R., Marsden, B. D., Kelm, S., Shi, J., Deane, C. M. and von Delft, F. (2017) 'A multi-crystal method for extracting obscured crystallographic states from conventionally uninterpretable electron density', *Nature Communications*, 8(1), p. 15123.

Perry, S.F., Braun, M.H., Noland, M., Dawdy, J. and Walsh, P.J. (2010) 'Do zebrafish Rh proteins act as dual ammonia-CO_2 channels?', *Journal of Experimental ZoologyPart A, Ecological genetics and physiology,* 313 (9), pp. 618-621.

Pflüger, T., Hernández, C. F., Lewe, P., Frank, F., Mertens, H., Svergun, D., Baumstark, M. W., Lunin, V. Y., Jetten, M. S. M. and Andrade, S. L. (2018) 'Signaling ammonium across membranes through an ammonium sensor histidine kinase', *Nature Communications*, 9(1), pp. 1–11.

Pitts, R.F. (1948) 'Renal excretion of acid', *Federation Proceedings,* 7 (2), pp. 418-426.

Pitts, R.F. (1971) 'The role of ammonia production and excretion in regulation of acid-base balance', *The New England Journal of Medicine,* 284 (1), pp. 32-38.

Pitts, R. J., Derryberry, S. L., Pulous, F. E. and Zwiebel, L. J. (2014) 'Antennal-Expressed Ammonium Transporters in the Malaria Vector Mosquito *Anopheles gambiae*', *PLoS One*, 9(10), pp. 1-11

Quentin, F., Eladari, D., Cheval, L., Lopez, C., Goossens, D., Colin, Y., Cartron, J.P., Paillard, M. and Chambrey, R. (2003) 'RhBG and RhCG, the putative ammonia transporters, are expressed in the same cells in the distal nephron', *Journal of the American Society of Nephrologyl,* 14 (3), pp. 545-554.

Rath, A., Glibowicka, M., Nadeau, V. G., Chen, G. and Deber, C. M. (2009) 'Detergent binding explains anomalous SDS-PAGE migration of membrane proteins', *Proceedings of the National Academy of Sciences*, 106(6), pp. 1760 LP – 1765

Reitzer, L. (2003) 'Nitrogen assimilation and global regulation in *Escherichia coli*'. *Annual Review Microbiology,* 57 155-176.

Rentsch, D., Laloi, M., Rouhara, I., Schmelzer, E., Delrot, S. and Frommer, W. B. (1995) '*NTR1* encodes a high affinity oligopeptide transporter in *Arabidopsis*', *FEBS Letters*, 370(3), pp. 264–268.

Rigaud, J.L. (2002) 'Membrane proteins: functional and structural studies using reconstituted proteoliposomes and 2-D crystals', *Braz J Med Biol Res,* 35 (7), pp. 753-766.

Rigaud, J.L., Paternostre, M.T. and Bluzat, A. (1988) 'Mechanisms of membrane protein insertion into liposomes during reconstitution procedures involving the use of detergents. 2. Incorporation of the light-driven proton pump bacteriorhodopsin'. *Biochemistry,* 27 (8), pp. 2677-2688.

Ripoche, P., Bertrand, O., Gane, P., Birkenmeier, C., Colin, Y. and Cartron, J. P. (2004) 'Human Rhesus-associated glycoprotein mediates facilitated transport of $NH_{(3)}$ into red blood cells', *Proceedings of the National Academy of Sciences of the United States of America,* 101 (49), pp. 17222-17227.

Sambrook, J., Fritsch, E.F. and Maniatis, T. (1989) 'Molecular Cloning: A Laboratory Manual.', *Cold Spring Harbor laboratory Press,*

Sayavedra-Soto, L.A., Hommes, N.G., Russell, S.A. and Arp, D.J. (1996) 'Induction of ammonia monooxygenase and hydroxylamine oxidoreductase mRNAs by ammonium in *Nitrosomonas europaea*', *Molecular Microbiology,* 20 (3), pp. 541-548.

Schmidt, I., Look, C., Bock, E. and Jetten, M.S.M. (2004) 'Ammonium and hydroxylamine uptake and accumulation in *Nitrosomonas*', *Microbiology,* 150 (5), pp. 1405-1412.

Schmidt, P.J. and Vos, G.H. (1967) 'Multiple phenotypic abnormalities associated with Rh-null (---/---)', *Vox Sanguinis,* 13 (1), pp. 18-20.

Shannon, R. (1976) 'Revised effective ionic radii and systematic studies of interatomic distances in halides and chalcogenides', *Acta Crystallographica Section A,* 32 (5), pp. 751-767.

Sidey, V. (2016) 'On the effective ionic radii for ammonium', *Acta Crystallographica Section B: Structural Science, Crystal Engineering and Materialsr,* 72 (Pt 4), pp. 626-633.

Simon, E., Martin, D. and Buerkert, J. (1985) 'Contribution of individual superficial nephron segments to ammonium handling in chronic metabolic acidosis in the rat. Evidence for ammonia disequilibrium in the renal cortex', *Journal of Clinical Investigation,* 76 (2), pp. 855-864.

Singleton, C.K., Kirsten, J.H. and Dinsmore, C.J. (2006) 'Function of ammonium transporter A in the initiation of culmination of development in *Dictyostelium discoideum*', *Eukaryotic Cell,* 5 (7), pp. 991-996.

Smith, D.G., Garcia-Pedrajas, M.D., Gold, S.E. and Perlin, M.H. (2003) 'Isolation and characterization from pathogenic fungi of genes encoding ammonium permeases and their roles in dimorphism', *Molecular Microbiol,* 50 (1), pp. 259-275.

Song, C. and Corry, B. (2009) 'Intrinsic ion selectivity of narrow hydrophobic pores', *The Journal of Physical Chemistry B,* 113 (21), pp. 7642-7649.

Soupene, E., He, L., Yan, D. and Kustu, S. (1998) 'Ammonia acquisition in enteric bacteria: physiological role of the ammonium/methylammonium transport B (AmtB) protein'. *Proc Natl Acad Sci U S A,* 95 (12), pp. 7030-7034.

Soupene, E., Ramirez, R.M. and Kustu, S. (2001) 'Evidence that fungal MEP proteins mediate diffusion of the uncharged species NH_3 across the cytoplasmic membrane'. *Molecular Cell Biology,* 21 (17), pp. 5733-5741.

Soupene, E., Lee, H. and Kustu, S. (2002) 'Ammonium/methylammonium transport (Amt) proteins facilitate diffusion of NH_3 bidirectionally', *Proceedings of the National Academy of Sciences*, 99(6), pp. 3926–3931.

Soupene, E., Inwood, W. and Kustu, S. (2004) 'Lack of the Rhesus protein Rh1 impairs growth of the green alga *Chlamydomonas reinhardtii* at high CO_2', *Proceedings of the National Academy of Sciences,* 101 (20), pp. 7787-7792.

Spinelli, J.B., Yoon, H., Ringel, A.E., Jeanfavre, S., Clish, C.B. and Haigis, M.C. (2017) 'Metabolic recycling of ammonia via glutamate dehydrogenase supports breast cancer biomass', *Science,* 358 (6365), pp. 941-946.

Stewart, A.K., Shmukler, B.E., Vandorpe, D.H., Rivera, A., Heneghan, J.F. and Li, X. (2011) 'Loss-of-function and gain-of-function phenotypes of stomatocytosis mutant RhAG F65S', *The American Journal of Physiology-Cell Physiology,* 301 (6), pp. C1325-1343.

Studier, F.W. (2005) 'Protein production by auto-induction in high density shaking cultures', *Protein expression and purification,* 41 (1), pp. 207-234.

Sudnitsyna, J.S., Skvertchinskaya, E.A., Dobrylko, I.A., Nikitina, E.R., Krivchenko, A.I., Gambaryan, S.P. and Mindukshev, I.V. (2016) 'Human erythrocyte ammonium transport is mediated by functional interaction of ammonium (RhAG) and anion (AE1) transporters', *Biochemistry (Moscow) Supplement Series A: Membrane and Cell Biology,* 10 (4), pp. 301-310.

Suzuki, I., Dular, U. and Kwok, S.C. (1974) 'Ammonia or ammonium ion as substrate for oxidation by *Nitrosomonas europaea* cells and extracts', *Journal of Bacteriology,* 120 (1), pp. 556-558.

Søgaard, R., Alsterfjord, M., Macaulay, N. and Zeuthen, T. (2009) 'Ammonium ion transport by the AMT/Rh homolog *Ta*AMT1;1 is stimulated by acidic pH', *Pflügers Archiv: European Journal of Physiology,* 458 (4), pp. 733-743.

Tannen, R.L. (1978) 'Ammonia metabolism', *American Journal of Physiology,* 235 (4), pp. F265-277.

ten Hoopen, F., Cuin, T.A., Pedas, P., Hegelund, J.N., Shabala, S., Schjoerring, J.K. and Jahn, T.P. (2010) 'Competition between uptake of ammonium and potassium in barley and *Arabidopsis roots*: molecular mechanisms and physiological consequences', *The Journal of Experimental Botany,* 61 (9), pp. 2303-2315.

Thomas, G.H., Mullins, J.G. and Merrick, M. (2000) 'Membrane topology of the Mep/Amt family of ammonium transporters'. *Molecular Microbiology,* 37 (2), pp. 331-344.

van den Berg, B., Chembath, A., Jefferies, D., Basle, A., Khalid, S. and Rutherford, J.C. (2016) 'Structural basis for Mep2 ammonium transceptor activation by phosphorylation', *Nature Communications,* 7 11337.

van Heeswijk, W.C., Hoving, S., Molenaar, D., Stegeman, B., Kahn, D. and Westerhoff, H.V. (1996) 'An alternative PII protein in the regulation of glutamine synthetase in *Escherichia coli*', *Molecular Microbiology,* 21 (1), pp. 133-146.

van Heeswijk, W.C., Westerhoff, H.V. and Boogerd, F.C. (2013) 'Nitrogen assimilation in *Escherichia coli*: putting molecular data into a systems perspective', *Microbiology and Molecular Biology Reviews,* 77 (4), pp. 628-695.

Verma, R., Holmans, P., Knowles, J. A., Grover, D., Evgrafov, O. V, Crowe, R. R., Scheftner, W. A., Weissman, M. M., DePaulo, J. R., Potash, J. B. and 213 Levinson, D. F. (2008) 'Linkage disequilibrium mapping of a chromosome 15q25-26 major depression linkage region and sequencing of *NTRK3*.', *Biological psychiatry*, 63(12), pp. 1185–9.

Wacker, T., Garcia-Celma, J. J., Lewe, P. and Andrade, S. L. (2014) 'Direct observation of electrogenic NH_4^+ transport in ammonium transport (Amt) proteins', *Proceedings of the National Academy of Sciences*, 111(27), pp. 9995–10000

Wall, S.M. and Koger, L.M. (1994) 'NH^+_4 transport mediated by $Na(^+)$-$K(^+)$-ATPase in rat inner medullary collecting duct', *American Journal of Physiology,* 267 (4 Pt 2), pp. F660-670.

Wang, J., Fulford, T., Shao, Q., Javelle, A., Yang, H., Zhu, W. and Merrick, M. (2013) 'Ammonium Transport Proteins with Changes in One of the Conserved Pore Histidines Have Different Performance in Ammonia and Methylamine Conduction', *PLoS ONE*, 8(5), p. e62745.

Wei, X., Sayavedra-Soto, L.A. and Arp, D.J. (2004) 'The transcription of the cbb operon in *Nitrosomonas europaea*', *Microbiology (Reading),* 150 (Pt 6), pp. 1869-1879.

Wei, X., Yan, T., Hommes, N.G., Liu, X., Wu, L., McAlvin, C., Klotz, M.G., Sayavedra-Soto, L.A., Zhou, J. and Arp, D.J. (2006) 'Transcript profiles of *Nitrosomonas europaea* during growth and upon deprivation of ammonia and carbonate'. *FEMS Microbiology Letters,* 257 (1), pp. 76-83.

Weidinger, K., Neuhäuser, B., Gilch, S., Ludewig, U., Meyer, O. and Schmidt, I. (2007) 'Functional and physiological evidence for a rhesus-type ammonia transporter in *Nitrosomonas europaea*', *FEMS Microbiology Letters,* 273 (2), pp. 260-267.

Westhoff, C.M., Ferreri-Jacobia, M., Mak, D.O. and Foskett, J.K. (2002) 'Identification of the erythrocyte Rh blood group glycoprotein as a mammalian ammonium transporter', *Journal of Biological Chemistry,* 277 (15), pp. 12499-12502.

Wilkins, M.R., Gasteiger, E., Bairoch, A., Sanchez, J.C., Williams, K.L., Appel, R.D. and Hochstrasser, D.F. (1999) 'Protein identification and analysis tools in the ExPASy server', *Methods in Molcular Biolology,* 112 531-552.

Williamson, G., Tamburrino, G., Bizior, A., Boeckstaens, M., Dias Mirandela, G., Bage, M., Pisliakov, A., Ives, C. M., Terras, E., Hoskisson, P. A., Marini, A.-M., Zachariae, U. and Javelle, A. (2020) 'A two-lane mechanism for selective biological ammonium transport', *eLife*, 9, pp. e57183

Williamson, G., Brito, A.S., Bizior, A., Tamburrino, G., Dias Mirandela, G., Harris, T., Hoskisson, P.A., Zachariae, U., Marini, A.M., Boeckstaens, M. and Javelle, A. (2022) 'Coexistence of Ammonium Transporter and Channel Mechanisms in Amt-Mep-Rh Twin-His Variants Impairs the Filamentation Signaling Capacity of Fungal Mep2 Transceptors', *mBio,* 13(2), pp. e0291321.

Winkler, F. K. (2006) 'Amt/MEP/Rh proteins conduct ammonia', European Journal of Physiology, 450, pp. 701–707

von Wirén, N. and Merrick, M. (2004) 'Regulation and function of ammonium carriers in bacteria, fungi, and plants', *in Molecular Mechanisms Controlling Transmembrane Transport. Berlin, Heidelberg: Springer Berlin Heidelberg*, pp. 95–120.

Wright, G., Noiret, L., Olde Damink, S.W. and Jalan, R. (2011) 'Interorgan ammonia metabolism in liver failure: the basis of current and future therapies', *Liver International,* 31 (2), pp. 163-175.

Yang, S., Hao, D., Cong, Y., Jin, M. and Su, Y. (2015) 'The rice *Os*AMT1;1 is a proton-independent feedback regulated ammonium transporter', *Plant Cell Reports,* 34 (2), pp. 321-330.

Zheng, L., Kostrewa, D., Bernèche, S., Winkler, F. K. and Li, X. D. (2004) 'The mechanism of ammonia transport based on the crystal structure of AmtB of *Escherichia coli*', *Proceedings of the National Academy of Sciences*, 101(49), pp. 17090–17095.

Zidi-Yahiaoui, N., Mouro-Chanteloup, I., D'Ambrosio, A.M., Lopez, C., Gane, P., Le van Kim, C., Cartron, J.P., Colin, Y. and Ripoche, P. (2005) 'Human Rhesus B and Rhesus C glycoproteins: properties of facilitated ammonium transport in recombinant kidney cells', *Biochemical Journal,* 391 (Pt 1), pp. 33-40.

Zidi-Yahiaoui, N., Ripoche, P., Le Van Kim, C., Gane, P., D'Ambrosio, A.M., Cartron, J.P., Colin, Y. and Mouro-Chanteloup, I. (2006) 'Ammonium transport properties of HEK293 cells expressing RhCG mutants: preliminary analysis of structure/function by site-directed mutagenesis', *Transfusion and Clinical Biology,* 13 (1-2), pp. 128-131.

Zidi-Yahiaoui, N., Callebaut, I., Genetet, S., Le Van Kim, C., Cartron, J.P., Colin, Y., Ripoche, P. and Mouro-Chanteloup, I. (2009) 'Functional analysis of human RhCG: comparison with *E. coli* ammonium transporter reveals similarities in the pore and differences in the vestibule', *American Journal of Physiology-Cell Physiology,* 297 (3), pp. C537-547.

Zuber, D., Krause, R., Venturi, M., Padan, E., Bamberg, E. andFendler, K. (2005) 'Kinetics of charge translocation in the passive downhill uptake mode of the Na^+/H^+ antiporter NhaA of *Escherichia coli*', *Biochimica et Biophysica Acta,* 1709 (3), pp. 240-250.

Appendices

Appendix: Publications

1. ‘A two-lane mechanism for selective biological ammonium transport’

2. ‘Coexistence of Ammonium Transporter and Channel Mechanisms in Amt/Mep/Rh Twin-His Variants Impairs the Filamentation Signaling Capacity of Fungal Mep2 Transceptors'

RESEARCH ARTICLE

A two-lane mechanism for selective biological ammonium transport

Gordon Williamson[1†], Giulia Tamburrino[2,3†], Adriana Bizior[1†], Mélanie Boeckstaens[4†], Gaëtan Dias Mirandela[1‡], Marcus G Bage[2,3], Andrei Pisliakov[2,3], Callum M Ives[2], Eilidh Terras[1], Paul A Hoskisson[1], Anna Maria Marini[4], Ulrich Zachariae[2,3]*, Arnaud Javelle[1]*

[1]Strathclyde Institute of Pharmacy and Biomedical Sciences, University of Strathclyde, Glasgow, United Kingdom; [2]Computational Biology, School of Life Sciences, University of Dundee, Dundee, United Kingdom; [3]Physics, School of Science and Engineering, University of Dundee, Dundee, United Kingdom; [4]Biology of Membrane Transport Laboratory, Department of Molecular Biology, Université Libre de Bruxelles, Gosselies, Belgium

Abstract The transport of charged molecules across biological membranes faces the dual problem of accommodating charges in a highly hydrophobic environment while maintaining selective substrate translocation. This has been the subject of a particular controversy for the exchange of ammonium across cellular membranes, an essential process in all domains of life. Ammonium transport is mediated by the ubiquitous Amt/Mep/Rh transporters that includes the human Rhesus factors. Here, using a combination of electrophysiology, yeast functional complementation and extended molecular dynamics simulations, we reveal a unique two-lane pathway for electrogenic NH_4^+ transport in two archetypal members of the family, the transporters AmtB from *Escherichia coli* and Rh50 from *Nitrosomonas europaea*. The pathway underpins a mechanism by which charged H^+ and neutral NH_3 are carried separately across the membrane after NH_4^+ deprotonation. This mechanism defines a new principle of achieving transport selectivity against competing ions in a biological transport process.

***For correspondence:**
u.zachariae@dundee.ac.uk (UZ);
arnaud.javelle@strath.ac.uk (AJ)

[†]These authors contributed equally to this work

Present address: [‡]Wellcome Trust Centre for Cell Biology, Michael Swann Building, The King's Buildings, University of Edinburgh, Edinburgh, United Kingdom

Competing interests: The authors declare that no competing interests exist.

Funding: See page 18

Received: 24 March 2020
Accepted: 13 July 2020
Published: 14 July 2020

Reviewing editor: Nir Ben-Tal, Tel Aviv University, Israel

Introduction

The transport of ammonium across cell membranes is a fundamental biological process in all domains of life. Ammonium exchange is mediated by the ubiquitous ammonium transporter/methyl-ammonium-ammonium permease/Rhesus (Amt/Mep/Rh) protein family. The major role of bacterial, fungal, and plant Amt/Mep proteins is to scavenge ammonium for biosynthetic assimilation, whereas mammals are thought to produce Rh proteins in erythrocytes, kidney, and liver cells for detoxification purposes and to maintain pH homeostasis (***Biver et al., 2008***; ***Huang and Ye, 2010***). In humans, Rh mutations are linked to pathologies that include inherited hemolytic anemia, stomatocytosis, and early-onset depressive disorder (***Huang and Ye, 2010***). Despite this key general and biomedical importance, so far, no consensus on the pathway and mechanism of biological ammonium transport has been reached.

High-resolution structures available for several Amt, Mep and Rh proteins show a strongly hydrophobic pore leading towards the cytoplasm (***Andrade et al., 2005***; ***Gruswitz et al., 2010***; ***Khademi et al., 2004***; ***Lupo et al., 2007***; ***van den Berg et al., 2016***). This observation led to the conclusion that the species translocated through Amt/Mep/Rh proteins is neutral NH_3. However, this view has been experimentally challenged, first for some plant Amt proteins (***Ludewig et al., 2002***; ***Mayer et al., 2006***; ***McDonald and Ward, 2016***; ***Neuhäuser et al., 2014***), followed by further *in-vitro* studies revealing that the activity of bacterial Amt proteins is electrogenic (***Mirandela et al.,***

2019; Wacker et al., 2014). Taken together, these findings renewed a long-standing debate on the mechanism by which a charged molecule is translocated through a hydrophobic pore and how selectivity for NH_4^+ over competing ions is achieved.

Here, we reveal the pathways, mechanism, and key determinants of selectivity of electrogenic ammonium transport in Amt and Rh proteins, unifying the diverse observations that led to these seemingly incompatible suggestions. The transport mechanism is underpinned by the separate transfer of H^+ and NH_3 on a unique two-lane pathway following NH_4^+ sequestration and deprotonation. This mechanism ensures that ammonium – which occurs mainly in protonated form in the aqueous phase – is efficiently translocated across the membrane, while maintaining strict selectivity against K^+, a monovalent cation of similar size. This previously unobserved principle is likely to form a new paradigm for the electrogenic members of the Amt/Mep/Rh family. Similar mechanisms may be utilized by other membrane transporters to facilitate the selective translocation of pH-sensitive molecules.

Results and discussion

AmtB and NeRh50 activity is electrogenic

Motivated by our finding that the activity of *Escherichia coli* AmtB is electrogenic (Mirandela et al., 2019), we first investigated the transport mechanism of the Rh50 protein from *Nitrosomonas europaea* (NeRh50). Rh and Amt proteins are distant homologs, and thus a functional distinction between both subfamilies has been proposed (Huang and Ye, 2010). The architecture of NeRh50 is highly representative of Rh proteins (Gruswitz et al., 2010; Lupo et al., 2007) which have been repeatedly reported to serve as electroneutral NH_3 or CO_2 gas channels (Cherif-Zahar et al., 2007; Hub et al., 2010a; Li et al., 2007; Lupo et al., 2007; Weidinger et al., 2007). The activity of purified NeRh50 reconstituted into liposomes was quantified using Solid-Supported Membrane Electrophysiology (SSME) (Bazzone et al., 2017) experiments, where we recorded a NH_4^+-selective current (Figure 1) with a decay rate that is strongly dependent on the lipid-to-protein ratio (LPR; Table 1, Figure 1—figure supplement 1). Expressed in a *Saccharomyces cerevisiae* triple-mepΔ strain, deprived of its three endogenous Mep ammonium transporters, NeRh50 complemented the growth defect on minimal medium containing ammonium as sole nitrogen source (Figure 1). The electrogenic transport activity observed for NeRh50 and AmtB may suggest a common transport mechanism amongst the distant Amt and Rh proteins, but more experiments are needed to conclusively confirm this. Also, the NH_4^+ selectivity of both transporters further highlighted the question of how these proteins achieve selective charge translocation through their hydrophobic pore.

Two interconnected water wires form an H^+ translocation pathway in AmtB

We next made use of the most substantive body of structural information available for the archetypal ammonium transporter AmtB from *E. coli* and its variants to decipher the molecular mechanism of electrogenic NH_4^+ transport (Dias Mirandela et al., 2018). Computational (Wang et al., 2012) and experimental studies (Ariz et al., 2018) have suggested that deprotonation of NH_4^+ is likely to be a major step in ammonium transport. We therefore aimed to identify dynamic polar networks across AmtB that could form a transfer pathway through the protein for the translocation of H^+, coming from NH_4^+ deprotonation. AmtB forms homotrimers in the cytoplasmic membrane, in which each monomer exhibits a potential periplasmic NH_4^+ binding region (S1) near residue D160, followed by a strongly hydrophobic pore leading towards the cytoplasm (Figure 2A; Khademi et al., 2004). Two highly conserved histidine residues, H168 and H318, protrude into the lumen, forming the family's characteristic 'twin-His' motif (Javelle et al., 2006). The only variation in the twin-His motif in members of the Amt/Mep/Rh family is in numerous fungal Mep transporters where the first His, corresponding to H168, is replaced by a Glu (Javelle et al., 2006). The general conservation pattern in the AmtB pore, as analysed with ConSurf (Ashkenazy et al., 2016), is shown in Figure 2—figure supplement 1.

To locate potential polar transfer routes, we performed atomistic molecular dynamics (MD) simulations of AmtB in mixed lipid bilayers. The simulations initially showed hydration of part of the putative hydrophobic NH_3 pathway from the twin-His motif to the cytoplasm (cytoplasmic water wire –

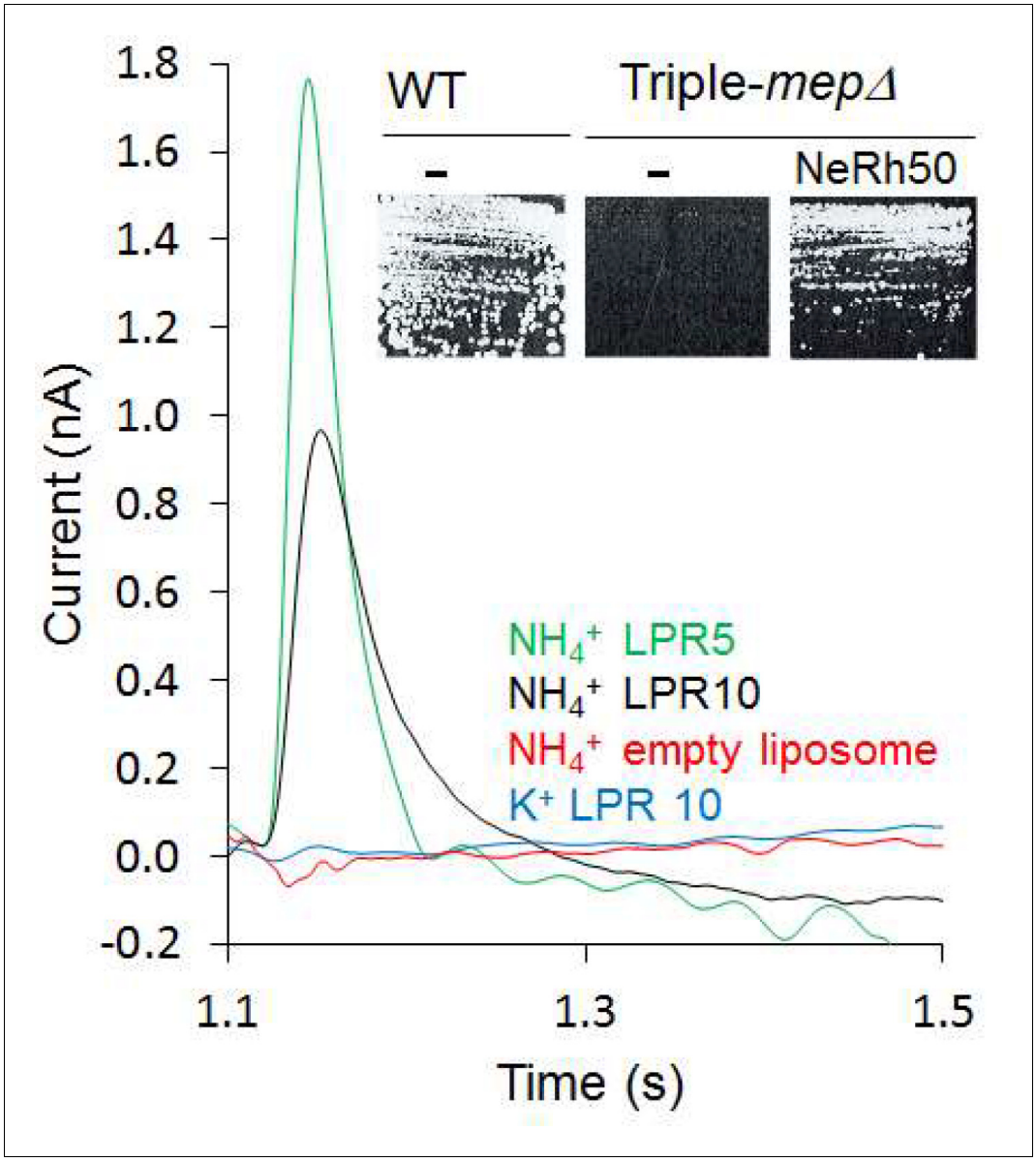

Figure 1. Characterization of the activity of NeRh50. Transient current measured using SSME after a 200 mM pulse (ammonium or potassium). *Insert:* Yeast complementation by NeRh50 (strain 31019b, *mep1Δ mep2Δ mep3Δ ura3*) on minimal medium supplemented with 3 mM ammonium as sole nitrogen source.
The online version of this article includes the following source data and figure supplement(s) for figure 1:

Source data 1. Characterization of the activity of NeRh50.
Figure supplement 1. Characterization of the activity of NeRh50.

CWW; ***Figure 2A***), confirming previous observations (***Lamoureux et al., 2007***). Notably, a new observation we made over longer simulation timescales is the presence of a previously unidentified second water-filled channel (periplasmic water wire - PWW). The PWW spans from residue D160 near the S1 region to the central twin-His motif (***Figure 2A***) and is formed both in simulations without and with applied membrane voltage V_m (***Figure 2A*** - ***Figure 2—figure supplement 2***; V_m in *E. coli* ~ −140 mV [***Felle et al., 1980***]).

As the protonation pattern of the twin-His motif has been found to play a role in the hydration of the protein (***Ishikita and Knapp, 2007***), two different tautomeric states of the twin-His motif were systematically probed in the simulations. The tautomeric state in which H168 is protonated on its N_δ and H318 is protonated on its N_ε atom is referred to as 'DE', while 'ED' terms the twin-His

Table 1. Decay time constants (s^{-1}) of transient currents triggered after an ammonium or potassium pulse of 200 mM in proteoliposomes containing AmtB at various LPR*.

	NH_4^+		K^+	
Variant	**LPR 10**	**LPR 5**	**LPR 10**	**LPR 5**
AmtB-WT	13.4 ± 1.5	18.7 ± 1.0	NC	NC
D160A	21.6 ± 1.2	24.3 ± 1.5	NC	NC
D160E	17.03 ± 2.84	19.53 ± 1.8	NC	NC
H168A H318A	29.5 ± 2.1	29.8 ± 2.6	NC	NC
S219A H168A H318A	NC	NC	NC	NC
H168A	28.3 ± 1.5	38.0 ± 1.0	2.7 ± 0.5	5.2 ± 1.0
H318A	22.56 ± 2.63	28.25 ± 3.1	10.07 ± 1.7	15.64 ± 2.1
NeRh50	24.0 ± 1.7	39.0 ± 3.6	NC	NC

*NC: No transient current recorded.

The online version of this article includes the following source data for Table 1:

Source data 1. Decay time constants (s^{-1}) of transient currents triggered after an ammonium or potassium pulse of 200 mM measured by SSME.

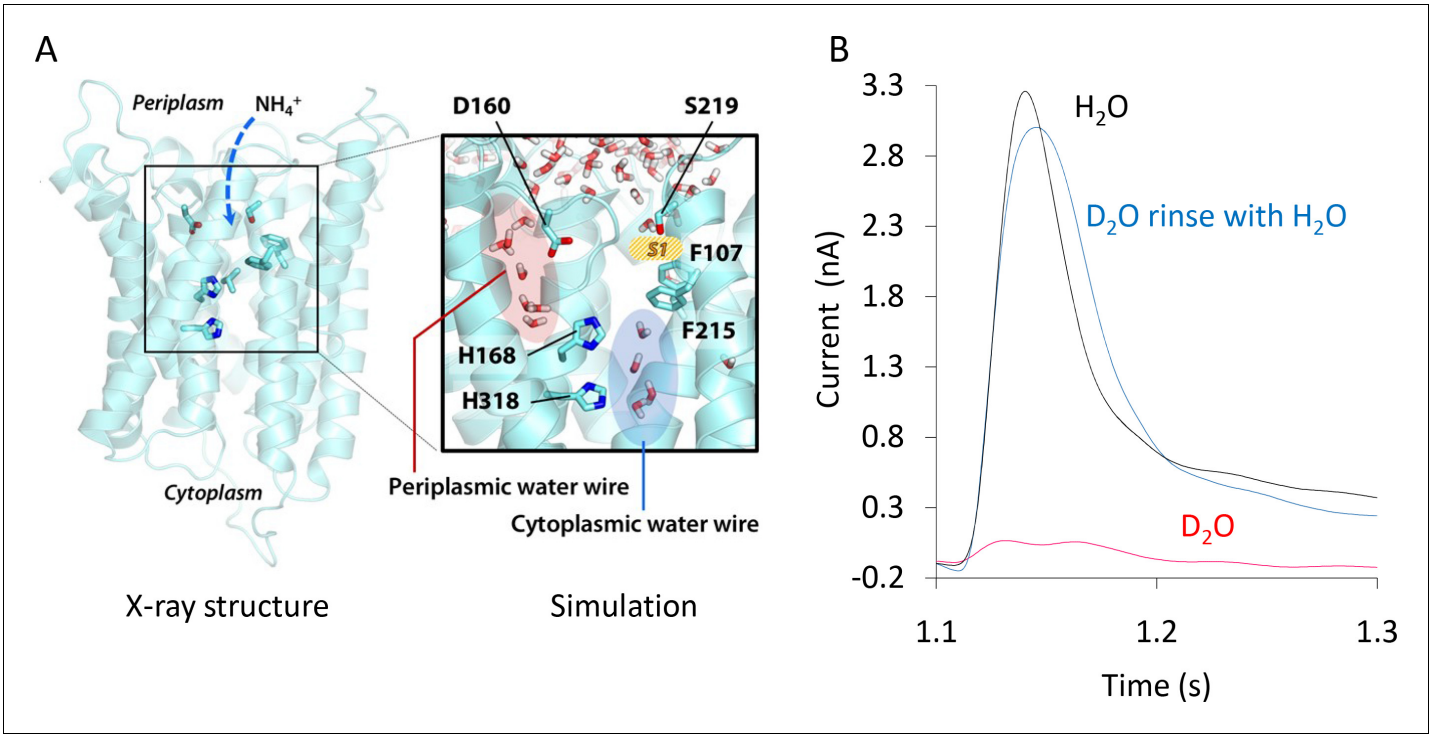

Figure 2. Formation and functionality of the periplasmic (PWW) and cytoplasmic (CWW) water wires in AmtB. (**A**) Extended atomistic simulations show a hydration pattern across the protein, in which cytoplasmic and periplasmic water wires, connected via H168, form a continuous pathway for proton transfer from the S1 NH_4^+ sequestration region to the cytoplasm. (**B**) Transient currents measured following a 200 mM ammonium pulse on sensors prepared with solutions containing either H_2O (black) or D_2O (red). D_2O sensors were rinsed with H_2O solutions and subsequently exposed to another 200 mM ammonium pulse (blue).

The online version of this article includes the following source data and figure supplement(s) for figure 2:

Source data 1. Functionality of the periplasmic (PWW) and cytoplasmic (CWW) water wires in AmtB.
Figure supplement 1. Evolutionary conservation of the proton and hydrophobic pathways for H^+ and NH_3 translocation in AmtB.
Figure supplement 2. Evolution and occupancy of the Periplasmic Water Wire (PWW).
Figure supplement 3. Evolution and occupancy of the Cytoplasmic Water Wire (CWW).
Figure supplement 4. The DE and ED twin-His motif configurations.

configuration where H168 is protonated on N_ε and H318 is protonated on N_δ (***Figure 2A***- ***Figure 2—figure supplement 2***, ***3***, ***4***). Formation of the CWW is observed to occur within a few nanoseconds at the beginning of each simulation. In the DE tautomeric state, the cytoplasmic pocket of each subunit almost continuously remains occupied by 3–4 water molecules for the rest of the simulation (***Figure 2A*** - ***Figure 2—figure supplement 2***, ***3***, ***4***; data for 0 mV membrane voltage). In the ED state, greater fluctuations in the number of water molecules in the chain are seen, and the average occupancy is decreased. Using a cut-off value of three water molecules per subunit, a complete water chain is present during 79% of the simulations in the DE state, and only during 12% of the simulated time in the ED state. The PWW is generally more transiently occupied than the cytoplasmic channel; however, we record up to 23% occupancy with at least three water molecules when the histidine sidechains are in the ED tautomeric state (***Figure 2A*** - ***Figure 2—figure supplement 2***, ***3***, ***4***).

Both water wires are connected via the twin-His motif, which bridges the aqueous chains, while preventing the formation of a continuous water channel in the simulations. Although neither the CWW nor the PWW are sufficiently wide to allow the transfer of solvated NH_4^+, water molecules and histidine side chains could serve as efficient pathways to facilitate proton transfer in proteins (***Acharya et al., 2010***). As shown in ***Figure 2—figure supplement 1***, the key residues that line both water wires in AmtB are highly conserved in the family.

The interconnected water wires are functionally essential to AmtB activity

To experimentally test if the water wires are essential for proton conduction during the AmtB transport cycle, we made use of the reduced deuteron mobility of heavy water D_2O. Because deuterons have twice the mass of a proton and the bond strength is increased, the deuteron mobility is reduced by 30% for each D_2O molecule compared to normal water (***Wiechert and Beitz, 2017***). Since the polar network of water we identified involves more than three water molecules (***Figure 2A***), AmtB should be nearly inactive if tested in the presence of D_2O. Indeed, we found that in an SSME-based assay where all buffers used to prepare the proteoliposomes and SSM sensors were made using D_2O, AmtB activity was completely abolished compared to buffer containing water (***Figure 2B***). After rinsing the sensor prepared in D_2O with water, AmtB re-gained 100% of its activity measured by SSME, showing that the presence of D_2O did not affect the protein itself or the integrity of the proteoliposomes (***Figure 2B***). Further calculations suggested that H^+ transfer between the water molecules is possible both within the PWW and CWW and could occur with high rates (the highest energy barrier is ~18 kJ/mol in the cytoplasmic wire near the twin-His motif; ***Table 2***). Taken together, the experimental and computational data suggest that proton transfer between water molecules, most likely the PWW and CWW detected in the simulations, may underpin the electrogenic activity of AmtB.

AmtB activity is not driven by the proton motive force

In the absence of ammonium, a proton pulse did not trigger a discernible current and additionally, in the presence of ammonium, an inward-orientated pH gradient did not increase AmtB activity (***Figure 3***). These findings suggest that there is no H^+-dependent symport activity of AmtB, showing instead that AmtB is not able to translocate a proton in the absence of NH_4^+, and indicating that the current induced by AmtB activity is generated by specific deprotonation of the substrate and subsequent H^+ translocation. Furthermore, they show that AmtB cannot act as an uncoupler, which raises the question of proton selectivity and the coupling between NH_3 and H^+ transfer (***Boogerd et al., 2011***; ***Maeda et al., 2019***). Our current data suggest that the PWW is transiently occupied and that its occupancy is strongly dependent on the particular state and conformation of D160, since even a D to E conservative change abolished presence of the PWW (***Figure 4A***). Any disruption of the PWW will, in turn, impede the capability of AmtB to transfer H^+. The functionally relevant conformation and protonation state of D160 that stabilize the PWW is likely to be coupled to the presence of a charged substrate binding near S1, thereby linking substrate binding and deprotonation to H^+ transfer.

Table 2. Free energies for proton translocation through the cytoplasmic and periplasmic water wires and neighboring water molecules (bulk)*.

			Z (Å)	Free energy (kJ/mol)
(bulk)	Peripl. water wire	wat1	14.7	0.0
		wat2	12.7	8.7
		wat3	10.7	15.0
		wat4	8.3	14.4
		wat5	6.1	7.5
D160		wat6	5.4	11.0
		wat7	3.2	14.4
		wat8	0.6	18.5
H168				
	cytopl. water wire	wat9	−0.4	17.3
		wat10	−0.8	14.4
		wat11	−3.2	12.1
H318		wat12	−5.1	13.8

*The vertical coordinate z was calculated relative to the position of the sidechain of H168. Positions of the sidechains of D160, H168 and H318 with respect to the periplasmic and cytoplasmic water wires are indicated in the left column.

The residue D160 is essential to stabilize the PWW

As the PWW is formed near the sidechain of D160, an invariant residue in the Amt/Mep/Rh superfamily (***Marini et al., 2006***; ***Thomas et al., 2000***), we further investigated the role of this residue in ensuring PWW and CWW stability by simulating the AmtB D160A and D160E mutants. Both mutants were stable on the time scale of our simulations and we did not detect major rearrangements in the protein. Moreover, all the elution profiles of the purified WT and variants proteins obtained by analytical size exclusion chromatography, before and after solubilization of the proteoliposomes in 2% DDM, were identical, showing a single monodisperse peak eluting between 10.4–10.6 ml (***Figure 4—figure supplement 1***). Taken together, these results suggest that major structural re-arrangements in the mutants are unlikely to occur. The simulations revealed no difference in the formation of the CWW in the D160A and D160E variants compared to the WT, however the formation of the PWW is almost completely abolished in the presence of these mutations (***Figure 4A***).

We then expressed wild-type AmtB as well as the D160A and D160E mutants in *S. cerevisiae* triple-*mep*Δ. Using ammonium as the sole nitrogen source, we found that cells expressing the mutants failed to grow, showing that $AmtB^{D160A}$ or $AmtB^{D160E}$ are unable to replace the function of the endogenous Mep transporters (***Figure 4B***).

The activity of the purified variants reconstituted into liposomes was next quantified using SSME. Electrogenic transport activity, triggered by a 200 mM ammonium pulse, led to a transient current with a maximum amplitude of 3.38 nA in AmtB, while $AmtB^{D160A}$ and $AmtB^{D160E}$ displayed reduced maximum currents of 0.63 nA and 1.42 nA respectively (***Figure 4B***, ***Figure 4—figure supplement 2***). Importantly, the lifetime of currents in both variants was unaffected by changes in liposomal LPR, and therefore the small transient current accounts for the binding of a NH_4^+ to the proteins and not a full translocation cycle (***Table 1***, ***Figure 4—figure supplement 2***; ***Bazzone et al., 2017***). Additionally, it was impossible to determine with confidence a catalytic constant (K_m) for both variants since no clear saturation was reached, even after an ammonium pulse of 200 mM (***Figure 4C***). These results thus demonstrate that $AmtB^{D160A}$ and $AmtB^{D160E}$ are transport-deficient. Our data show that residue D160 plays a central role in the transport mechanism as opposed to having a strictly structural role as previously suggested (***Khademi et al., 2004***). Moreover, the fact that the conservative D to E variation at position 160 impairs ammonium transport via AmtB indicates that D160 does not only show electrostatic interaction with NH_4^+ at the S1 site but is also involved in the translocation mechanism by stabilizing the PWW.

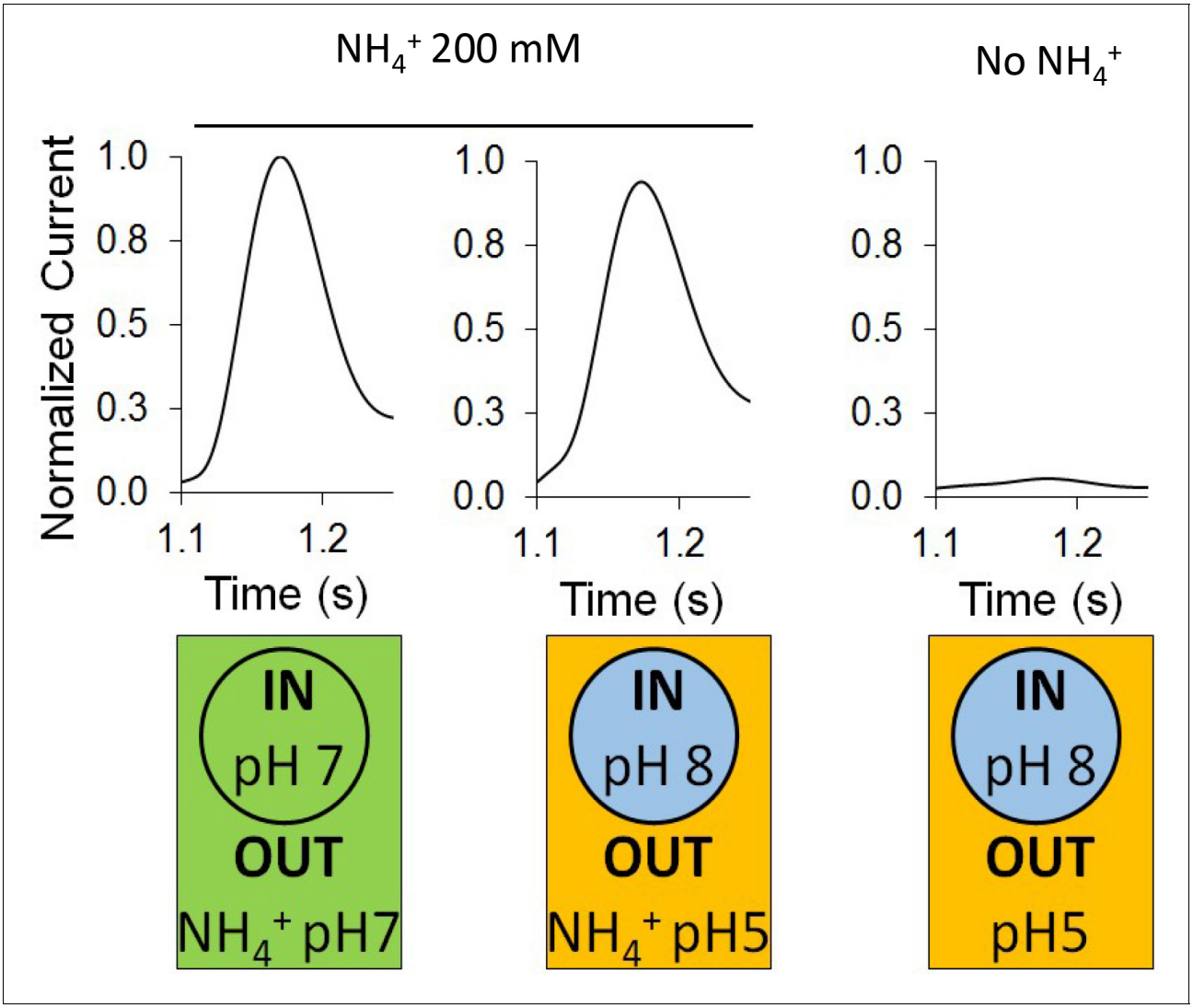

Figure 3. Effect of a proton gradient on AmtB activity. The transient currents were measured using SSME following an ammonium pulse of 200 mM at pH 7 (left) or under an inwardly directed pH gradient in the presence (center) or absence (right) of ammonium. eight sensors from two independent protein purification batches were measured, with three measurements recorded for each sensor. Single representative traces were chosen to visualize the results. Each sensor was measured in the order pH (in/out) 7/7, 8/5, 8/5 (this time without NH_4^+), and finally 7/7 again to be sure that the signals do not significantly decrease with time. The data are normalized against the measurements done at pH7 in/out for each sensor.
The online version of this article includes the following source data for figure 3:

Source data 1. Effect of a proton gradient on AmtB activity.

AmtB switches from transporter to channel-like activity in the absence of the 'twin-His' motif

The CWW and PWW are connected via the twin-His motif, which bridges the aqueous chains, while preventing the formation of a continuous water channel in the simulations (***Figure 2A***). We therefore next probed if the twin-His motif enables proton transfer between the two water wires by recording the activities of twin-His variants. Expressed in *S. cerevisiae* triple-*mep*Δ, $AmtB^{H168A/H318A}$ did not support cell growth on low ammonium (***Figure 5A***). *In-vitro* SSME measurements with this variant displayed LPR-independent current decay rates (***Figure 5A***, ***Figure 5—figure supplement 1***, ***Table 1***), showing that the residual current is caused by the association of NH_4^+ to AmtB without further transport. No current was recorded for the triple mutant $AmtB^{S219A/H168A/H318A}$, in which binding at the periplasmic face was further altered, confirming that the residual current reflects NH_4^+ interaction near S1 (***Figure 5—figure supplement 1***). The double-His mutant $AmtB^{H168A/H318A}$ is

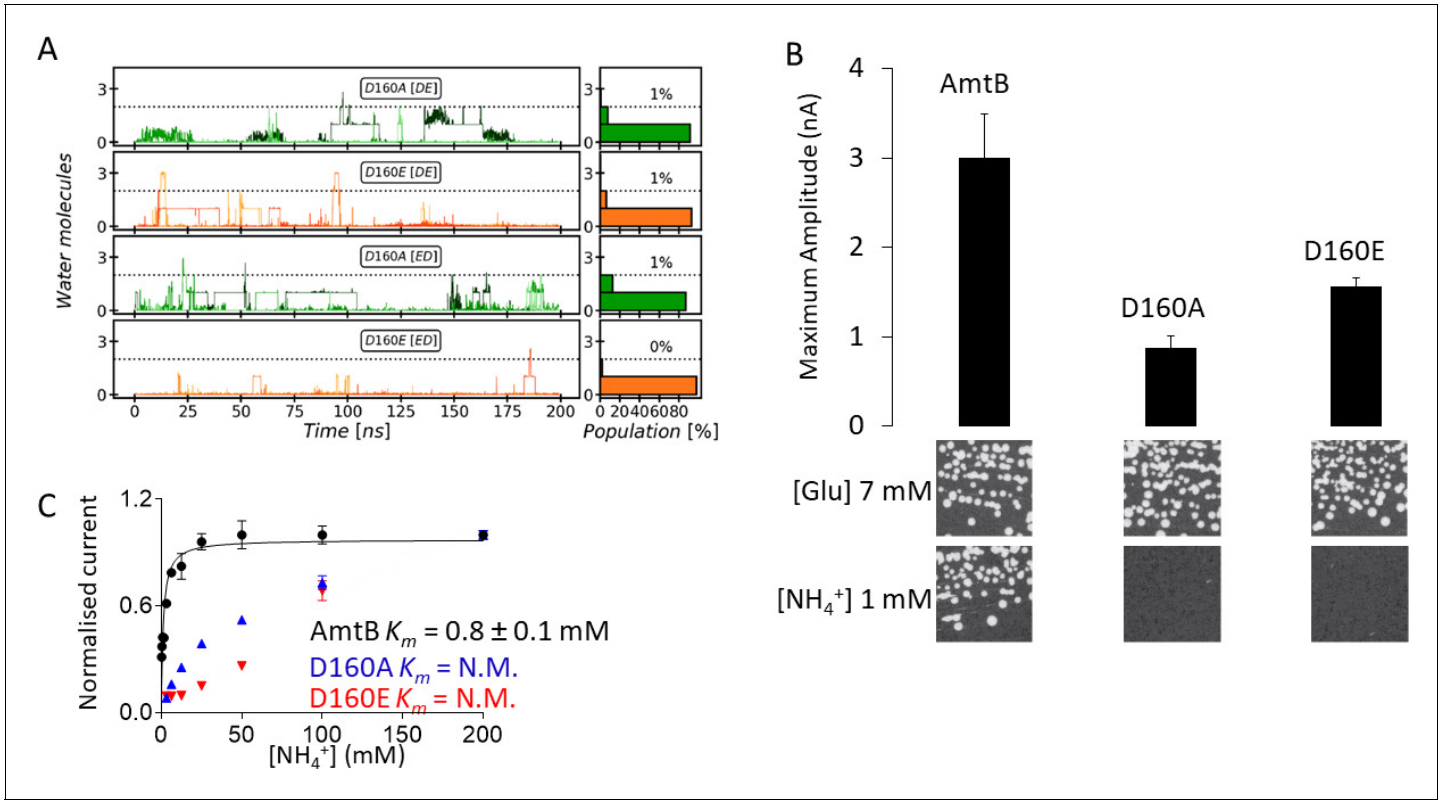

Figure 4. Effect of D160 substitutions. (**A**) The Periplasmic Water Wire (PWW) in the D160A and D160E variants. We observe no significant occupancy of the PWW above the threshold of at least three water molecules in the D160A and D160E AmtB variants, irrespective of the tautomeric protonation states of H168 and H318 (DE or ED, see Materials and method section). (**B**) *Upper panel:* maximum amplitude of the transient current measured using SSME following a 200 mM ammonium pulse. Eight sensors from two independent protein purification batches were measured, with three measurements recorded for each sensor (means ± SD). *Lower panel*: yeast complementation test (strain 31019b, *mep1Δ mep2Δ mep3Δ ura3*) using 7 mM Glutamate (Glu) or 1 mM ammonium as a sole nitrogen source. The growth tests have been repeated twice. (**C**) Kinetics analysis of the transport of ammonium. The maximum amplitudes recorded after a 200 mM ammonium pulse have been normalized to 1.0 for comparison. N.M.: Non Measurable. eight sensors from two independent protein purification batches were measured, with three measurements recorded for each sensor (means ± SD).
The online version of this article includes the following source data and figure supplement(s) for figure 4:

Source data 1. Effect of D160 substitutions on AmtB activity measured by SSME.
Figure supplement 1. Size Exclusion Chromatography analysis of AmtB.
Figure supplement 2. Characterization of the activity and specificity of AmtB variants.

thus able to interact with NH_4^+ but cannot transport the substrate across the membrane. This supports our previous structural analysis showing that the CWW in the pore of the double-His mutant $AmtB^{H168A/H318A}$ is absent (***Javelle et al., 2006***).

By contrast, the two single histidine-to-alanine substitutions in the twin-His motif unexpectedly produced an LPR-dependent current in our SSME recordings (***Figure 5A***, ***Figure 5—figure supplement 1***, ***Table 1***). Furthermore, triple-*mep*Δ yeast cells expressing these variants were able to grow in the presence of low ammonium concentrations (***Figure 5A***). Our previous crystal structure (***Javelle et al., 2006***) and our MD simulations (***Figure 5—figure supplement 2***) show increased hydration in the area around A168, which could potentially form a pathway for direct translocation of NH_4^+ without a deprotonation step. To test this hypothesis, we measured the activity of $AmtB^{H168A}$ and $AmtB^{H318A}$ in D_2O conditions, as described above. Crucially, the activity of both variants measured in the presence or absence of D_2O was similar (***Figure 5B***), in contrast to native AmtB where no activity was recorded in D_2O (***Figure 2B***), showing that proton transfer between water molecules is not a key mechanistic feature in the activity of the mutants. Additionally, the translocation of NH_4^+ is not saturable in the tested concentration range [12.5–200 mM] for $AmtB^{H168A}$ and $AmtB^{H318A}$ (***Figure 5C***). Summarizing, these results suggest that AmtB switches from

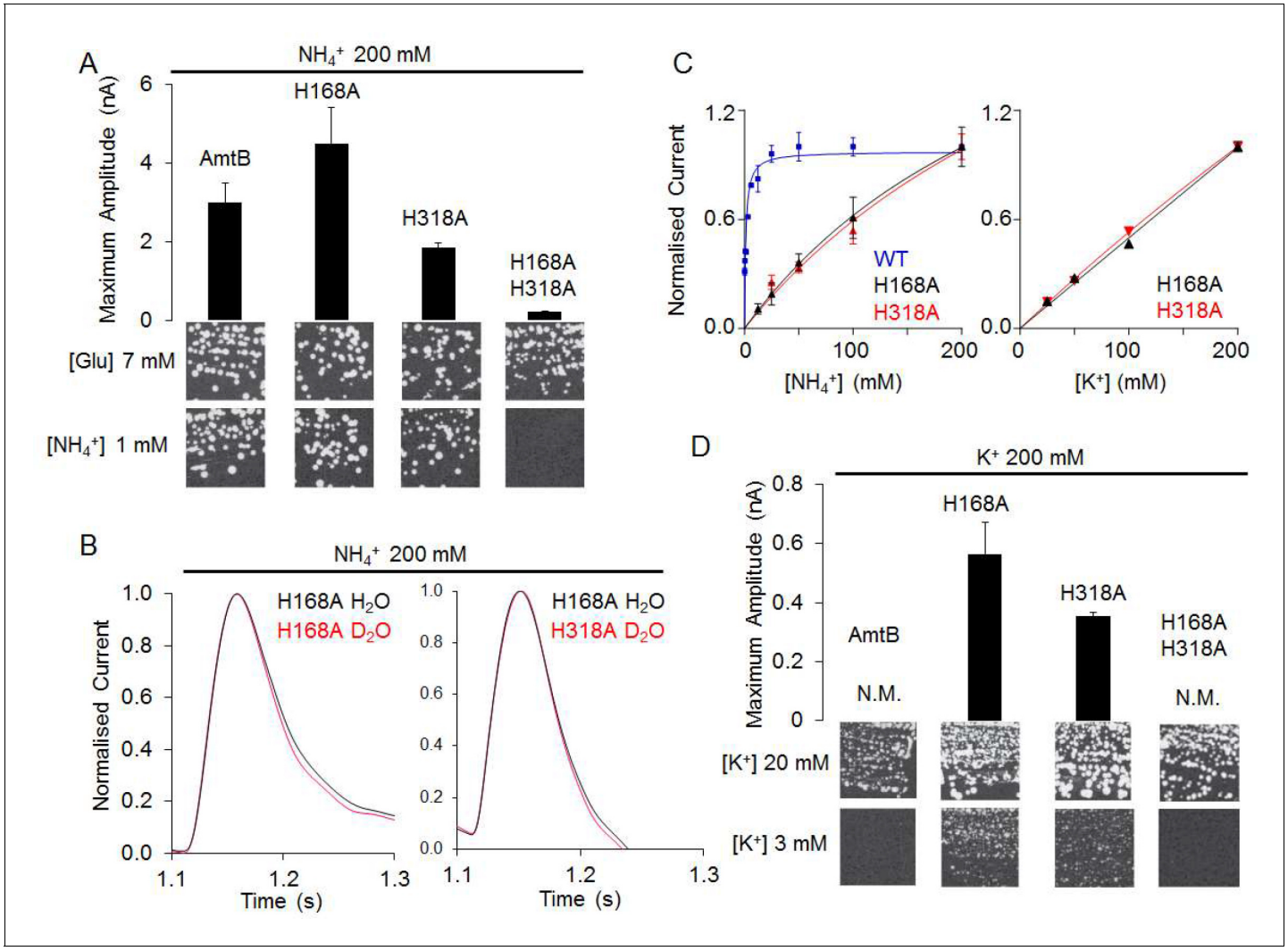

Figure 5. The AmtB^{H168A} and AmtB^{H318A} lose their specificity toward ammonium. (**A**) *Upper panels:* maximum amplitude of the transient current measure using SSME after a 200 mM ammonium pulse. Eight sensors from two independent protein purification batches were measured, with three measurements recorded for each sensor (means ± SD). *Lower panels*: yeast complementation test (strain 31019b, *mep1Δ mep2Δ mep3Δ ura3*) using 7 mM Glutamate (Glu) or 1 mM ammonium as a sole nitrogen source. The growth tests have been repeated twice. (**B**) Transient currents measured using SSME following a 200 mM ammonium pulse on sensors prepared with solutions containing either H_2O (black) or D_2O (red). The maximum amplitudes recorded after a 200 mM ammonium pulse on sensor prepared in H_2O have been normalized to 1.0 for comparison. eight sensors from two independent protein purification batches were measured, with three measurements recorded for each sensor (means ± SD). (**C**) Kinetics analysis of the transport of NH_4^+ (or K^+ in AmtB^{H168A} (black), AmtB^{H318A} (red) and WT-AmtB (bleu, only for NH_4^+, as no signal was measurable with K^+). The maximum amplitudes recorded after a 200 mM NH_4^+ or K^+ pulse have been normalized to 1.0 for comparison. Eight sensors from two independent protein purification batches were measured, with three measurements recorded for each sensor (means ± SD). (**D**) *Upper panels:* maximum amplitude of the transient current measured using SSME after a 200 mM potassium pulse. N.M. Non Measurable. Eight sensors from two independent protein purification batches were measured, with three measurements recorded for each sensor (means ± SD). *Lower panels*: yeast complementation test (strain #228, *mep1Δ mep2Δ mep3Δ trk1Δ trk2Δ leu2 ura3)* using media supplemented with 20 mM or 3 mM KCl. The growth test has been repeated twice.
The online version of this article includes the following source data and figure supplement(s) for figure 5:

Source data 1. Effect of H168 and/or H318 substitution on AmtB activity and selectivity measured by SSME.
Figure supplement 1. Characterization of the activity and specificity of AmtB variants.
Figure supplement 2. MD simulation of AmtB^{H168A} showing formation of a continuous water wire traversing the central pore region.

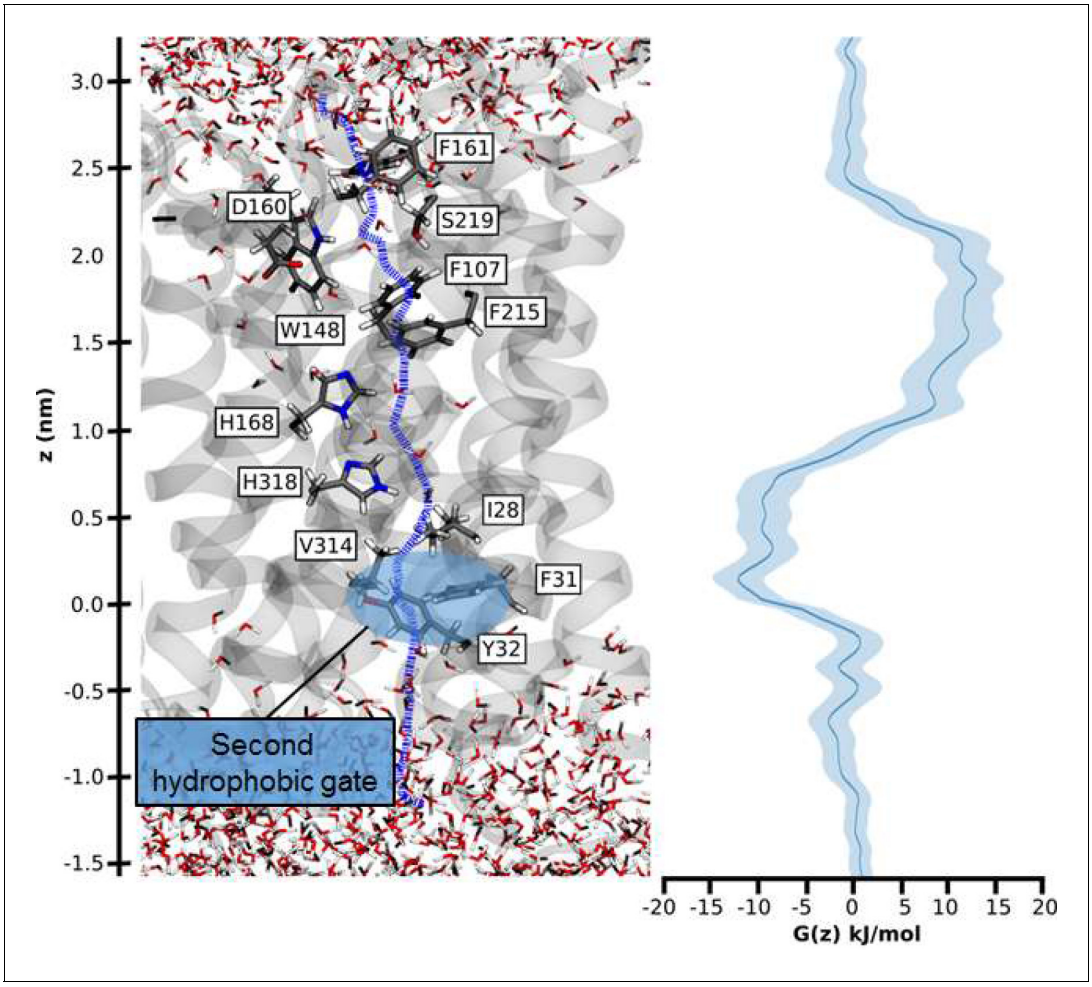

Figure 6. Hydrophobic pathway and energetics for NH_3 translocation in AmtB. We probed an optimal pathway for NH_3 transfer during our PMF calculations (left, purple dash trajectory) in the presence of both the PWW and CWW. The software HOLE (*49*) was used to determine the most likely transfer route. The pathway from the periplasm to the cytoplasm traverses the hydrophobic gate region (F107 and F215), crosses the cavity next to the twin-His motif (H168 and H318) occupied by the CWW, and continues across a second hydrophobic region (I28, V314, F31, Y32) before entering the cytoplasm.

transporter- to channel-like activity in the absence of the twin-His motif, directly translocating hydrated NH_4^+ through the pore. In the wild-types of Amt/Mep/Rh protein family members, the twin-His motif is highly conserved, which shows that transporter, as opposed to channel activity, is mechanistically crucial for the function of these proteins. The only variation seen in naturally occurring sequences is a replacement of the first His by Glu in some fungal Mep proteins (***Javelle et al., 2006***; ***Thomas et al., 2000***). Channel activity is so far only observed for the alanine mutants, not the wild-type. We hypothesized that transport activity might thus be key to ensure ion selectivity of AmtB, since NH_4^+ and K^+ are cations of similar size and hydration energy (***Aydin et al., 2020***).

The twin-His motif interconnects the two water wires to ensure the selectivity of AmtB

Since NH_4^+ was directly translocated in the absence of the twin-his motif and earlier studies implicated a role of the motif in AmtB selectivity (***Ganz et al., 2020***; ***Hall and Yan, 2013***), we repeated our SSME experiments on the $AmtB^{H168A}$ and $AmtB^{H318A}$ variants using the competing K^+ ion as substrate. A 200 mM K^+ pulse triggered currents in both variants, whose decay rates strongly depended on the LPR (***Figure 5D***, ***Table 1***, ***Figure 5—figure supplement 1***). Furthermore, the single His variants, but not native AmtB, complemented the growth defect of a yeast strain lacking its three endogenous ammonium (Mep) and potassium (Trk) transporters when a limited concentration

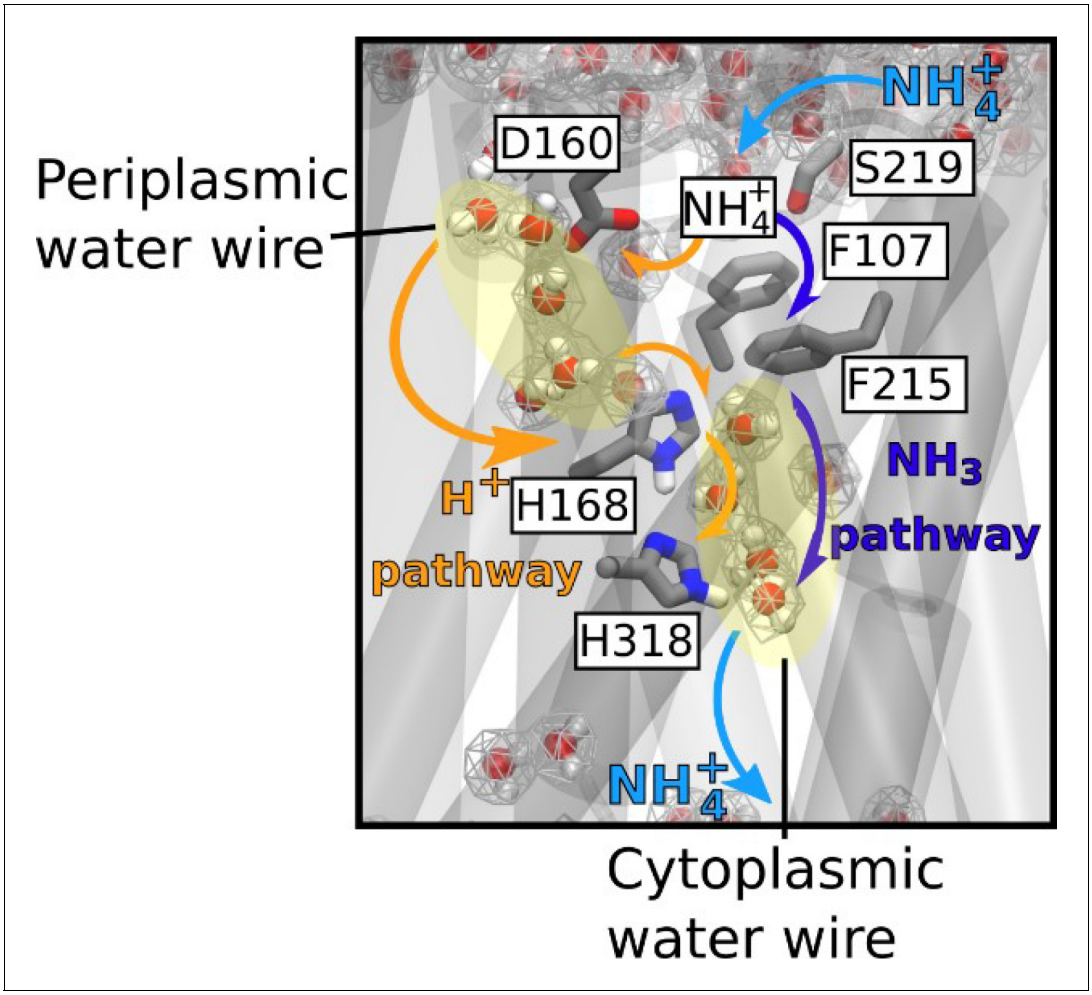

Figure 7. Mechanism of electrogenic NH_4^+ translocation in AmtB. Following sequestration of NH_4^+ at the periplasmic face, NH_4^+ is deprotonated and H^+ and NH_3 follow two separated pathways to the cytoplasm (orange arrows depict the pathway for H^+ transfer, dark blue arrows for NH_3), facilitated by the presence of two internal water wires. NH_3 reprotonation likely occurs near the cytoplasmic exit (***Figure 6***). The hydrated regions within the protein as observed in simulations are highlighted by wireframe representation, crucial residues involved in the transport mechanism are shown as sticks.

of $K^+$was present (***Figure 5D***). The K^+ translocation activity is not saturable in the substrate range [12.5–200 mM] (***Figure 5C***). These results demonstrate that both variants, $AmtB^{H168A}$ and $AmtB^{H318A}$, translocate K^+ ions across the membrane. The substitutions within the twin-His motif thus abolished selectivity for NH_4^+.

The presence of both histidine residues is therefore critical in ammonium transport, since permeability of ammonium transporters for K^+ would compromise ionic homeostasis and disrupt the membrane potential of *E. coli* cells, which crucially depends on maintaining K^+ concentration gradients across the membrane. Moreover, since AmtB is expressed in *E. coli* under nitrogen starvation conditions (low NH_4^+/K^+ ratio), loss of selectivity for NH_4^+ would impede ammonium uptake. Our results thus demonstrate that the twin-His motif, which is highly conserved amongst members of the family, is an essential functional element in the transport mechanism, preventing the transport of competing cations, whilst providing a pathway for proton transfer by bridging the periplasmic and the cytoplasmic water wires.

NH_3 permeation through the hydrophobic pore

Umbrella sampling free-energy calculations were performed to establish the rate limiting step of NH_4^+ transport. Our calculations show that NH_3 translocation experiences only a moderate energy barrier (~10 kJ/mol) at the periplasmic hydrophobic constriction region (F107 and F215) (***Figure 6***).

The starting points of the sampling windows were determined from the centers of HOLE calculations (**Smart et al., 1996**), optimizing the pathway of NH_3 translocation across the pore. A possible influence from this selection regarding the pathway was further reduced by allowing the molecule to move freely perpendicular to the pore axis within a radius of 5 Å in addition to extensive sampling; however, residual bias from window selection cannot be completely excluded. From the free energy profile of NH_3 translocation, we identified a shallow binding site below the twin-His motif (~5 kJ/mol). This is followed by a second hydrophobic region (I28, V314, F31 and Y32) that forms a small energy barrier between this binding site and the cytoplasmic exit. The increased residence time of NH_3 within this energy minimum suggests that reprotonation to NH_4^+, caused by the cytoplasmic pH, occurs in this region (**Figure 6**). Since both energy barriers for H^+ transfer along the water chains and NH_3 permeation are relatively small, we concluded that either initial deprotonation or proton transfer across the twin-His motif could be rate-limiting for overall NH_4^+ transport.

Conclusion

A new model for the mechanism of electrogenic ammonium transport therefore emerges from our findings (**Figure 7**). After deprotonation of NH_4^+ at the periplasmic side, a previously undiscovered polar conduction route enables H^+ transfer into the cytoplasm. A parallel pathway, lined by hydrophobic groups within the protein core, facilitates the simultaneous transfer of uncharged NH_3, driven by concentration differences. On the cytoplasmic face, the pH of the cell interior leads to recombination to NH_4^+, most likely near a second hydrophobic gate (**Figure 6**). The twin-His motif, which bridges the water chains constitutes the major selectivity gate for NH_4^+ transport preventing K^+ flow. We propose that this mechanism is conserved amongst the electrogenic members of the Amt/Mep/Rh family. Importantly, two RhAG polymorphisms associated to the overhydrated stomatocytosis human syndrome have also acquired the ability to transport K^+. Thus, deciphering the transport mechanism of two archetypal members of the family such as AmtB and NeRh50 could bring new insights to the understanding of substrate specificity determinants in Rh proteins in the context of human diseases (**Bruce et al., 2009**).

Our findings define a new mechanism, by which ionizable molecules that are usually charged in solution are selectively and efficiently transported across a highly hydrophobic environment like the AmtB/Rh pore. Alongside size-exclusion and ion desolvation (**Kopec et al., 2018**), it adds a new principle by which selectivity against competing ions can be achieved. Other biological transport systems, like the formate/nitrite transporters, may share similar mechanisms involving deprotonation-reprotonation cycles (**Wiechert and Beitz, 2017**).

Materials and methods

Key resources table

Reagent type (species) or resource	Designation	Source or reference	Identifiers	Additional information
Gene (*Escherichia coli*)	AmtB	**Zheng et al., 2004**	Uniprot: C3TLL2	
Gene (*Nitrosomonas europea*)	Rh50	**Lupo et al., 2007**	Uniprot Q82 × 47	
Strain, strain background (*Escherichia coli*)	C43 (DE3)	**Miroux and Walker, 1996**		Chemically competent cells
Strain, strain background (*Escherichia coli*)	GT1000	**Javelle et al., 2004**		Chemically competent cells
Recombinant DNA reagent	pET22b (+)	Novagen	Cat# - 69744	
Recombinant DNA reagent	pDR195	**Rentsch et al., 1995**	Addgene - 36028	High copy yeast expression vector
Recombinant DNA reagent	pAD7	**Cherif-Zahar et al., 2007**		pESV2-RH50$(His)_6$

Continued on next page

Continued

Reagent type (species) or resource	Designation	Source or reference	Identifiers	Additional information
Recombinant DNA reagent	p426MET25	***Mumberg et al., 1994***		
Recombinant DNA reagent	PZheng	***Zheng et al., 2004***		pET22b-AmtB(His)$_6$
Recombinant DNA reagent	pGDM2	This study		pET22b-AmtB (His)$_6^{H168AH318A}$
Recombinant DNA reagent	pGDM4	This study		pET22b-AmtB(His)$_6^{D160A}$
Recombinant DNA reagent	pGDM5	This study		pET22b-AmtB(His)$_6^{D160E}$
Recombinant DNA reagent	pGDM6	This study		pET22b-AmtB (His)$_6^{S219AH168AH318A}$
Recombinant DNA reagent	pGW2	This study		pET22b-AmtB(His)$_6^{H168A}$
Recombinant DNA reagent	pGDM9	This study		pDR195-AmtB(His)$_6^{D160A}$
Recombinant DNA reagent	pGDM10	This study		pDR195-AmtB(His)$_6^{D160E}$
Recombinant DNA reagent	pGDM12	This study		pDR195-AmtB (His)$_6^{H168AH318A}$
Recombinant DNA reagent	pGDM13	This study		pDR195-AmtB (His)$_6^{S219AH168AH318A}$
Recombinant DNA reagent	pGW7	This study		pDR195-AmtB(His)$_6^{H168A}$
Sequence-based reagent	AmtB^{S219A} F	IDT	PCR Primer (Mutagenesis)	GGTGGCACCGTGGTGG**ATA**T TAACGCCGCAATC
Sequence-based reagent	AmtB^{D160A} F	IDT	PCR Primer (Mutagenesis)	CTCACGGTGCGCTGG**CC**TTCG CGGGTGGCACC
Sequence-based reagent	AmtB^{D160E} F	IDT	PCR Primer (Mutagenesis)	CTCACGGTGCGCTGG**AG**TTCG CGGGTGGCACC
Sequence-based reagent	AmtB^{H168A} F	IDT	PCR Primer (Mutagenesis)	GGTGGCACCGTGGTGG**CCA**TT AACGCCGCAATC
Sequence-based reagent	AmtB^{H318A} F	IDT	PCR Primer (Mutagenesis)	TGTCTTCGGTGT**GGC**CGGCGT TTGTGGCATT
Sequence-based reagent	AmtB XhoI	IDT	PCR primer	AGTC**CTCGAG**ATGAAGATAGC GACGATAAAA
Sequence-based reagent	AmtB BamHI	IDT	PCR primer	AGTC**GGATCC**TCACGCGTTAT AGGCATTCTC
Sequence-based reagent	P5'NeRh	IDT	PCR primer	GCC**ACTAGT**ATGAGTAAACAC CTATGTTTC
Sequence-based reagent	P3'NeRh	IDT	PCR primer	GCC**GAATTC**CTATCCTTCTGA CTTGGCAC
Peptide, recombinant protein	AmtB(His)$_6$	This study		purified from *E. coli* C43 (DE3) cells
Peptide, recombinant protein	AmtB(His)$_6^{D160A}$	This study		purified from *E. coli* C43 (DE3) cells
Peptide, recombinant protein	AmtB(His)$_6^{D160E}$	This study		purified from *E. coli* C43 (DE3) cells
Peptide, recombinant protein	AmtB(His)$_6^{H168AH318A}$	This study		purified from *E. coli* C43 (DE3) cells

Continued on next page

Continued

Reagent type (species) or resource	Designation	Source or reference	Identifiers	Additional information
Peptide, recombinant protein	AmtB $(His)_6^{S219AH168AH318A}$	This study		purified from *E. coli* C43 (DE3) cells
Peptide, recombinant protein	$AmtB(His)_6^{H168A}$	This study		purified from *E. coli* C43 (DE3) cells
Peptide, recombinant protein	$AmtB(His)_6^{H318A}$	This study		purified from *E. coli* C43 (DE3) cells
Peptide, recombinant protein	*Ne*Rh50$(His)_6$	This study		purified from *E. coli* C43 GT1000 cells
Peptide, recombinant protein	XhoI	Promega	Cat# - R6161	
Peptide, recombinant protein	BamHI	Promega	Cat# - R6021	
Commercial assay or kit	Quikchange XL site-directed mutagensis kit	Agilent Technologies	Cat# 200516	
Chemical compound, drug	n-dodecyl-β-D-maltopyranoside (DDM)	Avanti	Cat#- 850520	
Chemical compound, drug	lauryldecylamine oxide (LDAO)	Avanti	Cat#- 850545	
Chemical compound, drug	*E. coli* Polar Lipids	Avanti	Cat#−100600	
Chemical compound, drug	Phosphotidylcholine (POPC)	Avanti	Cat#−850457	
Software, algorithm	Graphpad Prism software	GraphPad Prism (https://www.graphpad.com)		Version 6.01
Software, algorithm	Origin Pro Software	Origin Labs (https://www.originlab.com)		Origin 2017 Version 94E
Software, algorithm	$SURFE^2R$ Control Software	Nanion (https://www.nanion.de/en/)		V1.5.3.2

Mutagenesis

AmtB mutants were generated using the Quikchange XL site-directed mutagenesis kit (Agilent Technologies), according to the manufacturer's instructions. The primers used for mutagenesis are listed in Key resources table. The template was the *amtB* gene cloned into the plasmid pET22b(+), as previously described (***Zheng et al., 2004***; Key resources table).

AmtB and NeRh50 expression in yeast and complementation test

The different variants of *amtB* were amplified using *amtB* cloned into pET22b(+) (Key resources table) as a template with the primers AmtB XhoI and AmtB BamHI (Key resources table) and then sub-cloned into the plasmids pDR195 (Key resources table). The NeRh50 gene was amplified from *N. europaea* genomic DNA (kind gift from Daniel J. Arp and Norman G. Hommes, Department of Botany and Plant Pathology, Oregon State University, Corvallis, USA) using the primers P5'NeRh and P3'NeRh (Key resources table), and was then cloned into the SpeI and EcoRI restriction sites of the high-copy vector p426Met25 (Key resources table), allowing controlled-expression of NeRh50 by the yeast methionine repressible MET25 promoter.

Saccharomyces cerevisiae strains used in this study are the 31019b strain (*mep1Δ mep2Δ mep3Δ ura3*) and the #228 strain (*mep1Δ mep2Δ mep3Δ trk1Δ trk2Δ leu2 ura3*) (**Hoopen et al., 2010**; **Marini et al., 1997**). The plasmids used in this study are listed in Key resources table. Cell transformation was performed as described previously (**Gietz et al., 1992**). For growth tests on limiting ammonium concentrations, yeast cells were grown in minimal buffered (pH 6.1) medium and for growth tests on limiting potassium concentrations, a minimal buffered (pH 6.1) medium deprived of potassium salts was used (**Jacobs et al., 1980**). 3% glucose was used as the carbon source and, 0.1% glutamate, 0.1% glutamine or $(NH_4)_2SO_4$ at the specified concentrations were used as the nitrogen sources.

All growth experiments were repeated at least twice.

Protein purification

AmtB(His_6) cloned into the pET22b(+) vector (Key resources table) was overexpressed and purified as described previously (**Zheng et al., 2004**). The plasmid pAD7 (Key resources table) was used to overexpress NeRh50 in the *E. coli* strain GT1000 (**Javelle et al., 2004**). GT1000 was transformed with pAD7 and grown in M9 medium (**Elbing and Brent, 2002**), in which ammonium was replaced by 200 µg/ml glutamine as sole nitrogen source. NeRh50 was purified as described by **Lupo et al., 2007** with minor modifications, namely: the membrane was solubilized using 2% lauryldecylamine oxide (LDAO) instead of 5% *n*-octyl-β-D-glucopyranoside (OG), and 0.09% LDAO was used in place of 0.5% β-OG in the final size exclusion chromatography buffer (50 mL Tris pH 7.8, 100 mL NaCl, 0.09% LDAO).

AmtB and NeRh50 insertion into proteoliposomes

AmtB and NeRh50 were inserted into liposomes containing *E. coli* polar lipids/phosphatidylcholine (POPC) 2/1(wt/wt) as previously described (**Mirandela et al., 2019**). For each AmtB variant, proteoliposomes were prepared at lipid-to-protein ratios (LPRs) of 5, 10, and 50 (wt/wt). The size distribution of proteoliposomes was measured by dynamic light scattering (DLS) using a Zetasizer Nano ZS (Malvern Instruments, Malvern, UK). This analysis showed that the proteoliposomes had an average diameter of 110 nm (**Figure 8**). Proteoliposomes were divided into 100 µL aliquots and stored at −80˚C.

To ensure that all AmtB variants were correctly inserted into the proteoliposomes, the proteoliposomes were solubilized in 2% DDM and the proteins analyzed by size exclusion chromatography using a superdex 200 (10 × 300) enhanced column. The elution profile of all variants and the wild-type were identical, showing a single monodisperse peak eluting between 10.4–10.6 ml (**Figure 4—figure supplement 1**). This demonstrated that all proteins were correctly folded, as trimers, in the proteoliposomes.

Solid supported membrane electrophysiology

To form the solid-supported membrane, 3 mm gold-plated sensors were prepared according to the manufacturer's instructions (Nanion Technologies, Munich, Germany), as described previously (**Bazzone et al., 2017**). Proteoliposomes/empty liposomes were defrosted and sonicated in a sonication bath at 35 W for 1 min, diluted 10 times in non-activating (NA) solution (**Supplementary file 1**), and then 10 µl were added at the surface of the SSM on the sensor. After centrifugation, the sensors were stored at 4˚C for a maximum of 48 hr before electrophysiological measurements. For the D_2O experiments, all the solutions were prepared using D_2O instead of water.

All measurements were made at room temperature (21˚C) using a $SURFE^2R$ N1 apparatus (Nanion Technologies, Munich, Germany) with default parameters (**Bazzone et al., 2017**). Prior to any measurements, the quality of the sensors was determined by measuring their capacitance (15–30 nF) and conductance (<5 nS).

For functional measurements at a fixed pH, a single solution exchange protocol was used with each phase lasting 1 s (**Bazzone et al., 2017**). First, non-active (NA) solution was injected onto the sensor, followed by activating (A) solution containing the substrate at the desired concentration and finally NA solution (**Supplementary file 1**).

For the measurements under inwardly orientated pH gradient, a double solution exchange protocol was used (**Bazzone et al., 2017**), in which an additional resting solution phase of 15 min in NA solution at pH 8 was added to the end. The incubation phase adjusts the inner pH of the proteoliposomes to

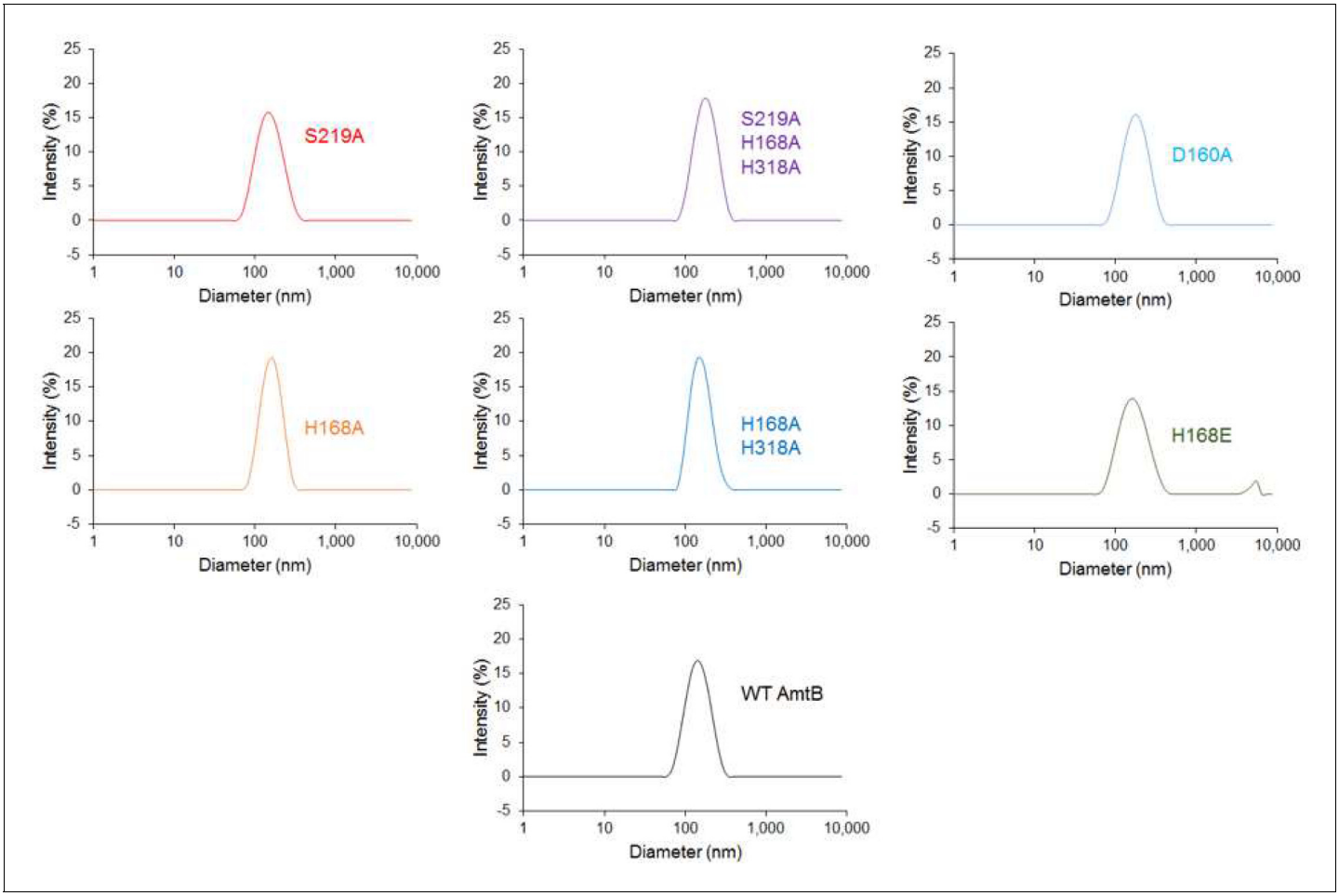

Figure 8. Size distribution of the proteoliposomes containing wild-type and variants of AmtB. Dynamic light scattering was used to determine the number-weighted distribution of liposome sizes in the detection reagent. The distribution was monodisperse, with a mean diameter of 110 nm.

pH 8 and establishes a pH gradient at the beginning of each measurement by pulsing the activation solution at pH 5.

Each sensor was measured in the order pH (in/out) 7/7, 8/5 (with NH_4^+), 8/5 (without NH_4^+), and finally again 7/7 to ensure that the signals do not significantly decrease with time. The data are normalized against the measurements conducted at pH7 in/out for each sensor. All measurements were recorded on 8 sensors from two independent protein purification batches, with 3 measurements recorded for each sensor.

The kinetic parameters were calculated using Graphpad Prism 6 (GraphPad Software, San Diego, California, USA) and fitted according to the Michaelis-Menten equation (Key resources table). Lifetime analysis of the current (decay time of the transient current) was performed to differentiate small pre-steady state currents, which arise due to the binding of a charged species to membrane proteins, from currents reflecting full transport cycles, which show faster decay rates under raised liposomal LPR (***Bazzone et al., 2017***). The decay time of the transient current (***Table 1***) was calculated by fitting the raw transient current data between the apex of the peak and the baseline (after transport) with a non-linear regression using OriginPro 2017 (OriginLab, Northampton, Massachusetts, USA). The regression was done using a one-phase exponential decay function with time constant parameter:

$$y = y_0 = A_1 e^{-x/t_1}$$

The fit was obtained using the Levenberg-Marquardt iteration algorithm, where x and y represent coordinates on the respective axis, y_0 represents the offset at a given point, A represents the amplitude, and t is the time constant.

Molecular Dynamics simulations

The AmtB trimer (PDB code: 1U7G) (**Khademi et al., 2004**) was processed using the CHARMM-GUI web server (**Lee et al., 2016**). Any mutations inserted during the crystallization process were reverted to the wild-type form. The N-termini and C-termini of the subunits were capped with acetyl and N-methyl amide moieties, respectively. The protein was then inserted into a membrane patch of *xy*-dimensions 13 × 13 nm. Unless otherwise specified, a membrane composition of palmitoyl oleoyl phosphatidyl ethanolamine and palmitoyl oleoyl phosphatidyl glycine (POPE/POPG) at a 3:1 ratio was used in order to approximate the composition of a bacterial cytoplasmic membrane. We employed the CHARMM36 forcefield for the protein and counter ions (**Best et al., 2012**). The water molecules were modeled with the TIP3P model (**Jorgensen et al., 1983**). Water bonds and distances were constrained by the Settle method (**Miyamoto and Kollman, 1992**), and all other bonds by the LINCS method (**Hess et al., 1997**). In simulations without ammonium, K^+ and Cl^- ions were added to neutralize the system and obtain a bulk ionic concentration of 250 mM. In simulations with ammonium, K^+ was replaced by NH_4^+. The parameters for NH_4^+ and NH_3 (umbrella sampling simulations) were adapted from **Nygaard et al., 2006**.

After a steepest descent energy minimization, the system was equilibrated by six consecutive equilibration steps using position restraints on heavy atoms of 1000 kJ/mol.nm^2. The first three equilibration steps were conducted in an NVT ensemble, applying a Berendsen thermostat (**Berendsen et al., 1984**) to keep the temperature at 310K. The subsequent steps were conducted under an NPT ensemble, using a Berendsen barostat (**Berendsen et al., 1984**) to keep the pressure at 1 bar. Production molecular dynamics simulations were carried out using a v-rescale thermostat (**Bussi et al., 2007**) with a time constant of 0.2 ps, and a Berendsen barostat with semi-isotropic coupling. A timestep of 2 fs was used throughout the simulations.

In a subset of simulations, we aimed to test the effect of membrane voltage on the internal hydration of AmtB using CompEL. For the CompEL simulations (**Kutzner et al., 2016**), the system was duplicated along the z-axis, perpendicular to the membrane surface. To focus on the physiologically relevant voltage gradient in *E. coli*, that is a negative potential on the inside of the cell of magnitude −140 to −170 mV (**Cohen and Venkatachalam, 2014**), an antiparallel orientation of the two trimers in the double bilayers was used (**Felle et al., 1980**). The final double system consisted of a rectangular box of 13 × 13×20 nm. For the CompEL simulations, 1000 positively charged (either NH_4^+ or K^+) and 1000 negatively charged ions (Cl^-) were added to the system, then the system was neutralized, and the desired ion imbalance established.

The Umbrella Sampling (US) Potential-of-Mean-Force (PMF) calculations (**Torrie and Valleau, 1977**) were set up as described previously by **Hub et al., 2010b**. A snapshot was taken from the simulation of the single bilayer system with the twin-His motif in the DE protonation state and both the CWW and PWW occupied. The pore coordinates were obtained using the software HOLE (**Smart et al., 1996**), removing the solvent and mutating F215 to alanine during the HOLE run only. Starting coordinates for each umbrella window were generated by placing NH_3 in the central x-y coordinate of the pore defined by HOLE at positions every 0.5 Å in the z coordinate. Solvent molecules within 2 Å of the ammonia's N atom were removed. Minimization and equilibration were then re-performed as described above. Unless otherwise stated, position restraints were used for all water oxygen atoms in the CWW with a 200 kJ/mol.nm^2 force constant; while the TIP3 molecules within the lower water wire were not restrained. For the US the N atom of ammonia was position-restrained with a force constant of 1000 kJ/mol.nm^2 on the z axis and a 400 kJ/mol.nm^2 cylindrical flat-bottomed potential with a radius of 5 Å in the x-y plane, as described earlier by **Hub et al., 2010a**. For some US window simulations, the ammonia z-axis restraints were increased and the time step reduced in the equilibration to relax steric clashes between sidechains and ammonia. After equilibration, US simulations were run for 10ns, using the parameters described above (**Lee et al., 2016**) and removing the initial two ns for further equilibration. The PMF profiles were generated with the GROMACS implementation of the weighted histogram analysis method (WHAM) with the periodic implementation (**Hub et al., 2010a**). Further US simulations were performed to as needed to improve sampling in regions of the profile that were not sufficiently sampled. The Bayesian bootstrap method was performed with 200 runs to calculate the standard deviation of the PMF.

Free energy calculations for proton translocation

The free energies for proton translocation were evaluated by protonating the water molecules at different sites along the periplasmic and cytoplasmic water wires. Electrostatic effects in proteins are often treated more effectively using semi-macroscopic models which can overcome the convergence problems of more rigorous microscopic models. Here we used the semi-macroscopic protein dipole/Langevin dipole approach of Warshel and coworkers in the linear response approximation version (PDLD/S-LRA) (***Kato et al., 2006***; ***Sham et al., 2000***). Positions of the water molecules in the PWW and CWW were obtained from the corresponding MD snapshots (***Figure 1***). All PDLD/S-LRA pK_a calculations were performed using the automated procedure in the MOLARIS simulations package (***Lee et al., 1993***) in combination with the ENZYMIX force field. The simulation included the use of the surface-constrained all atom solvent model (SCAAS) (***Warshel and King, 1985***) and the local reaction field (LRF) long-range treatment of electrostatics. At each site, 20 configurations for the charged and uncharged state were generated. The obtained pK_a values were then converted to free energies for proton translocation.

Acknowledgements

Special thanks to Prof. Iain Hunter (Strathclyde Institute of Pharmacy and Biomedical Sciences) for invaluable discussions and help during this project. We also thank Pascale Van Vooren for technical support and Thomas P Jahn for sharing the *triple-mepΔ trk,1,2Δ* yeast strain. Anna Maria Marini is a senior research associate FNRS and WELBIO investigator and thanks the help of FRFS-WELBIO grant ref: CR-2019A-05R.

Additional information

Funding

Funder	Grant reference number	Author
Tenovus	S17-07	Arnaud Javelle
Scottish Universities Physics Alliance		Ulrich Zachariae
Natural Environment Research Council	NE/M001415/1	Paul A Hoskisson
Fonds De La Recherche Scientifique - FNRS	WELBIO grant ref: CR-2019A-05R.	Anna-Maria Marini

The funders had no role in study design, data collection and interpretation, or the decision to submit the work for publication.

Author contributions

Gordon Williamson, Data curation, Formal analysis, Investigation, Methodology, Writing - review and editing; Giulia Tamburrino, Adriana Bizior, Data curation, Formal analysis, Investigation, Writing - review and editing; Mélanie Boeckstaens, Conceptualization, Data curation, Formal analysis, Methodology, Writing - review and editing; Gaëtan Dias Mirandela, Callum M Ives, Data curation, Formal analysis, Investigation; Marcus G Bage, Formal analysis, Investigation; Andrei Pisliakov, Conceptualization, Formal analysis, Methodology, Writing - review and editing; Eilidh Terras, Investigation; Paul A Hoskisson, Formal analysis, Funding acquisition, Writing - review and editing; Anna Maria Marini, Conceptualization, Methodology, Project administration, Writing - review and editing; Ulrich Zachariae, Conceptualization, Formal analysis, Methodology, Writing - original draft, Project administration; Arnaud Javelle, Conceptualization, Data curation, Formal analysis, Supervision, Investigation, Methodology, Writing - original draft, Project administration

Author ORCIDs

Gordon Williamson https://orcid.org/0000-0003-3053-8322
Mélanie Boeckstaens https://orcid.org/0000-0003-1629-7403

Gaëtan Dias Mirandela https://orcid.org/0000-0001-5871-6288
Andrei Pisliakov https://orcid.org/0000-0003-1536-0589
Callum M Ives http://orcid.org/0000-0003-0511-1220
Arnaud Javelle https://orcid.org/0000-0002-3611-5737

Decision letter and Author response
Decision letter https://doi.org/10.7554/eLife.57183.sa1
Author response https://doi.org/10.7554/eLife.57183.sa2

Additional files

Supplementary files

- Supplementary file 1. Supplementary Table 1.
- Transparent reporting form

Data availability

All data generated or analysed during this study are included in the manuscript and supporting files. Source data files have been provided for Figures 1-5 and Table 2. Simulation code is available on GitHub at https://github.com/UZgroup/A-two-lane-mechanism-for-selective-biological-ammonium-transport/ (copy archived at https://github.com/elifesciences-publications/A-two-lane-mechanism-for-selective-biological-ammonium-transport) and the trajectory files are available on Figshare (https://doi.org/10.6084/m9.figshare.12826316).

The following dataset was generated:

Author(s)	Year	Dataset title	Dataset URL	Database and Identifier
Tamburrino G, Zachariae U	2020	Molecular dynamics simulation trajectories, AmtB in twin-His HSD-HSE and HSE-HSD states	https://figshare.com/articles/dataset/Molecular_dynamics_simulation_trajectories_AmtB_in_twin-His_HSD-HSE_and_HSE-HSD_states/12826316	figshare, 10.6084/m9.figshare.12826316

References

Acharya R, Carnevale V, Fiorin G, Levine BG, Polishchuk AL, Balannik V, Samish I, Lamb RA, Pinto LH, DeGrado WF, Klein ML. 2010. Structure and mechanism of proton transport through the transmembrane tetrameric M2 protein bundle of the influenza A virus. *PNAS* **107**:15075–15080. DOI: https://doi.org/10.1073/pnas.1007071107, PMID: 20689043

Andrade SL, Dickmanns A, Ficner R, Einsle O. 2005. Crystal structure of the archaeal ammonium transporter Amt-1 from Archaeoglobus fulgidus. *PNAS* **102**:14994–14999. DOI: https://doi.org/10.1073/pnas.0506254102, PMID: 16214888

Ariz I, Boeckstaens M, Gouveia C, Martins AP, Sanz-Luque E, Fernández E, Soveral G, von Wirén N, Marini AM, Aparicio-Tejo PM, Cruz C. 2018. Nitrogen isotope signature evidences ammonium deprotonation as a common transport mechanism for the AMT-Mep-Rh protein superfamily. *Science Advances* **4**:eaar3599. DOI: https://doi.org/10.1126/sciadv.aar3599, PMID: 30214933

Ashkenazy H, Abadi S, Martz E, Chay O, Mayrose I, Pupko T, Ben-Tal N. 2016. ConSurf 2016: an improved methodology to estimate and visualize evolutionary conservation in macromolecules. *Nucleic Acids Research* **44**:W344–W350. DOI: https://doi.org/10.1093/nar/gkw408, PMID: 27166375

Aydin F, Zhan C, Ritt C, Epsztein R, Elimelech M, Schwegler E, Pham TA. 2020. Similarities and differences between potassium and ammonium ions in liquid water: a first-principles study. *Physical Chemistry Chemical Physics* **22**:2540–2548. DOI: https://doi.org/10.1039/C9CP06163K, PMID: 31942893

Bazzone A, Barthmes M, Fendler K. 2017. SSM-Based electrophysiology for transporter research. *Methods in Enzymology* **594**:31–83. DOI: https://doi.org/10.1016/bs.mie.2017.05.008, PMID: 28779843

Berendsen HJC, Postma JPM, van Gunsteren WF, DiNola A, Haak JR. 1984. Molecular dynamics with coupling to an external bath. *The Journal of Chemical Physics* **81**:3684–3690. DOI: https://doi.org/10.1063/1.448118

Best RB, Zhu X, Shim J, Lopes PE, Mittal J, Feig M, Mackerell AD. 2012. Optimization of the additive CHARMM all-atom protein force field targeting improved sampling of the backbone φ, ψ and side-chain χ(1) and χ(2) dihedral angles. *Journal of Chemical Theory and Computation* **8**:3257–3273. DOI: https://doi.org/10.1021/ct300400x, PMID: 23341755

Biver S, Belge H, Bourgeois S, Van Vooren P, Nowik M, Scohy S, Houillier P, Szpirer J, Szpirer C, Wagner CA, Devuyst O, Marini AM. 2008. A role for rhesus factor rhcg in renal ammonium excretion and male fertility. *Nature* **456**:339–343. DOI: https://doi.org/10.1038/nature07518

Boogerd FC, Ma H, Bruggeman FJ, van Heeswijk WC, García-Contreras R, Molenaar D, Krab K, Westerhoff HV. 2011. AmtB-mediated NH3 transport in prokaryotes must be active and as a consequence regulation of transport by GlnK is mandatory to limit futile cycling of NH4(+)/NH3. *FEBS Letters* **585**:23–28. DOI: https://doi.org/10.1016/j.febslet.2010.11.055, PMID: 21134373

Bruce LJ, Guizouarn H, Burton NM, Gabillat N, Poole J, Flatt JF, Brady RL, Borgese F, Delaunay J, Stewart GW. 2009. The monovalent cation leak in overhydrated stomatocytic red blood cells results from amino acid substitutions in the Rh-associated glycoprotein. *Blood* **113**:1350–1357. DOI: https://doi.org/10.1182/blood-2008-07-171140, PMID: 18931342

Bussi G, Donadio D, Parrinello M. 2007. Canonical sampling through velocity rescaling. *The Journal of Chemical Physics* **126**:014101. DOI: https://doi.org/10.1063/1.2408420, PMID: 17212484

Cherif-Zahar B, Durand A, Schmidt I, Hamdaoui N, Matic I, Merrick M, Matassi G. 2007. Evolution and functional characterization of the RH50 gene from the ammonia-oxidizing bacterium *Nitrosomonas europaea*. *Journal of Bacteriology* **189**:9090–9100. DOI: https://doi.org/10.1128/JB.01089-07, PMID: 17921289

Cohen AE, Venkatachalam V. 2014. Bringing bioelectricity to light. *Annual Review of Biophysics* **43**:211–232. DOI: https://doi.org/10.1146/annurev-biophys-051013-022717, PMID: 24773017

Dias Mirandela G, Tamburrino G, Ivanović MT, Strnad FM, Byron O, Rasmussen T, Hoskisson PA, Hub JS, Zachariae U, Gabel F, Javelle A. 2018. Merging In-Solution X-ray and neutron scattering data allows fine structural analysis of Membrane-Protein detergent complexes. *The Journal of Physical Chemistry Letters* **9**:3910–3914. DOI: https://doi.org/10.1021/acs.jpclett.8b01598, PMID: 29939747

Elbing K, Brent R. 2002. Media preparation and bacteriological tools. *Current Protocols in Molecular Biology* **59**:1. DOI: https://doi.org/10.1002/0471142727.mb0101s59

Felle H, Porter JS, Slayman CL, Kaback HR. 1980. Quantitative measurements of membrane potential in *Escherichia coli*. *Biochemistry* **19**:3585–3590. DOI: https://doi.org/10.1021/bi00556a026

Ganz P, Ijato T, Porras-Murrilo R, Stührwohldt N, Ludewig U, Neuhäuser B. 2020. A twin histidine motif is the core structure for high-affinity substrate selection in plant ammonium transporters. *Journal of Biological Chemistry* **295**:3362–3370. DOI: https://doi.org/10.1074/jbc.RA119.010891, PMID: 31988244

Gietz D, Jean AS, Woods RA, Schiestl RH. 1992. Improved method for high efficiency transformation of intact yeast cells. *Nucleic Acids Research* **20**:1425. DOI: https://doi.org/10.1093/nar/20.6.1425

Gruswitz F, Chaudhary S, Ho JD, Schlessinger A, Pezeshki B, Ho C-M, Sali A, Westhoff CM, Stroud RM. 2010. Function of human Rh based on structure of RhCG at 2.1 A. *PNAS* **107**:9638–9643. DOI: https://doi.org/10.1073/pnas.1003587107

Hall JA, Yan D. 2013. The molecular basis of K+ exclusion by the *Escherichia coli* ammonium channel AmtB. *The Journal of Biological Chemistry* **288**:14080–14086. DOI: https://doi.org/10.1074/jbc.M113.457952, PMID: 23546877

Hess B, Bekker H, Berendsen HJC, Fraaije JGEM. 1997. LINCS: a linear constraint solver for molecular simulations. *Journal of Computational Chemistry* **18**:1463–1472. DOI: https://doi.org/10.1002/(SICI)1096-987X(199709)18:12<1463::AID-JCC4>3.0.CO;2-H

Hoopen Ft, Cuin TA, Pedas P, Hegelund JN, Shabala S, Schjoerring JK, Jahn TP. 2010. Competition between uptake of ammonium and potassium in barley and Arabidopsis roots: molecular mechanisms and physiological consequences. *Journal of Experimental Botany* **61**:2303–2315. DOI: https://doi.org/10.1093/jxb/erq057

Huang C-H, Ye M. 2010. The Rh protein family: gene evolution, membrane biology, and disease association. *Cellular and Molecular Life Sciences* **67**:1203–1218. DOI: https://doi.org/10.1007/s00018-009-0217-x

Hub JS, de Groot BL, van der Spoel D. 2010a. g_wham—A Free Weighted Histogram Analysis Implementation Including Robust Error and Autocorrelation Estimates. *Journal of Chemical Theory and Computation* **6**:3713–3720. DOI: https://doi.org/10.1021/ct100494z

Hub JS, Winkler FK, Merrick M, de Groot BL. 2010b. Potentials of mean force and permeabilities for carbon dioxide, Ammonia, and water flux across a rhesus protein channel and lipid membranes. *Journal of the American Chemical Society* **132**:13251–13263. DOI: https://doi.org/10.1021/ja102133x, PMID: 20815391

Ishikita H, Knapp EW. 2007. Protonation states of Ammonia/ammonium in the hydrophobic pore of Ammonia transporter protein AmtB. *Journal of the American Chemical Society* **129**:1210–1215. DOI: https://doi.org/10.1021/ja066208n, PMID: 17263403

Jacobs P, Jauniaux J-C, Grenson M. 1980. A cis-dominant regulatory mutation linked to the argB-argC gene cluster in *Saccharomyces cerevisiae*. *Journal of Molecular Biology* **139**:691–704. DOI: https://doi.org/10.1016/0022-2836(80)90055-8

Javelle A, Severi E, Thornton J, Merrick M. 2004. Ammonium sensing in *Escherichia coli*. Role of the ammonium transporter AmtB and AmtB-GlnK complex formation. *The Journal of Biological Chemistry* **279**:8530–8538. DOI: https://doi.org/10.1074/jbc.M312399200, PMID: 14668330

Javelle A, Lupo D, Zheng L, Li XD, Winkler FK, Merrick M. 2006. An unusual twin-his arrangement in the pore of Ammonia channels is essential for substrate conductance. *Journal of Biological Chemistry* **281**:39492–39498. DOI: https://doi.org/10.1074/jbc.M608325200, PMID: 17040913

Jorgensen WL, Chandrasekhar J, Madura JD, Impey RW, Klein ML. 1983. Comparison of simple potential functions for simulating liquid water. *The Journal of Chemical Physics* **79**:926–935. DOI: https://doi.org/10.1063/1.445869

Kato M, Pisliakov AV, Warshel A. 2006. The barrier for proton transport in aquaporins as a challenge for electrostatic models: The role of protein relaxation in mutational calculations. *Proteins: Structure, Function, and Bioinformatics* **64**:829–844. DOI: https://doi.org/10.1002/prot.21012

Khademi S, O'Connell J, Remis J, Robles-Colmenares Y, Miercke LJ, Stroud RM. 2004. Mechanism of Ammonia transport by amt/MEP/Rh: structure of AmtB at 1.35 A. *Science* **305**:1587–1594. DOI: https://doi.org/10.1126/science.1101952, PMID: 15361618

Kopec W, Köpfer DA, Vickery ON, Bondarenko AS, Jansen TLC, de Groot BL, Zachariae U. 2018. Direct knock-on of desolvated ions governs strict ion selectivity in K^+ channels. *Nature Chemistry* **10**:813–820. DOI: https://doi.org/10.1038/s41557-018-0105-9

Kutzner C, Köpfer DA, Machtens JP, de Groot BL, Song C, Zachariae U. 2016. Insights into the function of ion channels by computational electrophysiology simulations. *Biochimica Et Biophysica Acta (BBA) - Biomembranes* **1858**:1741–1752. DOI: https://doi.org/10.1016/j.bbamem.2016.02.006, PMID: 26874204

Lamoureux G, Klein ML, Bernèche S. 2007. A stable water chain in the hydrophobic pore of the AmtB ammonium transporter. *Biophysical Journal* **92**:L82–L84. DOI: https://doi.org/10.1529/biophysj.106.102756, PMID: 17351012

Lee FS, Chu ZT, Warshel A. 1993. Microscopic and semimicroscopic calculations of electrostatic energies in proteins by the POLARIS and ENZYMIX programs. *Journal of Computational Chemistry* **14**:161–185. DOI: https://doi.org/10.1002/jcc.540140205

Lee J, Cheng X, Swails JM, Yeom MS, Eastman PK, Lemkul JA, Wei S, Buckner J, Jeong JC, Qi Y, Jo S, Pande VS, Case DA, Brooks CL, MacKerell AD, Klauda JB, Im W. 2016. CHARMM-GUI input generator for NAMD, GROMACS, AMBER, OpenMM, and CHARMM/OpenMM simulations using the CHARMM36 additive force field. *Journal of Chemical Theory and Computation* **12**:405–413. DOI: https://doi.org/10.1021/acs.jctc.5b00935, PMID: 26631602

Li X, Jayachandran S, Nguyen H-HT, Chan MK. 2007. Structure of the *Nitrosomonas europaea* Rh protein. *PNAS* **104**:19279–19284. DOI: https://doi.org/10.1073/pnas.0709710104

Ludewig U, von Wirén N, Frommer WB. 2002. Uniport of NH4+ by the root hair plasma membrane ammonium transporter LeAMT1;1. *Journal of Biological Chemistry* **277**:13548–13555. DOI: https://doi.org/10.1074/jbc.M200739200, PMID: 11821433

Lupo D, Li X-D, Durand A, Tomizaki T, Cherif-Zahar B, Matassi G, Merrick M, Winkler FK. 2007. The 1.3-A resolution structure of *Nitrosomonas europaea* Rh50 and mechanistic implications for NH3 transport by Rhesus family proteins. *PNAS* **104**:19303–19308. DOI: https://doi.org/10.1073/pnas.0706563104

Maeda K, Westerhoff HV, Kurata H, Boogerd FC. 2019. Ranking network mechanisms by how they fit diverse experiments and deciding on *E. coli*'s ammonium transport and assimilation network. *Npj Systems Biology and Applications* **5**:14. DOI: https://doi.org/10.1038/s41540-019-0091-6, PMID: 30993002

Marini AM, Soussi-Boudekou S, Vissers S, Andre B. 1997. A family of ammonium transporters in *Saccharomyces cerevisiae*. *Molecular and Cellular Biology* **17**:4282–4293. DOI: https://doi.org/10.1128/MCB.17.8.4282

Marini AM, Boeckstaens M, Benjelloun F, Chérif-Zahar B, André B. 2006. Structural involvement in substrate recognition of an essential aspartate residue conserved in Mep/Amt and Rh-type ammonium transporters. *Current Genetics* **49**:364–374. DOI: https://doi.org/10.1007/s00294-006-0062-5

Mayer M, Dynowski M, Ludewig U. 2006. Ammonium ion transport by the AMT/Rh homologue LeAMT1;1. *Biochemical Journal* **396**:431–437. DOI: https://doi.org/10.1042/BJ20060051

McDonald TR, Ward JM. 2016. Evolution of electrogenic ammonium transporters (AMTs). *Frontiers in Plant Science* **7**:352. DOI: https://doi.org/10.3389/fpls.2016.00352, PMID: 27066024

Mirandela GD, Tamburrino G, Hoskisson PA, Zachariae U, Javelle A. 2019. The lipid environment determines the activity of the *Escherichia coli* ammonium transporter AmtB. *The FASEB Journal* **33**:1989–1999. DOI: https://doi.org/10.1096/fj.201800782R, PMID: 30211659

Miroux B, Walker JE. 1996. Over-production of proteins *in Escherichia coli*: mutant hosts that allow synthesis of some membrane proteins and globular proteins at high levels. *Journal of Molecular Biology* **260**:289–298. DOI: https://doi.org/10.1006/jmbi.1996.0399, PMID: 8757792

Miyamoto S, Kollman PA. 1992. Settle: An analytical version of the SHAKE and RATTLE algorithm for rigid water models. *Journal of Computational Chemistry* **13**:952–962. DOI: https://doi.org/10.1002/jcc.540130805

Mumberg D, Muller R, Funk M. 1994. Regulatable promoters of *Saccharomyces cerevisiae*: comparison of transcriptional activity and their use for heterologous expression. *Nucleic Acids Research* **22**:5767–5768. DOI: https://doi.org/10.1093/nar/22.25.5767

Neuhäuser B, Dynowski M, Ludewig U. 2014. Switching substrate specificity of AMT/MEP/ Rh proteins. *Channels* **8**:496–502. DOI: https://doi.org/10.4161/19336950.2014.967618, PMID: 25483282

Nygaard TP, Rovira C, Peters GH, Jensen MØ. 2006. Ammonium recruitment and Ammonia transport by *E. coli* Ammonia channel AmtB. *Biophysical Journal* **91**:4401–4412. DOI: https://doi.org/10.1529/biophysj.106.089714, PMID: 17012311

Rentsch D, Laloi M, Rouhara I, Schmelzer E, Delrot S, Frommer WB. 1995. *NTR1* encodes a high affinity oligopeptide transporter in *Arabidopsis*. *FEBS Letters* **370**:264–268. DOI: https://doi.org/10.1016/0014-5793(95)00853-2

Sham YY, Chu ZT, Tao H, Warshel A. 2000. Examining methods for calculations of binding free energies: lra, LIE, PDLD-LRA, and PDLD/S-LRA calculations of ligands binding to an HIV protease. *Proteins: Structure, Function, and Genetics* **39**:393–407. DOI: https://doi.org/10.1002/(SICI)1097-0134(20000601)39:4<393::AID-PROT120>3.0.CO;2-H, PMID: 10813821

Smart OS, Neduvelil JG, Wang X, Wallace BA, Sansom MSP. 1996. HOLE: A program for the analysis of the pore dimensions of ion channel structural models. *Journal of Molecular Graphics* **14**:354–360. DOI: https://doi.org/10.1016/S0263-7855(97)00009-X

Thomas GH, Mullins JGL, Merrick M. 2000. Membrane topology of the Mep/Amt family of ammonium transporters. *Molecular Microbiology* **37**:331–344. DOI: https://doi.org/10.1046/j.1365-2958.2000.01994.x

Torrie GM, Valleau JP. 1977. Nonphysical sampling distributions in Monte Carlo free-energy estimation: Umbrella sampling. *Journal of Computational Physics* **23**:187–199. DOI: https://doi.org/10.1016/0021-9991(77)90121-8

van den Berg B, Chembath A, Jefferies D, Basle A, Khalid S, Rutherford JC. 2016. Structural basis for Mep2 ammonium transceptor activation by phosphorylation. *Nature Communications* **7**:11337. DOI: https://doi.org/10.1038/ncomms11337

Wacker T, Garcia-Celma JJ, Lewe P, Andrade SLA. 2014. Direct observation of electrogenic $NH4^+$ transport in ammonium transport (Amt) proteins. *PNAS* **111**:9995–10000. DOI: https://doi.org/10.1073/pnas.1406409111

Wang S, Orabi EA, Baday S, Bernèche S, Lamoureux G. 2012. Ammonium transporters achieve charge transfer by fragmenting their substrate. *Journal of the American Chemical Society* **134**:10419–10427. DOI: https://doi.org/10.1021/ja300129x, PMID: 22631217

Warshel A, King G. 1985. Polarization constraints in molecular dynamics simulation of aqueous solutions: The surface constraint all atom solvent (SCAAS) model. *Chemical Physics Letters* **121**:124–129. DOI: https://doi.org/10.1016/0009-2614(85)87168-2

Weidinger K, Neuhäuser B, Gilch S, Ludewig U, Meyer O, Schmidt I. 2007. Functional and physiological evidence for a rhesus-type Ammonia transporter in *Nitrosomonas europaea*. *FEMS Microbiology Letters* **273**:260–267. DOI: https://doi.org/10.1111/j.1574-6968.2007.00805.x, PMID: 17608700

Wiechert M, Beitz E. 2017. Mechanism of formate-nitrite transporters by dielectric shift of substrate acidity. *The EMBO Journal* **36**:949–958. DOI: https://doi.org/10.15252/embj.201695776, PMID: 28250043

Zheng L, Kostrewa D, Berneche S, Winkler FK, Li X-D. 2004. The mechanism of ammonia transport based on the crystal structure of AmtB of *Escherichia coli*. *PNAS* **101**:17090–17095. DOI: https://doi.org/10.1073/pnas.0406475101

AMERICAN SOCIETY FOR MICROBIOLOGY | mBio®

RESEARCH ARTICLE

Coexistence of Ammonium Transporter and Channel Mechanisms in Amt-Mep-Rh Twin-His Variants Impairs the Filamentation Signaling Capacity of Fungal Mep2 Transceptors

Gordon Williamson,[a] Ana Sofia Brito,[b] Adriana Bizior,[a] Giulia Tamburrino,[c] Gaëtan Dias Mirandela,[a,b] Thomas Harris,[a] Paul A. Hoskisson,[a] Ulrich Zachariae,[c] Anna Maria Marini,[b] Mélanie Boeckstaens,[b] Arnaud Javelle[a]

[a]Strathclyde Institute of Pharmacy and Biomedical Sciences, University of Strathclyde, Glasgow, United Kingdom
[b]Biology of Membrane Transport Laboratory, Department of Molecular Biology, Université Libre de Bruxelles, Gosselies, Belgium
[c]Computational Biology, School of Life Sciences, University of Dundee, Dundee, United Kingdom

Gordon Williamson, Ana Sofia Brito, and Adriana Bizior contributed equally to this work. Author order was determined by the time they have joined the project: most ancient first. Anna Maria Marini, Mélanie Boeckstaens, and Arnaud Javelle contributed equally to this work. Author order was determined by the time they have joined the project: most recent first.

ABSTRACT Ammonium translocation through biological membranes, by the ubiquitous Amt-Mep-Rh family of transporters, plays a key role in all domains of life. Two highly conserved histidine residues protrude into the lumen of the pore of these transporters, forming the family's characteristic Twin-His motif. It has been hypothesized that the motif is essential to confer the selectivity of the transport mechanism. Here, using a combination of *in vitro* electrophysiology on *Escherichia coli* AmtB, *in silico* molecular dynamics simulations, and *in vivo* yeast functional complementation assays, we demonstrate that variations in the Twin-His motif trigger a mechanistic switch between a specific transporter, depending on ammonium deprotonation, to an unspecific ion channel activity. We therefore propose that there is no selective filter that governs specificity in Amt-Mep-Rh transporters, but the inherent mechanism of translocation, dependent on the fragmentation of the substrate, ensures the high specificity of the translocation. We show that coexistence of both mechanisms in single Twin-His variants of yeast Mep2 transceptors disrupts the signaling function and so impairs fungal filamentation. These data support a signaling process driven by the transport mechanism of the fungal Mep2 transceptors.

IMPORTANCE Fungal infections represent a significant threat to human health and cause huge damage to crop yields worldwide. The dimorphic switch between yeast and filamentous growth is associated with the virulence of pathogenic fungi. Of note, fungal Mep2 proteins of the conserved Amt-Mep-Rh family play a transceptor role in the induction of filamentation; however, the signaling mechanism remains largely unknown. Amt-Mep-Rh proteins ensure the specific scavenging of NH_4^+ through a mechanism relying on substrate deprotonation, thereby preventing competition and translocation of similar-sized K^+. Our multidisciplinary approaches using *E. coli* AmtB, *Saccharomyces cerevisiae*, and *Candida albicans* Mep2 show that double variation of the family-defining Twin-His motif triggers a mechanistic switch from a specific transporter to an unspecific ion channel with both mechanisms still coexisting in single variants. Moreover, we show that this mechanistic alteration is associated with loss of signaling ability of Mep2, supporting a transport mechanism-driven process in filamentation induction.

KEYWORDS *Candida albicans*, *Escherichia coli*, *Saccharomyces cerevisiae*, ammonium assimilation, fungal filamentation, secondary transporter mechanism

Cellular ammonium transport is facilitated by the ubiquitous Amt-Mep-Rh superfamily, members of which have been identified in every branch of the tree of life (1). The physiological relevance of Amt-Mep-Rh proteins extends beyond their role in

Editor Michael Lorenz, University of Texas Health Science Center

Address correspondence to Anna Maria Marini, Anna.Maria.Marini@ulb.be, Mélanie Boeckstaens, melanie.boeckstaens@ulb.be, or Arnaud Javelle, arnaud.javelle@strath.ac.uk.

The authors declare no conflict of interest.

Received 4 October 2021
Accepted 26 January 2022

ammonium acquisition as a nitrogen source. In fungi, for instance, in the presence of very low ammonium concentrations, specific Amt-Mep-Rh transporters, the Mep2-like proteins, have been proposed to act as transceptors required for the development of filamentous growth, a dimorphic switch associated with the virulence of pathogenic fungi (2). However, it is currently unclear how the signal that leads to the pseudohyphal growth is initiated by Mep2-like transporters.

Despite the relevance of this protein family, the transport mechanism of Amt-Mep-Rh has remained largely elusive for decades. Crystal structures of various family members revealed a trimeric organization with a narrow conducting transport pore through each monomer lined with hydrophobic residues (3–8). While it was next shown that Amt-Mep-Rh proteins mediate NH_3 transport after NH_4^+ deprotonation (9), other functional studies demonstrated that *Archaeoglobus fulgidus* Amt1 and 3, *Escherichia coli* AmtB, and several plant Amts can mediate electrogenic ammonium transport (10–13), questioning the fate of the proton released by NH_4^+ fragmentation. We recently showed that two water wires connect the periplasmic side with the cytoplasmic vestibule of EcAmtB (12). These two water wires are interconnected via the H168 residue of the Twin-His, a highly conserved motif constituted of two histidine residues protruding into the lumen of the pore (12, 14). We showed that, after deprotonation of NH_4^+ at the periplasmic side, the two interconnected water wires and the Twin-His motif enable H^+ transfer into the cytoplasm. A parallel pathway, lined by hydrophobic groups within the protein core, facilitates the simultaneous transfer of uncharged NH_3.

Despite its high level of conservation, the Twin-His motif presents some variations in fungal Amt-Mep-Rh proteins (14–16). Specifically, the first histidine is present in Mep2 transceptors, whereas the Mep1- and Mep3-type proteins feature a natural occupation by a glutamic acid at the first histidine position, defining two functional Amt-Mep-Rh subfamilies in fungi. More recently, using functional characterization in *Xenopus* oocytes, we revealed that *Saccharomyces cerevisiae* Mep2 mediates electroneutral substrate translocation, while Mep1 performs electrogenic transport, and we proposed that the specific transport mechanism of Mep2 could be responsible for the signal leading to filamentation induction (17). We therefore sought to analyze in more detail the impact of Twin-His variation on the transport mechanism of Amt-Mep-Rh proteins.

Here, we report that altering the Twin-His motif within the pore of *E. coli* AmtB, *S. cerevisiae* and *Candida albicans* Mep2 does not impair ammonium transport function but abolishes the pore selectivity against potassium. We further demonstrate that this loss of selectivity is the result of a mechanistic switch from a transporter-like activity to a channel-like activity governed by a change in the hydrophobicity of the pore. Our findings show that the mechanism of substrate transport ensures the high specificity of the transport. Finally, we show that the mechanistic alteration impacts on the ability of fungal Mep2 proteins to act as transceptors in the development of pseudohyphal growth, supporting the hypothesis that the transport mechanism of Mep2-like proteins is connected to the signal leading to yeast filamentation.

RESULTS

Altering pore hydrophobicity does not disrupt transport activity of AmtB. To determine the effect of altering the hydrophobicity of the pore on transport activity, we first looked at the effect of single acidic substitutions H168E and H168D within the Twin-His motif of AmtB, mimicking the glutamate substitution present in the fungal Mep1/3-type transporters. We purified and reconstituted both AmtB variants into liposomes and measured their activities *in vitro* using solid supported membrane electrophysiology (SSME) and *in vivo* by yeast complementation assays. In proteoliposomes containing $AmtB^{H168D}$ or $AmtB^{H168E}$, an ammonium pulse of 200 mM elicited very high-current amplitudes of 14.23 nA and 22.28 nA, respectively, compared to 3.38 nA observed for the wild type (WT) (Fig. 1A). To confirm that the transient currents correspond to the translocation of ammonium into the proteoliposomes and not to a simple interaction between ammonium and the protein, we investigated the effect of varying

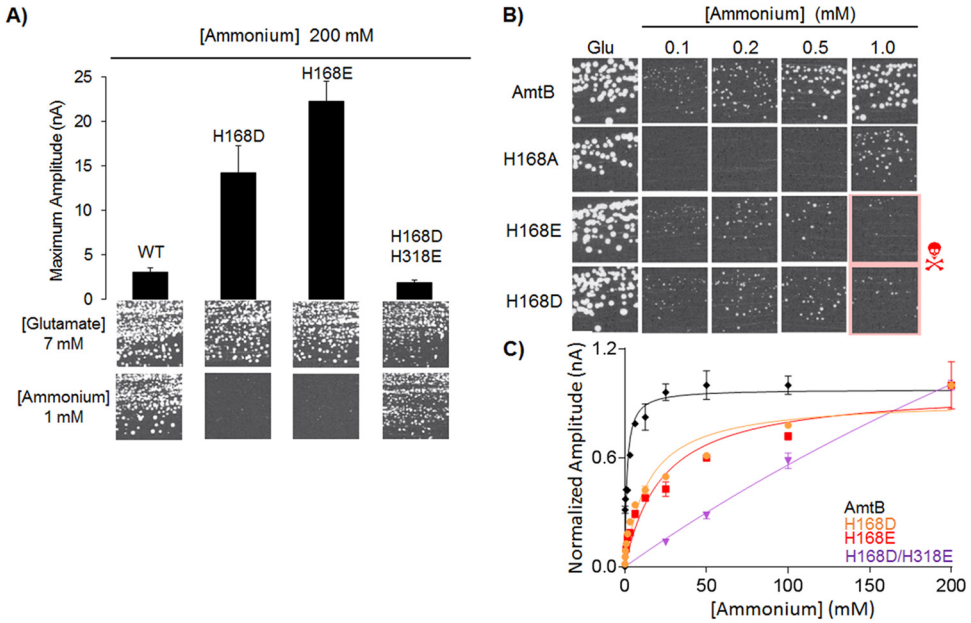

FIG 1 Effect of Twin-His substitution on AmtB ammonium transport activity. (A) (Upper panel) Maximum amplitude of the transient currents measured using SSME following a 200 mM ammonium pulse. (Lower panel) Yeast complementation test after 3 days at 29°C, on potassium glutamate (Glu, positive growth control) or ammonium as the sole nitrogen source. The strain 31019b (*mep1*Δ *mep2*Δ *mep3*Δ *ura3*) was transformed with the pDR195 plasmid, allowing expression of the various AmtB variants. (B) Yeast complementation test, after 5 days at 29°C, in the presence of a range of ammonium concentrations (0.1 mM to 1.0 mM) or glutamate. The red skull shows inhomogenous growth (C) Kinetics analysis for the transport of ammonium using SSME. The maximum amplitudes recorded after a 200 mM ammonium pulse have been normalized to 1.0 for comparison.

the protein density in the liposomes on the transient current. It is expected that increasing the protein density in the liposomes will prolong the decay time of the current if the current represents a complete transport cycle (18). The lifetime of the currents measured for both variants was dependent on the liposomal lipid:protein ratio (LPR), indicating that the currents indeed account for a full translocation cycle (Table 1). Additionally, we measured an increase of the catalytic constants (K_m) for both variants compared to the WT (Fig. 1C, Table 2).

Expressed in a *S. cerevisiae* triple-*mep*Δ strain deprived of its three endogenous Mep ammonium transporters, both variants were unable to restore growth on 1 mM ammonium after 3 days, suggesting a loss of function (Fig. 1A). However, after 5 days, an inhomogeneous weak growth was observed (Fig. 1B). Previous work has demonstrated that noncontrolled ammonium influx can be toxic to *S. cerevisiae* (19, 20). To test if this inhomogeneous growth could be linked to toxic ammonium influx, the yeast complementation assay was repeated with a lower range of ammonium concentrations (0.1 to 1.0 mM) (Fig. 1B). The complementation ensured by both AmtB^{H168D} and AmtB^{H168E} variants was improved by decreasing the ammonium concentrations. These

TABLE 1 Decay time constants (s^{-1}) of transient currents triggered after an ammonium, methylammonium, or potassium pulse of 200 mM in proteoliposomes containing AmtB variants at various LPR[a]

	Ammonium		MeA		Potassium	
Variant	LPR 10	LPR 5	LPR 10	LPR 5	LPR 10	LPR 5
WT	13.4 ± 1.5	18.7 ± 1.0	3.6 ± 0.5	8.3 ± 1.2	NC	NC
H168D	31.4 ± 1.3	38.1 ± 4.1	17.7 ± 2.1	26.4 ± 4.2	NC	NC
H168E	45.5 ± 4.8	53.9 ± 1.6	27.0 ± 1.9	36.4 ± 3.1	NC	NC
H168D/H318E	15.8 ± 1.1	17.8 ± 0.7	10.5 ± 2.5	13.9 ± 1.8	2.3 ± 0.4	4.9 ± 0.2

[a]NC, no transient current recorded.

TABLE 2 K_m (mM) of AmtB variants for ammonium, methylammonium, and potassium, using SSME[a]

Variant	Ammonium	MeA	Potassium
WT	0.8 ± 0.1	49.86 ± 4.76	NC
H168D	14.02 ± 4.08	55.09 ± 12.67	NC
H168E	12.87 ± 7.79	86.00 ± 9.46	NC
H168D/H318E	NA	NA	NA

[a]NC, no transient current recorded; NA, not applicable.

results suggest that the acidic substitution at position 168 drastically increases the ammonium flux through AmtB, rendering it toxic to yeast cells. We did not previously observe ammonium toxicity with the AmtB^{H168E} variant expressed in yeast (15). In those experiments, AmtB^{H168E} was expressed under the control of another promoter, *MET25*, repressible by methionine supplementation. The presence of ammonium under its sulfate salt may lead to partial repression of the *MET25* promoter. In the present experiment, the variants are expressed under the control of the *PMA1* promoter, a stronger promoter than *MET25*. Therefore, enhanced expression of the variants in the present experiment could explain the observed ammonium toxicity.

A double H168D/H318E mutation has previously been shown to impact AmtB specificity (21). To further probe the impact of pore hydrophobicity on the activity and specificity of AmtB, we substituted both residues of the Twin-His motif with acidic residues (AmtB$^{H168D/H318E}$). SSME measurements revealed that a 200 mM NH_4^+ pulse elicited an LPR-dependent transient current with a maximum amplitude of 1.84 nA in proteoliposomes containing AmtB$^{H168D/H318E}$, a 1.8-fold reduction compared to WT AmtB (Fig. 1A, Table 1). Additionally, a catalytic constant (K_m) for AmtB$^{H168D/H318E}$ could not be determined, as saturation could not be achieved, even following an ammonium pulse of 200 mM (Fig. 1C, Table 2). When expressed in the *S. cerevisiae* triple-*mep*Δ strain, AmtB$^{H168D/H318E}$ was able to restore cell growth on low ammonium concentrations (Fig. 1A). These data demonstrate that while AmtB$^{H168D/H318E}$ is still functionally active, its activity seems to be reduced compared to WT AmtB. The absence of saturable kinetics further suggests that the variant behaves like a channel rather than having transporter-like activity. We previously observed this type of behavior when we replaced the Twin-His motif with alanine residues, although the mechanism of this switch remained elusive (12).

Previously, methylammonium (MeA) was used as a substrate analogue for ammonium. However, it triggers transient currents of only 15 to 20% of those elicited by ammonium, indicating strong substrate discrimination by AmtB (11, 16, 22). To determine if this level of discrimination is maintained in the Twin-His variants, the AmtB^{H168D} and AmtB^{H168E} variants were subjected to a pulse of 200 mM MeA during SSME. Both AmtB^{H168D} and AmtB^{H168E} exhibited increased activity compared to WT AmtB (9-fold and 12-fold increase in current amplitude, respectively). The double mutant AmtB$^{H168D/H318E}$ showed a maximum amplitude comparable to WT AmtB (Fig. 2A), but it was not possible to determine a catalytic constant, again due to the lack of saturation (Fig. 2B, Table 2). These data indicate that the mutations do not alter the ability of AmtB to discriminate between MeA and ammonium *in vitro*. Yeast complementation was carried out in parallel. MeA cannot be metabolized by yeast cells and is toxic at high external concentrations (15, 23). The native AmtB and all the Twin-His variants allowed growth of triple-*mep*Δ *S. cerevisiae* cells on glutamate medium, but not when it was supplemented with MeA (Fig. 2A). This shows that all the variants are also active in transporting MeA in yeast.

Altering pore hydrophobicity abolishes transport selectivity. The findings reported above showed that altering the hydrophobicity of the pore does not inactivate AmtB but has a substantial impact on the transport mechanism. Thus, we next investigated whether the substitutions also affect the ammonium/MeA selectivity of AmtB against competing ions. We focused on K^+, as it has an ionic radius similar to that of NH_4^+. A 200 mM K^+ pulse failed to elicit a measurable current in AmtB^{H168D} or AmtB^{H168E} proteoliposomes but

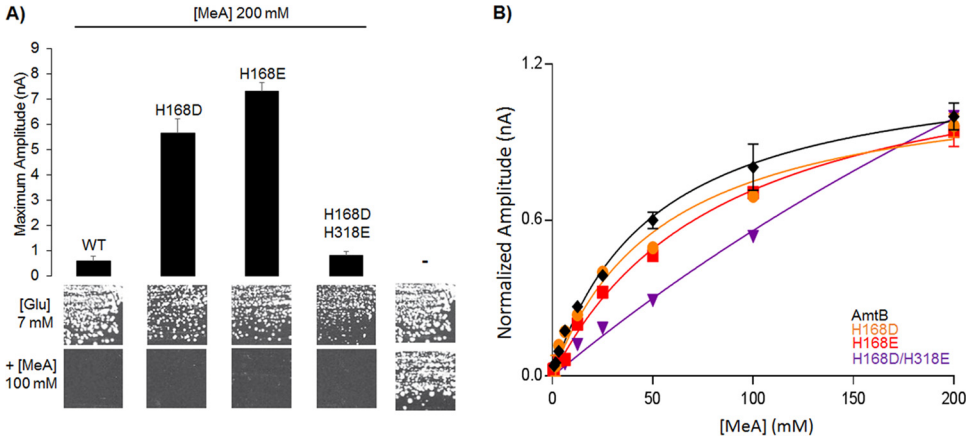

FIG 2 Effect of Twin-His substitution on AmtB methylammonium transport activity. (A) (Upper panel) maximum amplitude of the transient current measured using SSME following a 200 mM methylammonium (MeA) pulse. (Lower panel) Yeast complementation test, after 3 days at 29°C, on solid minimal medium containing, as the sole nitrogen source, potassium glutamate 7 mM (glu, positive growth control) supplemented or not with 100 mM methylammonium. The strain 31019b (*mep1*Δ *mep2*Δ *mep3*Δ *ura3*) was transformed with the empty pDR195 plasmid (–), or with pDR195 allowing expression of the various AmtB variants. (B) Kinetics analysis for the transport of methylammonium using SSME. The maximum amplitudes recorded after a 200 mM MeA pulse have been normalized to 1.0 for comparison.

was able to trigger a clear transient current in AmtB$^{H168D/H318E}$ (Fig. 3A). The amplitude and decay time of the currents recorded for AmtB$^{H168D/H318E}$ are LPR-dependent, confirming that they are caused by K^+ translocation and are not only the result of protein-substrate interaction (Fig. 3B, Table 1). It was not possible to determine a catalytic constant for AmtB$^{H168D/H318E}$, again due to the lack of saturation, indicating a channel-like rather than a transporter-like activity (Fig. 3C, Table 2). Moreover, all the variants, but not the WT, were able to complement the growth defect of a triple-*mep*Δ *trk*Δ *S. cerevisiae* strain,

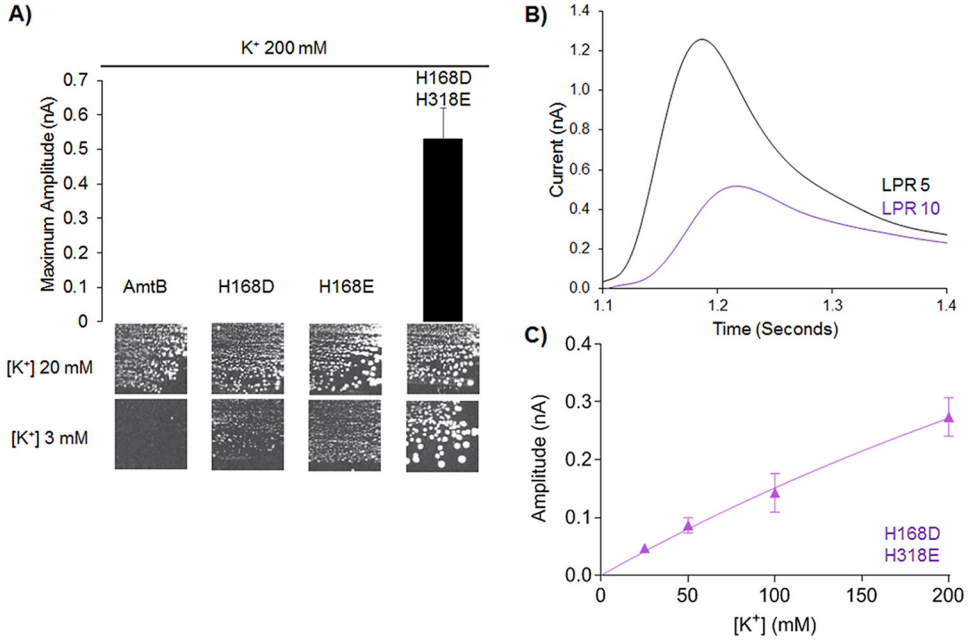

FIG 3 Potassium (K^+) transport in AmtB Twin-His variants. (A) (Upper panel) Maximum amplitude of the transient current measured using SSME following a 200 mM potassium pulse. (Lower panel) Yeast complementation test, after 5 days at 29°C, in the presence of 20 mM or 3 mM potassium. The #228 strain (*mep1*Δ *mep2*Δ *mep3*Δ *trk1*Δ *trk2*Δ *leu2 ura3*) was transformed with the pDR195 plasmid allowing expression of the various AmtB variants. (B) Transient currents measured using SSME following a 200 mM potassium pulse with AmtB$^{H168D/H318E}$ reconstituted into proteoliposomes at a LPR 5 (black) or 10 (purple). (C) Kinetics analysis for the transport of potassium using SSME.

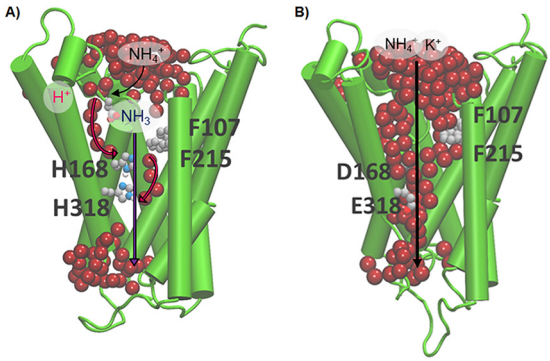

FIG 4 Schematic comparison of transport in WT AmtB and AmtB$^{H168D/H318E}$. (A) Molecular dynamic simulation of the AmtB monomer, showing the interconnected water wires (represented as red spheres). Following sequestration of NH_4^+ at the periplasmic face, NH_4^+ is deprotonated, before passing the "Phe-Gate," representing the first hydrophobic barrier, and H^+ and NH_3 follow two separate pathways to join the cytoplasm (magenta arrows depict the pathway for H^+ transfer, dark blue arrows for NH_3) facilitated by the presence of two internal water wires. (B) Molecular dynamic simulation of the AmtB$^{H168D/H318E}$ monomer, showing the pore filled with water molecules. Due to the increased hydration within the pore, periplasmic NH_4^+ and K^+ are translocated directly through the central pore to the cytoplasm.

which lacks the three endogenous ammonium (Mep) transporters and the 2 major potassium (Trk) transporters, in the presence of a limited concentration of K^+ (Fig. 3A). The complementation is clearly improved when AmtB$^{H168D/H318E}$ is expressed compared to AmtB^{H168D} or AmtB^{H168E}, showing that the single variants are also able to translocate potassium, albeit at a lower rate than AmtB$^{H168D/H318E}$. This could explain why we measured a current after a K^+ pulse in the proteoliposomes containing AmtB$^{H168D/H318E}$ but not with AmtB^{H168D} or AmtB^{H168E}. We reason that there could be an inverse relationship between the hydrophobicity of the central pore and the selectivity of AmtB.

Loss of AmtB selectivity is due to increased pore hydration accompanied by a mechanistic change. To understand the loss of substrate selectivity observed in the AmtB variants and the switch from transporter-like to channel-like activity observed in the SSME recordings with the AmtB$^{H168D/H318E}$ variant, molecular dynamics simulations were conducted. Our previously proposed model for the transport mechanism of AmtB suggests that, after deprotonation of NH_4^+ at the periplasmic side, two interconnected water wires enable H^+ transfer into the cytoplasm. A parallel pathway, lined with hydrophobic groups within the protein core, facilitates the simultaneous transfer of NH_3 (Fig. 4A) (12).

Molecular dynamics simulations based on alterations of the Twin-His motif by the introduction of charged residues show that this destabilizes and widens the pore, causing it to fill with water and forming a continuous aqueous channel (Fig. 4B). This represents a significant change from the ordered single-file chains of water molecules, separated by the Twin-His motif, observed in the simulations with the WT. The formation of a wide aqueous pore at the expense of discrete water chains disrupts the mechanism of transport and compromises the ability of AmtB to act as a specific transporter, since the newly flooded pore can enable the direct passage of hydrated cations.

To test if the single-file water wires are indeed disrupted by the substitutions, we employed a D_2O-based SSME assay. Because the strength of a covalent bond involving deuterium increases compared to hydrogen, proton mobility is reduced by 30% for each D_2O molecule compared to H_2O (24). If the water wires are intact and are required for the transport mechanism, replacement of H_2O with D_2O is expected to result in the complete abolishment of current when measured by SSME. If, however, the mechanism does not require the water wires, the substitution of H_2O with D_2O should not affect the observed current following an ammonium pulse. As previously observed in WT AmtB, no current was measured under D_2O conditions (Fig. 5) (12). In AmtB^{H168D} and AmtB^{H168E}, the current observed following a 200 mM ammonium pulse was diminished by about 4-fold in the presence of D_2O compared to H_2O, but not completely

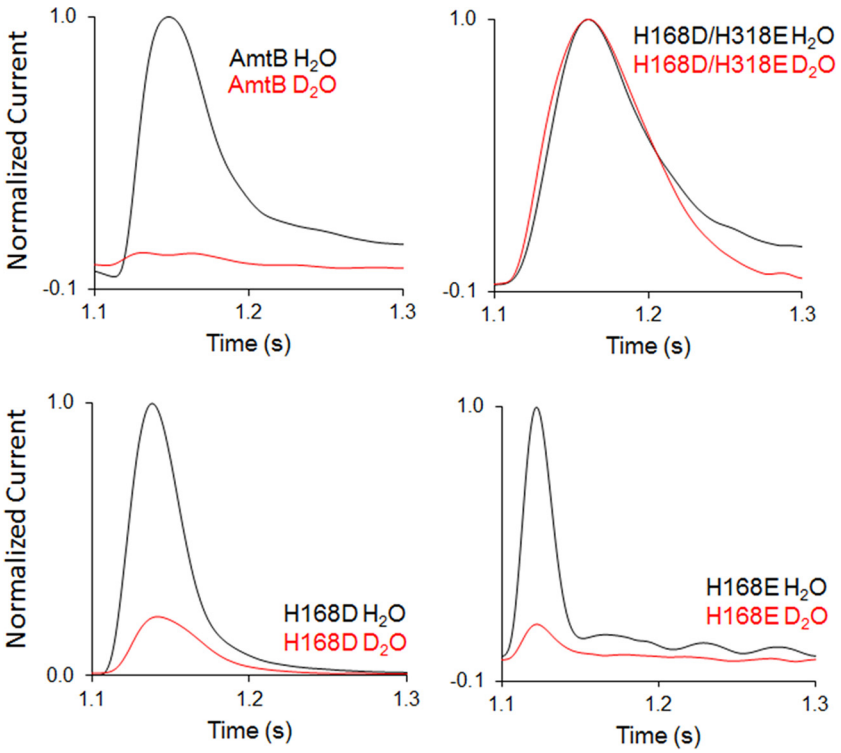

FIG 5 Hydrophobicity of the AmtB transport pore governs mechanistic switch. Transient currents measured using SSME following a 200 mM ammonium pulse on sensors prepared with solutions containing either H_2O (black) or D_2O (red) in WT AmtB, $AmtB^{H168D/H318E}$, $AmtB^{H168D}$, or $AmtB^{H168E}$. D_2O currents have been normalized to respective H_2O currents.

abolished (Fig. 5). The stark reduction of current in the presence of D_2O indicates that proton hopping remains a mechanistic feature within $AmtB^{H168D}$ and $AmtB^{H168E}$. However, the lack of complete abolition implies that some charge translocation is occurring by another mechanism. These data suggest that two transport mechanisms are used by these variants, one depending on NH_4^+ deprotonation, and the other allowing the occasional passage of hydrated NH_4^+ or K^+, as shown in Fig. 4. This result is in agreement with the capacity of these variants to transport K^+ in yeast (Fig. 3A).

In contrast, in $AmtB^{H168D/H318E}$, a 200 mM ammonium pulse elicits transient currents of similar magnitude with either D_2O or H_2O (Fig. 5). This indicates that the central mechanism of proton hopping observed in WT AmtB is no longer a mechanistic feature of $AmtB^{H168D/H318E}$ which gains the ability to directly transport NH_4^+ without deprotonation. These findings demonstrate that hydrophilic substitutions within the Twin-His motif gradually lead to a switch in the transport mechanism of AmtB protein from transporter to channel-like, which is observed in $AmtB^{H168D/H318E}$. In the latter, NH_4^+ is translocated as an intact cation in its hydrated form, abolishing transport specificity (Fig. 4). These data also explain why the ammonium/MeA/potassium transport activity cannot be saturated in proteoliposomes containing $AmtB^{H168D/H318E}$ and why this variant is highly efficient in potassium transport (Fig. 1, 2, and 3, Table 2).

The Twin-His motif is involved in the transport specificity of ScMep2. Previously, we showed that alanine mutations in the Twin-His motif ($AmtB^{H168A}$ and $AmtB^{H318A}$) also alter the selectivity of the AmtB pore, resulting in the ability of the variants to translocate K^+ ions (12). To understand the general importance of the hydrophobicity of the central pore in substrate selectivity, we simultaneously compared Twin-His variants of *S. cerevisiae* Mep2 with single or double mutations in alanine or glutamate residues in terms of ammonium, methylammonium, and potassium transport functionality. We chose a double Twin-His mutation to double E because the paralogue ScMep1 has an E at the His_1 position and E at the His_2-1 position. We wished to remain as close as possible

to a yeast protein situation known to be functional (ScMep1). We first tested if the *S. cerevisiae* triple-*mep*Δ strain expressing ScMep2^{H194A}, ScMep2^{H194E}, ScMep2^{H348A}, ScMep2^{H348E}, ScMep2$^{H194A/H348A}$, or ScMep2$^{H194E/H348E}$ was able to grow on low ammonium concentration, compared to cells expressing native ScMep2 as the positive control (Fig. 6A). We found that a single substitution of the first or second histidine of the Twin-His motif into alanine or glutamate does not affect in a major way the ammonium transport function of ScMep2 in a home-made buffered medium. However, the ScMep2 double Twin-His mutants (ScMep2$^{H194A/H348A}$ and ScMep2$^{H194E/H348E}$) do not support the growth of the triple-*mep*Δ cells on low ammonium (Fig. 6A). Fluorescence microscopy using Mep2 variants fused to the pHluorin version of green fluorescent protein (GFP) reveals that all variants reach the cell surface, except the double Twin-His variants, which seem to be additionally stacked in the endoplasmic reticulum (Fig. S3A). This could indicate that the failure to complement results from a trafficking problem of the double Twin-His variants.

We also tested the capacity of ScMep2 variants to intoxicate cells in the presence of high MeA concentrations. Contrary to ScMep1, native ScMep2 is unable to intoxicate cells in the presence of MeA, proposed to be due to a lower maximal transport rate (25). Expression of ScMep2 variants with single His substitutions reduced growth of the triple-*mep*Δ cells in the presence of MeA, suggesting a higher transport flux through the variants or an altered transport mechanism increasing the sensitivity of the cells to the toxic compound (Fig. 6A) (15). The substitution of both histidines in the Twin-His motif was not accompanied by an increased sensitivity of the cells to MeA, which is in agreement with the absence of ammonium transport by the ScMep2$^{H194A/H348A}$ and ScMep2$^{H194E/H348E}$ variants (Fig. 6A). As for AmtB, the Twin-His substitutions of ScMep2 do not affect ammonium/MeA discrimination.

The capacity of the ScMep2 variants to transport K^+ was next assessed in the triple-*mep*Δ strain further lacking its endogenous high-affinity potassium transporters Trk1/2 in the presence of limiting concentrations of K^+ (Fig. 6B). In contrast to native ScMep2, expression of any of the ScMep2 Twin-His variants rescues cell growth in the presence of low K^+ concentrations, with growth efficiency depending on the variant. Of note, the double Twin-His variants enable K^+ transport function, even if the pHluorin-fused versions are at least partially blocked in the endoplasmic reticulum (Fig. S3B), thereby suggesting that sufficient proteins reach the plasma membrane to produce this phenotype. These data show that ScMep2 Twin-His variants can translocate K^+, with variants possessing the H348A or H348E mutation being the most efficient in K^+ transfer (Fig. 6B). These results indicate that, as for AmtB, the mutations in the twin-His motif of the central pore of ScMep2 alters the transport selectivity.

Coexistence of different transport mechanisms in ScMep2 variants. It is of note that the medium used to test the ammonium transport capacity of the AmtB and ScMep2 variants in yeast contains about 180 mM K^+. Thus, it appears that single ScMep2 His-variants are able to ensure growth in the presence of 1 mM ammonium despite a very high K^+ concentration, indicating that potassium does not efficiently compete with ammonium recognition and transport in these variants. This indicates that the single His substitutions allow the coexistence of two transport mechanisms, as proposed for AmtB^{H168D} and AmtB^{H168E}. This finding suggests that the first mechanism allows the selective transport of NH_3 after NH_4^+ recognition and deprotonation (as in native Mep2) and is not sensitive to high K^+. The second mechanism, created by the substitution, could act as an ion channel pathway allowing the passage of K^+, and likely NH_4^+, and would thus be sensitive to competition between both ions. This prompted us to test if the absence of growth under low-ammonium conditions of cells expressing ScMep2$^{H194A/H348A}$ and ScMep2$^{H194E/H348E}$ could be linked to high concentrations of potassium in the medium used. We performed growth tests with the triple-*mep*Δ *trk*Δ strain in a medium allowing us to simultaneously address the capacity of the variants to transport K^+ and ammonium. As shown in Fig. 7, ScMep2$^{H194E/H348E}$ allows cell growth in the presence of 3 mM ammonium and equal or lower K^+ concentrations (1 mM and 3 mM), indicating that the ammonium transport mechanism of this variant is highly sensitive to the potassium concentration. Of note, cells

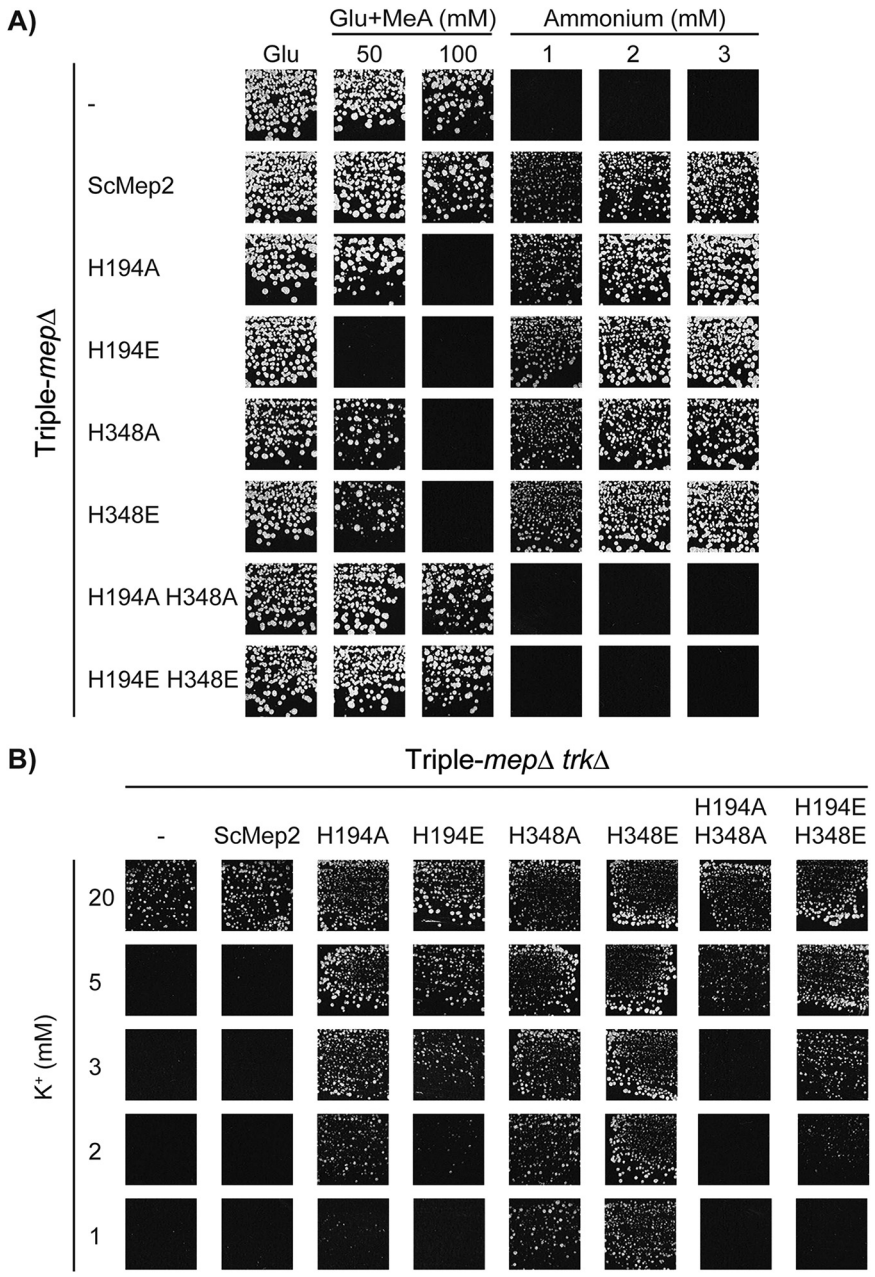

FIG 6 Effect of Twin-His substitutions on ScMep2 transport activity and specificity. (A) Growth tests, after 4 days at 29°C, on solid minimal medium containing, as the sole nitrogen source, ammonium 1, 2, and 3 mM or potassium glutamate (Glu, positive growth control) supplemented or not with 50 or 100 mM methylammonium (MeA). The *Saccharomyces cerevisiae* strain 31019b (*mep1*Δ *mep2*Δ *mep3*Δ *ura3*) was transformed with the pFL38 empty plasmid (–) or with YCpMep2, YCpMep2^{H194A}, YCpMep2^{H194E}, YCpMep2^{H348A}, YCpMep2^{H348E}, YCpMep2$^{H194A/H348A}$, or YCpMep2$^{H194E/H348E}$. (B) Growth tests, after 4 days at 29°C, on solid minimal medium containing different potassium concentrations (from 1 mM to 20 mM) and in the presence of sodium glutamate as the nitrogen source. The *Saccharomyces cerevisiae* strain #228 (*mep1*Δ *mep2*Δ *mep3*Δ *trk1*Δ *trk2*Δ *leu2 ura3*) was transformed with the pFL38 empty plasmid (–) or with YCpMep2, YCpMep2^{H194A}, YCpMep2^{H194E}, YCpMep2^{H348A}, YCpMep2^{H348E}, YCpMep2$^{H194A/H348A}$, or YCpMep2$^{H194E/H348E}$.

expressing the variant ScMep2^{H348E} appear to grow better when the ammonium concentration decreases specifically in the presence of 3 mM K^+ and not at higher K^+ concentrations. One possible explanation could be that upon lowering the concentration of the competitor K^+ ion, ammonium uptake increases up to toxic levels, as previously observed with AmtB^{H168E} and AmtB^{H168D} variants (Fig. 1B).

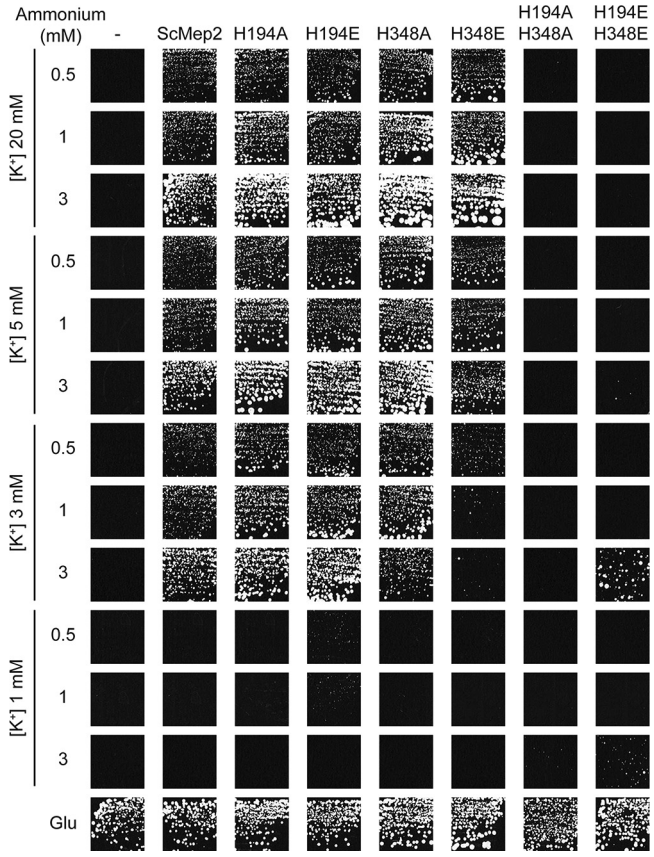

FIG 7 Different transport mechanisms in the ScMep2 Twin-His variants. Growth tests, after 12 days at 29°C, on solid minimal medium containing different potassium concentrations (from 1 mM to 20 mM) and in the presence of different ammonium concentrations (0.5, 1, or 3 mM) as the nitrogen source. The *Saccharomyces cerevisiae* strain #228 (*mep1*Δ *mep2*Δ *mep3*Δ *trk1*Δ *trk2*Δ *leu2 ura3*) was double transformed with the pFL46 and pFL38 empty plasmids (–) or with pFL46 and YCpMep2, YCpMep2^{H194A}, YCpMep2^{H194E}, YCpMep2^{H348A}, YCpMep2^{H348E}, YCpMep2$^{H194A/H348A}$, or YCpMep2$^{H194E/H348E}$. The same solid medium containing 20 mM potassium and potassium glutamate, as the sole nitrogen source, was used as the positive growth control (lower panel; the growth corresponds to day 5 at 29°C).

Consistent with the conclusions made for AmtB, these data support that simultaneous substitution of the two conserved histidines in ScMep2 results in the formation of a K^+/NH_4^+ channel pathway, while the transport mechanism dependent on NH_4^+ deprotonation is abolished. The observation that single histidine variants are able to ensure growth on low ammonium concentrations even in the presence of high potassium concentrations supports the hypothesis that both pathways, one based on ammonium deprotonation and the other linked to direct NH_4^+/K^+ transport, coexist in these variants.

Influence of the transport mechanism on the capacity of ScMep2 to induce filamentation. ScMep2, but not ScMep1 or ScMep3, is required for the dimorphic switch leading to yeast filamentation in the presence of very low ammonium concentrations (2). H194E and H348A mutations of ScMep2 were proposed to affect the filamentation signaling process under very low ammonium conditions (15, 17, 26). Here, we simultaneously compared the whole set of single and double mutants in the Twin-His motif of ScMep2 to assess the effect of the mechanistic switch from a transporter-like to a channel-like activity on the capacity of ScMep2 to induce filamentation on the appropriate synthetic low ammonium dextrose (SLAD) medium (100 μM ammonium) (Fig. 8A). Synthetic high ammonium dextrose (SHAD) medium (1 mM ammonium) was also used to check for potential constitutive induction of filamentation. In parallel, the ammonium transport functionality of the variants was also evaluated by growth tests

on these media (Fig. 8B). We show that, contrary to native ScMep2, filamentation is not observed in the presence of any of the His variants (Fig. 8A), as previously observed with ScMep2^{H194E} and ScMep2^{H348A} (15, 17, 26). As the single His substitutions into alanine slightly affect the functionality of ScMep2 on SLAD (Fig. 8B), the conclusion concerning its signaling capacity appears tricky. ScMep2$^{H194A/H348A}$ and ScMep2$^{H194E/H348E}$ are not able to ensure growth on SLAD (Fig. 8B), probably due to the high potassium concentration (30 mM) compared to the reduced ammonium concentration (100 μM) in this medium; therefore, we cannot draw conclusions on their capacity to induce filamentation. ScMep2^{H194E} and ScMep2^{H348E} have lost their signaling capacity, although they seem functional in ammonium transport function, revealing the importance of the pore hydrophobicity and/or the transport mechanism in the signaling process.

As potassium could compete with ammonium transport and a high potassium concentration is present in SLAD, we tested the capacity of the Twin-His variants to induce filamentation in a medium containing low potassium concentrations. Filamentation and growth tests were performed in a home-made medium, equivalent to yeast nitrogen base (YNB) medium and allowing control of potassium and ammonium concentrations (0.1 or 1 mM ammonium and a potassium concentration ranging from 0.1 to 20 mM) (Fig. 9A and B). Again, no filamentation is observed with the ScMep2 His variants (Fig. 9B). However, as shown in Fig. 9A, ScMep2$^{H194A/H348A}$ and ScMep2$^{H194E/H348E}$ are not able to sustain growth at 0.1 or 1 mM ammonium, even if the potassium concentration is reduced, suggesting that ammonium transport is strongly inhibited by potassium and is not sufficient to ensure growth. Of note, filamentous growth is not observed with cells expressing ScMep2 at very low potassium concentrations (0.1 mM, Fig. 9B). However, growth is also strongly impaired under this condition, indicating that a minimal potassium concentration is required to ensure optimal growth (Fig. 9A). ScMep2-dependent filamentation is also inhibited by increasing the potassium concentration, which could be due to the inhibition of ammonium translocation by potassium (Fig. 9B). This confirms that the simple presence of ScMep2 at the cell surface is not sufficient for its signaling property; translocation of the substrate is mandatory for signaling (15, 17, 27–29). Taken together, these data suggest that altering the transport mechanism of ScMep2 through Twin-His mutations is correlated with an impaired capacity of the protein to induce filamentation. This result supports the hypothesis that the capacity of ScMep2 to induce filamentation is associated with its substrate translocation mechanism (15, 17).

Coexistence of different transport mechanisms in CaMep2 variants and influence on filamentation. CaMep2 from *Candida albicans*, the orthologue of *S. cerevisiae* Mep2, is also required to induce filamentation of this human-pathogenic fungus (30). Expression of CaMep2 in *S. cerevisiae* cells deprived of endogenous ScMep2 restores filamentation, suggesting that a similar mechanism leads to filamentation in both species (17, 30). Here, we compared the impact of a set of Twin-His substitutions in CaMep2 by expressing the variants in *S. cerevisiae*. As observed with ScMep2, CaMep2 variants mutated in the first and/or second histidine CaMep2^{H188E}, CaMep2^{H342E}, and CaMep2$^{H188E/H342E}$ are able to translocate K^+ (Fig. 8C). Growth tests on SLAD and SHAD show that native CaMep2 and CaMep2^{H188E} are less functional in ammonium transport than ScMep2, while CaMep2^{H342E} and CaMep2$^{H188E/H342E}$ are completely nonfunctional, at least in the presence of high potassium concentrations (Fig. 8B). None of the CaMep2 variants are able to allow filamentation (Fig. 8A). Hence, as for ScMep2, the capacity of CaMep2 to induce filamentation also appears to be associated with its transport mechanism.

DISCUSSION

The data presented show that substitutions within the Twin-His motif of Amt-Mep-Rh decrease the specificity of transport. While this was previously proposed in *E. coli*, *S. cerevisiae*, and *Arabidopsis thaliana* (12, 15, 31), it was assumed that the Twin-His motif was central for the selectivity of the transporters. In this context, the natural occurrence of a glutamic acid in the place of the first histidine in fungal Mep1 and Mep3, but not Mep2 protein, was unclear. Here, our findings lead us to propose a new

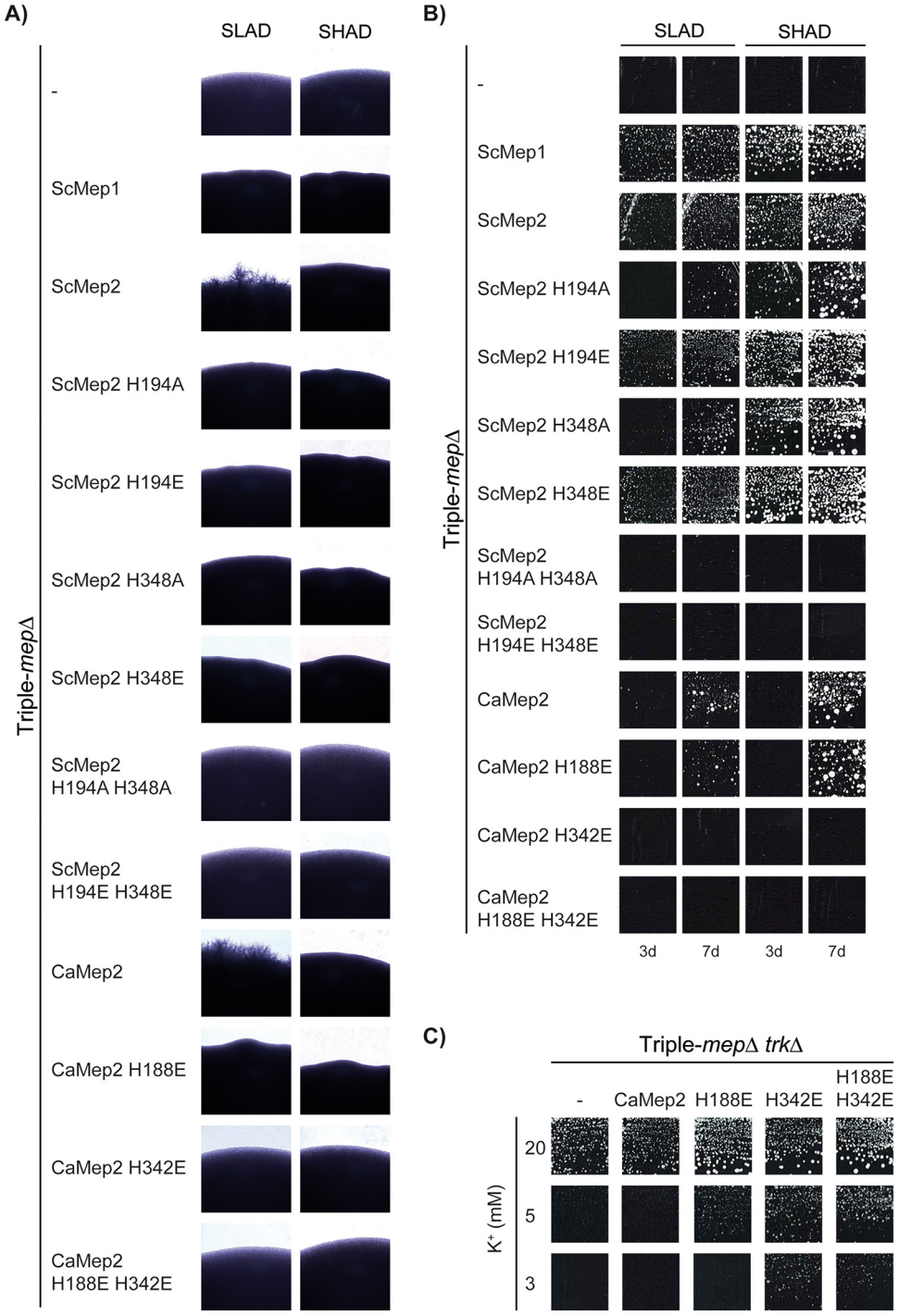

FIG 8 Effect of Twin-His substitutions on the capacity of ScMep2 and CaMep2 to induce fungal filamentation. Homozygous diploid triple-*mep*Δ *ura3* cells (strain ZAM38) were transformed with the pFL38 empty plasmid (–) or with YCpMep2, YCpMep2^{H194A}, YCpMep2^{H194E}, YCpMep2^{H348A}, YCpMep2^{H348E}, YCpMep2$^{H194A/H348A}$, YCpMep2$^{H194E/H348E}$, YCpCaMep2, YCpCaMep2^{H188E}, YCpCaMep2^{H342E}, or YCpCaMep2$^{H188E/H342E}$. (A) Pseudohyphal growth tests of high-density cell suspensions dropped on SLAD and SHAD media at day 7. (B) Growth tests of low-density cell suspensions on SLAD and SHAD media at days 3 (3d) and 7 (7d), at 29°C. (C) Growth tests, after 4 days at 29°C, on solid minimal medium containing different potassium concentrations (from 2 mM to 20 mM) and sodium glutamate as the nitrogen source. The *Saccharomyces cerevisiae* strain #228 (*mep1*Δ *mep2*Δ *mep3*Δ *trk1*Δ *trk2*Δ *leu2 ura3*) was transformed with the pFL38 empty plasmid (–) or with YCpCaMep2, YCpCaMep2^{H188E}, YCpCaMep2^{H342E}, or YCpCaMep2$^{H188E/H342E}$.

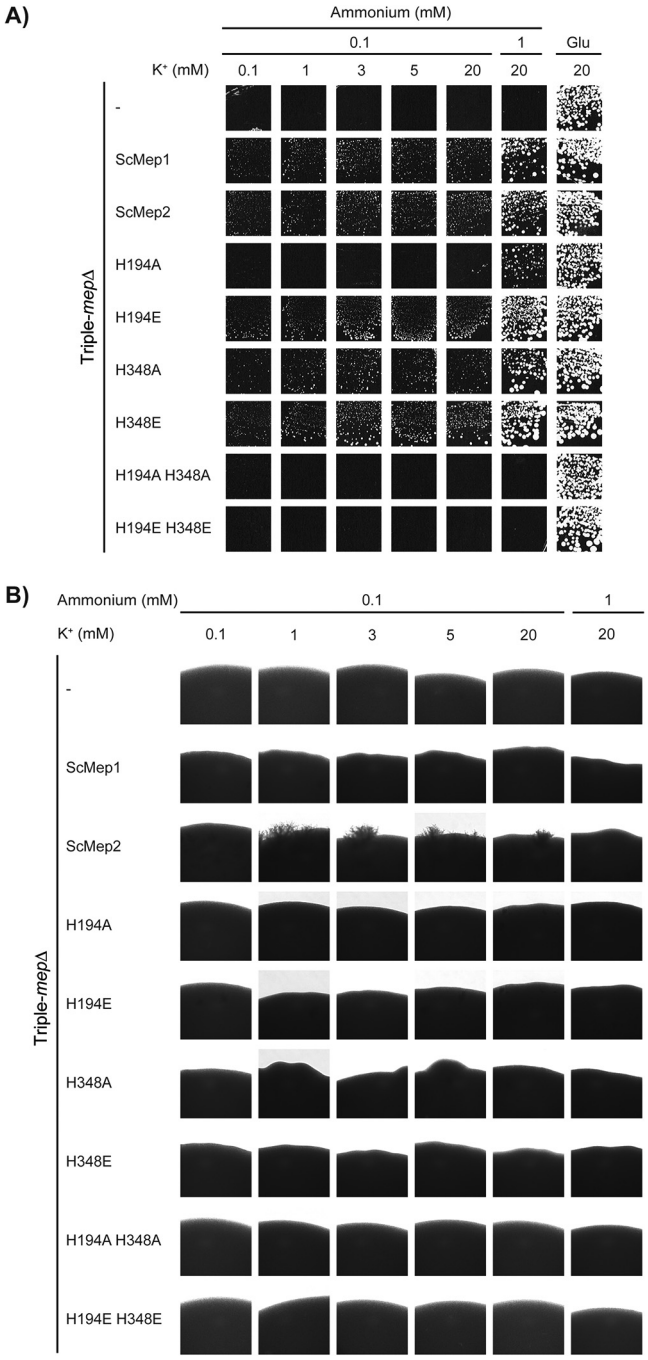

FIG 9 Effect of Twin-His substitutions on the capacity of ScMep2 to induce fungal filamentation at different K^+ concentrations. Homozygous diploid triple-*mep*Δ *ura3* cells (strain ZAM38) were transformed with the pFL38 empty plasmid (–) or with YCpMep1, YCpMep2, YCpMep2^{H194A}, YCpMep2^{H194E}, YCpMep2^{H348A}, YCpMep2^{H348E}, YCpMep2$^{H194A/H348A}$, or YCpMep2$^{H194E/H348E}$. (A) Growth tests, after 7 days at 29°C, on 183 medium containing different potassium concentrations (0.1 mM to 20 mM) and 0.1 mM or 1 mM ammonium, as the nitrogen source. The same medium containing 20 mM potassium and sodium glutamate (Glu), as the sole nitrogen source, was used as the positive growth control. (B) Pseudohyphal growth tests of high-density cell suspensions dropped on 183 medium containing different potassium concentrations (from 0.1 mM to 20 mM) and 0.1 mM or 1 mM ammonium, as the nitrogen source. Cells were incubated 7 days at 29°C.

model that explains the loss of specificity associated with variations in the Twin-His motif. We show that the modification of the Twin-His motif is associated with a change in the pore hydrophobicity increasing its hydration pattern. These findings are supported by our previous X-ray structural analysis, where we showed that the introduction of a charged

residue at the Twin-His position drastically enhanced the pore hydration level (14). This increase in hydration governs a switch of the translocation mechanism from a specific transporter, based on substrate fragmentation, to an unspecific channel-like activity, where NH_4^+ is transported in its hydrated form and K^+, an ion of similar size, is able to compete. The mechanism of substrate transport alone ensures the high specificity of the transporter. This is reminiscent of the formate/nitrite transporters that ensure transport selectivity by neutralizing the formate anion by protonation (deprotonation in Amt-Mep-Rh), followed by the passage of the neutral substrate through a lipophilic constriction zone (24). We anticipate that the selective mechanism here evidenced could also apply to Rh members of the Amt-Mep-Rh family, as human RhAG mutations are associated with overhydrated stomatocytosis (OhSt), a hemolytic anemia characterized by the loss of specificity and leakage of important monovalent cations (K^+, Na^+) inside red blood cells (32).

In this context, it is important to note that the residues that delineate and stabilize the water wires in AmtB are highly conserved across the whole Amt-Mep-Rh family, which implies that the model proposed for ammonium conduction in AmtB could be conserved among members of the family that exhibit electrogenic activity (12). In line with this hypothesis, our previous results for *Ne*Rh50, a phylogenetically distant homolog of AmtB, demonstrate that its activity is electrogenic (12). In addition, other groups have reported electrogenic activity in other Amt-Mep-Rh members, including Amt1 and Amt3 from *Archaeoglobus fulgidus*, Amt1;1 from *Lycopersicon esculentum*, and some human Rh proteins (10, 33, 34). However, electroneutral activity has also been reported for a number of Amt-Mep-Rh proteins (13, 17, 33, 35). Notably, protein isoforms within a single species have been characterized as having different activity. For example, in *Arabidopsis thaliana*, whose genome encodes 6 *AMT* genes, divided in 2 subfamilies, activity of Amt1 members is electrogenic, while activity of Amt2 is electroneutral (for review see reference 36 and references therein). A similar split is observed in *S. cerevisiae* and *C. albicans* Mep2 and Mep1/3 proteins (15, 17). These results suggest that the family possesses more than one unique transport mechanism and, if so, it may be advantageous in order to maintain multiple physiological functions (17). At the moment, the molecular basis underpinning the diversity in transport mechanism in the Amt-Mep-Rh protein family is not fully solved. Our study, however, offers a hint to better apprehend this complex question. We have shown that a single mutation in ScMep2 and AmtB changes a specific transporter to an unspecific ion channel. This is reminiscent of the ubiquitous and very large CLC family of chloride translocators in which apparently similar architecture supports various mechanisms of transport—strict Cl^- channel, weak coupled Cl^-/H^+ exchanger, strict Cl^-/H^+, or NO_3^-/H^+ antiporter (for review see reference 37). Hence, it is now necessary to further investigate the mechanism throughout the Amt-Mep-Rh family, alongside the energetics of the transport and the dynamics of the protein during the transport cycle.

Our results extend beyond the characterization of a new mechanism for selectivity and offer a gateway to better understand signaling mechanisms responsible for fungal filamentation. The mechanism of Mep2-mediated signaling in yeast filamentation remains largely unsolved. Two hypotheses are raised concerning the molecular mechanism of Mep2-mediated signaling. The first one is that Mep2 is a sensor, potentially interacting with signaling partners leading to the induction of filamentation (2). The other one proposes that the specific transport mechanism of Mep2 could underlie the signal leading to filamentation (15, 17). We showed that, in the Mep2 single Twin-His variants, an NH_4^+ deprotonation-dependent transport mechanism and a channel-like mechanism (direct NH_4^+ transport) coexist. We further showed that this mechanistic alteration impairs the capacity of the *S. cerevisiae* and *C. albicans* Mep2 protein to induce filamentation. Altogether, these results support the hypothesis of mechanism-dependent signaling in yeast filamentation. As previously suggested, the difference in the transport mechanism between fungal Mep2 and $Mep2^{H/E}$ could influence in an opposite way the intracellular pH (15, 17). This pH modification could be the signal leading to the dimorphic change. While Mep2 would transport NH_3 after NH_4^+ deprotonation,

the current data indicate that the Mep2^{H194E} variant transports NH_4^+, thereby leading to acidification. However, we cannot exclude that the mechanism alteration leading to the creation of an ionic channel in single Twin-His Mep2 variants precludes a conformational switch required to transmit the signal to partners. Filamentation is often related to the virulence of pathogenic fungi, such as the human pathogens *Candida albicans* (38), *Histoplasma capsulatum* (39), or *Cryptococcus neoformans* (40). In this context, our results are of particular importance, as the characterization of the conditions regulating the yeast dimorphism may be crucial to better understanding fungal virulence.

MATERIALS AND METHODS

Plasmids and mutagenesis. The plasmids used are listed in Table S1. AmtB mutants were generated using the Quikchange XL site-directed mutagenesis kit (Agilent Technologies), following the manufacturer's instructions. The *amtB* gene cloned into pET22b(+) was used as the template, as previously described (4).

Site-directed mutagenesis of *ScMEP2* was performed by GeneCust, using YCpMep2 as the template. The *CaMEP2* (orf19.5672) gene and the mutated *CaMEP2*^{H188E} and *CaMEP2*^{H342E} genes, with the *ScMEP2* promoter (–661 to −1) and terminator (1 to 262), were synthesized and cloned in pFL38 by GeneCust. Of note, compared to the equivalent plasmids used in reference 17, the *ScMEP2* promoter used in these new plasmids is longer (660 bp compared to 400 bp) and allows a better complementation in growth tests. Plasmid extraction from bacterial cells was performed using the GeneJET plasmid miniprep kit (Thermo Fisher). All constructs were verified by sequencing.

AmtB purification and solid supported membrane electrophysiology. AmtB(His)$_6$ cloned into the pET22b(+) vector was overexpressed in C43 cells (4, 41), purified (42), and inserted into liposomes (11) as previously described. The size distribution of proteoliposomes had an average diameter of 110 nm (Fig. S1). The elution profile of all variants and the wild type were identical, showing a single monodisperse peak eluting between 10.4 and 10.6 mL (Fig. S2). Then, 3-mm gold-plated sensors (Nanion Technologies) were prepared (18) and SSME measurements done (12) as previously described. See Text S1 for details.

Yeast strains and growth conditions. The *S. cerevisiae* strains used in this study are the 31019b strain (*mep1*Δ *mep2*Δ *mep3*Δ *ura3*) (43), the #228 strain (*mep1*Δ *mep2*Δ *mep3*Δ *trk1*Δ *trk2*Δ *leu2 ura3*) (44), and the ZAM38 strain (*mep1*Δ/*mep1*Δ *mep2*Δ/*mep2*Δ *mep3*Δ/*mep3*Δ *ura3*/*ura3*) (29). Cells were grown at 29°C. Cell transformation was performed as described previously (45).

For growth tests on limiting ammonium concentrations, yeast cells were grown on minimal buffered (pH 6.1) medium (167) containing potassium salts (46). For growth tests on limiting potassium concentrations, a similar minimal buffered (pH 6.1) medium (173) where potassium salts were replaced by sodium salts was used, and KCl was added at the specified concentration; 3% glucose was used as the carbon source. Nitrogen sources were added as required by the experiment and as specified in the text. The nitrogen sources used were 0.1% potassium glutamate, 0.1% sodium glutamate, or $(NH_4)_2SO_4$ at the specified concentrations referring to the ammonium moiety.

Pseudohyphal growth tests were performed as previously described (47). A suspension of diploid cells was patched onto synthetic low ammonium dextrose (SLAD) and synthetic high ammonium dextrose (SHAD) [0.68% yeast nitrogen base without amino acids and without $(NH_4)_2SO_4$, containing 3% glucose and 1% bacteriological agar (Oxoid)], respectively, supplemented with 50 μM or 0.5 mM $(NH_4)_2SO_4$. Pseudohyphal and growth tests on limiting potassium concentrations were performed on a home-made medium (183) equivalent to yeast nitrogen base medium without amino acids, $(NH_4)_2SO_4$ and potassium salts, and containing low NaH_2PO_4 concentrations. $(NH_4)_2SO_4$ and KCl were added as required by the experiment and as specified in the text. For growth tests, diploid cells were streaked on SLAD, SHAD, and 183 medium to follow the formation of colonies.

All growth experiments were repeated at least twice.

Molecular dynamics simulations. The AmtB trimer (PDB code 1U7G) (3) was processed using the CHARMM-GUI web server (48). Any mutations inserted during the crystallization process were reverted to the wild-type form. The studied mutations were introduced into the protein using PyMOL. The N termini and C termini of the subunits were capped with acetyl and N-methyl amide moieties, respectively. The protein was then inserted into a membrane patch of *xy*-dimensions 13 by 13 nm. Unless otherwise specified, a membrane composition of palmitoyl oleoyl phosphatidyl ethanolamine and palmitoyl oleoyl phosphatidyl glycine (POPE/POPG) at a 3:1 ratio was used in order to approximate the composition of a bacterial cytoplasmic membrane. We employed the CHARMM36 forcefield for the protein and counter ions (49). The water molecules were modeled with the TIP3P model (50). Water bonds and distances were constrained by the Settle method (51), and bonds involving hydrogen by the LINCS method (52). In simulations without ammonium, K^+ and Cl^- ions were added to neutralize the system and obtain a bulk ionic concentration of 250 mM. In simulations with ammonium, K^+ was replaced by NH_4^+.

After a steepest-descent energy minimization, the system was equilibrated by six consecutive equilibration steps using position restraints on heavy atoms of 1,000 kJ/mol.nm^2. The first three equilibration steps were conducted in a constant number, volume, and temperature (NVT) ensemble, applying a Berendsen thermostat (53) to keep the temperature at 310 K. The subsequent steps were conducted under an constant number, pressure, and temperature (NPT) ensemble, using a Berendsen barostat (53) to keep the pressure at 1 bar. Production molecular dynamics simulations were carried out using a v-

rescale thermostat (54) with a time constant of 0.2 ps and a Berendsen barostat with semi-isotropic coupling. A timestep of 2 fs was used throughout the simulations.

SUPPLEMENTAL MATERIAL

Supplemental material is available online only.

TEXT S1, DOCX file, 0.03 MB.

FIG S1, DOCX file, 2.1 MB.

FIG S2, DOCX file, 1.1 MB.

FIG S3, DOCX file, 1 MB.

TABLE S1, DOCX file, 0.03 MB.

TABLE S2, DOCX file, 0.02 MB.

ACKNOWLEDGMENTS

We thank Pascale Van Vooren for support and discussion. Special thanks go to Iain Hunter (Strathclyde Institute of Pharmacy and Biomedical Sciences) for invaluable discussions and help during this project.

A.B., G.W., and G.D.M. are supported by Ph.D. studentships from the University of Strathclyde. A.J. is supported by a Chancellor's Fellowship from the University of Strathclyde and Tenovus Scotland (S17-07). G.T. and U.Z. are supported by the Scottish Universities' Physics Alliance (SUPA). P.A.H. is supported by the Natural Environment Research Council (NE/M001415/1).

A.S.B. is a research fellow of the Fund for Scientific Research (F.R.S.-FNRS), A.M.M. is a senior research associate of the F.R.S.-FNRS and a WELBIO investigator, M.B. is a scientific research worker supported by WELBIO. A.M.M. received support for this work from F.R.S.-FNRS (CDR J017617F, PDR T011515F, PDR 33658167), the Fédération Wallonie-Bruxelles (Action de Recherche Concertée), WELBIO, and the Brachet Funds.

REFERENCES

1. Huang CH, Peng J. 2005. Evolutionary conservation and diversification of Rh family genes and proteins. Proc Natl Acad Sci U S A 102:15512–15517. https://doi.org/10.1073/pnas.0507886102.
2. Lorenz MC, Heitman J. 1998. The MEP2 ammonium permease regulates pseudohyphal differentiation in *Saccharomyces cerevisiae*. EMBO J 17:1236–1247. https://doi.org/10.1093/emboj/17.5.1236.
3. Khademi S, O'Connell J, III, Remis J, Robles-Colmenares Y, Miercke LJ, Stroud RM. 2004. Mechanism of ammonia transport by Amt/MEP/Rh: structure of AmtB at 1.35 Å. Science 305:1587–1594. https://doi.org/10.1126/science.1101952.
4. Zheng L, Kostrewa D, Bernèche S, Winkler FK, Li X-D. 2004. The mechanism of ammonia transport based on the crystal structure of AmtB of *Escherichia coli*. Proc Natl Acad Sci U S A 101:17090–17095. https://doi.org/10.1073/pnas.0406475101.
5. Andrade SL, Dickmanns A, Ficner R, Einsle O. 2005. Crystal structure of the archaeal ammonium transporter Amt-1 from *Archaeoglobus fulgidus*. Proc Natl Acad Sci U S A 102:14994–14999. https://doi.org/10.1073/pnas.0506254102.
6. Lupo D, Li XD, Durand A, Tomizaki T, Cherif-Zahar B, Matassi G, Merrick M, Winkler FK. 2007. The 1.3-A resolution structure of *Nitrosomonas europaea* Rh50 and mechanistic implications for NH_3 transport by Rhesus family proteins. Proc Natl Acad Sci U S A 104:19303–19308. https://doi.org/10.1073/pnas.0706563104.
7. Gruswitz F, Chaudhary S, Ho JD, Schlessinger A, Pezeshki B, Ho CM, Sali A, Westhoff CM, Stroud RM. 2010. Function of human Rh based on structure of RhCG at 2.1 A. Proc Natl Acad Sci U S A 107:9638–9643. https://doi.org/10.1073/pnas.1003587107.
8. van den Berg B, Chembath A, Jefferies D, Basle A, Khalid S, Rutherford JC. 2016. Structural basis for Mep2 ammonium transceptor activation by phosphorylation. Nat Commun 7:11337. https://doi.org/10.1038/ncomms11337.
9. Ariz I, Boeckstaens M, Gouveia C, Martins AP, Sanz-Luque E, Fernandez E, Soveral G, von Wiren N, Marini AM, Aparicio-Tejo PM, Cruz C. 2018. Nitrogen isotope signature evidences ammonium deprotonation as a common transport mechanism for the AMT-Mep-Rh protein superfamily. Sci Adv 4:eaar3599. https://doi.org/10.1126/sciadv.aar3599.
10. Wacker T, Garcia-Celma JJ, Lewe P, Andrade SL. 2014. Direct observation of electrogenic NH_4^+ transport in ammonium transport (Amt) proteins. Proc Natl Acad Sci U S A 111:9995–10000. https://doi.org/10.1073/pnas.1406409111.
11. Mirandela GD, Tamburrino G, Hoskisson PA, Zachariae U, Javelle A. 2019. The lipid environment determines the activity of the *Escherichia coli* ammonium transporter AmtB. FASEB J 33:1989–1999. https://doi.org/10.1096/fj.201800782R.
12. Williamson G, Tamburrino G, Bizior A, Boeckstaens M, Dias Mirandela G, Bage MG, Pisliakov A, Ives CM, Terras E, Hoskisson PA, Marini AM, Zachariae U, Javelle A. 2020. A two-lane mechanism for selective biological ammonium transport. Elife 9:e57183. https://doi.org/10.7554/eLife.57183.
13. Ludewig U, Neuhauser B, Dynowski M. 2007. Molecular mechanisms of ammonium transport and accumulation in plants. FEBS Lett 581:2301–2308. https://doi.org/10.1016/j.febslet.2007.03.034.
14. Javelle A, Lupo D, Zheng L, Li XD, Winkler FK, Merrick M. 2006. An unusual twin-his arrangement in the pore of ammonia channels is essential for substrate conductance. J Biol Chem 281:39492–39498. https://doi.org/10.1074/jbc.M608325200.
15. Boeckstaens M, Andre B, Marini AM. 2008. Distinct transport mechanisms in yeast ammonium transport/sensor proteins of the Mep/Amt/Rh family and impact on filamentation. J Biol Chem 283:21362–21370. https://doi.org/10.1074/jbc.M801467200.
16. Wang J, Fulford T, Shao Q, Javelle A, Yang H, Zhu W, Merrick M. 2013. Ammonium transport proteins with changes in one of the conserved pore histidines have different performance in ammonia and methylamine conduction. PLoS One 8:e62745. https://doi.org/10.1371/journal.pone.0062745.
17. Brito AS, Neuhauser B, Wintjens R, Marini AM, Boeckstaens M. 2020. Yeast filamentation signaling is connected to a specific substrate translocation mechanism of the Mep2 transceptor. PLoS Genet 16:e1008634. https://doi.org/10.1371/journal.pgen.1008634.
18. Bazzone A, Barthmes M, Fendler K. 2017. SSM-based electrophysiology for transporter research. Methods Enzymol 594:31–83. https://doi.org/10.1016/bs.mie.2017.05.008.

19. Hess DC, Lu W, Rabinowitz JD, Botstein D. 2006. Ammonium toxicity and potassium limitation in yeast. PLoS Biol 4:e351. https://doi.org/10.1371/journal.pbio.0040351.
20. Loque D, Mora SI, Andrade SL, Pantoja O, Frommer WB. 2009. Pore mutations in ammonium transporter AMT1 with increased electrogenic ammonium transport activity. J Biol Chem 284:24988–24995. https://doi.org/10.1074/jbc.M109.020842.
21. Hall JA, Kustu S. 2011. The pivotal twin histidines and aromatic triad of the Escherichia coli ammonium channel AmtB can be replaced. Proc Natl Acad Sci U S A 108:13270–13274. https://doi.org/10.1073/pnas.1108451108.
22. Javelle A, Lupo D, Li XD, Merrick M, Chami M, Ripoche P, Winkler FK. 2007. Structural and mechanistic aspects of Amt/Rh proteins. J Struct Biol 158:472–481. https://doi.org/10.1016/j.jsb.2007.01.004.
23. Roon RJ, Larimore F, Levy JS. 1975. Inhibition of amino acid transport by ammonium ion in *Saccharomyces cerevisiae*. J Bacteriol 124:325–331. https://doi.org/10.1128/jb.124.1.325-331.1975.
24. Wiechert M, Beitz E. 2017. Mechanism of formate-nitrite transporters by dielectric shift of substrate acidity. EMBO J 36:949–958. https://doi.org/10.15252/embj.201695776.
25. Dubois E, Grenson M. 1979. Methylamine/ammonia uptake systems in *Saccharomyces cerevisiae*: multiplicity and regulation. Mol Gen Genet 175:67–76. https://doi.org/10.1007/BF00267857.
26. Rutherford JC, Lin X, Nielsen K, Heitman J. 2008. Amt2 permease is required to induce ammonium-responsive invasive growth and mating in *Cryptococcus neoformans*. Eukaryot Cell 7:237–246. https://doi.org/10.1128/EC.00079-07.
27. Boeckstaens M, Andre B, Marini AM. 2007. The yeast ammonium transport protein Mep2 and its positive regulator, the Npr1 kinase, play an important role in normal and pseudohyphal growth on various nitrogen media through retrieval of excreted ammonium. Mol Microbiol 64:534–546. https://doi.org/10.1111/j.1365-2958.2007.05681.x.
28. Boeckstaens M, Llinares E, Van Vooren P, Marini AM. 2014. The TORC1 effector kinase Npr1 fine tunes the inherent activity of the Mep2 ammonium transport protein. Nat Commun 5:3101. https://doi.org/10.1038/ncomms4101.
29. Marini AM, Boeckstaens M, Benjelloun F, Cherif-Zahar B, Andre B. 2006. Structural involvement in substrate recognition of an essential aspartate residue conserved in Mep/Amt and Rh-type ammonium transporters. Curr Genet 49:364–374. https://doi.org/10.1007/s00294-006-0062-5.
30. Biswas K, Morschhauser J. 2005. The Mep2p ammonium permease controls nitrogen starvation-induced filamentous growth in *Candida albicans*. Mol Microbiol 56:649–669. https://doi.org/10.1111/j.1365-2958.2005.04576.x.
31. Ganz P, Ijato T, Porras-Murrilo R, Stührwohldt N, Ludewig U, Neuhäuser B. 2020. A twin histidine motif is the core structure for high-affinity substrate selection in plant ammonium transporters. J Biol Chem 295:3362–3370. https://doi.org/10.1074/jbc.RA119.010891.
32. Bruce LJ, Guizouarn H, Burton NM, Gabillat N, Poole J, Flatt JF, Brady RL, Borgese F, Delaunay J, Stewart GW. 2009. The monovalent cation leak in overhydrated stomatocytic red blood cells results from amino acid substitutions in the Rh-associated glycoprotein. Blood 113:1350–1357. https://doi.org/10.1182/blood-2008-07-171140.
33. Ludewig U, von Wirén N, Frommer WB. 2002. Uniport of NH_4+ by the root hair plasma membrane ammonium transporter LeAMT1;1. J Biol Chem 277:13548–13555. https://doi.org/10.1074/jbc.M200739200.
34. Caner T, Abdulnour-Nakhoul S, Brown K, Islam MT, Hamm LL, Nakhoul NL. 2015. Mechanisms of ammonia and ammonium transport by rhesus-associated glycoproteins. Am J Physiol Cell Physiol 309:C747–758. https://doi.org/10.1152/ajpcell.00085.2015.
35. Ludewig U. 2004. Electroneutral ammonium transport by basolateral rhesus B glycoprotein. J Physiol 559:751–759. https://doi.org/10.1113/jphysiol.2004.067728.
36. Hao DL, Zhou JY, Yang SY, Qi W, Yang KJ, Su YH. 2020. Function and regulation of ammonium transporters in plants. Int J Mol Sci 21:3557. https://doi.org/10.3390/ijms21103557.
37. Jentsch TJ. 2015. Discovery of CLC transport proteins: cloning, structure, function and pathophysiology. J Physiol 593:4091–4109. https://doi.org/10.1113/JP270043.
38. Lo HJ, Kohler JR, DiDomenico B, Loebenberg D, Cacciapuoti A, Fink GR. 1997. Nonfilamentous *C. albicans* mutants are avirulent. Cell 90:939–949. https://doi.org/10.1016/s0092-8674(00)80358-x.
39. Maresca B, Kobayashi GS. 1989. Dimorphism in *Histoplasma capsulatum*: a model for the study of cell differentiation in pathogenic fungi. Microbiol Rev 53:186–209. https://doi.org/10.1128/mr.53.2.186-209.1989.
40. Wickes BL, Edman U, Edman JC. 1997. The *Cryptococcus neoformans* STE12alpha gene: a putative *Saccharomyces cerevisiae* STE12 homologue that is mating type specific. Mol Microbiol 26:951–960. https://doi.org/10.1046/j.1365-2958.1997.6322001.x.
41. Miroux B, Walker JE. 1996. Over-production of proteins in *Escherichia coli*: mutant hosts that allow synthesis of some membrane proteins and globular proteins at high levels. J Mol Biol 260:289–298. https://doi.org/10.1006/jmbi.1996.0399.
42. Dias Mirandela G, Tamburrino G, Ivanovic MT, Strnad FM, Byron O, Rasmussen T, Hoskisson PA, Hub JS, Zachariae U, Gabel F, Javelle A. 2018. Merging in-solution X-ray and neutron scattering data allows fine structural analysis of membrane-protein detergent complexes. J Phys Chem Lett 9:3910–3914. https://doi.org/10.1021/acs.jpclett.8b01598.
43. Marini AM, Soussi-Boudekou S, Vissers S, Andre B. 1997. A family of ammonium transporters in *Saccharomyces cerevisiae*. Mol Cell Biol 17:4282–4293. https://doi.org/10.1128/MCB.17.8.4282.
44. ten Hoopen F, Cuin TA, Pedas P, Hegelund JN, Shabala S, Schjoerring JK, Jahn TP. 2010. Competition between uptake of ammonium and potassium in barley and *Arabidopsis* roots: molecular mechanisms and physiological consequences. J Exp Bot 61:2303–2315. https://doi.org/10.1093/jxb/erq057.
45. Gietz D, St Jean A, Woods RA, Schiestl RH. 1992. Improved method for high efficiency transformation of intact yeast cells. Nucleic Acids Res 20:1425. https://doi.org/10.1093/nar/20.6.1425.
46. Jacobs P, Jauniaux JC, Grenson M. 1980. A *cis*-dominant regulatory mutation linked to the *argB-argC* gene cluster in *Saccharomyces cerevisiae*. J Mol Biol 139:691–704. https://doi.org/10.1016/0022-2836(80)90055-8.
47. Gimeno CJ, Ljungdahl PO, Styles CA, Fink GR. 1992. Unipolar cell divisions in the yeast *S. cerevisiae* lead to filamentous growth: regulation by starvation and RAS. Cell 68:1077–1090. https://doi.org/10.1016/0092-8674(92)90079-R.
48. Lee J, Cheng X, Swails JM, Yeom MS, Eastman PK, Lemkul JA, Wei S, Buckner J, Jeong JC, Qi Y, Jo S, Pande VS, Case DA, Brooks CL III, MacKerell AD Jr, Klauda JB, Im W. 2016. CHARMM-GUI input generator for NAMD, GROMACS, AMBER, OpenMM, and CHARMM/OpenMM simulations using the CHARMM36 additive force field. J Chem Theory Comput 12:405–413. https://doi.org/10.1021/acs.jctc.5b00935.
49. Best RB, Zhu X, Shim J, Lopes PE, Mittal J, Feig M, Mackerell AD Jr. 2012. Optimization of the additive CHARMM all-atom protein force field targeting improved sampling of the backbone phi, psi and side-chain chi(1) and chi(2) dihedral angles. J Chem Theory Comput 8:3257–3273. https://doi.org/10.1021/ct300400x.
50. Jorgensen WL, Chandrasekhar J, Madura JD, Impey RW, Klein ML. 1983. Comparison of simple potential functions for simulating liquid water. J Chem Phys 79:926–935. https://doi.org/10.1063/1.445869.
51. Miyamoto S, Kollman PA. 1992. Settle: an analytical version of the SHAKE and RATTLE algorithm for rigid water models. J Comput Chem 13:952–962. https://doi.org/10.1002/jcc.540130805.
52. Hess B, Bekker H, Berendsen HJC, Fraaije JGEM. 1997. LINCS: a linear constraint solver for molecular simulations. J Comput Chem 18:1463–1472. https://doi.org/10.1002/(SICI)1096-987X(199709)18:12<1463::AID-JCC4>3.0.CO;2-H.
53. Berendsen HJC, Postma JPM, van Gunsteren WF, DiNola A, Haak JR. 1984. Molecular dynamics with coupling to an external bath. J Chem Phys 81:3684–3690. https://doi.org/10.1063/1.448118.
54. Bussi G, Donadio D, Parrinello M. 2007. Canonical sampling through velocity rescaling. J Chem Phys 126:e014101. https://doi.org/10.1063/1.2408420.